ISSN: 2153-1196 Volume 11, Number 11, November 2020

Scientific Research Publishing

# Journal of Modern Physics

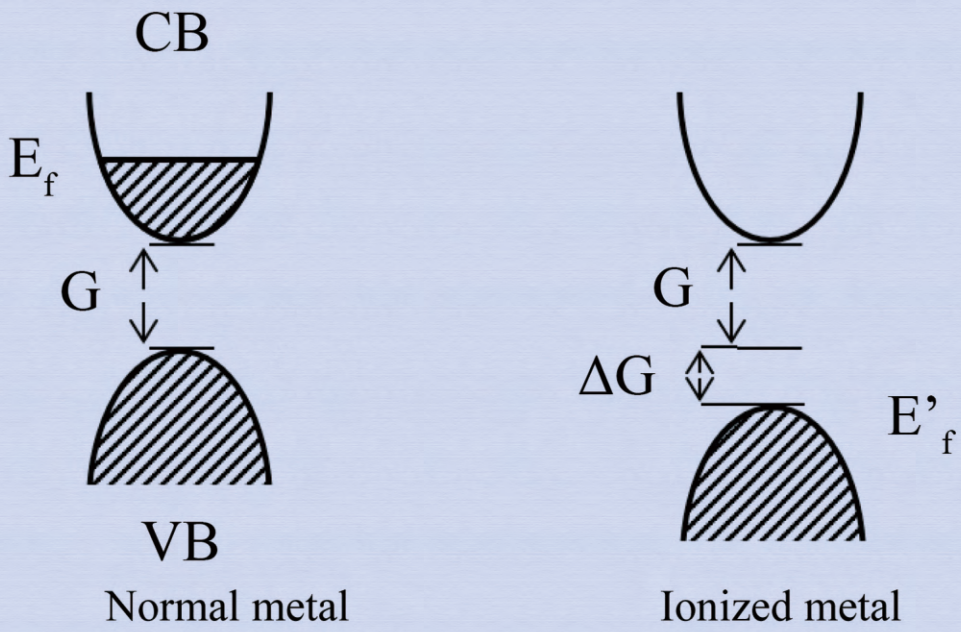


ISSN: 2153-1196

https://www.scirp.org/journal/jmp

# Journal Editorial Board

**ISSN: 2153-1196 (Print) ISSN: 2153-120X (Online)**
**https://www.scirp.org/journal/jmp**

## Editor-in-Chief



## Editorial Board

Scientific Research Publishing

Journal of Modern Physics, 2020, 11, 1743-1910
https://www.scirp.org/journal/jmp
ISSN Online: 2153-120X
ISSN Print: 2153-1196

# Table of Contents

Volume 11 Number 11 November 2020

Journal of Modern Physics, 2020, 11, 1743-1910
https://www.scirp.org/journal/jmp
ISSN Online: 2153-120X
ISSN Print: 2153-1196



The figure on the front cover is from the article published in Journal of Modern Physics, 2020, Vol. 11, No. 11, pp. 1743-1750 by Kai Wai Wong, Wan Ki Chow.

# Journal of Modern Physics (JMP)
# Journal Information

## SUBSCRIPTIONS

The *Journal of Modern Physics* (Online at Scientific Research Publishing, https://www.scirp.org/) is published monthly by Scientific Research Publishing, Inc., USA.

**Subscription rates:**
Print: $89 per issue.
To subscribe, please contact Journals Subscriptions Department, E-mail: sub@scirp.org

## SERVICES

**Advertisements**
Advertisement Sales Department, E-mail: service@scirp.org

**Reprints (minimum quantity 100 copies)**
Reprints Co-ordinator, Scientific Research Publishing, Inc., USA.
E-mail: sub@scirp.org

## COPYRIGHT



## PRODUCTION INFORMATION

For manuscripts that have been accepted for publication, please contact:
E-mail: jmp@scirp.org

Journal of Modern Physics, 2020, 11, 1743-1750
https://www.scirp.org/journal/jmp
ISSN Online: 2153-120X
ISSN Print: 2153-1196

# Principle for the Working of the Lithium-Ion Battery

**Kai Wai Wong[1], Wan Ki Chow[2]**

[1]Department of Physics and Astronomy, University of Kansas, Lawrence, USA
[2]Department of Building Services Engineering, The Hong Kong Polytechnic University, Hong Kong, China
Email: kww88ng@gmail.com

**How to cite this paper:** Wong, K.W. and Chow, W.K. (2020) Principle for the Working of the Lithium-Ion Battery. *Journal of Modern Physics*, **11**, 1743-1750.
https://doi.org/10.4236/jmp.2020.1111107

**Received:** September 16, 2020
**Accepted:** November 2, 2020
**Published:** November 5, 2020



## Abstract

The technological advances in Lithium-ion batteries have created many new applications, including electric vehicles. In this short note, we shall explain in simple terms the basic physics why and how it is possible to have high energy capacity in Lithium-ion batteries. However, heating has been a common problem and without appropriate design, they might give fire and explosion as reported.

## Keywords

Effective Coulomb Potential for Atomic Orbitals, Bohr Atomic Orbital Energies, Changes Due to Space Dimensions Symmetries, Change in Lithium Metal Ionized Valence Bands Binding

## 1. Introduction

Lithium-ion (Li-ion) batteries [1]-[8] have high specific energy, high efficiency and long service life and have become the power supply in many applications. Billions of units are manufactured per year as electrochemical storage systems in renewable energy plants, power systems for electric vehicles and as power sources for the electronics consumer market including smart phones, tablets, notebooks and laptops.

However, many field incidents occurred for Li-ion battery [9] [10] packs all over the world. Fires involving Li-ion batteries must therefore be studied more thoroughly when widely used. How a Li-ion battery will ignite by itself and what are the consequences under a flashover room fire should be studied. The first step is to understand the physics [11] [12] [13] behind why it is possible to have high energy capacity.

## 2. Physical Principles

Li has atomic number 3 with 1 electron at principal quantum number $n = 2$ and single pair or 2 elections at $n = 1$, 1 s. The atomic structure is similar to hydrogen $H$, except that in $H$, the outermost electron has principal quantum number $n = 1$. The electronic binding energy for $H$, from Bohr's model [14] [15] in 3D space symmetry is given by $-R$, where $R$ is the Rydberg constant. For the Li $n = 2$, 1 s electron, the electronic binding energy is given by $-R/4$, because the outermost electron experiences of the Pauli exclusion principle, each electron in the atom observed equally a net $+e$ charge due to the effective screening of the nucleus by the remaining the electron charge $-2e$ at $n = 1$. The total electron binding energy is thus $-2R - R/4 = -9R/4$. Should we ionize $H$, it will require an energy $E = R$. The first ionization energy of Li is not just $R/4$. Because when one electron is removed each of the remaining 2 electrons each would observe an effective +2e charge, due to charge screening of the nucleus by each of these two electrons, hence its total binding energy becomes $-4R$.

As compared to $-9R/4$, an energy of $7R/4$ is needed, instead of just the $R/4$ for $n = 2$ s orbital energy. This extra $3/2R$ amount is then stored up in the Li. But of course, Lithium is a metal having a 3D cubic crystal lattice periodic b.c. It is due to this lattice symmetry point group, the $n = 2$ s orbital becomes the conduction band (CB) electron, while the 2 $n = 1$ s orbitals formed the filled valence band (VB), with a separating gap $G$ roughly of $R/4$. In making Li into a battery, we remove the CB electron, thus making it a voltage source. For most other metals, this voltage is just corresponding to the last electron Coulomb binding, yet for Lithium, it is far greater; namely $3/2R$ greater. This extra amount requires that the VB 2 s orbitals be suppressed lower thus increasing the band gap by that same amount. In fact, what we have discussed is entirely based on 3D atomic symmetry. In a crystal structure, it is possible to make into a 2D thin film. Such a new 2D structure changes our Bohr model analysis. The 2D atomic levels are given by $-R/[n - 1/2]^2$, where $n = 1, 2, \cdots$. That means the outer most s orbital energy is $-4R/9$ instead of $-R/4$ while the lower 2 s orbital energy increases to $-8R$. By ionization of the CB electron the VB gap $G$ changes from $8R$ to $16R$, producing an extra potential energy of $8R$.

It is this physics that allows the technological advance of making the Lithium battery in terms of 2D layers. Of course, with the making of Li layers, its electronic orbitals are not perfect 2D, and the atomic energy gain is not exactly 2D. But it still increases the high energy capacity in the recharged battery. The wattage of the battery is proportional to the number of Li metal layers, while the voltage is layer thickness inverse dependent. The wattage limitation to such Li battery is completely due to the heat it generates.

The Hamiltonian with crystal lattice periodic boundary condition for the ionized Lithium orbitals is

$$H = \frac{P_1^2}{2m} + \frac{P_2^2}{2m} - \frac{3e^2}{r_1} - \frac{3e^2}{r_2} + \frac{e^2}{\left|\overline{r_1} - \overline{r_2}\right|} \tag{1}$$

where $H$ is the electrons Hamiltonian operator, $e$ the electron charge and $r$ the orbital radius under the Lithium metal periodic lattice boundary condition. Therefore the eigenvalues are given by the band structure as illustrated in Figure 1.

The repulsive electron-electron potential in effect is responsible for reducing the effective Hamiltonian to the 2 s states by realizing the Pauli exclusion principle to

$$H \cong \frac{P^2}{2m} - \frac{Ze^2}{r} \tag{2}$$

where $Z = 2$.

The band structure change of Li-ion metal is shown in Figure 1.

The Li-ion voltage $V$ is given by $E_f$ and $G$ as:

$$V = E_f + G + \Delta G \tag{3}$$

The quantum averaged potential change $\Delta G$ is:

$$\Delta G = \left\langle \frac{e^2}{r} \right\rangle \tag{4}$$

A schematic band structure for the Lithium metal and its corresponding ionized band structure are shown in Figure 1. The horizontal axis of each band diagram is in momentum unit.

Actually, the similar quantum chemistry approach can be applied to ionized Sodium, Na, which has atomic state $n$ = 3, 1 s. This Bohr state changes significantly the effective charges observed by the lower energy level electrons, and hence changes significantly the VB energy level changes, reducing the voltage capacity. However, it also reduces the heating when used as a battery material, but not enough for transportation application.

Perhaps sodium ion is in fact naturally derived from salt and used in bio-systems, such as the light emission in the firefly. Thus the future technological improvement lies in the design in heat insulation and dissipation and not in replacing Li by Na. Because Li-ion battery powered vehicles produce no emission, it is environmentally clean, compact, rechargeable, as well as maintenance free, making it the future choice replacing the combustion engine for transportation. Recently,

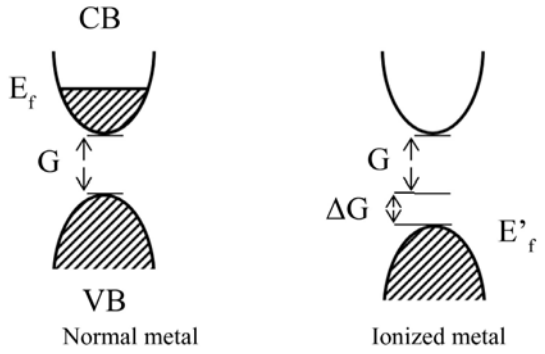


Figure 1. Band structure change.

a new Li-ion battery design that substantially increases its power was reported [11]. The problem to tackle the heating problem still remains.

## 3. Safety Aspects

Although Li-ion battery is rapidly adopted [16], safety concerns, both fire and explosion hazards, are threatening widespread adoption. Battery safety can be broadly classified into three categories:

1) Cell design depending on selected materials and circuitry.

Manufacturers are attempting to produce safer [17] products. There might be electric protection circuit.

2) Use of product in scenarios unexpected [18] by the supplier.

Fire and explosion hazards of Li-ion batteries in phones or electric cars in crowded space should be carefully watched [19]. For example, the thermal behavior of cellular phone models which have been complained to be too hot should be studied experimentally. Both smart phones and tablet computers might catch fires accidentally [20] and even explode by themselves. The consequence can be very hazardous in crowded areas allowing phone charging.

3) Accidents coming from normal recommended operating conditions, possibly due to thermal runaway.

Very limited theory is available on explaining thermal runaway. Thermal runaway can be described [10] by the situation when a cell undergoes spontaneous self-destruction under normal operating conditions with two events occurring in sequence:

- High power generation to result in high-temperature hot spots.
- Triggering of the propagation of negative electrode by such local hot spots to increase the temperature of the entire cell, giving further chemical reactions or even combustion.

Flammable gases released would pose fire and explosion hazards for the compartment housing the cells. However, there is little available information characterizing the flammability properties of the gases released after cell thermal runaway. Explosion characteristics, such as lower flammability limit, laminar flame speed, and maximum over-pressure have to be explained by physical principles as pointed out above.

In order to investigate the thermal failure propagation behaviors of Li-ion batteries, full-scale burning tests have to be conducted [21]. Theoretical physical principles have to be worked out on promoting fire safety design of large Li-ion battery energy storage equipment.

## 4. Suggestions

We mention above that heating problem is an important difficulty to overcome in the battery technology. So let us see the reasons behind the heating:

It is not due to the current flow in the battery. It is due to the high wattage, and the current it draws from the battery that must go through the battery con-

nection, and the inter layer possible voltage gradient due to the difference in the voltage caused by the atomic orbital of non-perfect 2D structure of the total N parallel 2D Lithium unit cell grouped in separated cross sections and the number of $n$ layers, that gives the battery voltage $V = nG$ as in Figure 2.

In many current Li-ion batteries, Li metal pieces are randomly mixed into $CoO_2$ [1] as in Figure 2(a). $CoO_2$ is an insulator, under its melting temperature. While as the battery energy is drawn, heat is generated if it contacts are normal conductors, causing short circuit and danger of fire or even exploding.

Both these problems can be eliminated if the material separating the layers and the connecting terminals are superconducting, as the superconducting separation between layers will equalize the voltage of all the layers, and will remove the connection heating as well.

High critical temperature (HTC) ceramics in its normal phase is a hole conductor, and as current is drawn, the Li-ions battery will lose its voltage as well as generate heat in the ceramic. However, if the HTC medium is in the superconducting phase as in Figure 2(b), the Li-ion will not lose energy. Such a Li-ion battery must then be housed within a temperature enclosure below the Tc of the HTC ceramic. In another word, such a battery design is only useful for use in very power intensive devices, such as electric vehicles.

When current is passed through a metal wire connected to an HTC superconductor, where the charge carriers are VB holes, due to an applied voltage, say from connecting to a Li-ion battery, it does not lose energy and due also to the effective mass difference; the electrons in the metal wire cannot fill the HTC holes. In fact, due to momentum conservation, it can only have elastic scattering and maintains current continuity. Meaning we can prevent a quick sudden heating as the Li-ion battery is connected to a superconductor instead of a normal conductor as current is drawn. There is of course certain minor loss in energy at the joint. Hopefully it can be dissipated by thermal conduction.

But a superconductor only works in a temperature bath below its critical

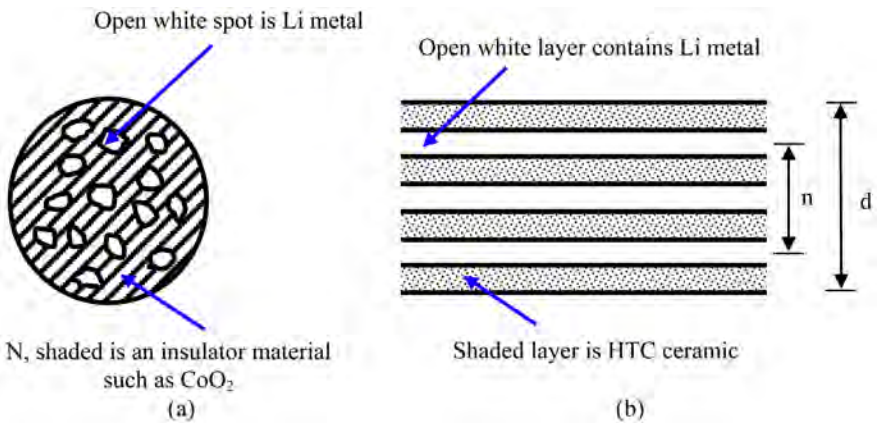


Figure 2. Grouped Li cells unit. It is vital that the Li layer is made of insulator material to prevent internal short circuit of the battery. (a) Li with insulation materials; (b) Li metal layers with HTC layers separation.

temperature Tc. Thus the higher the material Tc, the less cooling requirement would be needed. At the present, our best material is the HTC ceramics, such as YBCO/BiSCO. For these materials, we only need to maintain the battery in liquid nitrogen. With the above reasoning, we propose the battery manufacturing by using layer by layer disposition of Li micro particles with HTC powder, and heated under pressure. Actually, we had previously achieved a high current laser deposition of gold added TBCCO thin film on LaAlO substrate, which can be modified for the Li battery making [22]. First replace the substrate with an HTC ceramic. Then laser deposit a Li film, with the N cross section geometry, followed by a slightly thicker HTC film, and then the next Li film, etc., until it reaches n Li layers, and lastly sealed with a thick HTC top layer.

In order to improve both the Li-ion battery's voltage and its wattage power, there are two technical methods that one can implement in its design. In increasing the voltage, we must increase the VB binding. The space dimension restriction of the Lithium metal structure to as close as possible to 2D is achievable in applying nano deposition technology, while the increases in the battery wattage can be achieved by increasing the number of multiple separated layers of the Lithium metal. At present such techniques are limited by the potential current that is generated between the layers, that would generate internal heating, if the separation material between the Lithium layers is made of non-superconducting matter. Our suggested design of using HTC and keeping the battery at liquid nitrogen temperature is new.

Mining Lithium metal is energy intensive and mainly from South America and Australia. Thus it also contributes to environmental problem, despite the clean environment nature of using it as a battery. However, used and discarded Li-ion batteries can be recycled as the Lithium metal in it can be extracted and reused, without new supply from mining. Therefore, for environmental concern, we need to consider this recycling in mind as we design new batteries.

## 5. Conclusions

Basic physics behind Li-ion batteries has been explained in simple terms. Heating problem that will give fire and explosion as experienced has also been alerted to. Suggestions to solve the heating problem have also been proposed.

As we mentioned throughout this paper, the future of electrical power devices, including but not limited to electrical vehicles is the usage of the Lithium-ion battery. But current such batteries suffer from limitation on its voltage, and wattage due much by the internal heating problem that must be overcome. Our suggested new design is totally achievable from current HTC ceramics and laser deposition technologies, plus the thermal cycle cooling chamber technology in keeping the battery at liquid nitrogen temperature and thus minimizing that potential of battery fire danger during recharging and usage. Due to the carbon emission in current energy generators causing climate change, it is paramount that such carbon-based energy devices be eliminated completely within the next couple of decades. For which, the broad use of the Li-ion battery is a key com-

ponent.

## Funding

The work described in this paper was supported by a grant from the Research Grants Council of the Hong Kong Special Administrative Region for the Theme-Based Research Scheme Project "Safety, Reliability, and Disruption Management of High Speed Rail and Metro Systems" (T32-101/15-R) with account number3-RBAC.

## Acknowledgements

We thank Ms Winnie So for her careful help in editing.

## Conflicts of Interest

The authors declare no conflicts of interest regarding the publication of this paper.

## References

[1] Mizushima, K., Jones, P.C., Wiseman, P.J. and Goodenough, J.B. (1980) *Materials Research Bulletin*, **15**, 783-789. https://doi.org/10.1016/0025-5408(80)90012-4

[2] Mizushima, K., Jones, P.C., Wiseman, P.J. and Goodenough, J.B. (1981) *Solid State Ionics*, **3**, 171-174. https://doi.org/10.1016/0167-2738(81)90077-1

[3] Scrosati, B. and Garche, J. (2010) *Journal of Power Sources*, **195**, 2419-2430. https://doi.org/10.1016/j.jpowsour.2009.11.048

[4] Etacheri, V., Marom, R., Elazari, R., Salitra, G. and Aurbach, D. (2011) *Energy and Environmental Science*, **4**, 3243-3262. https://doi.org/10.1039/c1ee01598b

[5] Yan, L.M., Su, J.M., Sun, C. and Yue, B.H. (2014) *Advances in Manufacturing*, **2**, 358-368. https://doi.org/10.1007/s40436-014-0086-x

[6] Xu, J., Lin, F., Doeff, M.M. and Tong, W. (2017) *Journal of Materials Chemistry*, **5**, 874-901. https://doi.org/10.1039/C6TA07991A

[7] Ali, M.U., Zafar, A., Nengroo, S.H., Hussain, S., Alvi, M.J. and Kim, H.J. (2019) *Energies*, **12**, 446. https://doi.org/10.3390/en12030446

[8] Stampatori, D., Raimondi, P.P. and Noussan, M. (2020) *Energies*, **13**, 2638. https://doi.org/10.3390/en13102638

[9] Lisbona, D. and Snee, T. (2011) *Process Safety and Environmental Protection*, **89**, 434-442. https://doi.org/10.1016/j.psep.2011.06.022

[10] Zhang, Z.J., Ramadass, P. and Fang, W. (2013) Safety of Lithium-Ion Batteries. In: Pistoia, G., Ed., *Lithium-Ion Batteries Advances and Applications*, Elsevier, Amsterdam, Chapter 18, 409. https://doi.org/10.1016/B978-0-444-59513-3.00018-2

[11] Wu, M.S., Xu, B. and Ouyang, C.Y. (2016) *Chinese Physics B*, **25**, Article ID: 018206. https://doi.org/10.1088/1674-1056/25/1/018206

[12] Gao, J., Shi, S.-Q. and Li, H. (2016) *Chinese Physics B*, **25**, Article ID: 018210. https://doi.org/10.1088/1674-1056/25/1/018210

[13] Wong, K.W. and Chow, W.K. (2020) *Journal of Modern Physics*, **11**, 1058-1074. https://doi.org/10.4236/jmp.2020.117067

[14] Wikipedia, Bohr Model. https://en.wikipedia.org/wiki/Bohr_model#:~:text=In%20atomic%20physics%2C%2

0the%20Bohr,forces%20in%20place%20of%20gravity

[15] San Jose State University. A Generalization of the Bohr Equation for the Ionization Energy of the Outer Electron of Hydrogen-Like Atoms. https://www.sjsu.edu/faculty/watkins/bohrgen.htm

[16] Baird, A.R., Archibald, E.J., Marr, K.C. and Ezekoye, O.A. (2020) *Journal of Power Sources*, **446**, Article ID: 227257. https://doi.org/10.1016/j.jpowsour.2019.227257

[17] Johnson, S.K. (2020) Tesla Research Partnership Progresses on New Battery Chemistry, 14 August 2020. https://arstechnica.com/science/2020/08/tesla-research-partnership-progresses-on-new-battery-chemistry

[18] IEEE 1625:2008, IEEE Standard for Rechargeable Batteries for Multi-Cell Mobile Computing Devices.

[19] Kwok, J.H.Y., Cheng, C.H., Chow, W.K. and Chow, C.L. (2019) An Experimental Study on Possible Thermal Hazards of Cellular Phones. *Proceedings of the Third International Fire Safety Symposium* (*IFireSS* 2019), Ottawa, 5-7 June 2019, 597-606.

[20] Luk, S.Y. and Chow, W.K. (2020) Potential Thermal Fire Hazard of Smart Phones and Tablets. Article Submitted to Energy and Environment for Consideration to Publish.

[21] Chen, M.Y., Liu, J.H., Ouyang, D.X., Weng, J.W., Wu, X.Y., Cao, S.C. and Wang, J. (2020) *Journal of Energy Storage*, **31**, Article ID: 101657. https://doi.org/10.1016/j.est.2020.101657

[22] Wong, K.W., *et al.* (1994) *Laser in Engineering*, **2**, 319-324.

Journal of Modern Physics, 2020, 11, 1751-1760
https://www.scirp.org/journal/jmp
ISSN Online: 2153-120X
ISSN Print: 2153-1196

# Electron Transport under the Influence of Two Kinds of Friction in an Electron-Deuteron Plasma

**Mitsuaki Nagata**

Soft Creator Company, Kyoto, Japan
Email: nagata@heian-kogyo.jp

**How to cite this paper:** Nagata, M. (2020) Electron Transport under the Influence of Two Kinds of Friction in an Electron-Deuteron Plasma. *Journal of Modern Physics*, **11**, 1751-1760.
https://doi.org/10.4236/jmp.2020.1111108

**Received:** July 20, 2020
**Accepted:** November 3, 2020
**Published:** November 6, 2020



## Abstract

We discuss an electron transport in an ideal plasma which consists of electrons and deuterons. With respect to a frictional force to suppress an unlimited increase of a drift velocity, the Boltzmann equation with the Fokker-Planck collision term takes into consideration only a dynamical frictional force coming from the many-body collisions through the Coulomb force. However, we here bring forward a problem that there may be another frictional force besides the dynamical frictional force. Another frictional force was found in the weakly ionized plasma and appears only in the case where free paths (nearly straight lines in no external force field) can be defined. Then, we have inquired into the existence of physical quantities like free paths (or free times) in the field of the scattering through the Coulomb force and the existence of an effective radius of the Coulomb force of a deuteron.

## Keywords

Conductivity of Electrons in a Perfectly Ionized Plasma, Many-Body and Two-Body Collisions, Effective Radius of the Coulomb Force

## 1. Introduction

Electron transport in a fully ionized plasma has been classically analyzed based on the Boltzmann equation with the Fokker-Planck collision term $\delta f_c/\delta t$ ($t$: time) which is given by [1]-[6]

$$\frac{\delta f_c}{\delta t} = -\frac{\partial}{\partial \upsilon_r}\left( f \frac{\partial \mathrm{H}}{\partial \upsilon_r} \right) + \frac{1}{2}\frac{\partial^2}{\partial \upsilon_r \partial \upsilon_s}\left( f \frac{\partial^2 \mathrm{G}}{\partial \upsilon_r \partial \upsilon_s} \right) \tag{1}$$

Here, $f$ is a velocity distribution function of electrons, $\upsilon_{r(r=x,y,z)}$ and $\upsilon_{s(s=x,y,z)}$ are components of a velocity variable $\boldsymbol{\upsilon}$ of an electron,

$$\mathrm{H} \simeq \Gamma_{\upsilon} \frac{n_{\mathrm{p}}}{|\boldsymbol{\upsilon}|},\ \mathrm{G} \simeq \Gamma_{\upsilon} n_{\mathrm{p}} |\boldsymbol{\upsilon}|,\ \Gamma_{\upsilon} = 4\pi \left( \frac{q^2}{4\pi\varepsilon_0 m_{\mathrm{e}}} \right)^2 \left( \mathrm{n} \frac{4\pi\varepsilon_0 m_{\mathrm{e}} \boldsymbol{\upsilon}^2 \lambda_{\mathrm{D}}}{q^2} \right)$$

$-q$ is the electron charge $1.6 \times 10^{-19}$ C, $m_{\mathrm{e}}$ is the rest mass of an electron $9.1 \times 10^{-31}$ kg, $\varepsilon_0$ is the dielectric constant of vacuum $8.855 \times 10^{-12}$ Farad/m, $\lambda_{\mathrm{D}}$ is the Debye length $\left(\varepsilon_0 k_{\mathrm{B}} T / n_{\mathrm{p}} q^2\right)^{1/2}$, $n_{\mathrm{p}}$ is a deuteron density, $k_{\mathrm{B}}$ is the Boltzmann constant $1.38 \times 10^{-23}$ J/K and $T$ is electron temperature (=plasma temperature), $m_{\mathrm{e}} \ll m_{\mathrm{p}}$ (deuteron mass) and $|\boldsymbol{\upsilon}| \gg |\boldsymbol{\upsilon}_{\mathrm{p}}|$ (deuteron velocity magnitude). By integrating the Boltzmann equation multiplied by $m_{\mathrm{e}}\boldsymbol{\upsilon}$ all over the velocity space of electrons, the following equation for a drift velocity (denoted by $\mathbf{u}(t)$) is obtained:

$$m_{\mathrm{e}} \frac{\mathrm{d}\mathbf{u}(t)}{\mathrm{d}t} + q\boldsymbol{E} = \frac{m_e}{n_e} \int f \frac{\partial \mathrm{H}}{\partial \boldsymbol{\upsilon}} \mathrm{d}\boldsymbol{\upsilon} \tag{2}$$

Here, $\boldsymbol{E}$ is an electric field, a magnetic field $\boldsymbol{B} = 0$, $n_{\mathrm{e}}$ is an electron density which is not a function of position. Also, in (2), it has been taken into consideration that the dispersion due to work of the term containing G in (1) leaves the total momentum of the plasma unchanged. Furthermore, products between components of the drift velocity have been neglected. The right-hand side of (2) is the dynamical frictional force [1] (called DFF) coming from the many-body collisions between electrons and lots of surrounding charged particles.

On the other hand, we previously derived the momentum-transfer equation (given in (20) of Ref. [7]) in the case where electrons collide with neutral atoms and ions having an effective radius with respect to the Coulomb force (Determining the effective radius had remained as a pending question in Ref. [7]). As a result, two kinds of the frictional forces against an electric field, a part of DFF and another new frictional force, had appeared. An external electric field truncates or enlarges lengths of free times of electrons in the two-body collisions. We explained theoretically in **Appendix** of the other Ref. [8] that such a truncation-work of the electric field generates a new frictional force (called TFF) against an electron flow. TFF appears only in the case where a physical quantity like free times can be defined. We bring forward here a problem that, also in a field of scattering through the Coulomb force, there may be both DFF and TFF. In the following Section 2, we describe concretely DFF and TFF for comparison. And in Section 3, we try estimating an effective radius of the Coulomb force of a deuteron in the two-body collisions (called the e-$D^+$ collisions).

## 2. Two Kinds of the Frictional Force against Electric Field-Acceleration

First, for simplification of discussion, through this research we set the following physical conditions and the following ideal plasma:

* About external force fields;

◎ An electric field $\boldsymbol{E} = -\hat{z}E$ V/m.

◎ A magnetic field $\boldsymbol{B} = 0$ T.

∗ About an ideal plasma consisting of electrons and deuterons;

◎ Electron density $n_e = 10^{21}\,\mathrm{m}^{-3}$.

◎ Deuteron density $n_p = n_e\ \mathrm{m}^{-3}$.

◎ Plasma temperature $T = 4\times10^8\,\mathrm{K}$.

◎ A deuteron $D^+$ is regarded as a rest, heavy particle to an electron ($m \ll m_p$, $|\boldsymbol{\upsilon}| \gg |\boldsymbol{\upsilon}_p|$).

◎ Every electron is treated as a nonrelativistic particle with the same velocity $\bar{\upsilon}$ (= a mean thermal velocity $(8k_BT/\pi m_e)^{1/2} = 1.2\times10^8$ m/sec), except for calculation from (2) to (4).

◎ An influence [2] of the electron-electron interaction on the momentum-transfer from electrons to deuterons is disregarded.

◎ The Ramsauer effect also is disregarded.

1) The frictional force DFF in the field of the many-body collisions:

Substituting into (2)

$$\begin{cases} f = n_e\left(\dfrac{m_e}{2\pi k_BT}\right)^{3/2}\exp\left[-\dfrac{m_e}{2k_BT}\left(\boldsymbol{\upsilon}-\mathbf{u}(t)\right)^2\right] \\ \boldsymbol{E} = -\hat{z}E \ \text{ and } \ \mathbf{u}(t) = \hat{z}u(t), \end{cases} \tag{3}$$

We have [3] [4] in the limit of small $\left(\dfrac{m}{2k_BT}\right)^{1/2}u(t)$,

$$m_e\frac{\mathrm{d}u(t)}{\mathrm{d}t} - qE = -m_e\nu_D u(t) \tag{4}$$

where, by using $E_0 = \left(n_pm_e\Gamma/q\right)\left(2k_BT/m_e\right)$, $\Gamma = 4\pi\left(\bar{\upsilon}^2\right)^2p_\perp^2\ln\left(\lambda_D/p_\perp\right)$ and $p_\perp = q^2/\left(4\pi\varepsilon_0m_e\bar{\upsilon}^2\right)$ (Dreicer [3] used $3k_BT/\pi m_e$ instead of $\bar{\upsilon}^2\left(=8k_BT/\pi m_e\right)$),

$$\nu_D = \frac{qE_0}{m_e}\frac{4}{3\pi^{1/2}}\left(\frac{m_e}{2k_BT}\right)^{1/2} = n_p\pi p_\perp^2\bar{\upsilon}\left(4\ln\frac{\lambda_D}{p_\perp}\right)\frac{32}{3\pi^2} \tag{5}$$

Carrying out numerical calculations for $\lambda_D$, $p_\perp\nu_D$, we have

$$\lambda_D = \left(\frac{\varepsilon_0k_BT}{n_pq^2}\right)^{1/2} = 4.37\times10^{-5}\,\mathrm{m}$$

$$p_\perp = \frac{q^2}{4\pi\varepsilon_0m_e\bar{\upsilon}^2} = 1.76\times10^{-14}\,\mathrm{m}$$

($p_\perp$ is the impact parameter for π/2 -deflection in the e-$D^+$ collisions)

$$\nu_D \simeq 10^4\ \mathrm{sec}^{-1} \tag{6}$$

The right-hand side of (4) $-m_e\nu_Du(t)$ is commonly called DFF.

2) Another frictional force TFF in the field of the e-$D^+$ two-body collisions:

The momentum-transfer equation in the case where electrons do the two-body collisions both with neutral atoms and with ions is given by (20) of Ref. [7], as mentioned already. The equation reduces as follows, in the cases of no neutral atoms ($\nu^{en} = 0$) and no magnetic field ($\boldsymbol{B} = 0$,

$$\boldsymbol{F}_0 \times \hat{\mathbf{b}} = \left(-q\boldsymbol{E} + m_e \nu^{ep} \zeta \mathbf{u}(t)\right) \times \left(\boldsymbol{B}/|\boldsymbol{B}|\right) = 0),$$

$$m_e \frac{d\mathbf{u}(t)}{dt} + q\boldsymbol{E} = -m_e \nu^{ep} (1-\zeta)\mathbf{u}(t) - \kappa\left(-q\boldsymbol{E} + m_e \nu^{ep} \zeta \mathbf{u}(t)\right) \quad (7)$$

Here, $\nu^{ep} = n_p \pi p^2 \bar{\upsilon}$. In this work, this corresponds to the collision frequency of electrons in the e-$D^+$ collisions, and $p$ is an effective radius of the Coulomb force of $D^+$. Determining a value of $p$ had been remained as the pending question, $\zeta$ is the remaining ratio of $\mathbf{u}(t)$ in the e-$D^+$ anisotropic collisions (shown in **Figure 1** of Ref. [7]) and is given by

$$1-\zeta = 4\frac{\ln \Lambda}{\Lambda^2}$$

(where, $\Lambda = p/p_\perp$. In the isotropic scattering, $\zeta = 0$),

$$\kappa \equiv \beta_{02(\omega_c = 0)} = \frac{1}{3}$$

(where, $\omega_c = q|\boldsymbol{B}|/m_e$), and $-\kappa\left(-q\boldsymbol{E} + m_e \nu^{ep} \zeta \mathbf{u}(t)\right)$ is TFF. The quantity $\nu^{ep}(1-\zeta)$ with $p = \lambda_D$ is the same with $\nu_D$ of (5) in structure. Therefore, DFF ($= -m_e \nu_D \mathbf{u}(t)$ of (4)) contains $-m_e \nu^{ep}(1-\zeta)\mathbf{u}(t)$ as a part of itself. We presume that both DFF and TFF will work to suppress an unlimited increase of a drift velocity by acceleration of an external electric field.

## 3. An Effective Radius of a Deuteron on the Coulomb Force Scattering

We try estimating the upper limit of an impact parameter $p$ of $\nu^{ep}$ in (7). Since

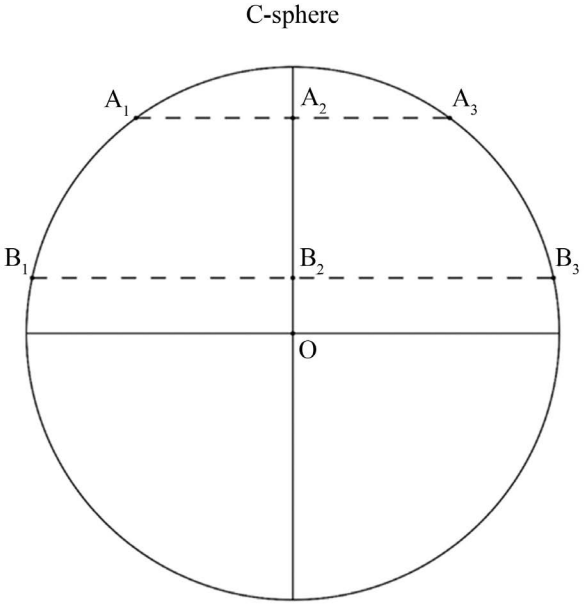


**Figure 1.** A proper influence-sphere (*C*-sphere), with respect to the Coulomb force, of a deuteron being at point O. The radius of *C*-sphere is $0.5d$. An electron flies two paths (from $A_1$ to around $A_3$ and from $B_1$ to around $B_3$). $\overline{OA_2} = 0.4d$, $\overline{OB_2} = 0.1d$, $\overline{A_1A_2} = \overline{A_2A_3} \simeq 0.33d$, $\overline{B_1B_2} = \overline{B_2B_3} \simeq 0.5d$. $d$ is a mean distance between deuterons.

a mean distance between deuterons is $n_p^{-1/3}$ $(=d=10^{-7}\,\mathrm{m})$, a deuteron has a proper influence-sphere (called $C$-sphere) whose radius is $0.5d$ with respect the Coulomb force [9]. We first compare deflection-angles by the many-body collisions with the ones by the two-body collisions in the cases where an electron passes the inside of $C$-sphere. In **Figure 1**, a deuteron $D^+$ is at point O and an electron with $\bar{\upsilon}\left(=1.2\times10^8\,\mathrm{m/sec}\right)$ flies two paths (from point $A_1$ to around point $A_3$ and from point $B_1$ to around point $B_3$) under no external force fields.

1) The case of the many-body collisions:

The magnitude of the dynamical frictional coefficient $\Delta\upsilon_{\parallel}$ in the Fokker-Planck collision term is given by

$$\Delta\upsilon_{\parallel}t=n_p\left[4\pi\bar{\upsilon}^2p_{\perp}^2\ln\left(\frac{\lambda_D}{P_{\perp}}\right)\right]t=1.21\times10^{12}t\quad\mathrm{m/sec}\tag{8}$$

where $t$ is flight time. Also, the dispersion coefficient $\Delta\upsilon_{\perp}$ is given by

$$\Delta\upsilon_{\perp}t\simeq\left(2\bar{\upsilon}\,\Delta\upsilon_{\parallel}t\right)^{1/2}=\quad\times10^{10}t^{1/2}\,\mathrm{m/sec}\quad\left(\Delta\upsilon_{\parallel}t\ll\bar{\upsilon}\right)\tag{9}$$

When an electron flies from $A_1$ to around point $A_3$ ( $t\simeq\left(2d/3\right)/\bar{\upsilon}$ ),

$$\Delta\upsilon_{\parallel}t=0.67\times10^{-3}\,\mathrm{m/sec}\quad(\text{Note: }\Delta\upsilon_{\parallel}t\ll\bar{\upsilon}).$$

$$\Delta\upsilon_{\perp}t=4\times10^{2}\,\mathrm{m/sec}\tag{10}$$

(Effects of $\Delta\upsilon_{\parallel}t$ on movement of an electron is disregarded in the after discussion).

Accordingly, a deflection angle $\chi_{\mathrm{many}}$ after the flight is

$$\chi_{\mathrm{many}(A_1\to A_3)}\simeq\frac{\Delta\upsilon_{\perp}t}{\bar{\upsilon}}=33.3\times10^{-7}\,\mathrm{radian}\tag{11}$$

2) The case of the e-$D^+$ collisions:

We denote deflection-angles of an electron for two impact parameters ( $\overline{OA_2}=0.4d$ , $\overline{OB_2}=0.1d$ ) by $\chi_{t1}$ , $\chi_{t2}$ , respectively.

a) $\overline{OA_2}=0.4d$ m . Since $p$ and $l$ in (A3) of **Appendix** are $0.4d$, about $0.33d$, respectively, we have

$$\tan\frac{\chi_{t1}}{2}=\frac{p_{\perp}}{0.4d}\cdot\frac{0.33d}{\left[\left(0.33d\right)^2+\left(0.4d\right)^2\right]^{1/2}}\quad\therefore\chi_{t1}\simeq5.64\times10^{-7}\,\mathrm{radian}\tag{12}$$

b) $\overline{OB_2}=0.1d$ m . Since $l\simeq0.5d$ , $\chi_{t2}\simeq36\times10^{-7}\,\mathrm{radian}$ . (13)

Now, we aim an electron (called Test electron) which starts at time $t=0$ from some point of a real plasma space. A scope of probable positions where Test electron is to exist at time $t$ expands from a dot to a tiny sphere (being supposed to be a round sphere and called $P$-sphere) due to the dispersion in a velocity space by the many-body collisions. Based on the dispersion given in (9), calculating a radius $P_{48d}$ of $P$-sphere after it has flied, for instance, the length $48d$, we have

$$P_{48d}=\int_0^{\frac{48d}{\bar{\upsilon}}}\Delta\upsilon_{\perp}t\mathrm{d}t=0.91\times10^{-10}\,\mathrm{m}\tag{14}$$

Since $d \gg P_{48d}$, $P$-sphere can be regarded to be a tiny particle with minus electric charge and an expanding volume. We analyze this orbit of the length $48d$ as follows:

1) The orbit of $P$-sphere consists of paths (called paths-in) which pass insides of $C$-spheres and paths (called paths-out) which do not pass the insides of $C$-spheres.

2) In paths-out, the dispersion makes a volume of $P$-sphere expand but does not make an advance-direction of $P$-sphere change.

3) In paths-in, the attraction by a deuteron at the center of each $C$-sphere gives proper, strong influence upon $P$-sphere. Because of this influence, "$P$-sphere suffers a small change of the advance-direction". However, unless $P$-sphere approaches a deuteron with too small impact parameters, the magnitude of the direction-changes are very small, as seen in the values of $\chi_{t1}$, $\chi_{t2}$ of (12), (13) and $\chi$ of (16). Also, since the direction-changes are done in disorder, we presume that $P$-sphere will advance straight macroscopically, although it is accompanied by small meanders.

4) As mentioned above, we have introduced a new element that the orbit of $P$-sphere is classified into straight parts in paths-out and the meandering parts in paths-in. The dynamical frictional coefficient decreases the speed of $P$-sphere and the dispersion coefficient makes the volume of $P$-sphere expand, but the above two coefficients do not make the advance-direction change. However, we consider that, when $P$-sphere (a tiny particle) goes deep a little into the inside of $C$-sphere, the orbit of $P$-sphere ought to suffer some fluctuation (or meander). The orbital meander in a real plasma space gives mainly swinging-motions to the velocity-point corresponding to the central point of $P$-sphere, besides the small movement by the dynamical frictional force. However, as mentioned in the above (3), small disorderly swinging-motions in the velocity-space does not obstruct that $P$-sphere advances straight macroscopically.

5) We estimate a mean length ($=\lambda_{\text{out}}$) of paths-out. If $C$-sphere is a solid sphere, $\lambda_{\text{out}}$ is given by $1/\left(n_{\text{p}}\pi d^2/4\right) = 4d/\pi = 1.27d$. But since plural $C$-spheres can hold the same space in common and furthermore since projections of $C$-spheres which are seen from $P$-sphere will overlap because of the big volume of $C$-sphere, we assume roughly that $\lambda_{\text{out}} \simeq 2.5d$.

Let us consider the case where $P$-sphere continues to fly over the length $48d$ and has come around point $O_1$ shown in **Figure 2**. This point is inside of $P$-sphere and Test electron is at this point. **Figure 2** shows an imaginary sight that the volume of a new probable positions-sphere of Test electron starting from point $O_1$ gradually expands. The new probable positions-sphere arrives at point $O_2$ on the surface of a $C$-sphere after having flied the length $\lambda_{\text{out}}$ without suffering meander and is about to make a head-on collision with a deuteron nucleus being at point $O_3$. The central point of the new probable positions-sphere does not suffer any meander in the head-on collision path from $O_2$ to $O_3$. Calculating a radius ($=p_{\text{up}}$) of the new probable positions-sphere near point $O_3$, we have

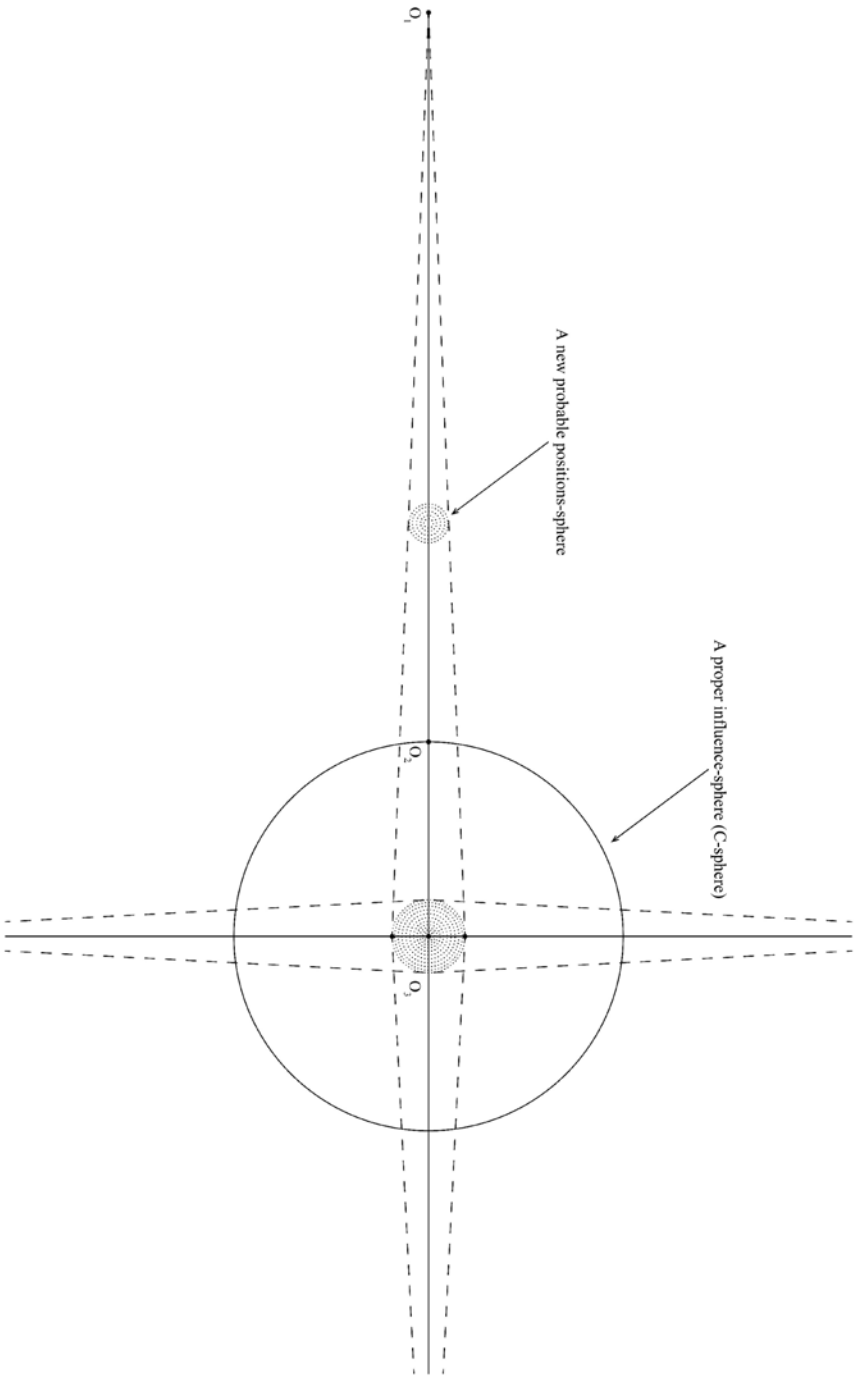


**Figure 2.** Expansion of a new probable positions-sphere of an electron by the dispersion. The central point of a new probable positions-sphere starts from point $O_1$ and makes a head-on collision with a deuteron nucleus being at point $O_3$. $\overline{O_1O_2} = 2.5d$ and $\overline{O_2O_3} = 0.5d$.

$$p_{\text{up}} = \int_0^{\frac{2.5d+0.5d}{\bar{\upsilon}}} \Delta\upsilon_\perp \text{d}t = \frac{2}{3}\times 1.71\times 10^{10}\left(\frac{3d}{\bar{\upsilon}}\right)^{3/2} = 1.43\times 10^{-12} = 81 p_\perp m \quad (15)$$

The above $p_{\text{up}}$ is the function of $\left(\overline{O_1O_3}\right)^{3/2}$. Considering that most of lengths

of paths-out is in the range between $d$ and $4d$ and calculating $p_{up}$ in two cases where $\overline{O_1O_3} = d + 0.5d$ and $\overline{O_1O_3} = 4d + 0.5d$, we have

$$\begin{cases} p_{up} = 81 p_{\perp} \times 0.35 & \text{for } \overline{O_1O_3} = 3d \times 0.5 \\ p_{up} = 81 p_{\perp} \times 1.84 & \text{for } \overline{O_1O_3} = 3d \times 1.5 \end{cases}$$

Though a mean length of paths-out depends also on a radius of $C$-sphere, now, we set an upper limit of an impact parameter for the e-$D^+$ two-body collisions to (15). A deflection-angle $\chi$ corresponding to $p_{up}$ of (15) is, from $\tan \chi/2 \simeq p_{\perp}/p_{up}$,

$$\chi = 1.4 \text{ degree} \tag{16}$$

Since a sphere with the radius $p_{up}$ is little tiny, we assume that $\nu^{ep}$ in (4) is $n_p \pi p_{up}^2 \bar{\upsilon}$. Then,

$$\nu^{ep} = 7.65 \times 10^5 \text{ sec}^{-1}, \quad 1 - \zeta = 4 \left( \frac{p_{\perp}}{p_{up}} \right)^2 \ln \left( \frac{p_{up}}{p_{\perp}} \right) = 2.7 \times 10^{-3}$$

$$\zeta = 0.9973, \quad \nu^{ep} (1 - \zeta) = 0.21 \times 10^4 \text{ sec}^{-1} \tag{17}$$

$(\nu_D)^{-1}$ is the characteristic time to change plasma conditions through the many-body collisions. On the other hand, since $(\nu^{ep})^{-1} = (\nu_D)^{-1}/77$, this time $(\nu^{ep})^{-1}$ is too short for the dispersion to play an important role.

Now, asking for the drift velocity u (the steady-state solution), we have the following results:

1) From (4);

$$\mathrm{u} = \mathrm{u}_{many} = \frac{qE}{m_e} \frac{1}{\nu_D} \simeq 1.76 \times 10^7 E \text{ m/sec} \tag{18}$$

If the influence of the electron-electron scattering [2] is taken into consideration as the frictional force,

$$\mathrm{u} = \mathrm{u}_{many} \simeq 1.76 \times 10^7 \times 0.58 E = 10^7 E \text{ m/sec} \tag{19}$$

2) From (7);

$$\mathrm{u} = \mathrm{u}_{two} = \frac{qE}{m_e} \frac{1 - \kappa}{\nu^{ep}(1 - \zeta) + \kappa \nu^{ep} \zeta} = 4.57 \times 10^5 E = \frac{\mathrm{u}_{many}}{38.5} \text{ m/sec} \tag{20}$$

The quantity $-m_e \nu^{ep} (1 - \zeta) \mathrm{u}(t)$ of (7) is a part of the dynamical frictional force, as already mentioned. Then, if $\nu^{ep}(1 - \zeta)$ of (20) is replaced with $\nu_D$, $\mathrm{u}_{two}$ becomes $4.4 \times 10^5 E$ m/sec. The dynamical frictional force may be too weak to suppress "the runaway instability". If the truncation frictional force works, the fear of outbreak of the runaway instability is somewhat lightened.

## 4. Conclusions

It is noted that the extension of positions of an electron in a real plasma space due to both the dispersion and the dynamical friction defined in a velocity-space is very small. The extension-region has been roughly regarded as a tiny sphere whose volume expands with time. The tiny sphere advances straight statistically

in no external force fields. But we have introduced the new element that the tiny sphere suffers fluctuation (or meander) near each deuteron and have imagined that tiny spheres starting from various positions make head-on collisions with a deuteron nucleus straight without suffering meander. Finally we put in order the consideration on the estimation of an effective radius of the Coulomb force of a deuteron:

1) There ought to be the mean length of paths by which a tiny sphere advances straight without suffering meander.

2) We set a Sphere with the radius of the mean length plus a half of the mean distance between deuterons. A deuteron is at the center of Sphere.

3) From every point on the surface of Sphere, each electron starts toward the deuteron at the same time.

4) Those electrons will form a cloud around the deuteron nucleus. We consider the cloud to be an effective region (for the two-body interaction) of the Coulomb force of a deuteron.

## Conflicts of Interest

The author declares no conflicts of interest regarding the publication of this paper.

## References

[1] Chandrasekhar, S. (1943) *Astrophysical Journal*, **97**, 255. https://doi.org/10.1086/144517

[2] Spitzer, L. and Härm, A. (1953) *Physical Review Journals Archive*, **89**, 997. https://doi.org/10.1103/PhysRev.89.977

[3] Dreicer, H. (1959) *Physical Review Journals Archive*, **115**, 238. https://doi.org/10.1103/PhysRev.115.238

[4] Linhart, J.G. (1961) Plasma Physics. 2nd Edition, North-Holland Publishing Co., Netherlands.

[5] Moffat, W.C. (1961) Thermodynamic and Electrical Properties of Dissociated Combustion Gases. MIT Magneto Gas Dynamic Lab. Reptort 5.

[6] Baral, K.C. and Mohanty, J.N. (1997) *Physics of Plasmas*, **4**, 2010. https://doi.org/10.1063/1.872396

[7] Nagata, M. (2011) *The European Physical Journal D*, **65**, 429-440. https://doi.org/10.1140/epjd/e2011-10464-2

[8] Nagata, M. (1999) *Journal of the Physical Society of Japan*, **68**, 2281-2286. https://doi.org/10.1143/JPSJ.68.2281

[9] Conwell, E. and Weisskoph, V. E. (1946) *Physical Review Journals Archive*, **69**, 258A.

[10] Landau, L. and Lifshitz, E. (1987) The Classical Theory of Fields. Sec. **3**8, 4th Revised English Edition, Butterworth & Heinemann, Amsterdam, 99.

## Appendix

We ask for a relation between a deflection angle $\chi$ and an impact parameter $p$ in the case where a relativistic electron with the velocity $\bar{\upsilon}$ is deflected by an electric field of a deuteron $D^+$. The deuteron $D^+$ is at the origin $x = y = 0$. An electron with the velocity $\bar{\upsilon}$ and the mass $m_{er}\left(=m_e\Big/\left(1-\bar{\upsilon}^2/c^2\right)^{1/2}\equiv m_e/\gamma_r\right)$ approaches the ion $D^+$ along the $x$-axis. A position $\mathbf{r}(t)$ of the electron at time $t$ is

$$\mathbf{r}(t) = \hat{x}\bar{\upsilon}t + \hat{y}p \quad \left(-\frac{l}{\bar{\upsilon}} < t \le 0\right) \tag{A1}$$

Variations of the velocity and the mass changing with time during the interaction with $D^+$ are disregarded. An electric field which the electron flying with the constant velocity $\bar{\upsilon}$ feels is given by [10]

$$\mathbf{E}(t'') = \frac{q\gamma_r^2\mathbf{r}(t)}{4\pi\varepsilon_0\left[\left(\bar{\upsilon}t\right)^2+\gamma_r^2p^2\right]^{3/2}} \equiv \hat{x}E_{\parallel}'' + \hat{y}E_{\perp}'' \tag{A2}$$

Then, a deflection angle $\chi$ of the electron by the deuteron $D^+$ is

$$\tan\frac{\chi}{2} \simeq \frac{\left|\int_{-\frac{l}{\bar{\upsilon}}}^{0}\frac{-qE_{\perp}''\gamma_r}{m_e}\mathrm{d}t\right|}{\bar{\upsilon}} = \frac{p_{\perp}\gamma_r}{p}\frac{l}{\left(l^2+\gamma_r^2p^2\right)^{1/2}} \quad (0<\chi\ll 1) \tag{A3}$$

where,

$$p_{\perp} = \frac{q^2}{4\pi\varepsilon_0 m_e\bar{\upsilon}^2}.$$

Journal of Modern Physics, 2020, 11, 1761-1778
https://www.scirp.org/journal/jmp
ISSN Online: 2153-120X
ISSN Print: 2153-1196

# Gravitational Space-Time Quantization for Charged Wormholes and the Diophantine Uncertainty Relation

**Yu. A. Khlestkov, A. Yu. Khlestkov, P. Yu. Lukashin, M. Yu. Lukashin, N. Yu. Lukashina**

National Research Nuclear University (MEPhI), Moscow, Russia
Email: khlestkov@yandex.ru

**How to cite this paper:** Khlestkov, Yu.A., Khlestkov, A.Yu., Lukashin, P.Yu., Lukashin, M.Yu. and Lukashina, N.Yu. (2020) Gravitational Space-Time Quantization for Charged Wormholes and the Diophantine Uncertainty Relation. *Journal of Modern Physics*, **11**, 1761-1778.
https://doi.org/10.4236/jmp.2020.1111109

**Received:** September 20, 2020
**Accepted:** November 6, 2020
**Published:** November 9, 2020



## Abstract

This research work proceeds from the assumption, which was still considered by Einstein, that the quantization of gravity does not require additional external procedures: quantum phenomena can be a consequence of the properties of the universal gravitational interaction, which maps any physical field upon the space-time geometry. Therefore, an attempt is made in this research work to reduce the quantization of physical fields in GRT to the space-time quantization. Three reasons for quantum phenomena are considered: Partition of space-time into a set of unconnected Novikov's R- and T-domains impenetrable for light paths; the set is generated by the invariance of Einstein's equations with respect to dual mappings; The existence of electric charge quanta of wormholes, which geometrically describe elementary particles in GRT. This gives rise to a discrete spectrum of their physical and geometric parameters governed by Diophantine equations. It is shown that the fundamental constants (electric charge, rest masses of an electron and a proton) are interconnected arithmetically; The existence of the so-called Diophantine catastrophe, when fluctuations in the values of physical constants tending to zero lead to fluctuations in the number of electric charges and the number of nucleons at the wormhole throats, which tend to infinity, so that the product of the increments of these numbers by the increment of physical constants forms a relation equivalent to the uncertainty relation in quantum mechanics. This suggests that space-time cannot but fluctuate, and, moreover, its fluctuations are bounded from below, so that all processes become chaotic, and the observables become averaged over this chaos.

## Keywords

Quantization of Gravitation, Novikov's R- and T-Domains, Diophantine Uncertainty Relations, Discretization of Space-Time

## 1. Statement of the Problem

A natural approach to the problem of quantizing gravity, to which Einstein (the creator of the general theory of relativity) inclined, is considered: quantum phenomena should be a consequence of the gravitational field properties. The logic is as follows: GRT (general theory of relativity) is a geometrizing model. Any physical field must be mapped onto the geometry of a curved space-time, the curvature of which, for its part, is equivalent to a universal gravitational field [1][1]. It is enough to solve the Einstein equations linking physics with geometry, together with Maxwell's equations for an electromagnetic field, to express all physical quantities characterizing, say, electromagnetic interaction, through the metric of pseudo-Riemannian space.

Moreover, the arbitrary functions of the radial coordinate arising in this case in the Cauchy problem for the initial conditions (the first integrals) describe the geometric images of the sources of the electromagnetic field, *i.e.* electric charges [2], which were not present in the formulation of the problem and which, therefore, are formed by the gravitational field itself. That is, the sources of the field are formed by space-time itself. As it turned out, they have a non-trivial topology of pulsating wormholes with non-closing static throats [2]. We got the opportunity to investigate the internal structure of elementary particles by eliminating in this way the main singularity in the flat space of the special theory of relativity, *i.e.* the Coulomb divergence of a point charge field.

That is, GRT can really reduce the quantization of a physical field to the quantization of the multidimensional pseudo-Riemannian space-time. Quantization of space-time means the existence of two phenomena: discretization of 4-dimensional pseudo-Riemannian space, *i.e.* dividing it into a set of unrelated domains, and the impossibility of accurately determining its geometric characteristics, which acquire a fluctuating character and, by analogy with quantum mechanics, are linked by the gravitational uncertainty relation. This is what we should get.

The results of the work are presented in three sections and in **Appendix 1**, which provides a proof for the complete geometrization of an electromagnetic spherically symmetric field consisting of a free radial electric field and dust-like neutral matter in a synchronous accompanying frame of reference. According to the exact particular solution of the Einstein and Maxwell equations [2], it is a periodic in space and time chain of pulsating wormholes with static throats (holes, necks) of extreme dimensions geometrically, which are geometric images of electric charges formed by the electromagnetic (and hence gravitational) field in curved space-time (**Figure 1**).

The second section describes a fundamental property of centrally symmetric Einstein's equations, *i.e.* their invariance in relation to dual mappings the mutual

[1]Recall that this relativistic principle of equivalence is well known in Newtonian nonrelativistic physics and is very accurately carried out experimentally in the form of equality of the inertial mass of a body (an analogue of matter) and its gravitational mass (an analogue of a gravitational field) in Newton's second law, as a result of which all bodies in a vacuum being in a gravitation field falls with the same acceleration.

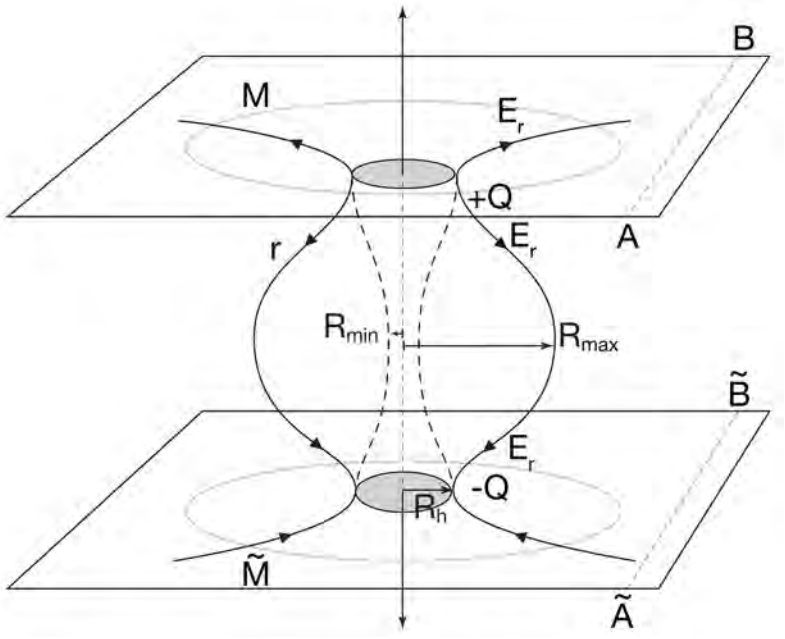


**Figure 1.** One period of a wormhole with two electric charges $\pm Q$—necks (throats) of radius $R_h$ that exit into two parallel static Reissner-Nordstrom vacuum worlds, in the state of maximum expansion ($R_{max}$) and in the state of maximum compression ($R_{min}$). The arrows show the direction of the radial electric field.

replacement of the time coordinate with the spatial radial coordinate. This leads to the existence of one more exact particular solution of the Einstein-Maxwell equations, dual conjugated to the given one, and to the emergence of a discrete set of so-called Novikov's R- and T-domains [3], which are closed and unconnected with each other, and which boundaries "B" are impenetrable for light paths (being isotropic geodesic lines) [4]. This is the first effect of natural "self-quantization" of the gravitational field.

As it will be illustrated in this section, this leads to the fact that the flux of photons continuously emitted by the source will come to an observer located at another point in space in discrete portions, *i.e.* quanta. This is the second effect of "self-quantization" of the curved space-time.

It was shown in [2] that the gravitational-electromagnetic interaction is sufficient to construct the simplest classical model uniting an electron, proton and neutron, with eliminating the main contradictory prohibitions, and to calculate their radii of curvature at unclosed throats of wormholes that go out into two parallel vacuum spaces. The radii of the proton and neutron are in good agreement with their experimental values (for a proton, with an accuracy of 0.04%). An electron, which in the flat space regarding to the special theory of relativity (SRT) would have to be single-point, *i.e.* structureless, also turns out to be a structural object in this model, having a finite radius of curvature of the throat much larger than that of a proton. Note that the very fact that the proton turned out to be not a single-point structured object is direct experimental evidence that the space-time in the microworld is also curved. That is, the gravitational inte-

raction is universal.

In the third section of this research work, it will be shown that, according to this exact solution of the Einstein's and Maxwell's equations, the relationship between the physical and geometric parameters of particles at the throat is described by a Diophantine equation (an integer variable equation with rational coefficients). This requirement of the rationality of the coefficients inevitably leads to the fact that an arithmetic relationship arises between the rest mass, electric charge and the radius of the Gaussian curvature of the throat, which has the discrete spectra nature. That is, the physical characteristics (masses and charges) are quantized.

The phenomenon of a "Diophantine catastrophe" is considered in the fourth section of this work. This phenomenon takes place when large fluctuations of the number of electric charges and the number of nucleons at the throats of wormholes arise under the action of small random fluctuations of physical constants (these always take place, as it can be assumed). Those fluctuations are related to each other with the Diophantine uncertainty relation: the product of an increment of the rational Diophantine equation coefficient, which depends on the increment of physical constants (rest masses of electrons, protons, and an electric charge), by the increment in the number of electric charges and the number of nucleons at the throat is not less than a certain value, that is, it is limited from below. This means that fluctuations of such quantities cannot but exist; they will be maintained by the gravitating system itself, since as the increments of physical constants tend to zero, the increment in the number of charges and the number of nucleons at the throat would tend to infinity, which is impossible.

## 2. Dual Spaces. Discretization of Novikov's R- and T-Domains

Einstein's equations in GRT:

$$G_{\mu\nu} = \kappa T_{\mu\nu}, \ \kappa = \frac{8\pi k}{c^4}, \ \mu,\nu = \{0,1,2,3\} \tag{1}$$

in 4-dimensional pseudo-Riemannian space in the coordinate system

$$x^{\mu} = \left\{x^0, x^i = x^1, x^2, x^3\right\} \tag{2}$$

in a set of arbitrary metrics that transform into each other,

$$x^{\tilde{\mu}} = x^{\tilde{\mu}}\left(x^{\alpha}\right), \tag{3}$$

with a non-degenerate Jacobian

$$\tilde{J} = \left|x^{\mu}_{,\alpha}\right|, \tag{4}$$

in a class of metrics

$$\mathrm{d}s^2 = g_{\mu\nu}\mathrm{d}x^{\mu}\mathrm{d}x^{\nu}, \tag{5}$$

with a Lorentzian signature

$$\text{signature} \quad g_{\mu\nu} = +---, \tag{6}$$

implemented by physical bodies [1]:

$$\begin{aligned} &g_{00} > 0, \\ &\begin{vmatrix} g_{00} & g_{01} \\ g_{10} & g_{11} \end{vmatrix} < 0, \\ &\det\begin{bmatrix} g_{00} & \cdots & g_{02} \\ \vdots & \ddots & \vdots \\ g_{20} & \cdots & g_{22} \end{bmatrix} > 0, \quad g = \det\left(g_{\mu\nu}\right) < 0, \end{aligned} \tag{7}$$

within the framework of centrally symmetric spaces with orthogonalized metric

$$\mathrm{d}s^2 = e^{\nu(\tau,r)}\mathrm{d}\tau^2 - e^{\lambda(\tau,r)}\mathrm{d}r^2 - R^2(\tau,r)\left(\mathrm{d}\theta^2 + \sin^2\theta\mathrm{d}\varphi^2\right), \tag{8}$$

which transform into themselves at the following dual mapping:

$$\begin{aligned} &x^0 \leftrightarrow x^1, \quad (\tau \leftrightarrow r), \\ &g_{00} \leftrightarrow g_{11}, \quad \left(e^{\nu} \leftrightarrow -e^{\lambda}\right), \\ &G_0^0 \leftrightarrow G_1^1 \quad \left(\nu^{\cdot} \leftrightarrow \lambda', \lambda^{\cdot} \leftrightarrow \nu'\right), \\ &\left(\cdot = \frac{\partial}{\partial\tau}, {}' = \frac{\partial}{\partial r}\right). \end{aligned} \tag{9}$$

with this mapping, the signature is preserved; the time coordinate $\tau\left(x^0 = \tau, g_{00} = g_{\tau\tau} > 0\right)$, and the radial coordinate $r\left(x^1 = r, g_{11} = g_{rr} < 0\right)$ change places and the whole 4-dimensional space-time is divided into Novikov's R- domains:

$$x^0 = \tau,\ x^1 = r,\ g_{00} = g_{\tau\tau} > 0,\ g_{11} = g_{rr} < 0 \tag{10}$$

and Novikov's T-domains [4]:

$$x^0 = r,\ x^1 = \tau,\ g_{00} = g_{rr} < 0,\ g_{11} = g_{\tau\tau} > 0 \tag{11}$$

which are new solutions of GRT equations being dually conjugated to a given one supplementing any exact particular solution of Equation (1) to a complete one that already describes the entire space-time. The latter means that the entire space-time, with the exception of a finite number of singular points and hypersurfaces "B" (boundary), on which the Jacobian (4) and the second-order determinant (7) degenerate:

$$\text{"B"}: x^{\tilde{0}}_{,0}x^{\tilde{1}}_{,1} - x^{\tilde{0}}_{,1}x^{\tilde{1}}_{,0} = 0 \text{ or } \infty,\ g_{\tilde{0}\tilde{0}}g_{\tilde{1}\tilde{1}} - g^2_{\tilde{0}\tilde{1}} = 0 \text{ or } \infty, \tag{12}$$

can be completely covered by a family of geodesic lines [5].

Thus, using the invariance of the GRT equations with respect to dual maps, we have a way to generate new exact partial solutions of the Einstein equations that describe space-time more fully.

Let's give a simple illustrative example. Let's take the well-known Schwarzschild solution for a gravitational field of a point mass $m$ [1]:

$$\mathrm{d}s^2 = \left(1 - \frac{r_g}{r}\right)\mathrm{d}\tau^2 - \frac{\mathrm{d}r^2}{\left(1 - \frac{r_g}{r}\right)} - r^2\left(\mathrm{d}\theta^2 + \sin^2\theta\mathrm{d}\varphi^2\right), \tag{13}$$

where $r_g$ is a gravitational radius. It has a singularity $r=0$ and an event horizon $r=r_g$ [1]. This is Novikov's R-domain. It describes the space of a black hole in the $r>r_g$ region (**Figure 2**, right side).

We now construct the dual-conjugate (13) Novikov's T-domain by the mapping $\tau \leftrightarrow r$, $e^{\nu} \leftrightarrow -e^{\lambda}$:

$$\mathrm{d}s^2 = \frac{\mathrm{d}\tau^2}{\left(\frac{r_g}{\tau}-1\right)} - \left(\frac{r_g}{\tau}-1\right)\mathrm{d}r^2 - \tau^2\left(\mathrm{d}\theta^2+\sin^2\theta\mathrm{d}\varphi^2\right). \tag{14}$$

One can make sure quite simply by substituting solution (14) into Einstein's Equation (1) [1] that we have obtained a new solution missing for the domain $r<r_g$, in which the radial coordinate $r$ has turned into a time coordinate $\tau$, and time $\tau$ has become a radial coordinate $r$ (**Figure 2**, left side).

Part of a boundary hypersurface "B" is a surface $r=r_g$ in R-domain, it is also $\tau=r_g$ in T-domain (**Figure 2**, left side).

Since the time and the radial coordinate that create the "B" boundary are different characteristics, then R- and T-domains are not related in any way. Therefore, no signal can cross the "B" boundary from the R domain to the T domain and back.

We construct a family of light paths for this example,

$$\mathrm{d}s^2 = 0. \tag{15}$$

Substituting (15) in (13) and (14), we obtain the expressions for the coordinate velocity of light $\beta_l^{\text{"R"}}$ and $\beta_l^{\text{"T"}}$ which is tangential for isotropic geodesic lines:

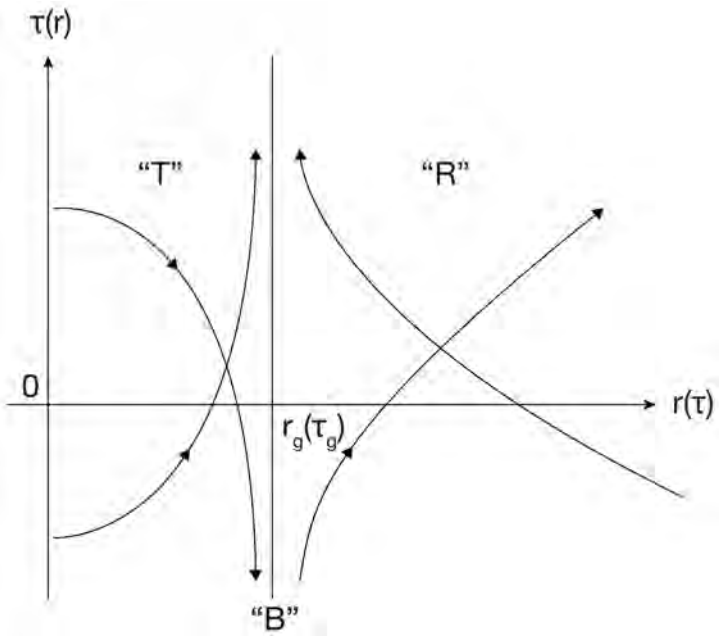


**Figure 2.** Parts of "R" and "T" Novikov regions in the Schwarzschild point mass field and light trajectories. In parentheses are the coordinate axes in the "T" area. "B" is the boundary between these regions—the event horizon, impenetrable for light trajectories. In the "T" region, the time coordinate $\tau$ and the radial coordinate $r$ are reversed.

$$\beta_l^{\text{“R”}} = \pm\left|1-\frac{r_g}{r}\right|,$$
$$\beta_l^{\text{“T”}} = \pm\frac{1}{\left|1-\frac{r_g}{\tau}\right|}. \tag{16}$$

It is easy to construct qualitatively the envelopes of the families themselves (**Figure 2**) along these tangents to the light paths. Two paths are constructed for each domain in **Figure 2**, one of which begins (ends) at the boundary “B” in asymptotics, the other ends (begins) at the boundary “B” in asymptotics.

What qualitative conclusions follow from this picture?

- Space-time is divided in a gravitational field into a discrete set of unconnected R-T-domains.
- R-domains are limited in space from below, and T-domains are limited in time from above.
- Time and radial coordinate are swapped at the boundary “B” between R- and T-domains; light paths do not cross the boundary “B”.
- Since T-domain is limited in time from above, then in the case of time-periodic solutions it will periodically disappear for observers in the R-domains. Consequently, the propagation of signals in the case of closed or semi-closed solutions (such as Friedman or Tolman solutions) will be discontinuous, that is, will occur in a quantum manner.

Attempts to accurately construct a family of geodesic paths for the solution in [2] describing the internal structure of elementary charged particles (electron, proton, neutron) in the microworld, as well as megamaximons in astrophysics in the megaworld [4] [6] [7] [8] [9] have not yet been successful, both analytically and numerically due to mathematical difficulties. Therefore, we have depicted in **Figure 3** only a qualitative picture of this family for semi-closed solutions, which clearly illustrates this phenomenon of curved space-time discretization.

If some observer resting in the “R”-domain continuously emits light rays, then observers in the “T”-domains will not see these signals at all, and observers at other points of the “R”-domains will see intermittent flux of light quanta. That is, the quantization of light turns out to be a property of curved space-time.

We also note that the integral gravitational action $S_g$ for each of these discrete domains of space-time is finite [1]:

$$S_g = -\frac{c^3}{16\pi k}\int \mathcal{R}\sqrt{-g}\,\mathrm{d}\Omega = \frac{e^2}{c}\psi\,, \tag{17}$$

where $\mathcal{R}$ is a trace of the Ricci tensor, $\frac{e^2}{c}$ is the gravitational “quantum of action”, $\mathrm{d}\Omega$ is an element of 4-dimensional volume, $\psi$ is a form factor depending on the geometry of R and T-domains. Note that if $\psi = 1/\alpha$, where $\alpha$ is the fine structure constant, then

$$S_g = \hbar\,, \tag{18}$$

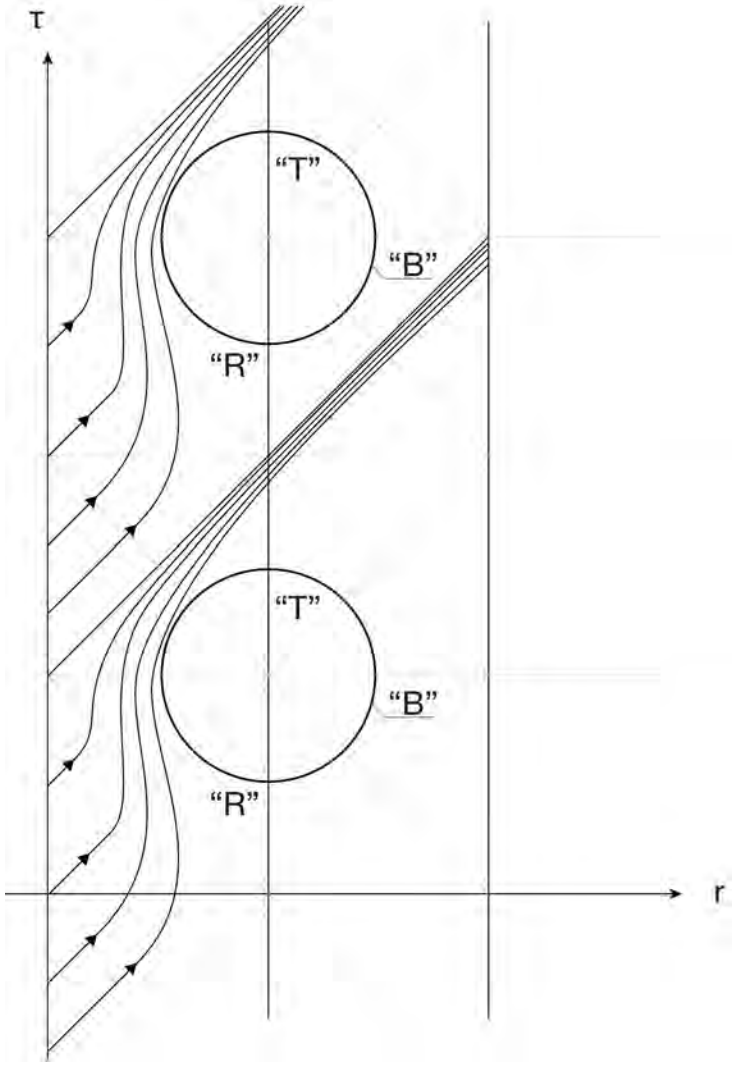


**Figure 3.** Quantization of a continuous stream of photons by "R" and "T" Novikov regions. "B" is the border between them, impenetrable for light trajectories.

where $\hbar$ is Planck's constant. Thus, the fundamental constant of quantum mechanics can also have a gravitational origin.

The results obtained in GRT allow us to take a fresh look at the event cone known in SRT (**Figure 4(a)**). This event cone consisting of two timelike domains of the past and future with a positive square of the interval $ds^2 > 0$, and of two spatially similar domains with a negative square of the interval $ds^2 < 0$ being unattainably "absolutely remote", with superluminal paths, can be interpreted differently. It represents the degeneration of "R"- and "T"-domains of curved space-time in the limiting case of disappearance of matter, therefore identical equality to zero of the Riemann-Christoffel curvature tensor according to the above-mentioned general relativistic principle of equivalence. This means flattening of this space. In this case, the entire space-time is divided into four time-like domains (**Figure 4(b)**): two "R"- and two "T"-ones, all with a positive square of the interval $ds^2 > 0$, which turns to zero at the boundaries of these

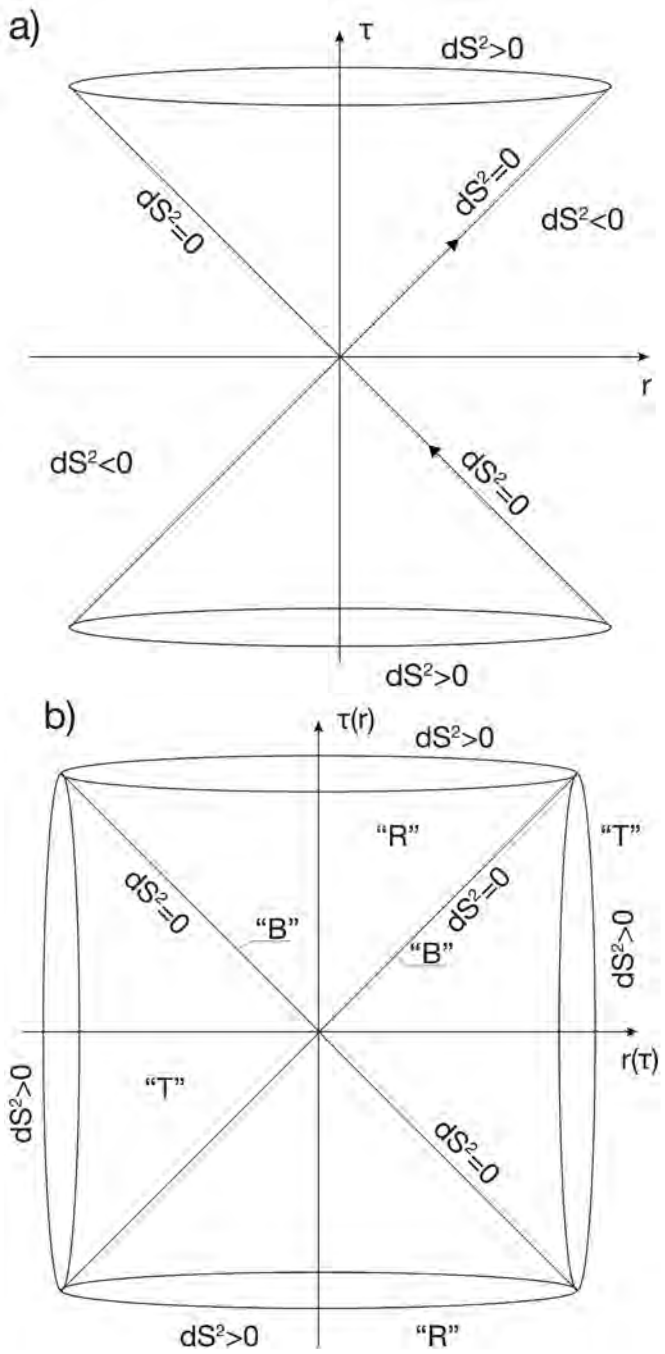


**Figure 4.** Degeneration of the light cone—"R" and "T"—Novikov regions in an empty flat space SRT. In parentheses are the coordinate axes in the "T" regions: (a) the usual interpretation of SRT, (b) possible representation of GRT.

domains, where the time and space coordinates are swapped in the neighbouring domains, and the metric remains Lorentzian, and the boundary "B" remained impassable. The presence of such a passage to the limit confirms that the chosen interpretation of the appearance of quantum properties in a curved space-time by means of its discretization by "R"- and "T"-dually conjugated domains is correct.

## 3. Discrete Diophantine Spectra of Wormhole Parameters and Relationship of Fundamental Constants

Consider the simplest centrally symmetric system consisting of a dusty substance (without pressure and temperature) and a free radial electric field (without sources) in an accompanying frame of reference. When integrating the Einstein and Maxwell equations in the Cauchy problem, three first integrals arise, being three arbitrary functions of the radial coordinate $r$, the setting of which is equivalent to setting the initial conditions for the dust energy density $\varepsilon_s$, the radius of the 2-dimensional Gaussian curvature $R$ and the rate of its change $R^{\cdot}$: the electric charge $Q$, the total energy of the gravitational field $\varepsilon_g$ and the function $f$ characterizing the curvature of space inside the wormhole and at its throats, through which it can be extended into two parallel external Reissner-Nordström vacuum spaces [5].

The GRT equations can be integrated to the end in three cases when one of the first integrals becomes a constant [2] [10]. We will consider the simplest solution, in which the electric charge becomes a constant:

$$Q = const = eN_Q, \tag{19}$$

where $e$ is a fundamental charge, it is an irrational number for our world and $N_Q$ is an integer number of such charges.

If we take into account that we initially considered a free electric field without sources, then the appearance of a new physical constant $\pm Q$ during integration means that space-time itself has formed a source of the electromagnetic field, *i.e.* an electric charge $\pm Q$ (for elementary particles $\pm e$) geometrically representing a pulsating wormhole [2]:

$$\begin{aligned} e^{\nu} &= 1, \\ e^{\lambda} &= \frac{R'^2}{f^2}, \\ R &= \frac{R_g}{2\left(1-f^2\right)}\left(1-\delta\sin\eta\right), \\ \tau &= \frac{R_g}{2\left(1-f^2\right)^{3/2}}\left(\eta-\delta\sin\eta-\pi\right), \\ \delta &= \sqrt{1-\frac{4R_c^2}{R_g^2}\left(1-f^2\right)}, \end{aligned} \tag{20}$$

with two static throats, the radius of the 2-dimensional Gaussian curvature $R_h$ of which is always equal to twice the classical (electromagnetic) radius:

$$R_f = \frac{Q^2}{2\varepsilon_g(r)} \tag{21}$$

At the throats under $r = 0, r = r_h$ [2]:

$$R_h = 2R_{fh} = \frac{R_{gh}}{2}\xi^2 = \xi R_c. \tag{22}$$

Here $R_g = \frac{\kappa\varepsilon_g}{4\pi}$ is a gravitational radius proportional to the total gravitational energy $\varepsilon_g(r)$,

$$R_c = \frac{Q\sqrt{k}}{c^2} \tag{23}$$

is the critical radius proportional to the electric charge $Q$ of the particle, which is always paired with its antiparticle, the throat of which can be extended into a parallel vacuum space;

$$\xi = \frac{Q}{M_{gh}\sqrt{k}} \geq 1 \tag{24}$$

is the charge to the mass ratio of the inner world, $M_g = \varepsilon_g / c^2$, taken at the throat.

Recall that there are two fundamental constants in the GRT: $k$ is an Einstein's constant, which relates physics with geometry (that is, makes them indistinguishable), and $c$ is the speed of light, which locally limits the speed of propagation of any signals. The fundamental electric charge $Q$ appears only when integrating the equations of GRT. Its quantum $e$ can be found purely geometrically by measuring the space-time curvature values at any of its points, both inside an elementary particle, and in the Reissner-Nordström vacuum space glued to it through the throats:

$$e = \frac{c^2}{\sqrt{k}} \mathcal{K}_{0r}^{(2)^{-1}} \left( \mathcal{K}_0^{(1)} - \mathcal{K}^{(4)} \right)^{1/2}, \tag{25}$$

where $\mathcal{K}_{0r}^{(2)} = \frac{1}{R^2(\tau, r)}$ is the intrinsic Gaussian curvature of 2-spheres $r = const$.

$\mathcal{K}_0^{(4)} = G_0^0$ is the curvature of 4-dimenional areas orthogonal to the time coordinate $\tau$ and equal to the zero mixed component of the geometric Einstein tensor $G_\mu^\nu$.

$\mathcal{K}^{(4)} = G$ is the scalar (Gaussian) space-time curvature equal to the trace of the Einstein tensor.

Thus, we can say that $e$ is a geometric quantum of electric charge, *i.e.* a topological characteristic of a given particle. Along with it, we can introduce a quantum of mass, the critical mass $m_c$ that differs from the charge only by a constant:

$$m_c = \frac{e}{\sqrt{k}} \tag{26}$$

and the quantum of length, which is a critical radius $r_c$:

$$r_c = \frac{e\sqrt{k}}{c^2}, \tag{27}$$

where the classical (electromagnetic) and gravitational radius are compared in magnitude.

Taking into account (24), Equation (22) could be as follows with introducing the mass at the throat

$$M_h = m_p N_p + m_e N_e , \tag{28}$$

where $N_e$ is the number of electrons at the throat of the wormhole, taking into account that

$$N_e = N_p - N_Q , \tag{29}$$

can be rewritten in the form of a Diophantine equation:

$$N_p = \lambda N_Q , \tag{30}$$

where $N_p$ and $N_Q$ are integer variables; $\lambda$ is a rational coefficient equal to:

$$\lambda = \frac{m_e + m_c/\xi}{m_e + m_p} . \tag{31}$$

Despite the seeming simplicity of relations (30), (31), they contain a new meaning for us. The logic behind this decision is simple. Equation (30) has non-trivial solutions only if $\lambda \in \mathbb{Z}$, belongs to the set of rational numbers. Let us assume that the masses of an electron, a proton and the mass of the $m_c$ quantum are irrational. Let particle in (31) is a friedmon for simplicity, *i.e.* $\xi = 1$. Then, for there to be a solution to Equation (30), the sums of irrational numbers in the numerator and in the denominator must be rational. This is possible, but not for all $m_e, m_c, m_p$. The admissible values of these physical quantities will form a discrete spectrum:

$$\begin{aligned} m_e + m_c &\in \mathbb{Z}, \\ m_e + m_p &\in \mathbb{Z}. \end{aligned} \tag{32}$$

We will not solve arithmetic relations (31) and (32) here. We will make only a qualitative conclusion: first, the masses of the electron $m_e$, quanton $m_c$, and proton $m_p$ are related arithmetically, *i.e.* depend on each other. Second, they have discrete spectra of values, outside of which the conditions for the existence of a stationary throat are not satisfied. Therefore, the considered gravitational system (wormhole) will be nonequilibrium, which means that it will fluctuate. This statement obtained within the framework of this gravitational model obviously can be verified experimentally. That is, the nature of quantum fluctuations is non-fulfilment of arithmetic equilibrium conditions.

We present below the procedure for solution of the Diophantine equation (30). We represent the rational coefficient $\lambda$ as the sum of an integer $\Lambda$ and a proper fraction $\frac{a}{b}$, $|a| < b$, where $a, b \in \mathbb{Z}$, then, dividing the fraction by the greatest common divisor (GCD) $(a, b)$ (or the fraction $b = 10^n, n = 1, 2, \cdots$) in the decimal representation, we transform the fraction $\frac{a}{b}$ into an irreducible fraction $\frac{a_1}{b_1}$.

$$\lambda = \Lambda + \frac{a}{b} = \Lambda + \frac{a}{10^n} = \Lambda + \frac{a_1}{b_1} = \Lambda + \frac{a/(a,b)}{10^n/(a,10^n)}. \tag{33}$$

Diophantine Equation (30) has the following discrete spectrum of solutions:

$$\begin{aligned} N_Q &= b_1 i, \ \ i = 1,2,\cdots \\ N_p &= (\Lambda b_1 + a_1) i. \end{aligned} \tag{34}$$

Or, in more detail:

$$N_Q = \frac{10^n}{(a,10^n)} i, \ \ N_p = \left( \Lambda \frac{10^n}{(a,10^n)} + \frac{a}{(a,10^n)} \right) i. \tag{35}$$

Here is the simplest illustrative example of this arithmetic:

$$N_2 = 32.25 N_1 = \left(32 + \frac{25}{10^2}\right) N_1 = \left(32 + \frac{1}{4}\right) N_1,$$

$$a = 25, b = 10^2, (a,b) = 25, a_1 = 1, b_1 = 4, n = 2, \Lambda = 32,$$

$$N_1 = b_1 i = 4i = 4,8,12,\cdots$$

$$N_2 = (\Lambda b_1 + a_1) i = (32 \times 4 + 1) i = 129,258,387,\cdots$$

Using this example, let's see what happens to the equilibrium spectrum of integer solutions $N_1$, $N_2$ of this solution if we introduce a perturbation for a rational coefficient of the given equation $\lambda = 32.25$, say, with 1/1000. Let

$$\tilde{\lambda} = 32.251 : \Lambda = 32, a = 251, b = 10^3, (a,b) = 1, a_1 = 251, b_1 = 10^3,$$

$$\tilde{\lambda} = \lambda + \delta\lambda, \lambda = 32,25, \delta\lambda = 10^{-3},$$

$$\widetilde{N_1} = N_1 + \Delta N_1 = 10^3 i = 1000;2000;3000;\cdots$$

$$\widetilde{N_2} = N_2 + \Delta N_2 = \left(32 \times 10^3 + 251\right) i = 32251;64502;96753;\cdots,$$

$$\Delta N_1 = 996;1992;3988;\cdots,$$

$$\Delta N_2 = 32122;64254;96366;\cdots.$$

The result is obvious: With small perturbations of the physical constants included in the rational coefficient of the Diophantine equation, the spectra of the required number of charges $N_Q$ increase sharply in their magnitude, so that as the fluctuations of the constants tend to zero, the fluctuations of the required number of electric charges $N_Q$ and the number of nucleons $N_p$ tend to infinity: $\delta\lambda \to 0$, $\Delta N_{Q,p} \to \infty$. This is a Diophantine catastrophe. We will discuss it below.

The same qualitative disturbances will be expected for the spectrum of the necessary throat radii:

$$R_h = r_p \frac{N_Q}{\lambda\left(1 + m_e/m_p\right)}. \tag{36}$$

As a result, if there would be no such values of $m_e, m_p$, fluctuations of the values of $N_Q, N_p$ will not decay in principle.

## 4. Fluctuations of Fundamental Constants, Wormhole Parameters and Diophantine Uncertainty Relation

What is the cause of a Diophantine catastrophe? The fluctuations of physical constants (electric charge, rest masses of elementary particles) tending to zero cause an infinitely large required increment in the number of charges and the number of nucleons to ensure a stationary state of wormhole throats. Since such numbers are not found, the gravitational system begins to fluctuate.

The perturbed system is described by a perturbed Diophantine equation:

$$\widetilde{N_p} = \tilde{\lambda}\widetilde{N_Q}, \tag{37}$$

in which the perturbed rational coefficient can be represented as:

$$\tilde{\lambda} = \lambda + \delta\lambda, \tag{38}$$

and we write the fluctuation $\delta\lambda \ll \lambda$ itself in the form:

$$\delta\lambda = \frac{\alpha}{10^{m+n}},\ m = 1,2,\ \alpha = 1,2,3,\cdots \tag{39}$$

The unperturbed rational coefficient has the same form:

$$\lambda = \Lambda + \frac{a}{10^n} \tag{40}$$

Therefore, the perturbed coefficient is as follows:

$$\tilde{\lambda} = \Lambda + \frac{a}{10^n} + \frac{\alpha}{10^{n+m}}. \tag{41}$$

Hence, the solution for an integer $\widetilde{N_Q}$ with perturbation $\tilde{\lambda}$ looks like this:

$$\widetilde{N_Q} = c10^{n+m},\ c = 1,2,3,\cdots \tag{42}$$

and for the integer value $\widetilde{N_p}$:

$$\widetilde{N_p} = \left(\Lambda + \frac{a}{10^n} + \frac{\alpha}{10^{n+m}}\right)c10^{n+m}, \tag{43}$$

or

$$\widetilde{N_p} = c\left(\Lambda 10^{n+m} + a10^m + \alpha\right). \tag{44}$$

Now let's find the increment $\Delta N_p$:

$$\Delta N_p = \widetilde{N_p} - N_p = c\left(\Lambda 10^{n+m} + a10^m + \alpha\right) - i\left(\Lambda b_1 + a_1\right). \tag{45}$$

Find the product of fluctuations $\delta\lambda$ and $\Delta N_p$:

$$\delta\lambda\Delta N_p = \alpha\left(c\left(\Lambda + a10^{-n} + \alpha 10^{-(n+m)}\right) - \left(\Lambda b_1 + a_1\right)i10^{-(n+m)}\right). \tag{46}$$

Let $\delta\lambda \to 0$, so $n, m \gg 1$, therefore,

$$\Delta N_p \to \infty. \tag{47}$$

From (45), leaving the largest term and taking into account the arbitrariness of $c = 1,2,\cdots$, we obtain the required Diophantine uncertainty relation:

$$\delta\lambda\Delta N_p \geq \alpha\Lambda. \tag{48}$$

Proceeding in the same way with $\Delta N_Q$, we obtain a similar relation for it:

$$\delta\lambda\Delta N_Q \geq \alpha . \tag{49}$$

Consequently, when the number of fundamental charges is bounded from above, the fluctuations of the physical constants are bounded from below. This means that the gravitational system of elementary particles cannot but fluctuate.

## 5. Conclusions

The invariance of Einstein's equations in GRT with respect to dual mappings is considered. First, this symmetry makes it possible to obtain new exact partial solutions of the Einstein equations that complement the obtained ones to a more complete description of space-time. Secondly, this symmetry leads to discretization of space-time, or its division into a set of unconnected Novikov's R- and T-domains impenetrable for light paths. This is the first effect of "self-quantization" of the gravitational field. This, in turn, leads to discretization of the flux of photons continuously emitted by an emitter in separate portions, or quanta. This is the second self-quantization effect of a curved space-time.

It is shown that the relationship between physical and geometric parameters at the wormhole throats, which are exact particular solutions of the Einstein-Maxwell equations, and which describe the internal structure of elementary charged particles, is described by a Diophantine equation in integer variables with a rational coefficient. This leads to the appearance of discrete spectra of physical and geometric parameters of wormholes. This is the third effect of "self-quantization" of the gravitational field.

Finally, the presence of arbitrarily small fluctuations of fundamental constants (charges, masses and radii of elementary particles) leads to the phenomenon of "Diophantine catastrophe", when the increments of the number of charges and the number of nucleons at the throats tend to infinity as the increments of the fundamental constants tend to zero. A Diophantine uncertainty relation arises, which is similar to the uncertainty relation in quantum mechanics: the product of the increment at the throat in the number of charges or the number of nucleons (elementary particle, atomic nucleus) required to maintain equilibrium by the increment in physical constants (rational coefficient of the Diophantine equation) must be no less than a certain value.

The authors thank Jane Gao for her cooperation.

## Conflicts of Interest

The authors declare no conflicts of interest regarding the publication of this paper.

## References

[1] Landau, L.D. and Lifshitz, E.M. (1975) The Course of Theoretical Physics. Vol. 2, The Classical Theory of Fields. Butterworth-Heinemann, London.

[2] Khlestkov, A.Yu. and Khlestkov, Yu.A. (2019) *Russian Physics Journal*, **62**, 264-283.

https://doi.org/10.1007/s11182-019-01709-9

[3] Novikov, I.D. (1964) Soobshenie GAISh. No. 132.

[4] Khlestkov, Yu.A., Sukhanova, L.A. and Trushkin, N.S. (2016) *Chinese Journal of Physics*, **54**, 614-627. https://doi.org/10.1016/j.cjph.2016.07.008

[5] Hawking, S.V. and Ellis, G.F.R. (1973) The Large Scale Structure of Space-Time. Cambridge University Press, Cambridge. https://doi.org/10.1017/CBO9780511524646

[6] Khlestkov, Yu.A., Lukashina, N.Yu., Lukashin, M.Yu. and Lukashin, P.Yu. (2019) *Journal of Modern Physics*, **10**, 1299-1309. https://doi.org/10.4236/jmp.2019.1011086

[7] Khlestkov, Yu.A. (2003) Nauchnaya Sessiya MEPhI-2003. Vol. 5, Moscow, 177.

[8] Khlestkov, A.Yu., Sukhanova, L.A. and Khlestkov, Yu.A. (2005) Nauchnaya Sessiya MEPhI-2005. Vol. 11, Sbornik Nauchnich Trudov, Moscow, 128-138.

[9] Gavrilin, D.Yu., Matyuk, N.N., Podoplelov, A.M., Lukashina, N.Yu. and Khlestkov, A.Yu. (2005) Nauchnaya Sessiya MEPhI-2005. Vol. 11, Sbornik Nauchnich Trudov, Moscow, 123-128.

[10] Khlestkov, Yu.A. (2005) *Zh. Eksp. Theor. Fiz.*, **128**, 300-311.

## Appendix 1. Geometrization of an Electromagnetic Field and Dusty Matter

Consider a pseudo-Riemannian centrally symmetric geometry with a metric

$$\mathrm{d}s^2 = e^{\nu}\mathrm{d}\tau^2 - e^{\lambda}\mathrm{d}r^2 - R^2\left(\mathrm{d}\theta^2 + \sin^2\theta\mathrm{d}\varphi^2\right) \tag{A1}$$

And the geometric conservative Einstein tensor $G_{\mu\nu}$ expressed through it; it is generated by an electromagnetic field of strength $E_r$ with an energy density $\varepsilon_f$, with an electric charge $Q$, a dusty substance with an energy density $\varepsilon_s$ and with a total gravitational energy $\varepsilon_g$. According to the exact particular solution of the Einstein and Maxwell equations in GRT, these physical characteristics are expressed through the geometry [2]:

$$\begin{aligned}
\varepsilon_f &= \frac{1}{\kappa}\left(G_0^0 - G\right),\\
\varepsilon_s &= \frac{1}{\kappa}G,\\
Q &= \frac{c^2}{\sqrt{k}}\sqrt{G_0^0 - G}R^2,\\
E_r &= \frac{c^2}{\sqrt{k}}\sqrt{G_0^0 - G},\\
\varepsilon_g &= \frac{1}{2}\frac{c^4R^3}{k}\left(G_0^0 - G\right) + \frac{1}{2}\frac{c^4R}{k}\left(1 - e^{-\lambda}R'^2 + e^{-\nu}\dot{R}^2\right).
\end{aligned} \tag{A2}$$

Here $' = \dfrac{\partial}{\partial r}$, $\dot{} = \dfrac{\partial}{\partial \tau}$.

The problem is in expressing the scalar potential $A_0$ in terms of geometry. The partial derivative of $A_0$ with respect to the radial coordinate is expressed in the synchronous accompanying frame of reference through the radial component of the electric field strength:

$$A_0' = -e^{\frac{\lambda}{2}}E_r. \tag{A3}$$

Substituting $E_r$ from (A2) into (A3), we obtain:

$$A_0' = -\frac{c^2}{\sqrt{k}}e^{\frac{\lambda}{2}}\sqrt{G_0^0 - G}. \tag{A4}$$

Using the Lorentz gage,

$$A^{\mu}_{,\mu} = 0, \tag{A5}$$

and equality to zero of the spatial components of the vector potential in the given frame of reference, we obtain from (A5) an expression for the partial time derivative $A_0$ with regard to time:

$$\dot{A_0} = -\left(\frac{\dot{\lambda}}{2} + 2\frac{\dot{R}}{R}\right)A_0. \tag{A6}$$

Knowledge of the two partial derivatives $A_0'$ and $\dot{A_0}$ makes it possible to find the connection between $A_0(\tau, r)$ and the geometry through the integral equation:

$$A_0 = -\int\left(\frac{\dot{\lambda}}{2}+2\frac{\dot{R}}{R}\right)A_0 \mathrm{d}\tau - \int\frac{c^2}{\sqrt{k}}e^{\lambda/2}\sqrt{G_0^0-G}\,\mathrm{d}r + const. \tag{A7}$$

However, using the permutation of the second partial derivatives

$$\dot{A}_0' = A_0'', \tag{A8}$$

and, substituting the partial derivatives $A_0'$ and $\dot{A}_0$ from (A5) and (A6) in (A8),

$$\left(\left(\frac{\dot{\lambda}}{2}+2\frac{\dot{R}}{R}\right)A_0\right)' = \frac{c^2}{\sqrt{k}}\left(e^{\frac{\lambda}{2}}\sqrt{G_0^0-G}\right)^{\cdot}, \tag{A9}$$

it is possible to obtain from (A9) the explicit required expression for the scalar potential $A_0$ in terms of the geometry:

$$A_0 = \frac{c^2}{\sqrt{k}}\frac{\left(e^{\frac{\lambda}{2}}\sqrt{G_0^0-G}\right)^{\cdot}+\left(\frac{\dot{\lambda}}{2}+2\frac{\dot{R}}{R}\right)e^{\lambda/2}\sqrt{G_0^0-G}}{\left(\frac{\dot{\lambda}}{2}+2\frac{\dot{R}}{R}\right)'}. \tag{A10}$$

Journal of Modern Physics, 2020, 11, 1779-1784
https://www.scirp.org/journal/jmp
ISSN Online: 2153-120X
ISSN Print: 2153-1196

# Why the Spacetime Embedding Incompressible Cores of Pulsars Must Be Conformally Flat?

**Ahmad A. Hujeirat**

IWR, Universität Heidelberg, Heidelberg, Germany
Email: AHujeirat@iwr.uni-heidelberg.de

**How to cite this paper:** Hujeirat, A.A. (2020) Why the Spacetime Embedding Incompressible Cores of Pulsars Must Be Conformally Flat? *Journal of Modern Physics*, **11**, 1779-1784.
https://doi.org/10.4236/jmp.2020.1111110

**Received:** October 1, 2020
**Accepted:** November 8, 2020
**Published:** November 11, 2020



## Abstract

The multi-messenger observations of the merger event in GW170817 did not rule out the possibility that the remnant might be a dynamically stable neutron star with $\mathcal{M}_{rm} \geq 2.69\mathcal{M}_{\odot}$. Based on this and other recent events, I argue that the universal maximum density hypothesis should be revived. Accordingly, the central densities in the cores of ultra-compact objects must be upper-limited by the critical density number $n_{cr}$, beyond which supranuclear dense matter becomes purely incompressible. Based on the spacetime-matter coupling in GR, it is shown that the topology of spacetime embedding incompressible quantum fluids with $n = n_{cr}$ must be Minkowski flat, which implies that spacetime at the background of ultra-compact objects should be bimetric.

## Keywords

Relativity: Numerical, General, Black Hole Physics, Pulsars, Neutron Stars, Pulsars, Superfluidity, Superconductivity, Incompressibility, Gluons, Quarks, Plasmas, QCD

Most theoretical investigations indicate that pulsars, neutron stars and magnetars, that comprise the family of ultra-compact objects (UCOs), whose masses $\mathcal{M}_{NS} \geq 1.4\mathcal{M}_{\odot}$, should have central densities much larger than the nuclear one [1] [2] [3] [4] [5]. Theoretically this posses an upper limit of their maximum mass $\mathcal{M}^{NS}_{\max} \leq 2.3M_{\odot}$ for almost all EOSs, though none of these objects have been ever observed with $\mathcal{M}^{NS}_{\max} \geq 2.1M_{\odot}$ (see [1] and the references therein).

Indeed, the multi-messenger observations of the merger of the two neutrons stars in GW170817 did not rule the formation of a massive NS with $\mathcal{M}^{NS} \approx 2.79M_{\odot}$ [5] [6] [7] [8]; hence the mechanisms that limit their theoretical mass range must be revisited.

Let us assume that there is a universal maximum energy density $\varepsilon_{\max}$, beyond which supranuclear dense fluids becomes incompressible. Under these circumstances the solution of the field equations:

$$R^{\mu\nu} - \frac{1}{2} g^{\mu\nu} R = 8\pi G T^{\mu\nu} \tag{1}$$

reads:

$$\mathrm{d}s^2 = g_{\mu\nu}\mathrm{d}x^{\mu}\mathrm{d}x^{\nu} = \frac{1}{S^{\kappa}}\mathrm{d}t^2 - \frac{\mathrm{d}r^2}{S} - r^2\mathrm{d}\Omega^2, \tag{2}$$

where $S = 1 - r_s/r$, $\kappa = \frac{1+3\alpha_0}{2}$, $\alpha_0 = P_b^L/\varepsilon_{\max}$ and $\Omega^2 = \mathrm{d}\theta^2 + \sin^2(\varphi)$. $P_b^L$ here is the local baryonic pressure.

In order to find out whether this spacetime is Weyl-transformable into a conformally flat spacetime of the type:

$$\mathrm{d}s^2 = \hat{g}_{\mu\nu}\mathrm{d}\hat{x}^{\mu}\mathrm{d}\hat{x}^{\nu} = e^f\left(\mathrm{d}\tau^2 - \mathrm{d}\rho^2 - \rho^2\mathrm{d}\Sigma^2\right), \tag{3}$$

we need to analyse the relation between both coordinate systems, solve for the conformal factor $e^f = F(\tau, \rho, \vartheta, \psi)$ and discuss their physical consistences (see [9] [10] and the references therein). As the line element, d$s$, should be invariant under the transformation, both metrics are related to each other through:

$$\hat{g}_{\mu\nu} = \frac{\partial x^{\mu}}{\partial \hat{x}^{\nu}}\frac{\partial x^{\mu}}{\partial \hat{x}^{\nu}} g_{\mu\nu}. \tag{4}$$

Using algbraic manipulation and setting $\frac{\partial x^{\mu}}{\partial \hat{x}^{\nu}} = \delta^{\mu}_{\nu}$, the following equalities are obtained:

$$e^f = \left(\frac{1}{S}\right)^{\kappa}\left(\frac{\partial t}{\partial \tau}\right)^2 = \left(\frac{1}{S}\right)\left(\frac{\partial r}{\partial \varrho}\right)^2 = \left(\frac{r}{\rho}\right)^2\left(\frac{\partial \Omega}{\partial \Sigma}\right)^2. \tag{5}$$

A strictly flat spacetime would correspond to $e^f = 1$. In this case, the relation between both coordinates systems read:

$$\begin{aligned}
&\frac{\mathrm{d}\tau}{\mathrm{d}t} = \frac{1}{S^{\kappa/2}} \Leftrightarrow \mathrm{d}\tau = \frac{1}{\left(1 - a_0 r^2\right)^{\kappa/2}}\mathrm{d}t \\
&\frac{\mathrm{d}\rho}{\mathrm{d}r} = \frac{1}{\sqrt{S}} \Leftrightarrow \mathrm{d}\rho = \frac{1}{\sqrt{1 - a_0 r^2}}\mathrm{d}r \\
&\qquad\qquad \Rightarrow \rho = \frac{\arcsin\left(\sqrt{a_0}\, r\right)}{\sqrt{a_0}} r \\
&\frac{\mathrm{d}\Sigma}{\mathrm{d}\Omega} = \frac{1}{S} \Leftrightarrow \mathrm{d}\Sigma = \frac{\sqrt{a_0}\, r}{\arcsin\left(\sqrt{a_0}\, r\right)}\mathrm{d}\Omega
\end{aligned} \tag{6}$$

Consequently, the spacetime:

$$\mathrm{d}s^2 = \left(\frac{1}{S}\right)^{\kappa/2}\mathrm{d}t^2 - \left(\frac{1}{S}\right)\mathrm{d}r^2 - r^2\mathrm{d}\Omega^2, \tag{7}$$

appears to be conformal to the flat spacetime:

$$\mathrm{d}s^2 = \mathrm{d}\tau^2 - \mathrm{d}\rho^2 - \rho^2\mathrm{d}\Sigma^2. \tag{8}$$

Mathematically, while $\kappa$ may accept other values, but $\kappa=1$ is most reasonable as the volume-expansion rate of the incompressible core in both dual-spacetimes is equal and independent of the core's compactness, *i.e.*

$$\frac{\mathrm{d}\rho}{\mathrm{d}\tau}=\frac{\mathrm{d}r}{\mathrm{d}t}. \tag{9}$$

Note that since the matter inside the core is incompressible and stationary, then the spatial and temporal variations must vanish. This implies that the state of matter in both spacetimes are identical and that remote observers can measure the variations of the core's radius only. In most cases, modelings of the interiors of UCOs usually relay on using one single EOS throughout the entire object and obeying: $P_b^L \le 1/3\varepsilon$ This requires a strong spatial variation of $\varepsilon$ in the neighborhood of $r=0$, where the regularity condition is imposed. However this egularity condition is practically equivalent to imposing zero-compressibility, *i.e.* $\nabla P=\nabla\varepsilon\big|_{r=0}=0$. To overcome this inconsistency, the central density is manually increased to be much higher than the nuclear number density, $n_0$, therefore giving rise to causality violation. On the other hand, recently it was suggested that at $n_{cr}\approx 3\times n_0$ and zero-temperature, the neutrons at the very central regions of massive pulsars ought to undergo a phase transition, through which they merge together to form embryonic super-baryons (SB, see **Figure 1** as well as [3] [4] and the references therein). The number density of the enclosed incompressible gluon-quark superfluid would attain the value $n_{cr}$, which could be easily reached by NSs with moderate masses. The state of the fluid on the verge of merger is said to be maximally compressible (MC) and the corresponding stress-energy tensor becomes traceless: $\boldsymbol{T}=\varepsilon_{cr}-3P_b^L=0$. Although the MC state is expected to be a short-living transient phase, $\boldsymbol{T}=0$ insures that the matter-field correspondence, and specifically the incompressibility character of the quantum fluid, is invariant under Weyl and conformal transformations.

When the compressible matter surrounding the cores of NSs cools down on the cosmic time, the curved spacetime at the background would compress the baryons at the center together, thereby decreasing the separation distance between the baryons, $d_b$, down to values comparable to the average distance $d_g$, between quarks (see **Figure 2**), thereby giving rise a free darg energy, a free dark energy $\Delta\varepsilon_b^+$ of order $c\hbar/2d_b$. For $d_b=d_q$, $\Delta\varepsilon_b^+$ is comparable to the rest energy of an isolated baryon, *i.e.*

$$\frac{\Delta\varepsilon_b^+}{\Delta\varepsilon_q}\sim\frac{2d_q}{d_q+d_b}\to\begin{cases}0; & d_b\gg d_q\\ 1; & d_b=d_q\end{cases} \tag{10}$$

where $\Delta\varepsilon_q=0.939$ GeV. Hence $\Delta\varepsilon_b^+$ is capable of deconfining the quarks inside baryons, thereby rendering merger of the baryons possible. Moreover, the pressure $P_{UP}$, induced by the uncertainty principle, and $\Delta\varepsilon_b^+$ become duals that oppose compression/contraction of the core's matter, whilst enhancing the effective mass of the core. The state of matter in the post merger phase is governed by EOS: $P_{UP}=\Delta\varepsilon_b^+=\varepsilon_{cr}=a_0n_{cr}^2$. The mass of the field quanta goes to

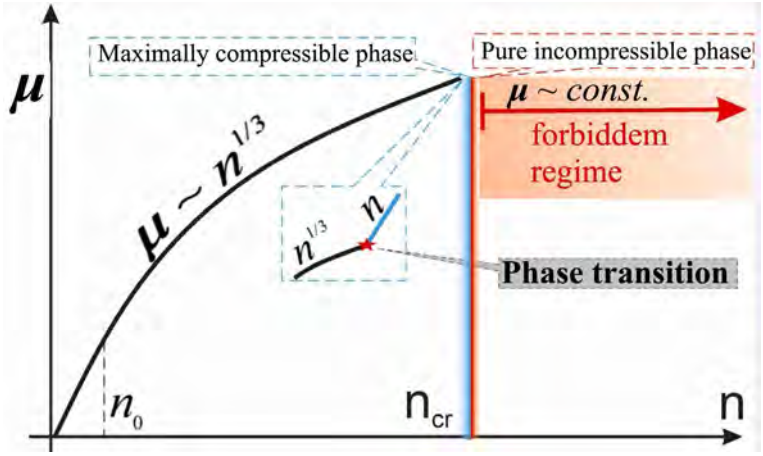


**Figure 1.** The development of the chemical potential $\mu$ of ultradense quantum fluids with the number density $n$. For $n_0 \le n < n_{cr}$, $\mu \sim n^{1/3}$. As $n \to n_{cr}$ the quantum fluid converges to the maximally compressible state and undergoes a phase transition into the incompressible state, where $P = \varepsilon_{cr} = c_0 n_{cr}^2$. The forbidden region correspond to number densities that are beyond the universal maximum allowable value $n_{cr}$.

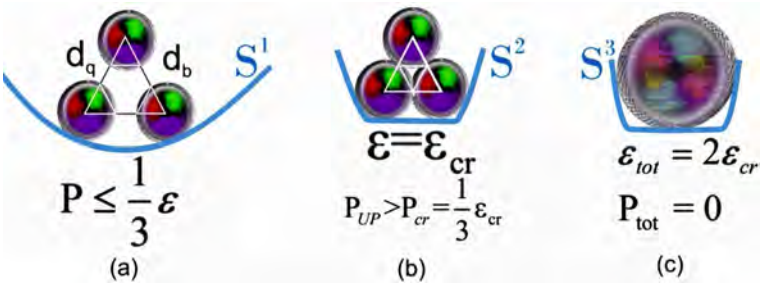


**Figure 2.** A schematic description of the spacetime curvature (denoted with $S$) as opposed to the EOS and number density. $d_b$ and $d_q$ denote the mean distances between two arbitrary baryons and quarks, respectively. The case (a) corresponds to compressible quantum fluid embedded in a Schwarzschild-like spacetime ($S^1$), (b) to the maximally compressible fluid phase, where the boundaries of baryons overlap, *i.e.* $d_b = d_g$ and the pressure $P_{UP}$ induced by the uncertainty principle becomes comparable to $\varepsilon_{cr}$. Here the spacetime start flattening to become nearly a Minkowski-type spacetime ($S^2$). (c) corresponds to the final state in which baryons start merging to form a super-baryon, whose interior is made of incompressible gluon-quark superfluid embedded by a strictly flat spacetime ($S^3$).

zero and therefore the quarks communicate with each other via the massless gluons at the speed of light [11] [12].

The dark energy contribution $\Delta\varepsilon^+$ must be stored locally; it goes specifically into enhancing the surface tension of the super-baryon and acts as a confining force for the enclosed ocean of quarks. At a certain point of the cosmic time, the core would decay and dark energy would be liberated, thereby provoking a hadronization process of the guon-quark superfluid.

For a given super-baryon resulting from the merger of $N$-baryons, the effective energy is expected to be:

$$\varepsilon_{SB}^{tot} \approx 2N \times \varepsilon_0. \tag{11}$$

This appears to be in line with the short-living pentaquark formation observed at the LHC-experiment (see [13] and the references therein), though the entropy and density regimes are totally different from those in the cores of UCOs.

Noting that the core must be 3D spherically symmetric with zero-entropy enclosed matter which behaves as a single quantum entity embedded in a flat spacetime, the governing physics is predicated to be mirrored onto its two-dimensional surface in accord with the holographic principle. However, it is not clear at all, how and what kind of information could be still storable on the surface under zero-entropy conditions?

Finally, when combining the result-presented here with the following arguments:

- The remnant of GW170817 didn't necessarily collapse into a BH.
- BHs with $\mathcal{M}_{BH} \le 5M_{\odot}$ may be safely ruled out.
- The first generation of stars may have formed massive pulsars that should be dark by now.
- The glitch phenomena in pulsars are triggered by topological changes of the bimetric spacetime embedding pulsars (see [14] and the references therein); then the existence of a universal maximum energy density is an inevitable conclusion. It should be noted however, that the existence of a universal maximum density, $n_{cr}$, does not necessary rule out BHs as astrophysical objects, whose existence is observationally well-verified; however, it argues against their classical formation scenario as well as against the existence of matter singularities at their centers.

## Acknowledgements

Dr. Emre Dil is gratefully acknowledged for valuable discussions.

## Conflicts of Interest

The author declares no conflicts of interest regarding the publication of this paper.

## References

[1] Ozel, F. and Freire, P. (2016) *Annual Review of Astronomy and Astrophysics*, **54**, 401-440. https://doi.org/10.1146/annurev-astro-081915-023322

[2] Camenzind, M. (2007) Compact Objects in Astrophysics. Springer, Heidelberg. https://doi.org/10.4236/jmp.2018.91004

[3] Hujeirat, A.A. (2018). *Journal of Modern Physics*, **9**, 51-69.

[4] Hujeirat, A.A. (2018) J*ournal of Modern Physics*, **9**, 532-553. https://doi.org/10.4236/jmp.2018.94037

[5] Raithel, C.A. (2019) *The European Physical Journal A*, **55**, Article No. 80. https://doi.org/10.1140/epja/i2019-12759-5

[6] Piro, L., Troja, E., Zhang, B., *et al.* (2019) *Monthly Notices of the Royal Astronomical Society*, **483**, 1912-1921. https://doi.org/10.1093/mnras/sty3047

[7] Abbott, B.P., *et al.* (2019) *Physical Review X*, **9**, Article ID: 011001.

[8] Hujeirat, A.A. and Samtaney, R. (2020) *Journal of Modern Physics*, **11**.

[9] Dil, E. and Zafer, T. (2016) *Journal of Gravity*, **2016**, Article ID: 7636493. https://doi.org/10.1155/2016/7636493

[10] Brito, I. and Ramos, M.P.M. (2019) *General Relativity and Gravitation*, **51**, Article No. 28. https://doi.org/10.1007/s10714-019-2514-5

[11] Zeldowich, Ya.B. (1962) *Soviet Physics—JETP*, **14**, 5.

[12] Bludman, S.A. and Ruderman, M.A. (1968) *Physical Review*, **170**, 1176. https://doi.org/10.1103/PhysRev.170.1176

[13] LHCb Collaboration (2015) *Physical Review Letters*, **115**, Article ID: 072001.

[14] Hujeirat, A.A. and Samtaney, R. (2020) *Journal of Modern Physics*, **11**, 395-406.

Journal of Modern Physics, 2020, 11, 1785-1798
https://www.scirp.org/journal/jmp
ISSN Online: 2153-120X
ISSN Print: 2153-1196

# The Remnant of GW170817: A Trapped Neutron Star with a Massive Incompressible Superfluid Core

**Ahmad A. Hujeirat[1], Ravi Samtaney[2]**

[1]IWR, Universität Heidelberg, Heidelberg, Germany
[2]Applied Mathematics and Computational Science, CEMSE Division, KAUST, Thuwal, KSA
Email: AHujeirat@iwr.uni-heidelberg.de, ravi.samtaney@kaust.edu.sa

**How to cite this paper:** Hujeirat, A.A. and Samtaney, R. (2020) The Remnant of GW170817: A Trapped Neutron Star with a Massive Incompressible Superfluid Core. *Journal of Modern Physics*, **11**, 1785-1798.
https://doi.org/10.4236/jmp.2020.1111111

**Received:** June 19, 2020
**Accepted:** November 8, 2020
**Published:** November 11, 2020





## Abstract

Our bimetric spacetime model of glitching pulsars is applied to the remnant of GW170817. Accordingly, pulsars are born with embryonic incompressible superconducting gluon-quark superfluid cores (SuSu-matter) that are embedded in Minkowski spacetime, whereas the ambient compressible and dissipative media (CDM) are imbedded in curved spacetime. As pulsars cool down, the equilibrium between both spacetime is altered, thereby triggering the well-observed glitch phenomena. Based thereon and assuming all neutron stars (*NSs*) to be born with the same initial mass of $M_{NS}(t=0)\approx 1.25M_{\odot}$, we argue that the remnant of GW170817 should be a relatively faint *NS* with a massive central core made of SuSu-matter. The effective mass and radius of the remnant are predicted to be $\left[2.8\mathcal{M}_{\odot}<\mathcal{M}_{rem}\le 3.351\mathcal{M}_{\odot}\right]$ and $R_{rem}=10.764$ km, whereas the mass of the enclosed SuSu-core is $\mathcal{M}_{core}=1.7M_{\odot}$. Here, about $1/2\,\mathcal{M}_{core}$ is an energy enhancement triggered by the phase transition of the gluon-quark-plasma from the microscopic into macroscopic scale. The current compactness of the remnant is $\alpha_c=0.918$, but predicted to increase as the CDM and cools down, rendering the remnant an invisible dark energy object, and therefore to an excellent black hole candidate.

## Keywords

Relativity: Numerical, General, Black Hole Physics, Magnetars, Neutron Stars, Pulsars, Superfluidity, Superconductivity, Gluons, Quarks, Plasmas, QCD

## 1. Introduction

The astronomical event GW170817 marks the beginning of a new era of multi-

messenger astronomy, in which detectors of gravitational waves and electromagnetic radiation operated almost simultaneously to follow up the merger event. Using LIGO detectors and advanced Virgo in combination with Fermi and INTEGRAL gamma-ray telescopes the event was localized to the galaxy 4993, in which two compact objects, most likely two neutron stars, were found inspiraling and to subsequently merge and form a massive compact object [see [1], and the references therein]. The component masses were inferred to lie between $\left[1.0M_\odot \le M_1, M_2 \le 1.89M_\odot\right]$ in the high spin case and $\left[1.16M_\odot \le M_1, M_2 \le 1.60M_\odot\right]$ in the low case. Approximately 10% of the total mass is predicted to have gone forming an accretion disk, ejecta, jets, X-ray flares and/or outflows [see [2], and the references therein]. While the exact nature of the remnant depends strongly on the final baryonic mass, it may still fall in one of the following three categories:

■ **A massive neutron star (HMNS)**

Based on observational and theoretical considerations, the possibility that the merger of the two *NSs* yielded a short-living massive neutron star (HMNS) appears to be widely accepted [see [3] [4] [5], and the references therein]. On the long-term however, it is not clear if such a massive object would survive a gravitational collapse and end up as a stellar BH [see [6], and the references therein].

On the other hand, there are several observational signatures that obviously favor the formation a MNS. Namely, the occurrence of the gamma-ray burst GRB170817 approximately 1.7 seconds after the merger event [7] and the appearance of certain features 155 days later is a clear indication for reactivation of the central object. Moreover, the formation of a structured off-axis jet [3] [8], the detected emission powered by the radioactive decay of r-process nuclei synthesized in the ejecta [9] and that a surface magnetic field of order $10^{12}$ G is required to match the EM-radiation hint that the remnant must be neutron-rich with a hard surface [see [4], and the references therein].

In particular, the observed steady brightening of GW170817 lasting less than 160 days after the merger, which is most likely powered by non-thermal synchrotron emission from plasmas propagating at relativistic speeds, may be well-considered for ejecta from a central compact object with hard surface. The Lorentz factors, $\Gamma s$, that correspond to plasma propagation in micro-quasar systems generally fall in the range of $\left[3 \le \Gamma \le 10\right]$, whereas $\Gamma s$ of the observed ejecta in GW170817 hardly reach the lower range of this interval.

■ **A stellar black hole (SBH)**

Whether the remnant was a short or is a long-living HMNS, its total mass is $\mathcal{M}_{tot} \ge 2.6M_\odot$ to 90% confidence [see [11], and the references therein]. In the absence of extraordinary stiff EOSs with exotic repulsive nuclear forces of unknown origin, the object should ultimately collapse into a stellar black hole. Indeed, the revealed low X-ray flux from GW170817 indicates weak magnetic field that is typical to stellar BHs [12]. Other arguments favoring the formation of a BH have been discussed, though the results obtained may be biased, as these

studies assume a prior the formation of a BH [see [6], and the references therein].

However, it should be noted here that determining the nature of the remnant would require solving the time-dependent general relativistic Navier-Stokes equations with radiative transfer and magnetic fields at the background of a dynamically varying spacetime, which is beyond the state-of-the-art simulations today. Also, the capability of receiving gravitational wave signals that carry information about the spin and compactness of the *NSs* shortly before and of the remnant immediately after the merger event are outside the sensitivity range of LIGO.

■ **Another type of a compact object**

In the absence of direct and founded observational signatures that determine conclusively the nature of the remnant, the possibility that it might be neither a classical *NS* nor a stellar BH, but rather a new type of a compact object cannot be excluded. The fact that the mass of the remnant falls in the range of $\left[2.5M_{\odot} \le \mathcal{M} \le 5M_{\odot}\right]$, where neither stellar BHs nor normal neutron stars have ever been observed, makes this conjecture viable.

In the following, we discuss this conjecture in detail and argue that the remnant is most likely made of incompressible gluon-quark superfluid core embedded in a flat spacetime and surrounded by a shell of compressible and dissipative matter with a curved spacetime at the background as visualized in Figure 1.

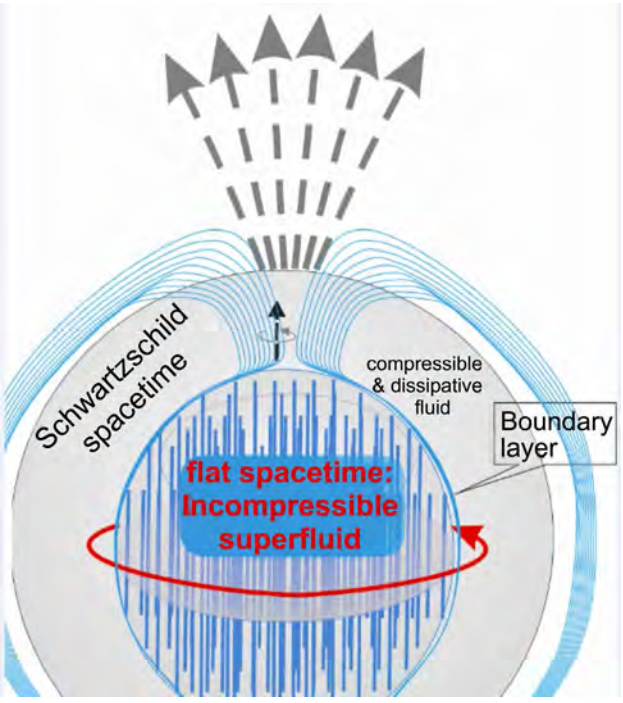


Figure 1. A schematic description of the interior of the remnant of GW170817 as predicted by the bimetric spacetime scenario. While the incompressible superfluid in the core is enclosed in a Minkowski spacetime, the surrounding compressible and dissipative media is set to be imbedded in a curved spacetime. Both media are separated by geometrically thin boundary layer, where the pulsar's dynamo action is expected to operate.

## 2. The Remnant of GW170817 and Its Internal Structure

In the case of a quasi-static contraction of a massive *NS*: as the event horizon, $R_{\mathcal{H}}$, and the star radius, $R_{\star}$, approach each other, the stiffness of the EOS and therefore the compactness must increase. The sound speed should increase and reach roughly the speed of light at $R_{\star} = R_{\mathcal{H}}(1+\epsilon)$, where $\epsilon$ is a sufficiently small number. Indeed, it was repeatedly argued that the sound speed inside HMNS*s* must be larger than $c/\sqrt{3}$ [see [13], and the references therein]. A possible limiting EOS may have the form:

$$P_L = n^2 \frac{\partial}{\partial n}(\varepsilon/n) \xrightarrow{\varepsilon \to a_0 n^2} \varepsilon, \tag{1}$$

where $a_0, n, P_L, \varepsilon$ denote a constant coefficient, number density, local pressure and the density of internal energy, respectively. Here the rate of interaction of sub-nuclear particles, namely mesons and gluons, reaches the saturation limit, at which the chemical potential, *i.e.* energy per particle, attains its universal maximum value, which was predicted to be around $n_{cr} \approx 3 \times n_0$, where $n_0$ is the nuclear number density [14]. In this case,

$$\varepsilon = a_0 n^2 \xrightarrow[n \to n_{cr}]{} a_0 n_{cr}^2 \doteq \varepsilon_{cr} = \mathcal{O}\left(10^{36}\right) \mathrm{erg/cc} \tag{2}$$

In the present study, this EOS governs fluids that are the maximally compressible or purely incompressible. Under these conditions, the constituents are capable of resisting all kinds of external perturbations, including further contractions by gravity. However an EOS of the type $\varepsilon = P_L = const.$ is incompatible with traceless mass-energy tensors (METs) and therefore does not obey conformal invariance [13]. Similar to weakly compressible terrestrial fluids, the pressure in incompressible fluids loses its local thermodynamical character and turns into a mathematical term only[1], which nevertheless must be chosen, so to ensure that $\mathrm{d}P_L/\mathrm{d}\varepsilon \le 1$.

In fact, fluids governed by the limiting EOS: $P = \varepsilon(> \varepsilon_0)$ cannot accept stratification by gravity or, equivalently by the curvature of spacetime. Indeed, it was recently verified that once the matter at the very center of massive *NSs* become purely incompressible, then the embedding spacetime must flatten and become conformally flat [see [15], and the references therein]. The total energy of a stationary and zero-stratified supradense nuclear matter should consist of the rest energy only, as otherwise, thermal, magnetic and kinetic energies can be affected directly by gravity. Thus the energy state of purely incompressible supradense nuclear fluids should correspond to the universal lowest-possible energy state. Based thereon, our argument may be summarized as follows:

1) Under certain conditions, supradense nuclear fluids may become maximally compressible, *i.e.* purely incompressible, at which the energy density attains the universal maximum value $\varepsilon_{\max}$. Here the interaction rate between the constituents saturates as they communicate with each other at the speed of light. Energy divergence is prohibited as massless gluons are the mediators whilst the

[1]In terrestrial weakly incompressible fluid the pressure is treated as a Lagrangian multiplier.

quarks must motionless in space, but oscillatory in time. These conditions should apply to the gluon-quark-plasma inside individual baryons at zero-entropy.

2) The classical pressure in purely incompressible supradense nuclear fluids loses its local thermodynamical character. In fact, as the constituents communicate with each other at the speed of light, the interaction-power is sufficiently strong to smooth out all possible potential barriers between individual baryons, thereby enhancing their merger and forming an ocean of gluon-quark superfluid.

3) Purely incompressible supradense nuclear matter governed by the EOS,

$$P = \varepsilon_{\max} = const. \tag{3}$$

should have zero-entropy and embedded in a flat spacetime. This strong conjecture raises the possibility that entropy of matter and curvature of spacetime may have hidden connections.

## 3. Basic Assumptions and the Solution Strategy

Very recently, we applied the bimetric spacetime scenario of glitching pulsars to investigate the internal structures both of the Crab and Vela pulsars [16]. The model was capable of re-producing and explaining several mysterious features that observed to accompany both pulsars, namely the deriving mechanisms underlying the glitch phenomena and their rate of reoccurrence, the origin of under/overshootings observed to associate their glitch events as well as their cosmological fate. Based thereon, newly born pulsars are predicated to have the initial mass of $1.25M_\odot$ and an embryonic SuSu-core of $0.029M_\odot$ to evolve into a Crab-like pulsar after 1000 years and subsequently into a Vela-like pulsar 10,000 years later to finally fade away as an invisible dark energy object after roughly 10 Myr. The cores of both pulsars were predicted to have the masses: $\mathcal{M}_{core}^{Crab} = 0.15M_\odot$ and $\mathcal{M}_{core}^{Vela} = 0.55M_\odot$ [10].

In order to apply the model to the remnant of GW170817, the following assumptions must be made:

- The masses of the two merging *NSs* read: $\mathcal{M}_{tot}^1 = \mathcal{M}_{tot}^2 = 1.4M_\odot$, which fall in the mass-range revealed by observations [1]. Although our results are not too sensitive to these exact values, both masses are remarkably close to that of the Crab pulsar and therefore we may assume that both *NSs* should have the same cosmic evolution. Specifically, both *NSs* should have identical initial conditions, are perfectly isolated with no energy loss or gain from or to their surroundings. As in the case of the Crab and Vela pulsars, any mass-difference is due to age-difference: as the object ages, it becomes colder, the inertia of its SuSu-core increases, which is associated with a topological change of spacetime embedding its interior.

The total mass of the object consists of core's mass, half of which is baryonic matter while the other half is due to the enhanced gluon cloud enclosing the quarks on the macroscopic scale. The other contribution to $\mathcal{M}_{tot}^1$ comes from the ambient normal fluid.

Based thereon each of two the *NSs* prior merger should have approximately the same age, same total masses as the Crab pulsar and therefore the same core's masses: $\mathcal{M}_{core}^{Crab} = 0.15 M_{\odot}$ [see [10], for further details].

- The incompressible superfluid cores of both objects should have survived the violent merger and preserved their inertia. While this assumption appears to be too strong, it may be supported by the following arguments:

– Similar to gluon-quark plasma inside individual baryons, the incompressible gluon-quark superfluid inside the cores of pulsars cannot live in free space, but hidden behind a confining quantum barrier. The effective energy of the potential barrier is sufficiently strong to protect the core against deformations by tidal forces. Indeed, the sound crossing time of each core is predicated to be one million times shorter than the dynamical time scale during the inspiraling phase of both *NSs* prior merger.

– In QCD, the bag energy confining gluon-quark plasmas inside individual baryons is of order 300 MeV. When $N$ baryons are set to merge together under zero-temperature and pure incompressibility conditions, then the size, $V$, and mass of the resulting super-baryon must increase with $N$, *i.e.* $\mathrm{d}V/\mathrm{d}N = const$. Recalling that roughly 99% of the effective energy of an individual baryon is due to the gluon field, then the energy of the gluon cloud confining the quarks inside the super-baryon must moderately increase with $N$, *i.e.* an energy enhancement of the type: $\mathrm{d}\varepsilon^{gluon}/\mathrm{d}N = \alpha_0 N^{\beta}$ is forbidden as $N$ is typically of order $\mathcal{O}\left(10^{57}\right)$, so that any value of $\beta > 0$ would lead energy divergence. A reasonable prediction would be that the merging process of $N$-neutrons at zero-temperature is energetically upper-bounded by the constant: $\mathrm{d}\varepsilon^{gluon}/\mathrm{d}N = 2\varepsilon_0$, where $\varepsilon_0$ is the rest energy of a neutron.

One may conjecture that the extra energy originates from the gluon field necessary for stably confining the quark-ocean inside the super-baryons and shield it from the outside universe [17]. Indeed, the effective energy stored in the creation of the short-living pentaquark that was detected in the LHC experiment was found to be about 4.5 GeV, which is consistent with our scenario [18], though the physical conditions are completely different: while the plasma at the LHC is characterized by very high temperature and extremely low density, the matter in the central cores of pulsars should be supradense nuclear with temperature much lower than the corresponding Fermi one.

– The incompressible supranuclear dense matter inside the cores of *NSs* must have the lowest possible energy state and behaves as a single quantum entity. Such a fluid is expected to be well-equipped to resist all types of external perturbations, including tidal deformation. In this case, the only source left for energy emission would be the ambient compressible and dissipative nuclear fluid in the shell.

## 4. The Numerical Approach

Based on the above-mentioned arguments, the mass and size of the remnant's core may be obtained here by extrapolating the sizes of the cores of the well-studied

Crab and of the Vela pulsars as well as recalling that the remnant should turn invisible, once the object has metamorphosed entirely into a SuSu-object. Thus a *NS* with the initial mass of $M_0 = M\left(t=0\right) = 2.5M_\odot$ will double its mass at the end of its visible lifetime, *i.e.* $M\left(t=\infty\right) = 5M_\odot$.

In **Figure 2** we show the distribution of effective masses of the cores versus the total masses of the objects. Here we use the tabulated values shown in **Figure 2** to construct the quadratic mass-function in units of $M_\odot$:

$$\mathcal{M}_{core} = 0.108507\mathcal{M}_{tot}^2 + 0.652778\mathcal{M}_{tot} - 0.976562, \tag{4}$$

which applies for $\mathcal{M}_{tot} \geq 1.25M_\odot$.

Let $t = t_0$ denote the time, at which the two *NSs* merged together. Based on observations the total mass of both objects is: $M_{tot}\left(t = t_0 - \epsilon_{t_0}\right) = 2.8M_\odot$, which consists of $2.5M_\odot$ baryonic matter and $0.3M_\odot$ of dark energy, where $t = t_0 - \epsilon_{t_0}$ corresponds to the time shortly before the merger event and $\epsilon_{t_0}$ denotes a short instant.

Based on the mass-function $\mathcal{M}_{core}$, the core's mass of the remnant appears to have undergone a dramatic increase during the merger from $0.3M_\odot$ to $1.7M_\odot$, which implies an additional input of dark energy that amounts to $0.55M_\odot$, yielding a massive *NS* of $3.351M_\odot$, and consisting of $2.5M_\odot$ in the form of baryonic matter and $0.85M_\odot$ of dark energy.

The mechanism underlying the injection of dark energy into the system here may be explained as follows:

When the matter at the center of a massive *NS* is compressed by the surrounding curved spacetime, the separation between two arbitrary baryons, $\ell_b$, may decrease down and become comparable to the mean free path $\ell_g$, between quarks in individual baryons and at zero-temperature. In this case a free energy $\Delta\varepsilon^+$ of order $c\hbar/2\ell_g$ would be generated and may easily surpass the 0.939 GeV limit, beyond which baryon's merger becomes a viable process. $\Delta\varepsilon^+$ is expected to be stored locally, and specifically to enhance the surface tension needed for confining the enclosed ocean of quarks. At certain time, this energy would be liberated, once the core has decayed into a pure baryonic matter.

Based thereon, the Tolman-Oppenheimer-Volkov equation (TOV) was solved, using the core mass and its energy-density as input parameters. In the present case, the inertia of the core is expected to significantly enhance the curvature of spacetime and therefore the distribution of matter in the shell surrounding the core. The matter here is set to obey the polytropic EOS: $P = \mathcal{K}\rho^\gamma$. In order to obtain the optimal values of $\mathcal{K}$ and $\gamma$, the TOV equation was solved for the maximum possible mass that can be obtained using the EOSs "alf4" and "sly" [19] [20]. As shown in **Figure 3**, the resulting mass turns to be: $\mathcal{M}_{NS}^{\max} = 2.075M_\odot$, which is approximately equal to that of PSR J0348+0435.

Interestingly enough, using "alf4" and "sly" EOSs, the central density obtained here roughly equal to the universal maximum value: $\rho_{\max} = 6\times\rho_0$, at which the fluid turns purely incompressible superfluid.

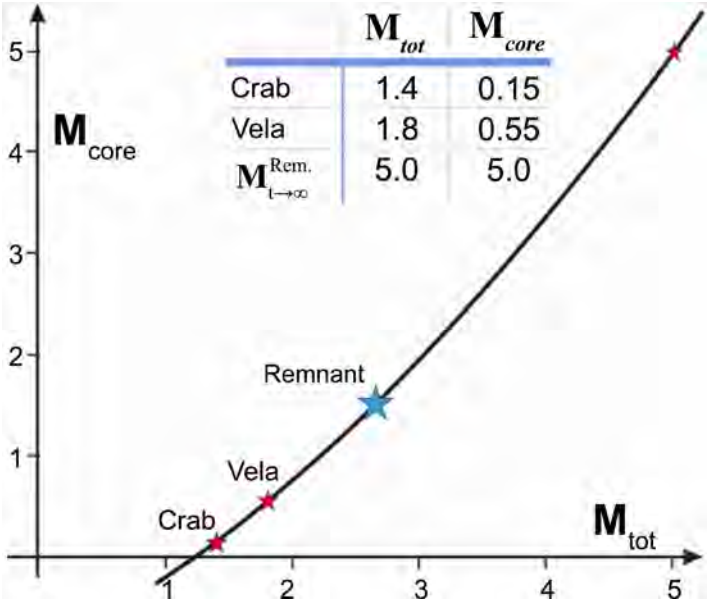


**Figure 2.** The total mass of the core (baryonic and dark energy) versus total mass of the entire object (*i.e.* the mass of the core and overlying baryonic shell) are displayed, using a polynomial interpolation of the values tabulated in the figure. Part of these values have been adopted from [10].

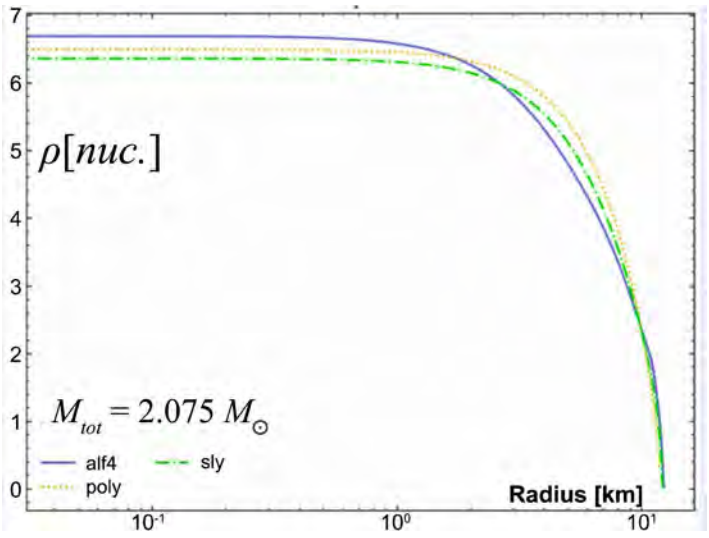


**Figure 3.** The internal structure of a marginally stable massive *NS* using the three different EOSs: alf4 [19], sly [20] and poly (*i.e.* the polytropic EOS in which the coefficient $\mathcal{K}$ and $\gamma$ were optimized to fit the other two profiles). Except poly, non of the EOSs, including other 12 models, where capable of stably modelling the interiors of *NSs* more massive than $2.075M_{\odot}$.

The fitting procedure of the polytropic EOS with "alf4" and "sly" (see **Figure 3**), yielded the following values:

$$\begin{aligned}\mathcal{K} &= 1.98183\times 10^{-6}\\ \gamma &= 2.72135\end{aligned} \tag{5}$$

Assuming $\rho_{\max}$ to exist in our universe, then the physical conditions governing

both the cores of MNS and of the remnant of GW170817, must be identical.

In order to accurately capture the strong gradients in the vicinity of the remnant's surface, the explicit adaptive mesh refinement (EAMR) method has been employed [16]. Here approximately $10^5$ grid points have been used reaching an aspect ratio of $\mathrm{d}r_{\max}/\mathrm{d}r_{\min} \approx 10^5$ (see **Figure 4**). In **Figure 5** the profiles of the normalized total energy density and the total pressure throughout the entire object versus radius are shown. These are defined as follows:

$$\varepsilon_d = \varepsilon_{bar} + \varepsilon_\phi, \quad P_{tot} = P_{bar} + P_\varphi, \tag{6}$$

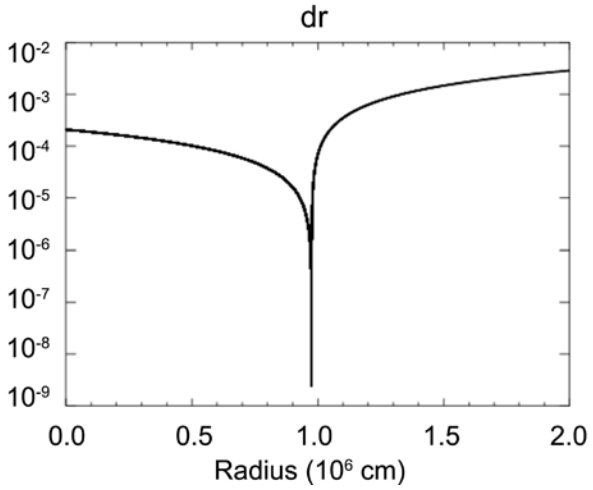


**Figure 4.** The non-linear distribution of the grid spacing versus radii. Here the density of grid points was optimized in order to capture the fine structures of the remnant in the vicinity of its surface.

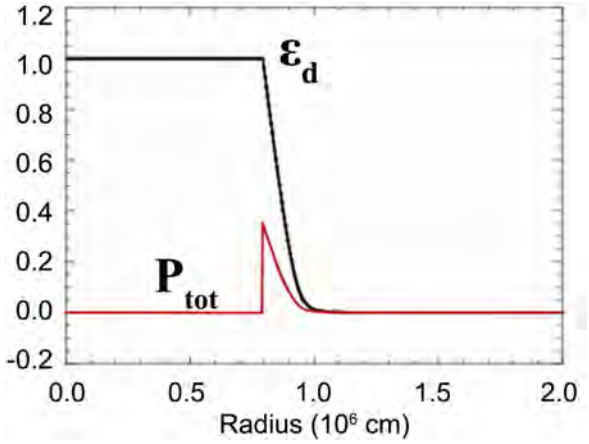


**Figure 5.** The profiles of the energy density $\varepsilon_d$ and the total pressure, $P_{tot}$, versus radius in units of $2\varepsilon_{cr}$. Inside the core, where the spacetime is flat, the energy density attains the constant value $\varepsilon_d = 2\varepsilon_{cr}$ (see Equation (2), Equation (6) and Equation (7)). Outside the core, where the matter is compressible and dissipative, the radial-distribution of $\varepsilon_d$ is determined by solving the TOV equation at the background of a Schwarzschild spacetime using the "poly" EOS. The total pressure inside the core is the superposition of the normal local pressure and the negative pressure due to vacuum. While $P_{tot}$ vanishes inside the core, it becomes equal to the local pressure outside it.

where

$$\varepsilon_{\phi} = \frac{1}{2}\dot{\phi}^2 + V(\phi) + \frac{1}{2}(\nabla\phi)^2$$
$$P_{\phi} = \frac{1}{2}\dot{\phi}^2 - V(\phi) - \frac{1}{6}(\nabla\phi)^2 \quad (7)$$

Here $\phi, V(\phi)$ generally denote the scalar field and its interaction potential with the baryonic matter. In the present case, $\phi$ is a spatially averaged gluon field and $V(\phi)$ is the potential energy of the gluon-cloud embedding the quarks inside the super-baryon. The subscript "bar" denotes the contribution due to baryonic matter whereas $\varphi$ due to vacuum. The scalar field, $\phi$, is assumed to be significantly enhanced when undergoing a phase transition from the micro into the macroscale. Such enhancement is necessary in order to maintain the super-baryon stable, while hiding it from the outside world [see [21], and the references therein]. Inside the core, the incompressible superfluid is stationary and therefore $\phi$ is spatially and temporary constant, *i.e.*

$$\dot{\phi} = \nabla\phi = 0. \quad (8)$$

In this case $V(\phi) = \varepsilon_{bar}$, which is equal to the effective resistive pressure, $P_L$, required to maintain the quarks apart at a minimum distance $\ell_{\min}$ which is of order 0.6 fm.

Consequently, inside the core we have $\varepsilon_d = 2\varepsilon_{bar}$, but a vanishing total pressure $P_{tot}$. Outside the core, however, $\varepsilon_d$ runs as dictated by the TOV-equation at the background of a Schwarzschild spacetime and using the polytropic EOS with the parameters specified in Equation (5).

Following Equation (4), the total mass of the core is $1.7M_{\odot}$, half of which is made of baryonic matter and the other half is due to the macroscopic enhancement of the gluon field (see **Figure 6**). Using the polytropic EOS with the parameters

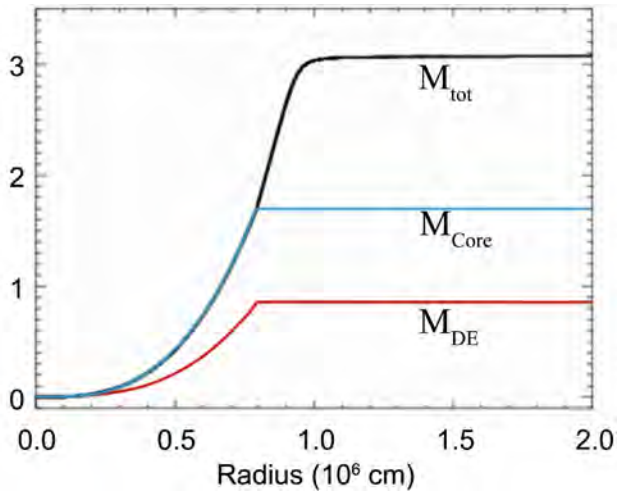


**Figure 6.** The radial-distributions of the total effective mass of the remnant $M_{tot}$, the total mass of the core, $M_{core}$, and the contribution of dark energy, $M_{DE}$, to the effective mass of the core. The final masses here read: $M_{tot} = 3.351M_{\odot}$, $M_{core} = 1.7M_{\odot}$ and $M_{DE} = 0.85M_{\odot}$.

given in Equation (5), the TOV equation was integrated to determine the radius and therefore the compactness of the remnant. Our high-resolution numerical calculations yielded the radius of $R_{rm} = 10.764$ km for a remnant mass of $3.351 M_{\odot}$ to give rise to a compactness parameter: $\alpha_c = 0.918$ as shown in **Figures 6-8**.

Obviously, the predicated value of the remnant's radius here is consistent with the recent investigations [see [22], and the references therein].

In **Figure 7** we show the Schwarzschild matric exponent, $\Psi$, which is, in the limit of weak gravitational field, reduces to the gravitational potential. Inside the core, where the embedding spacetime is flat, $\Psi$ attains a negative constant value, but increases abruptly throughout the ambient medium and goes to zero at infinity. Across the surface, $\Psi$ undergoes a dramatic spatial variation. This can be seen from $\mathrm{d}\Psi/\mathrm{d}r$, which vanishes inside the core, but then decreases and increases dramatically in the vicinity of the remnant's surface. Thus free particles in this region would experience rapid acceleration and deceleration, thereby

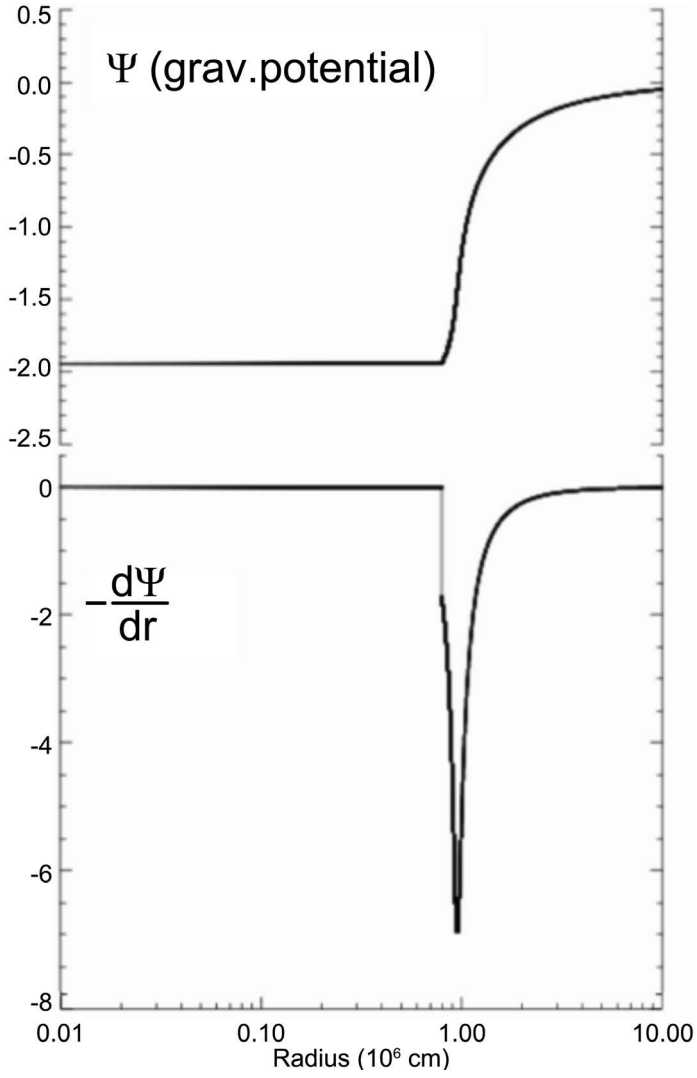


**Figure 7.** The radial distribution of the gravitational potential, $\Psi$, and its negative radial derivative throughout the remnant and the surrounding space.

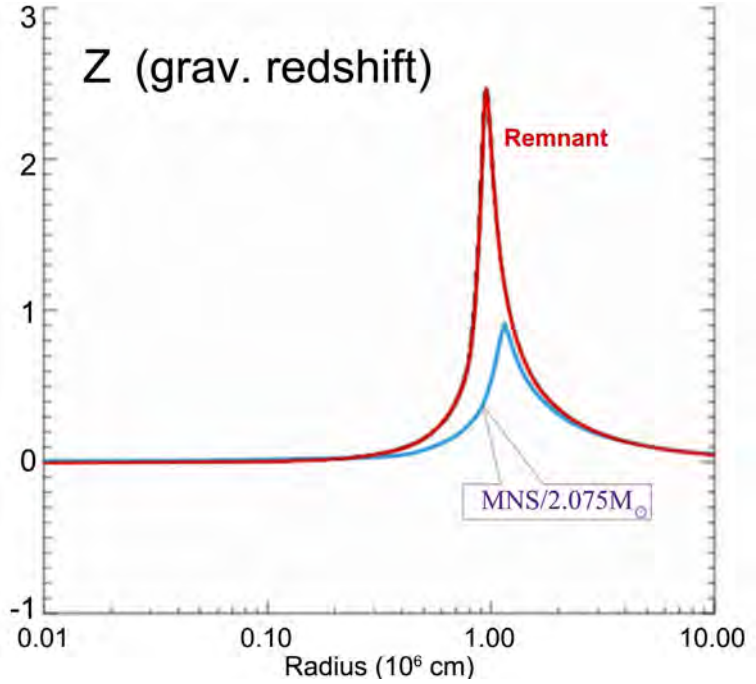


**Figure 8.** The radial distribution of the gravitational redshift, $Z$, throughout the remnant and the surrounding space (red-colored) to be compared to that of a massive *NS* (MNS/blue-colored) with $\mathrm{MNS} = 2.075 M_{\odot}$. $Z$ at the surface of the remnant is roughly four times larger than $Z$ at the surface of the MNS.

giving rise to radiation emission that are strongly redshifted and may appear four times fainter than those emitted from the surface of massive and highly compact *NSs* (see **Figure 8**).

## 5. Summary

In this paper we have presented a model for the remnant of GW170817, which is based on the bimetric spacetime scenario of glitching pulsars. Accordingly, the core is made of incompressible superconducting, gluon-quark superfluid (Su-Su-matter) embedded in a flat spacetime, whereas the ambient compressible and dissipative medium is set to be imbedded in a Schwarzschild spacetime.

The present study relies on our previous investigation of the cosmic evolution of the Crab and Vela pulsars as well as on the topological change of spacetime inside pulsars as the driving mechanism for the glitch phenomena in pulsars.

Based thereon we have found that the remnant must have a total mass of $\mathcal{M}_{tot}^{rem} = 3.351 M_{\odot}$, a radius $R_{rem} = 10764\,\mathrm{km}$ and it should enclose a massive SuSu-core of $\mathcal{M}_{core}^{rem} = 1.7 M_{\odot}$. The matter inside the shell surrounding the core is compressible and dissipative and its stratification is dictated by the curvature of the embedding Schwarzschild spacetime. The massive object is deeply trapped in spacetime and the radiation emitted from its surface would be redschifted, reaching $Z \approx 3$, *i.e.* approximately 5 to 7 times more fainter than $Z$'s at the surfaces of normal *NSs*.

Thus the remnant is actually a *NS*, which has a massive SuSu-core overlaid by

a neutron-rich matter. On the cosmological time scale, when all secondary energies in the shell have exhausted[2], its compactness would saturate around one, thereby turning the object invisible and making it an excellent black hole candidate.

The dark energy in the SuSu-core of the remnant is predicated to be $0.85M_{\odot}$. This energy enhancement originates from the phase transition of the gluon field from microscopic scale inside separated baryons into the macroscopic scale, where the core behaves as a single quantum entity, but still hidden from the outside universe.

However, while the model is based on several reasonable assumptions, work must be still done to verify their validities, specifically:

- The existence of a universal maximum density and the state of pure incompressibility;
- The origin of gravitation and its hidden connection to entropy;
- The viability of the bimetric spacetime scenario inside pulsars;
- The mechanisms underlying the glitch phenomena in pulsars and young neutron stars.

Finally, similar to newly born pulsars, a significant part of the rotational energy prior to the merger should have been stored both in the core and in the overlying shell of the remnant. The resulting configuration is expected to considerable deviate from spherical symmetry and therefore serves a rich source for the emission of gravitational radiation with $\nu > 10^3$ Hz. However, this range of frequencies is far beyond the current sensitivity range of LIGO.

Moreover, when correlating the total entropy production to the revealed radiation power from GW170817, we find that the entropy is much below the expected value from an object of $2.78M_{\odot}$, irrespective of whether the remnant is a massive *NS* or a stellar BH [4]. Indeed, a massive entropy-free superfluid core may nicely explain the origin of the entropy deficiency here.

Assuming the next generation of high resolution observations would render our scenario reasonable, then current scenarios related to the fate of the first generation of *NSs*, the relatively small number of *NSs* and BHs in the Galaxy, the origin of dark matter and dark energy in the universe must be revisited.

## Conflicts of Interest

The authors declare no conflicts of interest regarding the publication of this paper.

## References

[1] Abbott, *et al.* (2019) *Physical Review X*, **9**, Article ID: 011001.

[2] Shibata, M., Fujibayashi, S., Hotokezaka, K., *et al.* (2017) *Physical Review D*, **96**, Article ID: 123012. https://doi.org/10.1103/PhysRevD.96.123012

[3] Margutti, R., Alexander, K.D., Xie, X., *et al.* (2018) *APJ*, **856**, L18. https://doi.org/10.3847/2041-8213/aab2ad

[2]Energies other than the rest one.

[4] Piro, L., Troja, E., Zhang, B., *et al.* (2019) *MNRAS*, **483**, 1912. https://doi.org/10.1093/mnras/sty3047

[5] Banagiri, S., Coughlin, M.W., Clark, J., *et al.* (2020) *MNRAS*, **492**, 4945. https://doi.org/10.1093/mnras/staa181

[6] Gill, R., Nathanail, A. and Rezzolla, L. (2019) *APJ*, **876**, 139. https://doi.org/10.3847/1538-4357/ab16da

[7] Abbott, B.P., *et al.* (2017) *APJ*, **848**, L12.

[8] Mooley, K.P., Frail, D.A., *et al.* (2018) *APJ*, **868**, L11. https://doi.org/10.3847/2041-8213/aaeda7

[9] Yu, Y.-W., *et al.* (2018) *APJ*, **861**, 114. https://doi.org/10.3847/1538-4357/aac6e5

[10] Hujeirat, A.A. and Samtaney, R. (2020) *Journal of Modern Physics*, **11**, 395-406. https://doi.org/10.4236/jmp.2020.113025

[11] Ai, S., Gao, H. and Zhang, B. (2020) *APJ*, **893**, 146. https://doi.org/10.3847/1538-4357/ab80bd

[12] Pooley, D., Kumer, P., Wheeler, C. and Grossan, B. (2018) *APJ*, **859**, L23. https://doi.org/10.3847/2041-8213/aac3d6

[13] Bedaque, P. and Steiner, A. (2015) *Physical Review Letters*, **114**, Article ID: 031103. https://doi.org/10.1103/PhysRevLett.114.031103

[14] Hujeirat, A.A. (2018) *Journal of Modern Physics*, **9**, 51-69. https://doi.org/10.4236/jmp.2018.91004

[15] Hujeirat, A.A. (2020) Why the Spacetime Embedding Incompressible Supradense Nuclear Matter Is Conformally Flat?

[16] Hujeirat, A.A. and Samtaney, R. (2019) *Journal of Modern Physics*, **10**, 1696-1712. https://doi.org/10.4236/jmp.2019.1014111

[17] Witten, E. (1984) *Physical Review D*, **30**, 272-285. https://doi.org/10.1103/PhysRevD.30.272

[18] LHCb Collaboration (2015) *Physical Review Letters*, **115**, Article ID: 072001.

[19] Alford, M., Braby, M., Paris, M.W. and Reddy, S. (2005) *APJ*, **629**, 969. https://doi.org/10.1086/430902

[20] Douchin, H.P. (2001) *A&A*, **380**, 151. https://doi.org/10.1051/0004-6361:20011402

[21] Hujeirat, A.A. (2018) *Journal of Modern Physics*, **9**, 532. https://doi.org/10.4236/jmp.2018.94037

[22] Capano, C.D., Tews, I. and Brown, S.M. (2019) Stringent Constraints on Neutron-Star Radii from Multimessenger Observations and Nuclear Theory.

Journal of Modern Physics, 2020, 11, 1799-1806
https://www.scirp.org/journal/jmp
ISSN Online: 2153-120X
ISSN Print: 2153-1196

# On the Quantization of Time, Space and Gravity

**Joseph Kongani Wamukoya**

Department of Science Physics, British School of Lomé, Lomé, Togo
Email: joseph.wamukoya@bsl.tg

**How to cite this paper:** Wamukoya, J.K. (2020) On the Quantization of Time, Space and Gravity. *Journal of Modern Physics*, **11**, 1799-1806.
https://doi.org/10.4236/jmp.2020.1111112

**Received:** October 4, 2020
**Accepted:** November 8, 2020
**Published:** November 11, 2020



## Abstract

We combine the de Broglie Matter Wave Equation with the Heisenberg Uncertainty Principle to derive an equation for time as a wave. This happens to be the first time that these two statements have been combined in this manner to derive an equation for time. The result is astounding. Time turns out to be a minuscule blob of quantum electromagnetic energy in perpetual angular momentum. From this time equation, we derive an equation for space which turns out to also predict a string (like the string of string theory). We then combine the time equation with the space equation to derive an equation for the inverse of quantum gravity which is also surprisingly electromagnetic in nature. This last statement implies that space is multidimensional and gravity in multidimensional space is not quantized, but its inverse (which is single-dimensional) is.

## Keywords

Heisenberg Uncertainty Principle, de Broglie Wave Equation, String Theory, Motion in a Gravitational Field Equation, Linear Displacement, Quantum Photon Energy

## 1. Introduction

In this paper, the goal is to mathematically derive fundamental quantum equations for time, space and inverse gravity. The three equations show that all three quantities are electromagnetic energy in nature. Since everything known so far can only exist in space and time and must occupy space, we can safely say everything is electromagnetic energy in nature. The mathematical manipulations also show that fundamental quantum energy is much smaller than the known quantum photon energy ($hf$). It turns out that the new tiny energy is the inverse

of the photon energy; that is, ( $\frac{1}{hf}$ ).

## 2. Quantum Equations

### 2.1. Derivation of the Equation of Time as a Wave

According to the Heisenberg Uncertainty Principle [1]:

$$\Delta E \Delta t \geq \frac{h}{4\pi} \tag{1}$$

The symbol ≥ suggests there is a limiting condition when:

$$\Delta E \Delta t = \frac{h}{4\pi} \tag{2}$$

We can drop the delta symbol the same way we do when calculating tunneling time and express it as:

$$4\pi E t = h \tag{3}$$

Also according to the de Broglie Matter Wave Equation [2]:

$$\lambda = \frac{h}{mv} \tag{4}$$

which is called the "de Broglie wavelength" for every particle moving at a velocity $v$ as seen by a stationary observer [3]. This can be rewritten as:

$$\lambda mv = h \tag{5}$$

Since the $h$ in Equation (3) is the same as ($h$) in Equation (5), we can equate these two equations to get the following:

$$4\pi E t = \lambda mv \tag{6}$$

Since the $mv$ on the right-hand side of Equation (6) represents momentum, the energy ($E$) on the left-hand side of Equation (6) must be kinetic for the two sides to balance and make sense. Both sides of the equation must be dynamic in nature.

Making time ($t$) to be the subject of the equation we get:

$$t = \frac{\lambda mv}{4\pi \frac{1}{2} mv^2} \tag{7}$$

Equation (7) reduces to:

$$t = \frac{\lambda}{2\pi v} \tag{8}$$

This equation establishes the following:

- Time is a wave since it has a wavelength ( $\lambda$ ).
- Since wavelengths are the "number of units of length per wave" [4] and are countable in whole numbers, we can say that time is made up of whole number wavelengths ($n$).

We can therefore write Equation (8) as:

$$t = \frac{n\lambda}{2\pi v} \quad \text{where} \quad n = 1, 2, 3, \cdots \tag{9}$$

But we know, from $v = \lambda f$ , that:

$$\frac{h}{v} = \frac{1}{f} \tag{10}$$

So Equation (9) becomes:

$$t = \frac{n}{2\pi f} \tag{11}$$

Since frequency is the number of wavelengths per unit time [5], the ($n$) in Equation (11) still makes sense since it now refers to the countable number of wavelengths per unit time.

## 2.2. Derivation for the Angular Momentum Equation

Let there be $n$ wavelengths of a standing wave on the circumference of a circle; see **Figure 1**.

Then the circumference of the circle is an integral number ($n$) of wavelengths [6]:

$$n\lambda = 2\pi r \quad \text{where } r \text{ is the radius of the circle} \tag{12}$$

Rewriting gives:

$$\lambda = \frac{2\pi r}{n} \tag{13}$$

But from de Broglie's Matter Wave Equation in Equation (4):

$$\lambda = \frac{h}{mv}$$

Equating Equation (4) to Equation (13) we get:

$$\frac{2\pi r}{n} = \frac{h}{mv} \tag{14}$$

After cross-multiplying:

$$nh = mvr(2\pi) \tag{15}$$

Dividing both sides by (2π) yields:

$$\frac{nh}{2\pi} = mvr \tag{16}$$

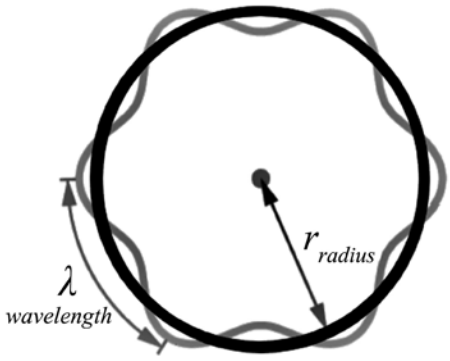


**Figure 1.** Standing wave on a circle.

But we know that ($mvr$) is angular momentum [7]; therefore, $\frac{nh}{2\pi}$ is angular momentum.

We can now turn Equation (11) into an equation of energy since the ($f$) in the denominator on the right-hand side of Equation (11) is a proxy symbol for quantum energy. Similarly, the term $\frac{n}{2\pi}$ on the right-hand side of Equation (11) is also a proxy for angular momentum.

Multiply the right-hand side of Equation (11) by $\frac{h}{h}$ so that:

$$t = \frac{n}{2\pi f} \times \frac{h}{h} \tag{17}$$

This can be written as:

$$t = \frac{nh}{2\pi} \times \frac{1}{hf} \tag{18}$$

In Equation (18), the first term is angular momentum and the second term is the inverse of a bundle of quantum energy.

Equation (18) can be reduced to:

$$t = \frac{nh}{2\pi E} \tag{19}$$

From the above equation, we can see that:

- Time is quantized because of the ($n$).
- We also see that the elementary bundle of energy is the inverse of the bundle of the photon. We could baptize it as an "inverquant".

### 2.3. Derivation of the Equation for Quantum Space

Equation (9) can be written as:

$$tv = \frac{n\lambda}{2\pi} \tag{20}$$

Space in a single direction can be defined by a line which is linear displacement; defined as the movement of an object in a particular direction over a certain distance [8]. This is given by:

$$vt = d \tag{21}$$

Substituting ($d$) for ($vt$) in Equation (20) and multiplying the RHS by $\frac{h}{h}$, we get:

$$d = \frac{n\lambda}{2\pi} \times \frac{h}{h} \tag{22}$$

But we know that:

$$\lambda = \frac{v}{f} \tag{23}$$

Replacing ( $\lambda$ ) in Equation (22) by $\frac{v}{f}$ gives:

$$d = \frac{nh}{2\pi} \times \frac{v}{hf} \tag{24}$$

This can be reduced to:

$$d = \frac{nhv}{2\pi E} \tag{25}$$

This implies the following:

- Space is quantized with a combination of angular momentum represented by the term $\frac{nh}{2\pi}$.
- This angular momentum is combined with linear velocity ($v$). Hence, this combination might produce wobbling motion of the inverse of a bundle of photon energy. This might resemble the motion of a string as suggested in string theory [9]:

$$\frac{1}{E} = \frac{1}{hf} \tag{26}$$

## 2.4. Derivation of the Equation of Quantum Gravity

We use the equation of motion in a gravitational field for an object in free-fall near the Earth from rest position; see **Figure 2**.

The displacement is given as follows [10]:

$$d = ut + \frac{1}{2}gt^2 \tag{27}$$

Since the object falls from rest $u = 0$.

Then:

$$g = \frac{2d}{t^2} \tag{28}$$

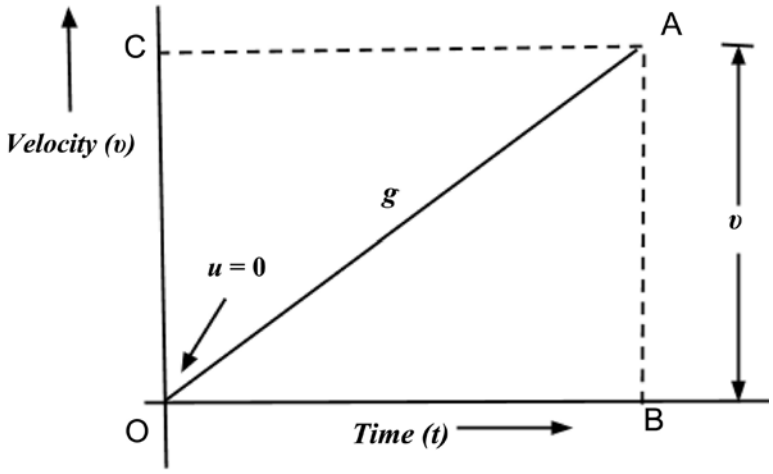


**Figure 2.** The area of the velocity-time graph gives the object's displacement.

By Equation (25), we see that:

$$2d = \frac{2nh\nu}{2\pi E} \tag{29}$$

By Equation (18), we can write:

$$t^2 = \frac{n^2h^2}{4\pi^2E^2} \tag{30}$$

Now substituting Equation (29) and Equation (30) in Equation (28) gives:

$$g = \frac{nh}{2\pi} \times \frac{2\nu}{hf} \times \frac{4\pi^2}{n^2h^2} \times h^2 f^2 \tag{31}$$

It reduces to:

$$g = \frac{2\pi}{nh} \times 2\nu \times hf \tag{32}$$

Equation (32) does not show quantization since the ($n$) that allows counting is in the denominator with the irrational pi in the numerator. This suggests that gravity is not quantized. However, on turning Equation (32) upside down by getting its inverse, we can write:

$$\frac{1}{g} = \frac{nh}{2\pi} \times \frac{1}{2\nu} \times \frac{1}{E} \tag{33}$$

Equation (33) is quantized, so the inverse of gravity is quantized.

But what is the inverse of gravity?

Does this not suggest that gravity is a value obtained from all the dimensions of space so that ($\frac{1}{g}$) appears to be the fraction of ($g$) we obtain when we consider only one dimension of that gravity? This then suggests gravity is multidimensional and that only a single dimension out of the total is quantized. This implies that gravity has many dimensions but if one dimension is singled out of the many, that is ($\frac{1}{g}$), then the single dimension of ($g$) becomes quantized.

## 3. Concluding Remarks

We set out to mathematically demonstrate that time, space and inverse gravity are quantized. We were also interested in establishing the fundamental nature of the three quantities. From our mathematical derivations, we can conclude the following:

1) We have just mathematically shown that time, space and inverse gravity are quantized.

2) It has also been established that each of the three quantities is fundamentally electromagnetic energy in nature.

3) We have shown that this energy is dynamic in the sense that it is perpetually in angular momentum.

4) We have also shown that while gravity is not quantized, its inverse is.

5) We further interpret the inverse of gravity to mean a fraction of gravity; that is $(1/g)$. This seems to suggest that $(g)$ is a collective value combining several dimensions such that if only one of those dimensions is considered, that is to say $(1/g)$, or 1 out of $(g)$, then the result becomes quantized.

6) On the basis of this latter argument, we have concluded that each of the three quantities is quantized with a caveat that $(g)$ is quantized if only a single dimension of gravity is considered. This statement assumes that gravity is multi-dimensional in nature as evidenced by our mathematical manipulations and subsequent interpretation.

7) We also conclude that the energy is much smaller than quantized photon energy which is $(hf)$. We establish that the quantum energy for each of the three quantities is $\left(\frac{1}{hf}\right)$.

## Conflicts of Interest

The author declares no conflicts of interest regarding the publication of this paper.

## References

[1] Heisenberg, W.K. (1927) *Zeitschrift für Physik*, **43**, 172-198. https://doi.org/10.1007/BF01397280

[2] Logiurato, F. (2014) *Journal of Modern Physics*, **5**, 1-7. https://doi.org/10.4236/jmp.2014.51001

[3] Butto, N. (2020) *Journal of High Energy Physics, Gravitation and Cosmology*, **6**, 567-578. https://doi.org/10.4236/jhepgc.2020.64038

[4] Hecht, E. (1987) Optics. 2nd Edition. Addison-Wesley, Boston, 15-16.

[5] Leckey, C.A., and Banerjee, S. (2020) Computational Nondestructive Evaluation Handbook: Ultrasound Modeling Techniques. CRC Press, Boca Raton. https://doi.org/10.1201/9780429456909

[6] Goel, A. (2006) Wave Mechanics. Discovery Publishing House Pvt. Limited., India.

[7] Edmonds, A.R. (2016) Angular Momentum in Quantum Mechanics. Princeton University Press, Princeton.

[8] Richards, J. (2018) The Comprehensive Textbook of Biomechanics. Elsevier Health Sciences, Netherlands.

[9] Salem, M. (2015) *Journal of Modern Physics*, **6**, 374-380. https://doi.org/10.4236/jmp.2015.64040

[10] Mohazzabi, P. and Kohneh, Z.A. (2005) *The Physics Teacher*, **43**, 114-115. https://doi.org/10.1119/1.1855750

## Nomenclature

$d$: Displacement
$f$: Frequency
$g$: Gravitational constant
$h$: Planck's constant
$m$: Mass
$t$: Time
$u$: Initial velocity
$v$: Velocity
$\Delta E$: Uncertainty in energy
$\Delta t$: Uncertainty in time
$\lambda$ : Wavelength

Journal of Modern Physics, 2020, 11, 1807-1826
https://www.scirp.org/journal/jmp
ISSN Online: 2153-120X
ISSN Print: 2153-1196

# Experimental Ferrogravitational Field around Untwisting Closed Superconductor

**Robert A. Sizov**

Individual Researcher, Moscow, Russia
Email: sizov.robert@gmail.com

**How to cite this paper:** Sizov, R.A. (2020) Experimental Ferrogravitational Field around Untwisting Closed Superconductor. *Journal of Modern Physics*, **11**, 1807-1826.
https://doi.org/10.4236/jmp.2020.1111113

**Received:** October 15, 2020
**Accepted:** November 10, 2020
**Published:** November 13, 2020





## Abstract

The study by the author of magnetic scattering neutrons in the structures of ferrimagnets, as well as his experiments with the separation of magnetic charges in dipole pairs ±g in magnetic field, showed that fundamental magnetic particles (magnetic charges) are real structural components of atoms and substance. It is the magnetic poles, and not the moving electric charges are the direct sources of all magnetic fields and magnetic manifestations in Nature. Basic reasons of ignoring the magnetic fundamental particles by world physical theory, for almost 150 years, are the ultra-harsh confinement of these particles in substance which radically is different from the confinement electrons, as well as the vicious concept of the electric magnetism Maxwell. Rotating magnetic dipoles in conductors which are untwisted by electric current, are direct sources of the vortex magnetic field $\mathrm{rot}\boldsymbol{H}$. One should also expect the formation of a vortex electric field $\mathrm{rot}\boldsymbol{E}$ forming by rotating electric dipoles which are untwisted by the current of magnetic charges. This article provides an experimental answer to the question: what field is formed around a conductor if joint direct currents of electric $\boldsymbol{J}_{\mathrm{e}}$ and magnetic $\boldsymbol{J}_{\mathrm{g}}$ charges are passed through it? The author's experiments have shown that in this case the vortex electromagnetic current is realized which manifests itself as the vortex electromagnetic (gravitational) field. It is possible to implement such a process, according to the results of the author's research, exclusively in superconductors. The vector character of the gravitational field is in many respects similar to the vortex magnetic field which makes it possible to introduce such it states as paragravitation and ferrogravitation into representations. To create joint currents of electric and magnetic charges, the author used the inertial forces of these particles under conditions of acceleration and deceleration of the rotational motion of the closed lead superconductor. The result of this experiment was the gravitational, as it turned out later, the ferrogravitational field, which was detected by effect repulsion of trial cargos from the coil with a superconducting winding at the stage of its untwist. The

latter process is defined by the author as an effect of the gravitational (ferro-gravitational) levitation. The values of ferrogravitational (levitational) forces noted in this experiment were: 120 mg for a tungsten trial cargo and 50 and 25 mg for a lead cargo with an error of ±15 mg. The values of ferrogravitational (levitational) forces noted in this experiment are: 120 mg for from tungsten trial cargo and 50 and 25 mg for a cargo from lead, with an error of ±15 mg. The "anomaly" noted by the author in this study was in the absence of any absence of a gravitational effect on stage a braking of the coil. Probable cause of the noted "anomaly" is discussed in the Discussion of Results chapter.

## Keywords

Magnetic Charges, Magnetons, Antimagnetons, Magnetic Dipoles, True Antielectrons, S-Gravitons, Gravitational Field, Ferro- and Paragravitation, Gravitational "Dark Energy", Gravitational Levitation

## 1. Introduction to the Physics of Magnetic Charges and True Antielectrons in Composition of Substance

The author's experimental and theoretical studies which have been carried out since 1968 have shown that magnetic poles (magnetic charges) are real structural components of atoms and substance [1] [2] [3] [4] [5]. It is magnetic charges, but not moving electrons are the direct sources of all magnetic fields and magnetic manifestations in Nature. The charges of magnetic spinor particles (g) which together with electrons and true antielectrons form a shells of atoms, correspond condition g = e, where e is the electron charge. Magnetic charge with negative sign g-received the author's name magneton (not to be confused with the so-called magneton of Bohr). By antiparticle to a magneton is the antimagneton with positive magnetic charge $g^+$. The main state of fundamental magnetic charges in Nature, as well as electric charges, is its existence in composition of the corresponding bispinors, which most often appear in the form of dipoles [6].

**Note 1.** The bispinor is a pair of spinor particles, *i.e.* charged particles, in the composition: a spinor and a corresponding antispinor. Spinors are, for example, electrons and magnetons. Antispinors are fundamental particles with a positive charge, such as true antielectrons and antimagnetons. In the absence of external influences the bispinor, as a result of close contact in a pair of constituent it particles, is in a state complete closure a spins. In this case, complete mutual compensation of the spinor fields of the particles that make up the bispinor is realized, which, in this state, does not manifest itself by the external spinor fields, *i.e.* are practically undetectable. It is the noted effect of complete spin closure in the interaction of an electron with a positron that is the cause of such a global theoretical delusion as the annihilation of particles in a particle-antiparticle pair.

Under the influence of the electric current $\boldsymbol{J}_e$ the vortices of the above-mentioned magnetic dipoles are realized in the conductor which is described by the

expression $\mathrm{rot}\boldsymbol{J}_g$, and the equation of the process of their formation has the form:

$$k_1\boldsymbol{J}_e = \mathrm{rot}\boldsymbol{J}_g. \quad (1)$$

It is the vortices of magnetic charges formed in conductor under the influence of an electric current are direct sources of the vortex magnetic field $\mathrm{rot}\boldsymbol{H}$, the formation of which is described by the equation

$$k_2\mathrm{rot}\boldsymbol{J}_g = \mathrm{rot}\boldsymbol{H}. \quad (2)$$

The well-known, so-called first Maxwell's equation

$$k\boldsymbol{J}_e = \mathrm{rot}\boldsymbol{H}, \quad (3)$$

is extremely erroneous, since it combines into a single action two physically different processes mentioned above. This equation appeared as a result of the superficial impression of the Great Theoretician from the famous Experience of Oersted [7].

Unfortunately, at the time of the formation of his vicious electromagnetic concept and the introduction of the super-harmful Equation (3) in 1873, Maxwell, apparently, did not even assume that real magnetic poles could exist in Nature. It is also important to emphasize here that moving electric charges in the described process (1) are just intermediaries, whose role is, exclusively, in the unwinding of vortices of magnetic dipoles actually existing in the conductor [8] [9]. The aforementioned Great misconception by Maxwell led to numerous errors in physical science, giving rise, for example, to such a vicious theoretical direction as relativism.

The first person to experimentally observe real magnetic charges in a substance was the remarkable Austrian physicist Felix Ehrenhaft. Based on the results of his research which lasted for more than 40 years, he published about 30 articles in physical journals [10]. It is important to note that Ehrenhaft's experiments were repeated by numerous followers who confirmed his results and conclusions (see, for example [11]).

The Ehrenhaft experiments are a magnetic analog of well-known Milliken tests from determining the value of the electron charge. Very small particles of solids substance were placed in a vertical uniform magnetic field free of residual electrical charges. The particles were illuminated by concentrated beam of light. The optical system allowed to determine the parameters of the particles movement. The basic experimental result of investigation Ehrenhaft consisted in the fact that it was found a logical movement of particles along power lines of the magnetic field. With the change in the direction of the field, the direction of movement of the particles also was changed. According to conclusions Ehrenhaft motions of particles, that observed in his experiments, are determined their charging by the magnetic charges of different signs.

Experimental and theoretical studies of the author, with compelled interruptions, have been carried out since 1968 have shown that electrons and magnetic charges in a normal conductor are under conditions of radically different phys-

ics of their confinement. Electrons populate real conduction bands which allow them to participate in the composition of the electric current. As for magnetic charges that are not included in atomic structures, they are in potential zones of conduction and their movement in a normal conductor is possible only in the processes of the noted rotations around the lines of electric current.

However, the situation with the confinement of magnetic charges in conductors, changes dramatically under conditions of superconductivity when these charges leave potential zones and pass into real conduction zones. In this case, magnetic dipoles, in the process of their rotation around the electric current lines, do not experience "friction" against the superconductor lattice, what and determines its zero electrical resistance or superconducting effect. It is important to note that true anti-electrons ($e^+$), along with the magnetic charges, as well as are in substance under hard confinement conditions.

The author's research has shown that the positron is not an anti-electron, as it follows from modern physical concepts, since represents the mass, *i.e.* atomic-like structure. As for the true antielectron, it "sits" in the positron as a nucleus and determines its positive charge $e^+$ [12] (see also [6]).

The conditions for the confinement of electric and magnetic charges in a substance are presented in **Figure 1**, which shows the layout of the levels of electrons, true anti-electrons and magnetic charges (magnetons and anti-magnets) on the energy scale. As you know, electronic levels are in a potential "well" and for an electron to come out into a free state from connection with the conductor lattice, it is necessary to increase its internal energy, for example, by heating. As for the magnetic charges and true anti-electrons, their energy levels are located under the potential "dome" and for these particles to enter the free state, the substance should be cooled, *i.e.* reduce his internal energy.

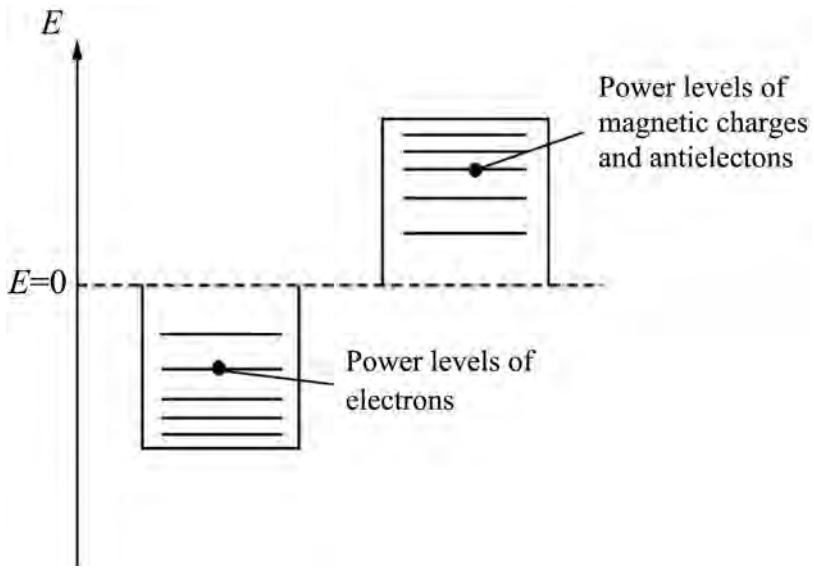


**Figure 1.** Schematic diagram of the location on the energy scale of the levels of electrons (in the energy well) and magnetic charges with true anti-electrons (under the energy dome).

At deep stages of cooling of some substances, their superconducting state is realized, which associated with exit of magnetic charges and true antielectrons into a state free from coupling with the superconductor lattice. It is the special conditions of the confinement of magnetic spinor particles, as well as of true antielectrons in substance noted above that played a very "cruel joke" with the physical theory, which manifested itself, for example, in the form vicious electric magnetism of Maxwell.

It is important to note that the vicious ignoring of real magnetic charges, as well as true electrons, did not pass without a trace for the existing physical theory. These unrecognized fundamental particles were perforce replaced, more or less, by suitable theoretical surrogates. For example, magnetic charges in atomic shells were substitute with such "fig leaves" as the magnetic moments of electrons (3d or 4f), and the true antielectrons by Dirac holes or electron vacancies [13] [14].

According to the author of the article, the famous Dirac monopole should also be referred to the above-mentioned surrogate-substitutes for real elementary particles. The position taken by Dirac in questions related to magnetic poles is more than strange. On the one hand, he argues that it would be surprising if nature did not use this possibility, that is, the realization of magnetic poles in the structures of substance and showed, that quantum electromagnetic theory fully admits their existence. But, on the other hand, it fills its monopole with a magnetic field, which is created in ultra-thin filaments-solenoids fed by electric current. Thus, if to remove the filaments-solenoids of Dirac, *i.e.* if you disconnect the monopole from the source of electric current, then the magnetic monopole will not be able to be realized. In other words, despite lofty goals, Dirac and his magnetic monopoly failed to avoid being infected by the vicious Maxwell virus. In addition, the magnetic field emitted by the Dirac monopole can only be a vortex field, which is described by vortex vector $\mathrm{rot}\boldsymbol{H}$, since only such a magnetic field can be formed around a conductor with a constant electric current. It is also important to note that Dirac did not associate his monopole with magnetic fields and magnetic manifestations which surround man, because he did not see any prospects for this [15].

At the end of the seventies (1979), the author asked himself an interesting question, what can happen if we pass joint linear currents of electric and magnetic charges through a superconductor? Of course, there are no problems with the implementation of electric current, but where to get the source of the current of magnetic charges? The solution to this problem was the use of inertial forces of magnetic and electric charges in the conditions of untwist or braking a coil with a closed winding from of the superconducting wire. The author assumed that if you spin a closed loop of a superconductor and then abruptly stop its rotation, then due to inertial forces in the superconductor, joint currents of electric and magnetic charges are realized, *i.e.* an electromagnetic current is generated. In this process, as the author assumed, these currents will not remain linear, but their mutual twisting will occur with the formation of an eddy electromagnetic

current, which, most likely, will manifest itself as a vortex electromagnetic (gravitational) field.

The fact that magnetic charges have the property of inertia is evidenced, for example, by the effect of self-induction. The fact that after removing the electrical voltage in the conductor, for some time, the electric current is maintained, according to the author, is determined by the inertia of magnetic charges in the composition eddy dipole currents involved in the process of self-induction according to the equation $k\mathrm{rot}\boldsymbol{J}_{\mathrm{g}} = \boldsymbol{J}_{\mathrm{e}}$ [16].

## 2. Experimental Ferrogravitational Field around Untwisting Closed Superconductor

### 2.1. Experimental Technique

The schematic diagram of the setup on which dynamic experiments were performed to create joint currents of electric and magnetic charges in superconductors using inertial forces, is shown in Figure 2. The setup was a large helium cryostat (1), 140 cm high with reinforced wall of the inner (helium) vessel. In the lower part of the inner vessel, on a rolling bearing 2, a coil 3 with windings consisted of lead wire 0.8 and 1 mm in diameter. As part of the coil windings, both one section with a wire with a diameter of 0.8 mm (**Experiment I**) and two

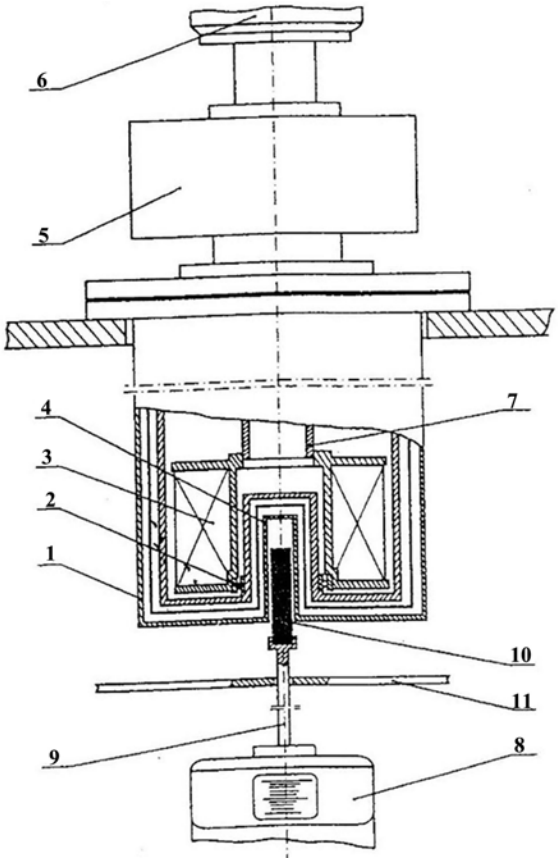


Figure 2. Schematic of experimental setup for obtaining a vortex electromagnetic (gravitational) field by means of a rotating superconductor.

independent sections with a wire diameter of 1 mm (**Experiment II**) were implemented.

In order to connect the ends of the winding in each section, they were welded in an inert atmosphere. No surface insulation of the wire was made. The coil, after winding and securing the wire, was carefully balanced. The "appendix" 4 was made in the lower part of the cryostat, allowing the introduction of a "warm atmosphere" into the coil cavity. A wedge-type braking device 5 and an electric motor 6 (1.5 kW and 2900 rpm) were installed on the cryostat cover. The transmission of rotation from the electric motor to the coil was carried out by means of a stainless steel pipe 7.

The electromechanical balance 8 with a weighing accuracy of ± 10 mg served as an indicator of the expected effect. On the movable part of the balance, on an aluminum rod 9, cylindrical weights 10 of tungsten and lead with a diameter of 16 mm and a length of 70 mm were fixed. The cargos were inserted into the "appendix" so that a third of their length would enter the coil cavity. To exclude parasitic influences on the balance mechanism, a screen 11 made of "Armco" iron sheets was installed between the cryostat and the balance.

The technology of the experiments was as follows.

After filling the cryostat with liquid helium to a level exceeding the top of the coil, the cryostat-coil system was held for ~15 minutes to equalize the temperature. Then the coil was spun up to the maximum engine speed. After holding in this mode for 10 - 15 seconds, the coil rotation was abruptly stopped by means of the braking device. The untwist time of the coil to the maximum speed was, according to the author's estimate, 2 - 2.5 seconds, and the time the stop of rotation was ~1.5 seconds. The effect of changing the weight of the cylindrical cargos in the course of the experiment was recorded visually on a scale of the balance.

In total, two complete experiments were carried out, in which from 4 to 5 cycles were implemented (unwinding-braking). The limited number of experiments was explained, in particular, by the high consumption of liquid helium, especially in the dynamic part of the experiments. After each cycle, it was necessary to add helium again, cool and hold the system to equalize the temperature.

## 2.2. Experimental Results

**Experiment I.** The coil winding consisted of one closed section with lead wire of 0.8 mm in diameter. The total weight of lead in section is 14.2 kg. In the course of the experiment, 4 cycles were performed (untwist-braking). In none of the noted cycles was there any change in the weight of the tungsten cargo, both at the stage of untwisting and at the stage of braking.

**Experience II.** The coil winding consisted of 2 independent sections with wire of diameter of 1 mm. The total weight of the wire in the 2 coil sections was 15.3 kg. During the experiment 5 cycles were performed (untwisting-braking): 2 cycles with tungsten cargo and 3 cycles with lead cargo.

In none of the five cycles of the experiment was any reaction of the scales observed at the stage of braking the rotation of the coil, although it was at this stage

that the appearance of the gravitational effect was expected. At the same time, at the stage of untwist the coil, a clear and very significant reaction of the balances was found. Two reliable changes in the weight of the cargos were noted: one in the 1st cycle of the experiment with a tungsten cargo (ΔP = 120 ± 15 mg) and one in the 3rd cycle with a lead cargo (ΔP = 50 ± 15 mg). The maximum error in estimating the change in the weight of the cargos (±15 mg) was adopted by us proceeding from the instrument error of the balance (±10 mg), plus a possible error (±5 mg) in the visual reading of ΔP on the scale of the balance under the conditions of the fast dynamics of the experiment.

The noted effects, which, no doubt, were of a gravitational nature, were, at first, qualified by the author as the attraction of the weights to the coil, in accordance with the well-known law of universal gravitation. Problems with the sign of the observed gravitational effects, *i.e.* the attraction or repulsion of cargos that occurred in this pilot study are described in detail in the Discussion of Results below.

Changes in weights of the cargos from W and Pb which were obtained by the author in conditions of primary fixation of effect on visual observation of scale of the weights, are shown in Figure 3 by the dotted lines. In addition, in Figure 3, by means of bold solid lines, the nature of these changes is shown after clarifying the sign of interactions between the cargos and coil using the results of subsequent experiments by the author. These latest results indicate that under the conditions of the described **Experiment II** only of the ferrogravitational field is realized around the superconductor. The essence of vector States of the gravitational

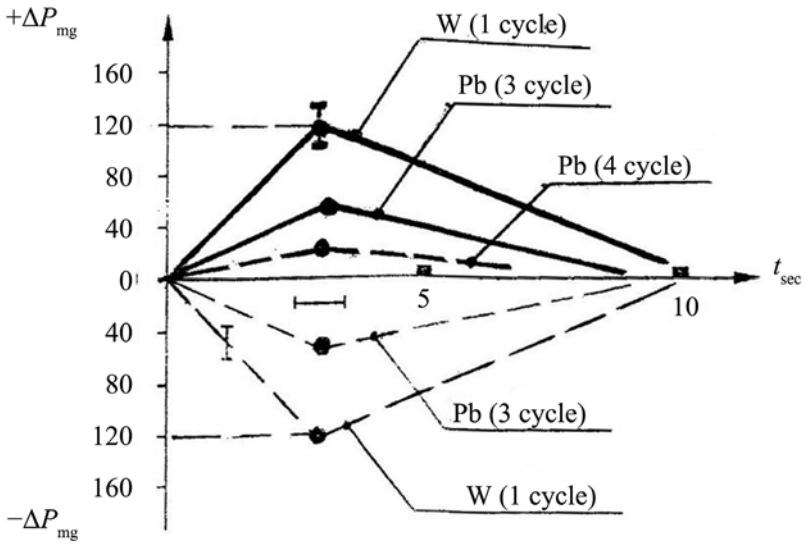


Figure 3. Values of changes in the weights (ΔP) of tungsten and lead cargos found in the author's experiments with rotating superconductors. The shows the nature and magnitude of the change in ΔP of the weights (vertical axis) as a function of time *t* from the moment the untwist began (plotted along the horizontal axis). A possible error in determining the time in the noted process is estimated by us as ±0.5 sec. The values of reliable changes in weights of the cargos turned out to be very significant (120 and 50 mg with an error of ±15 mg).

field formed based on the results of the author's experimental research, is presented in Section 4 of the article.

The behavior of the scales in the 4th cycle of the experiment with a lead weight turned out to be peculiar. In this cycle, it was not a decrease in the weight of the weights that was observed, but its increase, which corresponds to pushing the weight out of the coil cavity at the stage of untwist. The noted value of ΔP in this case was 25 ± 15 mg. The effect of the weight repulsion from the rotating coil was reliably detected as a result of the fact that the zero division of the scale of the balance fell into a single field of view together with the value ΔP of the weight change.

In connection with the small value of this last effect and the strange sign of interaction, from the point of view of existing gravitational concepts, the author initially considered it as a kind of parasitic effect or "strange tendency". However, it was noticed that as the coil continued to spin, this "strange tendency" disappeared in about the same ~10 seconds as with the other weight changes noted above.

It is important to note, paradoxical as it may seem, but it was the last "tendency" that served as the basis for the author to revise his initial impressions of the described experiment and to conduct further experimental studies to clarify a real sign of the gravitational impact which was noted in the article.

In cycles 2 and 5 of **Experiment II**, no weight reactions were observed even at the trend level.

**Note 2.** The experiments with rotating superconductors presented in the article were carried out by the author in 1979-1981 on the territory of the Institute of Theoretical and Experimental Physics (building 7) in Moscow. The subsequent experiments of the author on the creation of a magneto-moving force (MMF) and constant current of magnetic charges ( $\boldsymbol{J}_g$ ) in superconductor, on the basis of which the s were clarified of the real signs of above the gravitational effects, were presented on Russian in publications of the author [17] and in [5] and, briefly, on English in [3]. In addition, an English-language publication is currently being prepared with a detailed description of these very important and informative experiments.

The reasons that delay the timely publication of the results of this very important and effective experiment in physics journals are set out below in the Discussion of Results section.

### 2.3. The Discussion of the Results

It is important to note that the experiments presented in the article had the main goal of obtaining an answer to the question: does the effect take place within the framework of this technology, and if so, then conduct a detailed study of it in subsequent experiments. In addition, an important point here was testing working capacity the setup in real experimental conditions. Namely, the circumstances described above and the goals associated with the conduct of this experiment are an explanation for the author's insufficient attention to such an im-

portant parameter of a possible gravitational manifestation as its sign.

Changes in the weights of the cargos found in **Experiment II**, according to the author, indicate the presence of a matched eddy electromagnetic current in the superconducting winding of the coil, which is realized in the process of its untwist and manifests itself through the vortex electromagnetic (gravitational) field. The observed effects are related precisely to the dynamics of superconductors, since preliminary tests performed on the facility at temperatures of 293 and 80˚K were negative.

Below in this chapter important aspects related to this study are considered, the clarification of the circumstances of which contributed to the successful interpretation of the experimental results by the author.

1) First of all, the manifestation of gravitational effect at the stage of untwist the coil was unexpected. It was assumed that this effect should be expected at the stage of braking. This "strangeness" can be explained by the differences in the conditions of confinement of magnetic and electric charges at the indicated stages of the experimental process. Before untwist the coil the conditions of confinement of magnetic and electric charges in the conduction band of the superconductor are presented to be quite close, what suggests the possibility of realizing a stable mutual ordering of charges in the eddy electromagnetic current during the movement the superconductor lattice. It is under such conditions that one can expect the formation of a stable EM-current and, consequently, the manifestation of the gravitational effects in the form of the change in the weights of the cargos. Under the conditions of the maximum revolutions of the coil and keeping it in this rotation, the conditions for holding magnetic and electric charges in the superconductor lattice can differ significantly, what will prevent the formation of a stable matched EM-current.

2) The value of the change in the weight $\Delta P$ of the tungsten cargo, noted in the experiment, significantly exceeds the corresponding value noted for the lead cargo, which testifies in favor of the gravitational nature of the observed effects (specific weights: W—19.30, Pb—11.34 g/cm$^3$). At the same time, it was noted that for equal conditions for the manifestation of the gravitational effect, the change in the weight of the lead weight would have to be 70.5 mg, if we take into account that for tungsten this change is 120 mg. By the explanation of the latter circumstance is the exit of the upper section of the coil from the superconducting state. The weights of the coil winding sections, measured after the experiment, were: 10.2 kg for the lower section and 5.1 kg for the upper section. Thus, the version of disabling the upper section from the realization of the effect is quite possible, since the calculated gravitational effect with its participation could be 47 mg. Recall that the value of the measured $\Delta P$ for the lead cargo in the third cycle of **Experiment II** was 50 ± 15 mg.

3) The collision noted in Chapter 2.2 with of the manifestation of the so-called the "strange tendency" in the 4th cycle of **Experiment II** requires a thorough explanation. As noted above, **Experiment II**, which followed negative **Experiment I**, had its main purpose to determine whether there was any effect within

the framework of this experiment or not? Therefore, all attention during visual observation of the scale weights was focused on fixing the magnitude of the change in the weight of the cargos (ΔP) and of the time parameters of the process of these changes. At the same time, the sign of the change in the weights ΔP of the weights remained outside the author's line of attention, under the conditions of a rapidly running experiment, *i.e.* the question of what takes place in this experiment: the attraction of cargo by a coil or their repulsion. The last question did not seem to the author to be any significant, considering that this experiment was carried out in 1981. At that time, the author was firmly convinced that the only possible gravitational manifestation here could be solely the attraction of the cargo to coil, in accordance with the law of the world gravitation. In addition, a feature of the scale of the balance used was that zero division of the scale and values ΔP of the weight changes of the cargos in cycles 1 and 3, did not fall into the single field of view of the observer. As for cycle 4 in **Experiment II**, so the magnitude of the change in the weight of the lead cargos ΔP and the zero division of the scale of the balance were within the framework of a single visual field, what and led the author to discover of the noted "anomalous tendency". The subsequent resolution of the issue with the "anomalous tendency", which lasted for more than 20 years, led the author to the discovery of such important states of the gravitational field as paragravitation and ferrogavitation, as well as to effect of the gravitational (ferrogravitational) levitation [18] [19].

4) Due to the large mass of substance participating in the presented dynamic experiment, as well as the relatively small ΔT˚ K between the temperature of liquid helium (4.2˚ K) and the temperature of the superconducting transition of lead (7.2˚ K), gravitational effects which manifested in the Experiments, according to the author are turned out to be in an acute dependence on local temperature conditions in the volume of lead windings. Very critical condition for the realization of the expected electromagnetic current is the provision of superconducting conditions at the points where the ends of the coil windings were closed (fused). It is the local exit of parts of the coil winding from the superconductivity mode that, according to the author, is a possible reason for the absence of the effect in **Experiment I**, as well as in cycles 2 and 5 of **Experiment II**. Local violations of the superconducting state regimes in the coil windings can also serve as an explanation for the observed mismatches in the measured ΔP values in the effective cycles of **Experiment II**.

**Note 3.** It should, with regret, add that the author was unable to continue his experiments with rotating superconductors within the framework of the experimental technology described above and, therefore, to repeat and investigate the discovered effects, in result of change his working situation in 1982. This change was, in many ways, a consequence of his so-called "vicious hobby" for the search for real magnetic charges in atoms and substance. Under new circumstances the author was able to continue his research, but in a more modest experimental scales and was able, using other approaches, to explain the real physics of the "anomalous tendency" discovered in **Experiment II**. It should be added that it is

precisely the life circumstances noted above that are the reason that these subsequent studies by author stretched out for more than 20 years.

The introduction of real magnetic charges, as well as true anti-electrons into basic physics allowed the author to formulate the concept of the World Physical Triad (WPT) which is extremely important for physical science, according to which the real World formed by three fundamental phases: Matter, Antimatter and Energo-phase (Energo-medium). This concept introduces into Physics the such a physical essence as "Dark energy", *i.e.* a global force factor responsible for all effects on particles and masses existing in Nature. The WPT concept, as well as the important implications for fundamental physical theory arising from it, is briefly presented in Chapter 5.

## 3. Other Experiments with Rotating Superconductors

It is important to note that later and independently of the results of the experiments of the present author presented in the article experiments with rotating superconductors were performed by: Podkletnov E. and Nieminen R. in 1992 [20], as well as Tajmar M. and de Matos C. in 2003 [21]. In these experiments, according to their authors, gravitational effects were obtained.

In [20] the experimental gravitational field was obtained using a rotating superconducting metal-ceramic disk in strong magnetic field. Our analysis of the results of these experiments suggests that the effects observed are of gravitational nature. Under the conditions of these experiments, an eddy electromagnetic current is formed in the superconductor, *i.e.* a system of polarized S-gravitons that manifest themselves through an experimental gravitational field. It is important to note that the gravitational field generated in experiments [20] is the ferrogravitational field, which manifests itself in the processes of repulsion of adjacent masses from the superconducting disk. In essence, this effect is the effect of gravitational levitation, discovered by the present author and described in his publications and in this article (see Chapters 4 and 5).

The gravitational manifestations in the experiment of Tajmar M. and de Matos C. [21], which were detected during the accelerated rotation of the superconducting niobium ring, were interpreted by the authors as a manifestation of the gravimagnetic field. According to the interpretation of the author of this article, noted in [21] so-called gravimagnetic effects are manifestations of the real gravitational, or more precisely, the ferrogravitational field. The latest results are in good agreement with the gravitational effects obtained in the studies of the present author. It should also be noted that the magnitudes of gravitational effects obtained in the author's experiments are more than $10^3$ times higher than the effects found in the study of Tajmar M. and de Matos C.

Experimental and theoretical studies of the author of the article related to the discovery and detailed study of real magnetic charges existing in atoms and substance have shown that the gravitational field is a vortex electromagnetic field and is formed in joint vortex processes of electric and magnetic charges (see Chapter 4).

However, the authors of the above other experiments when interpreting the results obtained, did not involve magnetic poles in their explanations, *i.e.* they, de facto, remained within Maxwell's flawed electromagnetic concept.

**Note 4.** In this article, the author named the date of his experiments with rotating superconductors 1979-1982. At the same time, the first official publication of their results was made only in 2001 (see [2]). The above date of these experiments, if any questions arise, can be confirmed by the technical specialists who participated with the author in the conduct of these experiments. The author presented the personalities of these specialists in the Acknowledgments section of this article.

## 4. Paragravitation and Ferrogravitation, Ferrogravitational Levitation, Physical Nature of Mass

The results of the experiments presented in the article, as well as other experimental and theoretical studies of the author, allowed him to establish the physical parameters and the place of real magnetic charges in the structures of atoms and matter. For example, the author showed that atomic shells consist of electric and magnetic spinor particles, the charges of which meet the condition e = g, and the shells themselves are electromagnetic, not purely electronic, as has always been believed [22] [23]. It is also important to emphasize that the number of magnetic spinor particles in atomic structures is approximately equal to the number of electrical particles. It is the electromagnetic shells of atoms that are natural sources (generators) of the gravitational field, which, in reality, is a vortex electromagnetic field. The elementary source of the gravitational field in the composition of atomic shells is a spinor electromagnetic quasiparticle, which received the author's name S-Graviton (S from Engl. a source). The S-graviton contains two spinors (an electron and a magneton) and two corresponding antispinors. The S-graviton can be represented as as a copula of magnetic and electric dipole revolving in antiphase in the same atomic orbit. This quasiparticle can also be represented in the form of two joint antiphase orbital currents of electric and magnetic charges.

The above-described model of an elementary vortex EM-current or S-Graviton can be written in mathematical form as: $\mathrm{rot}\left[\boldsymbol{J}_{\mathrm{e}}-\boldsymbol{J}_{\mathrm{g}}\right]$, где $\boldsymbol{J}_{\mathrm{e}}$ и $\boldsymbol{J}_{\mathrm{g}}$ are the vectors of the instantaneous current density of electric (e) and magnetic (g) charges corresponding to their vortex (circular) flows. Then the equation of the process of formation of the gravitational field is written in the following form:

$$k\,\mathrm{rot}\left[\boldsymbol{J}_{\mathrm{e}}-\boldsymbol{J}_{\mathrm{g}}\right]=\mathrm{rot}\left[\boldsymbol{E}-\boldsymbol{H}\right], \tag{4}$$

where $\boldsymbol{E}$ and $\boldsymbol{H}$ are the vectors of instantaneous electric and magnetic field strengths at each point of the vortex electromagnetic (gravitational) field, and $k$ is the proportionality coefficient. The vortex vector $\mathrm{rot}\left[\boldsymbol{E}-\boldsymbol{H}\right]$ corresponds to an elementary quantum of the gravitational field emitted by one S-Graviton.

The minus signs, set in the above equation of the process of formation of the

gravitational field (4), correspond both to the antiphase relation between the eddy currents of electric and magnetic charges in the S-Graviton, and to the antiparallel orientation of vectors of instantaneous strengths electric and magnetic fields at each point of the gravitational field. It is the minus signs, set in the above Equation (4), that correspond to the minimization of "Dark energy", which is realized in the Energy-phase under the influence of the fields of the S-graviton, presented in the article [24]. Thus, in contrast to the vortex magnetic field, each point of which corresponds to one vector of instantaneous intensity $\boldsymbol{H}$, each point of the elementary gravitational field corresponds to two vectors of instantaneous field strengths $\boldsymbol{E}$ и $\boldsymbol{H}$, equal in magnitude and directed antiparallel to each other.

Vector-vortex analogy between magnetic (**a**) and gravitational (**b**) of fields is shows in Figure 4. Unlike from vortex magnetic field of every point of which is answered one vector of instantaneous tension of $\boldsymbol{H}$, of every point of the elementary gravitational field is responsible two vectors of instantaneous tension of the fields of $\boldsymbol{E}$ and $\boldsymbol{H}$ equal by value and oriented antiparallel to each other.

If polarization of vortex vectors $\mathrm{rot}\left[\boldsymbol{J}_e - \boldsymbol{J}_g\right]$ of S-gravitons is realized in the structures of physical masses (atoms, nucleons, substance, etc.), what is accompanied by polarization of vortex vectors $\mathrm{rot}\left[\boldsymbol{E} - \boldsymbol{H}\right]$, then in analogy with magnetic fields ferromagnetics the gravitational fields being emitted by these masses can be called a **ferrogravitational** fields (FGF). The gravitational field formed by physical masses in the absence polarization of the vortex vectors of s-gravitons in their structures is a tensor or quasi-scalar field. And again, in analogy with magnetism, such field can to define as **paragravitational** field (PGF). Vector

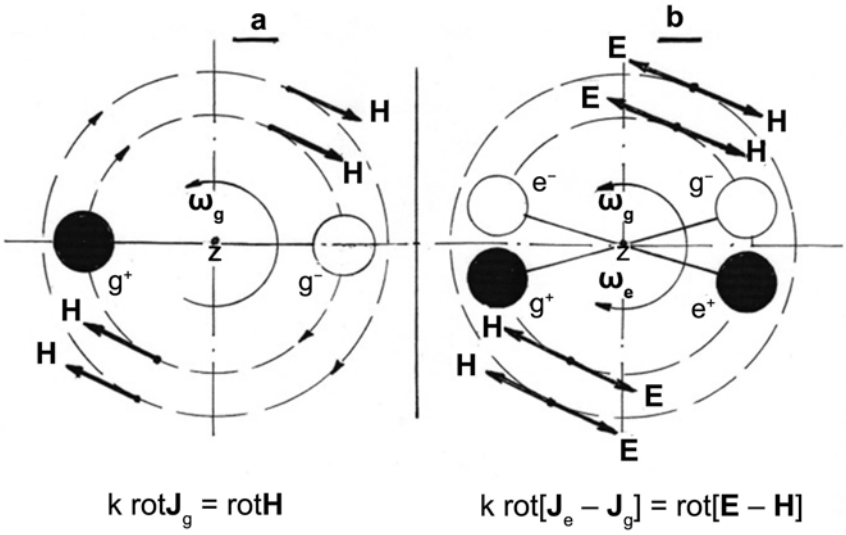


Figure 4. Schemes of mechanisms formation of the vortex spinor fields: magnetic (a) and electromagnetic (gravitational) (b). By white circles in the figure showed negative charged electric and magnetic spinors: electron ($e^-$) and magneton ($g^-$) and black circles—positively charged antispinors corresponding to them with charges $e^+$ and $g^+$. The classical equations of the processes formation magnetic and electromagnetic (gravitational) of fields also show in the figure.

conditions corresponding to these fields are written in the following form: $< \mathrm{rot}[\boldsymbol{E} - \boldsymbol{H}] > \neq 0$ for ferrogravitational field and $< \mathrm{rot}[\boldsymbol{E} - \boldsymbol{H}] > = 0$ for the field paragravitational.

Since 2001 (see [2]), the author in his publications tried to explain that all varieties of Physical Mass (PM) are electromagnetic structures atomic type, consisting of electric and magnetic spinor particles. One of the main characteristic properties of all varieties of PM is their ability to emit a gravitational field that is formed as the result of joint orbital currents of electric and magnetic charges and is the vortex electromagnetic field. Thus, all types of physical mass (atoms, nucleons, substance etc.) are dynamic electromagnetic structures that emit a gravitational field and consist of electric and magnetic spinor particles. In other words: everything that creates a gravitational field is Mass. If magnetic poles (magnetic charges) are removed from the FM composition, then only electric particles will remain in this "place" which themselves are not able to form either mass or gravitational field.

At the same time, in modern mathematical physics, in conditions of complete disregard for real magnetic particles, the function of endow particles Mass entrusted to Higgs field, the quantum of which is his known boson [25]. The paradox of the situation with such "endow" is that the existing representation of mass is purely mathematical. Any real, general physical representation of the essence of FM is absent in modern physics. Therefore, the process of imparting mass to spinor particles is also mathematical and, as shown by the research of present author, has nothing to do with reality.

It is important to emphasize that Physical Mass and, for example, Matter are completely different of physical categories. The physical masses are, for example, nucleons and atoms. It is important to note that the individual spinor particles, as electric so and magnetic, are massless, because the mass is the result of their joint "structural operations". For example, the electron is massless particle and no "divine bosons" can't give him Mass. It should also be added that substance, atoms, nucleons *i.e.* the physical masses cannot be identified with Matter, as is now accepted in modern physical science.

The physical masses, emitting ferrogravitational field is push off from sources paragravitational field, for example, from the Earth. The last action is a manifestation levitation effect, which was first discovered by the author of this article and very widely distributed in Nature. In principle, such effects as gravitational volatility of atoms (molecules) of light gases, for example, hydrogen and also convectional processes in liquids and gas media should be also attributed to the natural levitation manifestations. The fact of participation of the gravitational levitation in the volatility of atoms (molecules) of hydrogen was detected in the experiment performed by the author of this article (see [19]). The levitation forces, which is caused by natural ferrogravitational fields, emitting by cells, are responsible for vertical growth (development) of plants and trees, as well as maintain them in an upright position. Namely, the forces of gravitational levita-

tion are responsible for the amazing "aerobatics" of bumblebees, and also allow swifts and migratory birds to stay in the air for a long time.

Results of experiments author with magnetic charges and their currents in superconductors has allow him to develop technology to produce of the technical ferrogravitational field (FGF). Technical FGF and levitation forces formed by them can be used in transport, lifting and space engineering, in power engineering, as well as in numerous Gravito-Physical and Gravito-Chemical technologies (see publications author's [26] [27] [28]).

## 5. World Physical Triad and "Dark Energy" in the Physics of Gravitational Influences

The detection and multi-year research of the real magnetic charges in atoms and substance allowed the author to formulate the conception of the World Physical Triad (WPT), according to which the Real World consists of three fundamental phases: Matter, Antimatter and Energo-phase (Energo-medium) [29] (см. также [23]). All spinor particles with negative charge belong to Matter, and particles with a positive charge constitute Antimatterial phase. Such names of spinor particles as "lepton" and "antilepton", as well as "fermion" and "antifermion" are determined by the natural essence of the particles that is their material or antimaterial nature.

**Note 5.** It should be noted that in existing physical concepts, for example, atoms or nucleons are often referred to as matter. In his articles the author tries to explain that atoms, nucleons are not is matter at all. These structural formations consisting of material and antimaterial particles with electric and magnetic charges are, exclusively, of Physical masses. In addition, such physical essence as Antimatterial phase under no circumstances can it be can't be antisubstance.

The Energo-phase (Energo-medium) is superhigh-density of gas-like medium that fills the entire World Space and consists of its own massless and spinless particles, which are called the Energions (author's title) and are designated as ε. It is important to note that the Energo-phase can also be referred to as Energo-ether can find the points of contact between the Energo-phase and the Physical vacuum.

The energetic derivative from the Energo-phase is the so-called "Dark energy" ("DE") which is determined by the non-equilibrium states of Energo-phase in the form of local pressure fields ($P_\varepsilon$) created by the Energions.

Figure 5 shows the scheme of the World Physical Triad which includes three fundamental world phases: Matter, Antimatter and Energo-medium (Energo-phase). The fundamental particles that constitute the Phases of the Triad are indicated on the diagram, *i.e.* the spinors, antispinors and energions. In Figure 5 marked and such derivatives from the phases of Triad, as the spinor fields and "Dark energy". Outside of this scheme remain are condensates consisting of spinor particles of Matter and Antimatter, called Masses.

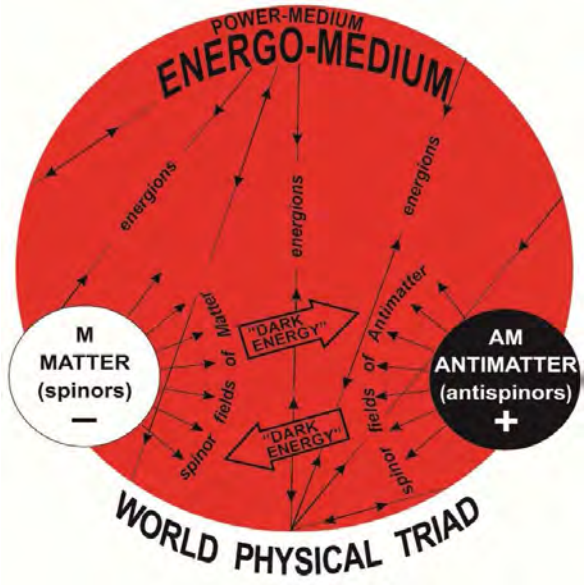


Figure 5. The diagram of the world physical triad.

The formations of "Dark energy" induce by spinor fields, *i.e.* fields of charged particles. Under this all varieties of spinor fields, including gravitational fields, themselves have no have essential of the force value. They are only intermediaries that influence on the local energy state of Energo-medium and induce the formation of "Dark energy" in it. Namely the "Dark energy" is global force factor which performs all the power acts with particles and masses, both in the scales of cosmos (the motion of galaxies, stars, planets, etc.), so and in the microcosm (the dynamics and so called interactions between Atoms and Charged Particles in compositions of Mass).

Between the Masses (atoms, bodies and other) which emit paragravitational field implemented the so-called the attraction or gravity. It is this last process, which is carried out, most often, by the forces of the gravitational "Dark energy" is the determining process in the physics of chemical bonding.

The Masses which emit the ferrogravtational field are repulsed from masses-sources of the paragravitational field, for example, from Earth, what constitute effect of the Gravitational levitation (GL) discovered and researched by author present article. An example of the so-called the ferrogravitational atom, *i.e.* atom emitting the FGF, is protium which is also called light hydrogen (designated as $^{1}$H).

The measure of the gravitational mass is the magnitude of the force of the gravitational "Dark energy" ($G$ "DE") which is realized, for example, in pairs of bodies or atoms. The equation of the so-called Law of universal gravitation should be written in the form $F_{DE} = \pm G\frac{M_1 \cdot M_2}{r^2}$, where the + sign refers to the case when the gravitational "DE" is implemented in of the pairs atoms or bodies emitting PGF. The masses, in this case, are pressed to each other by the force of the gravitational "DE" what is mistakenly perceived as their attraction. If the ef-

fect of gravitational levitation is realized between bodies or atoms what, as a rule, takes place in a pair of masses emitting PGF and FGF, then before the constant $G$, in the above equation, a minus sign is set. In reality, of course, the gravitational constants, in the two cases of gravitational interactions noted above, will differ. Therefore, different symbols should be used for their designation. So, for example, the letter L (from the word "levitation") can be used to denote the constant of interactions between paragravitational and ferrogravitational masses which refers this new concept to processes of gravitational levitation.

It is important to note that the forces of the gravitational "DE" between masses over very small distances (e.g. less than 1 Angstrom) are not sufficiently studied. There is high probability that on small distances between the sources of the gravitational fields, the forces of the gravitational "Dark energy" are comparable with forces so called of electrostatic attraction and can even exceed its. In connection with the physical essence of "Dark energy" presented in the article and its global participation in the force effects on particles and masses, the term "interaction" between particles and masses does not correspond to the real state of affairs and is exclusively fictitious.

The reason that were closed all the possibilities of approaching of physical science to explaining real processes associated with the action of the gravitational "Dark energy" is the perverse performance about actual physics of the gravitational field.

As is generally known, in the existent official physical approaches, the gravitational field, more than one hundred years, binds with curvature of the four-dimensional space-time. In addition, a limiting factor here was the lack in of the representations of World Physical Triad which, according to the author, to a greater extent than the Physical vacuum or traditional Ether is meets the Reality.

## 6. Conclusions

Magnetic spinor particles (magnetic charges) that actually exist in the structures of atoms and substance are not recognized in the official physical theory and are not included in the standard model. The results of the author's research have shown that the basic reasons responsible for ignoring the noted fundamental particles by the world physical theory, for almost 150 years, are the special conditions of confinement of these particles in substance, which is radically different from the confinement electrons. In addition, the vicious concept of electric magnetism Maxwell, as well as such a "magnetic" surrogate as the theoretic monopole of Dirac, played a very negative role here. It is exclusively under the influence of these vicious concepts that the world's physical theory has ignored the existence in atoms and substance, practically, the three quarters of fundamental spinor particles, have left yourself only negative electric and neutral particles for "convenience" of physical interpretations

The investigations of F. Ehrenhaft and the author of the article allow us to assert that ignoring in physics real magnetic spinor particles, as well as true an-

ti-electrons in the structures of substance and following the vicious teaching of Maxwell, is a tragic delusion of the existing official physical theory. Namely a mysticism that Maxwell laid down in the process of forming magnetic field, is responsible for the occurrence of such global theoretical misconceptions as the curvature of 4-dimensional space-time, which explains the phenomenon of gravity; the global expansion of the Universe and the Big Bang; the Annihilation of particles in particle-antiparticle pairs; the introduction of a fictitious Higgs boson to "endow" particles with mass and a great many others.

The vicious electrical magnetism of Maxwell, given its general-physical harmfulness, can associate with the "cancerous formation" in the "body" of physical science, the "metastases" of which have hit its many areas and directions. Conducting global "chemotherapy" of modern physical theory with the purpose of eliminating the numerous misconceptions generated by Maxwell's vicious concept, according to the author, is the most urgent task for today. All this needs to be done as soon as possible, because another 10 - 15 years and even robots will laugh at us.

## Acknowledgements

The author expresses deep gratitude to Elena Sizova and Vitaly Sizov who for many years helped and supported him which largely contributed to the implementation of his research activities.

The author is grateful to the technical specialists: Alexander Davydov, Nikolai Koshelev, Alexander Lomakin, Evgeni Moiseenkov and Sergei Staritsyn who together with him conducted the main experiments connected with the discovery and investigation of real magnetic charges.

## Conflicts of Interest

The author declares no conflicts of interest regarding the publication of this paper.

## References

[1] Sizov, R.A. (1971) *Journal of Experimental and Theoretical Physics*, **60**, 1363-1370.

[2] Sizov, R.A. (2001) New Presentation of Nature Magnetism, Gravitation and Nuclear Forces of Bonding. Akademizdat Center "Science", Moscow, 62 p.

[3] Sizov, R.A. (2015) *Journal of Modern Physics*, **6**, 1013-1022. https://doi.org/10.4236/jmp.2015.68106

[4] Sizov, R.A. (2020) *Journal of Modern Physics*, **11**, 1245-1261. https://doi.org/10.4236/jmp.2020.118078

[5] Sizov, R.A. (2008) Electric and Magnetic Spinor Particles as Structure Forming Components of Mass and Electromagnetic Source Gravitation. Akademizdat-Center "Science", Moscow, 260 p.

[6] Sizov, R.A. (2020) *OSP Journal of Nuclear Science*, **2**, JNS-2-111.

[7] Maxwell, J.C. (1873) Treatise on Electricity and Magnetism. Volume 1-2, Clarendon Press, Oxford.

[8] Sizov, R.A. (2019) *Applied Physics Research*, **11**, 49-55. https://doi.org/10.5539/apr.v11n3p49

[9] Sizov, R.A. (2019) *Applied Science and Innovative Research*, **3**, 257-263. https://doi.org/10.22158/asir.v3n4p257

[10] Ehrenhaft, F. (1910) Wiener Berichte 119(11a) 836; (1942) Jour. Frank. Inst. Mar., 235; (1951) Acta Phys. Austriaca, 5, 12.

[11] Mikhailov, V.F. and Ruzicka, J. (1989) *Acta Physica Universitatis Comenianae*, **29**, 97-148.

[12] Sizov, R.A. (2018) *Journal of Modern Physics*, **9**, 145-171. https://doi.org/10.4236/jmp.2018.92010

[13] Dirac, P.A.M. (1931) *Proceedings of the Royal Society A*, **133**, 60-72. https://doi.org/10.1098/rspa.1931.0130

[14] Sizov, R.A. (2015) *Journal of Modern Physics*, **6**, 2280-2289. https://doi.org/10.4236/jmp.2015.615232

[15] Sizov, R.A. (2018) *Physics & Astronomy International Journal*, **2**, 17-20.

[16] Sizov, R.A. (2017) *Journal of Modern Physics*, **8**, 964-981. https://doi.org/10.4236/jmp.2017.86061

[17] Sizov, R.A. (2007) Magnetic Fundamental Particles (Magnetons) in Physics of Magnetic and Electromagnetic Effects. Akademizdat-Center "Science", Moscow, 149 p.

[18] Sizov, R.A. (2012) Levitation as a Spread Force Manifestation of Natural Ferrogravitation. Akademizdat-Center "Science", Moscow, 96 p.

[19] Sizov, R.A. (2015) *Journal of Modern Physics*, **6**, 1591-1601. https://doi.org/10.4236/jmp.2015.611161

[20] Podkletnov, E. and Nieminen, R. (1992) *Physica C*: *Superconductivity*, **203**, 441-444. https://doi.org/10.1016/0921-4534(92)90055-H

[21] Tajmar, M. and de Matos, C. (2003) *Physica C*: *Superconductivity*, **385**, 551-554. https://doi.org/10.1016/S0921-4534(02)02305-5

[22] Sizov, R.A. (2016) *Journal of Modern Physics*, **7**, 2374-2397. https://doi.org/10.4236/jmp.2016.716206

[23] Sizov, R.A. (2017) *Journal of Modern Physics*, **8**, 1072-1086. https://doi.org/10.4236/jmp.2017.87069

[24] Sizov, R.A. (2016) *Journal of Modern Physics*, **7**, 558-572. https://doi.org/10.4236/jmp.2016.76059

[25] Higgs, P.W. (1964) *Physics Letters*, **12**, 132-133. https://doi.org/10.1016/0031-9163(64)91136-9

[26] Sizov, R.A. (2013) Transference of People and Loads in the Terrestrial Space by Means of Technical Ferrogravitation. Akademizdat-Center "Science", Moscow, 118 p.

[27] Sizov, R.A. (2020) *Applied Science and Innovative Research*, **4**, 1. https://doi.org/10.22158/asir.v4n1p1

[28] Sizov, R.A. (2020) *Open Journal of Physical Chemistry*, **10**, 48-67. https://doi.org/10.4236/ojpc.2020.101003

[29] Sizov, R.A. (2011/2012) Matter, Antimatter and Energo-Medium Is Physical Triad of the Real World. Akademizdat-Center "Science", Moscow, 192 p.

Journal of Modern Physics, 2020, 11, 1827-1841
https://www.scirp.org/journal/jmp
ISSN Online: 2153-120X
ISSN Print: 2153-1196

# Describing a Baryon as a Meson Pair

**Teruo Kurai**

IEEE, Tokyo, Japan
Email: kurai.teruo@topaz.plala.or.jp

**How to cite this paper:** Kurai, T. (2020) Describing a Baryon as a Meson Pair. *Journal of Modern Physics*, **11**, 1827-1841.
https://doi.org/10.4236/jmp.2020.1111114

**Received:** September 18, 2020
**Accepted:** November 10, 2020
**Published:** November 13, 2020





## Abstract

We propose a new description of a baryon as a pair of mesons. This description is an extension of the previously proposed description of a nucleon as a pair of pions. The purpose of this article is to show the following two possibilities. The first one is that it shows the qualitative explanation to support our description of a nucleon as a pair of pions and the second one is that it gives the systematic way of estimation of baryon mass not only for light baryons but also for heavy baryons (charm baryons and bottom baryons). Each isospin group is constructed of both baryons and antibaryons. This way of construction is consistent with that of mesons. The results obtained are listed in tables (Tables 1-9). This shows that the generalized Gell-Mann-Nishijima relation equation holds under the condition that the baryon number is 0 and that the obtained masses are fairly good, even for heavy baryons. Our description also yields several examples of baryon decay modes.

## Keywords

Baryon Description, Baryon Isospin, Baryon Mass, Baryon Decay Mode

## 1. Introduction

The widely accepted theory of baryon composition is the SU(6) quark model [1] [2] based on the eightfold way proposed by Gell-Mann [3] and Ne'eman [4]. According to this theory, baryons are composed of three quarks and antibaryons are composed of three antiquarks. The isospin group is constructed of only baryons, and that of antibaryons is constructed of only antiquarks. This theory is well supported by evidence and seems to be a complete formalism under the condition that the intrinsic spin of composing quarks determines baryon spin. However, in 1987, the European Muon Collaboration discovered that proton spin is not determined by the intrinsic quark spin [5]. Presently, it is clear that the contribution of the intrinsic spin of quarks to proton spin is at most 30% [6]. This result means that proton spin cannot tell us the number of composing

quarks. In other word, it is not evident that a proton is composed of three quarks. From this fact, a different possibility for the composition of a proton can be considered. In this report, we propose a description of a nucleon as a pair of pions and obtain a plausible result for nucleon electromagnetic form factors (e.m. FFs) [7]. Because all baryons decay to a proton as a final state, it is a fair consideration that any baryon spin is not determined by the intrinsic spin of composing quarks. Thus, it is not obvious that any baryons are composed of three quarks. From this view point, we extend our consideration of proton composition to all baryons by describing a baryon as a pair of mesons. In this case, we have to reconsider the way that isospin groups are constructed. In the case of mesons, all isospin groups are constructed from both a particle and an antiparticle. Thus, it is consistent that any isospin group of baryons is also constructed from both a particle and an antiparticle. Our proposition is based on this consideration. Mass splitting of baryons is explained well by the Gell-Mann-Okubo equation [3] [8] for light baryons, but this equation no longer holds when heavy baryons (charm baryons and bottom baryons) are included. For example, their generalized equation gives us equal mass for $\Xi_c$ and $\Xi_c'$ (each charged and neutral cases) because all isospin, strangeness, and $C$ value are same for both baryons, but their masses are different about 100 MeV (100 MeV is almost 70% of the mass difference between $\Xi^*$ and $\Omega^-$; thus, we cannot neglect it). There is no useful formula to estimate baryon mass. Therefore, we need another way of estimating baryon mass. In this paper, we estimate baryon mass even though one generalized including $C$ and $B$ values. The previous description of a nucleon as a pair of pions shows good results for e.m. FF, especially, $G_E/G_D$ for proton), but it is not obvious the reason why a nucleon can be described as a pair of pions. In this paper, we show the qualitative aspect of baryon description as a pair of mesons. This gives a support to our proposition of a nucleon description as a pair of pions.

## 2. Description of Properties

The basic meson operator is defined by the Bethe-Salpeter-like amplitude of the hadronic operator as

$$\chi(1,2) = \langle 0 | q(1,2) | P \rangle \tag{1}$$

where $|0\rangle$ and $|P\rangle$ denote a vacuum and physical state, respectively.

The gauge-invariant bi-local operator $q(1,2)$ is defined in the non-Abelian gauge field as

$$q(1,2) = T_r^c q_\beta^+(2) P \exp\left( ig \int_1^2 \mathrm{d}\bar{x} \overrightarrow{A^a}(x) \frac{\lambda_a}{2} \right) q_\alpha(1) \tag{2}$$

Here $\alpha$ and $\beta$ denote the Dirac indices, $P$ denotes the path ordering, and the $\frac{\lambda_a}{2}$ component generates the adjoint representation of the SU($N$) color gauge group. The trace is calculated for color spin $a$. Suura first proposed this

definition [9] [10], and later we applied it to the case of the t'Hoot model, the light meson mass spectra and the pion e.m. FF [11] [12]. We then proposed that a nucleon can be described as a pair of pions and obtained the e.m. FFs and distribution functions of nucleon [7]. The results of Ref. [7] encouraged us to extend this kind description to the consideration that a baryon can be described as a pair of mesons. In Ref. [7], a nucleon operator is defined as

$$\chi(1;2,3)=\langle 0|q(1;,2,3)|P\rangle \tag{3}$$

$$\text{where}\quad q(1;2,3)=q(1,2)+q(1,3) \tag{4}$$

Extending this consideration to all baryons, any baryon operator is defined as having the same form as Equation (3) and Equation (4), but quark field considerations indicate u, d, s, c, and b quarks instead of only u, d quarks for the nucleon case. For the case that antiquarks are bounded, it is easy to describe by using $\chi(1,2;3)$ instead of $\chi(1;2,3)$.

We show baryons described as a pair of mesons composed of u,d, and s quarks in **Table 4** (spin 1/2) and **Table 5** (spin 3/2). Baryons described as a pair of mesons composed of c and b quarks are shown in **Tables 6-9** (**Table 6** and **Table 7** for spin 1/2, **Table 8** and **Table 9** for spin 3/2). The terms listed in columns are paired mesons, isospin, the third component of isospin, strangeness, *c* value, *b* value, binding quarks, binding energy, excited energy, estimated mass and mass measured by experiment.

It is obvious to see that each baryon satisfies the generalized Gell-Mann-Nishijima relation equation [13] [14]. The generalized Gell-Mann-Nishijima relation equation is given as

$$Q=I_3+\frac{1}{2}(S+B_a+C+B) \tag{5}$$

where $Q$: charge value;

$I_3$ : the third component of isospin;

$B_a$ : baryon number;

$S$: strangeness;

$C$: $c$-value $c=+1,\overline{c}=-1$ ;

$B$: $b$-value $b=-1,\overline{b}=+1$ .

Because a baryon is composed of a pair of mesons, we need these values to determine the isospin, the third component of isospin, and the strangeness and to estimate the mass of each baryon. **Table 1** shows the properties of mesons composed of u, d, and s quarks only for the spin 0 case.

**Table 2** shows the properties of mesons with spin 0 composed by c and b quarks baryons.

**Table 3** shows the properties of mesons with spin 1 composed by c and b quarks baryons.

Using the values of **Tables 1-3**, we construct the isospin of a baryon and describe a baryon as a pair of mesons. To construct the isospin, we regroup the

**Table 1.** Properties of mesons (u,d,s quarks only).

| Meson | $I$ | $I_3$ | $S$ | $B_a$ | Mass (MeV) |
|---|---|---|---|---|---|
| $\pi^+$ | 1 | 1 | 0 | 0 | 139.57 |
| $\pi^0$ | 1 | 0 | 0 | 0 | 134.98 |
| $\pi^-$ | 1 | −1 | 0 | 0 | 139.57 |
| $f^0$ | 0 | 0 | 0 | 0 | 440.50 |
| $\eta^0$ | 0 | 0 | 0 | 0 | 547.86 |
| $\kappa^+$ | $\frac{1}{2}$ | $\frac{1}{2}$ | 1 | 0 | 493.68 |
| $\kappa^-$ | $\frac{1}{2}$ | $-\frac{1}{2}$ | −1 | 0 | 493.68 |
| $\kappa_s^0$ | 0 | 0 | 0 | 0 | 497.61 |
| $\kappa_L^0$ | 0 | 0 | 0 | 0 | 497.61 |
| $\kappa^0$ | $\frac{1}{2}$ | $\frac{1}{2}$ | 1 | 0 | 497.61 |
| $\overline{\kappa^0}$ | $\frac{1}{2}$ | $-\frac{1}{2}$ | −1 | 0 | 497.61 |

Notes: The listed mass of $f^0$ is from ref [12]. All other mass are from Oliver *et al.* [15]. We use $\kappa_s^0, \kappa_L^0$ (short and long decay time of $\kappa^0$) instead of $\kappa^0, \overline{\kappa^0}$ because $\kappa^0, \overline{\kappa^0}$ are strong eigenstates that are considered not to decay. Normally, $\kappa_s^0, \kappa_L^0$ are both noted not to be eigenstates of strangeness, however, we denote strangeness 0 for these because the quark representation of these two are $\frac{d\bar{s}+\bar{d}s}{\sqrt{2}}$ and $\frac{d\bar{s}-\bar{d}s}{\sqrt{2}}$, respectively, and from these expression we can consider their strangeness to be 0. By setting this strangeness value, isospin of $\kappa_s^0, \kappa_L^0$ must be 0, due to the Gell-Mann-Nishijima relation equation. All isospin and strangeness values (except $\kappa_s^0$ and $\kappa_L^0$) are from Ref. [15].

**Table 2.** Properties of mesons (c,b quarks; spin 0).

| Meson | Composing quarks | $I$ | $I_3$ | $S$ | $C$ | $B$ | Mass (MeV) |
|---|---|---|---|---|---|---|---|
| $D^+$ | $c\bar{d}$ | $\frac{1}{2}$ | $\frac{1}{2}$ | 0 | 1 | 0 | 1869.61 |
| $D^-$ | $\bar{c}d$ | $\frac{1}{2}$ | $-\frac{1}{2}$ | 0 | −1 | 0 | 1869.61 |
| $D^0$ | $c\bar{u}$ | $\frac{1}{2}$ | $\frac{1}{2}$ | 0 | 1 | 0 | 1864.84 |
| $\overline{D^0}$ | $\bar{c}u$ | $\frac{1}{2}$ | $-\frac{1}{2}$ | 0 | −1 | 0 | 1864.84 |
| $D_s^+$ | $c\bar{s}$ | 0 | 0 | 1 | 1 | 0 | 1968.30 |
| $D_s^-$ | $\bar{c}s$ | 0 | 0 | −1 | −1 | 0 | 1968.30 |
| $B^+$ | $u\bar{b}$ | $\frac{1}{2}$ | $\frac{1}{2}$ | 0 | 0 | 1 | 5279.26 |
| $B^-$ | $\bar{u}b$ | $\frac{1}{2}$ | $-\frac{1}{2}$ | 0 | 0 | −1 | 5279.26 |
| $B^0$ | $d\bar{b}$ | $\frac{1}{2}$ | $\frac{1}{2}$ | 0 | 0 | 1 | 5279.58 |
| $\overline{B^0}$ | $\bar{d}b$ | $\frac{1}{2}$ | $-\frac{1}{2}$ | 0 | 0 | −1 | 5279.58 |
| $B_s^0$ | $s\bar{b}$ | 0 | 0 | −1 | 0 | 1 | 5366.77 |
| $\overline{B_s^0}$ | $\bar{s}b$ | 0 | 0 | 1 | 0 | −1 | 5366.77 |

Notes: The listed values are taken from Ref. [15] including mass values. All baryon numbers are 0. The listed isospin values are determined by the fact that the isospin of u( $\bar{u}$ ) and d( $\bar{d}$ ) quarks is $\frac{1}{2}$, and that of other quarks is 0.

**Table 3.** Properties of mesons (c,b quarks; spin 1).

| Meson | Composing quarks | $I$ | $I_3$ | $S$ | $C$ | $B$ | Mass (MeV) |
|---|---|---|---|---|---|---|---|
| $D^{*+}$ | $c\bar{d}$ | $\frac{1}{2}$ | $\frac{1}{2}$ | 0 | 1 | 0 | 2010.26 |
| $D^{*-}$ | $\bar{c}d$ | $\frac{1}{2}$ | $-\frac{1}{2}$ | 0 | −1 | 0 | 2010.26 |
| $D^{*0}$ | $c\bar{u}$ | $\frac{1}{2}$ | $\frac{1}{2}$ | 0 | 1 | 0 | 2006.96 |
| $\overline{D^{*0}}$ | $\bar{c}u$ | $\frac{1}{2}$ | $-\frac{1}{2}$ | 0 | −1 | 0 | 2006.96 |
| $D_s^{*+}$ | $c\bar{s}$ | 0 | 0 | 1 | 1 | 0 | 2112.10 |
| $\overline{D_s^{*-}}$ | $\bar{c}s$ | 0 | 0 | −1 | −1 | 0 | 2112.10 |
| $B^{*+}$ | $u\bar{b}$ | $\frac{1}{2}$ | $\frac{1}{2}$ | 0 | 0 | 1 | 5325.20 |
| $B^{*-}$ | $\bar{u}b$ | $\frac{1}{2}$ | $-\frac{1}{2}$ | 0 | 0 | −1 | 5325.20 |
| $B^{*0}$ | $d\bar{b}$ | $\frac{1}{2}$ | $\frac{1}{2}$ | 0 | 0 | 1 | 5325.20 |
| $\overline{B^{*0}}$ | $\bar{d}b$ | $\frac{1}{2}$ | $-\frac{1}{2}$ | 0 | 0 | −1 | 5325.20 |
| $B_s^{*0}$ | $s\bar{b}$ | 0 | 0 | −1 | 0 | 1 | 5415.40 |
| $\overline{B_s^{*0}}$ | $\bar{s}b$ | 0 | 0 | 1 | 0 | −1 | 5415.40 |

Notes: The listed values are taken from Ref. [15] including mass values. All baryon numbers are 0.

baryons including antiparticles. For example, in the nucleon case, we consider $p^-$ (an antiparticle of proton $p^+$) and constitute $p^+$, $p^0$ ($n^0$: neutron), $p^-$ as one group so that the isospin is 1 instead of the normally considered value of $\frac{1}{2}$. This isospin determination is following. The isospin of pions is 1, thus the the possible isospin of a pair of pions is 2, 1 and 0 because of 1 + 1 = 2. Then, we take 1 for the isospin of proton group. We use this way of determination of isospin for other baryons. The composing meson pairs are selected by their charge and composing quarks and mass. We show the results of light baryons with the spin $\frac{1}{2}$ case in **Table 4**. We use a baryon number of 0 for all baryons as proposed in Ref. [7].

The binding energies for uu, dd, ud are determined by the mass difference between a proton and the sum of the masses of $\pi^+$ and $\pi^0$. We call this binding energy the strong binding energy, and calculate it to be 664.02 MeV. A similar consideration gives the binding energy for us and ds, using the mass difference between $\Lambda^0$ and the sum of the masses of $\pi^+$ and $\kappa^-$ or $\pi^-$ and $\kappa^+$. We call this the weak binding energy and calculate it to be 482.43 MeV. The estimated mass of each baryon is obtained by the following equation.

$$\begin{aligned}\text{Mass of baryon} = &\text{Sum of mass of composing mesons}\\ &+\text{Binding energy}+\text{Excited energy}\end{aligned} \tag{6}$$

In **Table 4**, there is no excitation energy term, although this term appears in later tables.

**Table 4.** Properties of light baryons (spin 1/2).

| Baryon | Pair of mesons | $I$ | $I_3$ | $S$ | Binding quarks | Binding energy | Mass (MeV) (estimated) | Mass (MeV) (measured) |
|---|---|---|---|---|---|---|---|---|
| $p^+$ | $\pi^+ + \pi^0$ | 1 | 1 | 0 | uu or $\overline{dd}$ | 664.02 | 938.27 (setting) | 938.27 |
| $p^0$ ($n^0$) | $\pi^+ + \pi^-$ | 1 | 0 | 0 | ud or $\overline{ud}$ | 664.02 | 943.16 | 939.57 |
| $p^-$ | $\pi^- + \pi^0$ | 1 | −1 | 0 | $\overline{uu}$ or dd | 664.02 | 938.27 | – |
| $\Lambda^0$ | $\pi^+ + \kappa^-$ or $\pi^- + \kappa^+$ | 0 | 0 | 0 | us or $\overline{us}$ | 482.43 | 1115.68 (setting) | 1115.68 |
| $\Sigma^+$ | $\pi^+ + \eta^0$ | 1 | 1 | 0 | us or $\overline{ds}$ | 482.43 | 1169.76 | 1189.37 |
| $\Sigma^0$ | $\pi^0 + \eta^0$ | 1 | 0 | 0 | us, ds or $\overline{us}$, $\overline{ds}$ | 482.43 | 1165.27 | 1192.64 |
| $\Sigma^-$ | $\pi^- + \eta^0$ | 1 | −1 | 0 | ds or $\overline{us}$ | 482.43 | 1169.76 | 1197.45 |
| $\Xi^+$ | $f^0 + \kappa^+$ | $\frac{1}{2}$ | $\frac{1}{2}$ | 1 | $\overline{us}$, $\overline{ds}$ | 482.43 | 1316.61 | – |
| $\Xi^-$ | $f^0 + \kappa^-$ | $\frac{1}{2}$ | $-\frac{1}{2}$ | −1 | us, ds | 482.43 | 1316.61 | 1321.71 |
| $\Xi^0$ | $f^0 + \kappa_s^0$ or $f^0 + \kappa_L^0$ | 0 | 0 | 0 | us, ds or us, ds | 482.43 | 1320.54 | 1314.86 |

Notes: All values of the baryon number $B_a$ are 0. All $C$ and $B$ values are 0.

The measured mass in Table 4 and in later tables is taken from Beringer *et al.* [16].

Table 5 shows the properties of light baryons with spin $\frac{3}{2}$.

The excited energy for Δ baryons is determined using the fact that $\Delta^+$ and $\Delta^0$ are normally considered as the excitation states of $p^+$, and $p^0$ ($n^0$) (proton and neutron), respectively. Thus, by setting the mass of $\Delta^+$ of 1232 MeV, we obtain this excited energy value of 293.43 MeV.

Table 6 shows the properties of heavy baryons with spin $\frac{1}{2}$ composed by c quarks.

Note that we denote the isospin of $\Sigma_c^0$ to be 0. Because the total isospin of a pair of mesons is 3 (we consider that $\Sigma_c^0$ is a mixture of $D^+ + \pi^-$ and $D^- + \pi^+$, thus $\frac{3}{2} + \frac{3}{2} = 3$), the possible isospin is 3, 2, 1, and 0. Thus we can take 0 for the isospin of $\Sigma_c^0$. The same consideration determines that the strangeness and C value become 0. Another possible meson pair of $\Sigma_c^0$ is the mixture of $D^0 + \pi^0$ and $\overline{D^0} + \pi^0$. Although we do not adopt this pair in our consideration, we address it in the Discussion. We use the same consideration for the $\Xi_c^0$ and $\Xi_c'^0$ cases, and adopt it in later tables.

To extend our consideration to heavy baryons, the binding energy for cu and cd is determined by the mass difference between the mass of $\Lambda_c^+$ and the sum of the masses of $D^+$ and $\pi^0$. To determine the binding energy for cs, we use the the difference between strong and weak binding energies (664.02 − 482.43 = 181.59 MeV).

The binding energy for cs is determined by the subtraction of above energy difference from the binding energy for cu and cd (281.87 − 181.59 = 100.28 MeV).

**Table 5.** Properties of light baryons (spin 3/2).

| Baryon | Pair of mesons | $I$ | $I_s$ | $S$ | Binding quarks | Binding energy (MeV) | Excited Energy (MeV) | Mass (estimated) (MeV) | Mass (measured) (MeV) |
|---|---|---|---|---|---|---|---|---|---|
| $\Delta^{++}$ | $\pi^+ + \pi^+$ | 2 | 2 | 0 | $uu, \overline{dd}$ | 664.02 | 293.43 | 1236.59 | 1232 |
| $\Delta^{+}$ | $\pi^+ + \pi^0$ | 2 | 1 | 0 | $uu, \overline{dd}, \overline{ud}$ | 664.02 | 293.43 | 1232 (setting) | 1232 |
| $\Delta^{0}$ | $\pi^+ + \pi^-$ | 2 | 0 | 0 | $uu, dd, ud$ | 664.02 | 293.43 | 1236.59 | 1232 |
| $\Delta^{-}$ | $\pi^- + \pi^0$ | 2 | −1 | 0 | $\overline{uu}, dd, ud$ | 664.02 | 293.43 | 1232.0 | 1232 |
| $\Delta^{--}$ | $\pi^- + \pi^-$ | 2 | -2 | 0 | $\overline{uu}, dd$ | 664.02 | 293.43 | 1236.59 | 1232 |
| $\Sigma^{*+}$ | $\pi^+ + \eta^0$ | 1 | 1 | 0 | $uu, \overline{dd}, \overline{ud}$ | 664.02 | 0 | 1351.45 | 1382.8 |
| $\Sigma^{*0}$ | $\pi^0 + \eta^0$ | 1 | 0 | 0 | $uu, dd, ud$ | 664.02 | 0 | 1346.86 | 1383.7 |
| $\Sigma^{*-}$ | $\pi^- + \eta^0$ | 1 | −1 | 0 | $\overline{uu}, dd, ud$ | 664.02 | 0 | 1356.59 | 1387.2 |
| $\Xi^{*+}$ | $\kappa^+ + f^0$ | $\frac{1}{2}$ | $\frac{1}{2}$ | 1 | $uu, ud$ | 664.02 | 0 | 1598.20 | – |
| $\Xi^{*-}$ | $\kappa^- + f^0$ | $\frac{1}{2}$ | $-\frac{1}{2}$ | −1 | $\overline{uu}, \overline{dd}$ | 664.02 | 0 | 1598.20 | 1535..0 |
| $\Xi^{*0}$ | $\kappa_s^0 + f^0$ or $\kappa_L^0 + f^0$ | 0 | 0 | 0 | $ud, dd$ or $ud, dd$ | 664.02 | 0 | 1602.13 | 1531.80 |
| $\Omega^{+}$ | $\kappa^+ + \eta^0$ | $\frac{1}{2}$ | $\frac{1}{2}$ | 1 | $uu, ud$ | 664.02 | 0 | 1705.54 | – |
| $\Omega^{-}$ | $\kappa^- + \eta^0$ | $\frac{1}{2}$ | $-\frac{1}{2}$ | −1 | $\overline{uu}, \overline{dd}$ | 664.02 | 0 | 1705.04 | 1672.45 |

Note: All values of the baryon number $B_a$ are all 0.

**Table 6.** Properties of heavy baryons (c quark; spin 1/2).

| Baryon | Pair of mesons | $I$ | $I_3$ | $S$ | $C$ | Binding quarks | Binding energy (MeV) | Excited energy (MeV) | Mass (estimated) (MeV) | Mass (measured) (MeV) |
|---|---|---|---|---|---|---|---|---|---|---|
| $\Lambda_c^+$ | $D^+ + \pi^0$ | $\frac{1}{2}$ | $\frac{1}{2}$ | 0 | 1 | $cu$ | 281.87 | 0 | 2286.46 (setting) | 2286.46 |
| $\Lambda_c^-$ | $D^- + \pi^0$ | $\frac{1}{2}$ | $-\frac{1}{2}$ | 0 | −1 | $\overline{cu}$ | 281.87 | 0 | 2286.46 | – |
| $\Sigma_c^{++}$ | $D^+ + \pi^+$ | $\frac{3}{2}$ | $\frac{3}{2}$ | 0 | 1 | $cu$ | 281.87 | 131.01 | 2422.06 | 2453.98 |
| $\Sigma_c^{+}$ | $D^+ + \pi^0$ | $\frac{3}{2}$ | $\frac{1}{2}$ | 0 | 1 | $cu$ | 281.87 | 131.01 | 2417.47 | 2452.9 |
| $\Sigma_c^{-}$ | $D^- + \pi^0$ | $\frac{3}{2}$ | $-\frac{1}{2}$ | 0 | −1 | $\overline{cu}$ | 281.87 | 131.01 | 2417.47 | – |
| $\Sigma_c^{--}$ | $D^- + \pi^-$ | $\frac{3}{2}$ | $-\frac{3}{2}$ | 0 | −1 | $\overline{cu}$ | 281.87 | 131.01 | 2422.06 | – |
| $\Sigma_c^{0}$ | $D^+ + \pi^-$ or $D^- + \pi^+$ | 0 | 0 | 0 | 0 | $cu, \overline{cu}$ | 281.87 | 131.01 | 2422.06 | 2453.74 |
| $\Xi_c^{+}$ | $D^+ + \kappa_s^0$ or $D^+ + \kappa_L^0$ | $\frac{1}{2}$ | $\frac{1}{2}$ | 0 | 1 | $cs$ | 100.28 | 0 | 2458.80 | 2467.8 |
| $\Xi_c^{-}$ | $D^- + \kappa_s^0$ or $D^- + \kappa_L^0$ | $\frac{1}{2}$ | $-\frac{1}{2}$ | 0 | −1 | $\overline{cs}$ | 100.28 | 0 | 2463.57 | – |
| $\Xi_c^{0}$ | $D^+ + \kappa^-$ or $D^- + \kappa^+$ | 0 | 0 | 0 | 0 | $cs, \overline{cs}$ | 100.28 | 0 | 2458.80 | 2470.88 |
| $\Xi_c'^{+}$ | $D^+ + \kappa_s^0$ or $D^+ + \kappa_L^0$ | $\frac{1}{2}$ | $\frac{1}{2}$ | 0 | 1 | $cd$ | 281.87 | 0 | 2640.59 | 2575.6 |
| $\Xi_c'^{-}$ | $D^- + \kappa_s^0$ or $D^- + \kappa_L^0$ | $\frac{1}{2}$ | $-\frac{1}{2}$ | 0 | −1 | $\overline{cd}$ | 281.87 | 0 | 2640.59 | – |
| $\Xi_c'^{0}$ | $D^+ + \kappa^-$ or $D^- + \kappa^+$ | 0 | 0 | 0 | 0 | $cd, \overline{cd}$ | 281.87 | 0 | 2644.32 | 2577.9 |

**Continued**

| | | | | | | | | | | |
|---|---|---|---|---|---|---|---|---|---|---|
| $\Xi_{cc}^{++}$ | $D^+ + D_s^+$ | $\frac{1}{2}$ | $\frac{1}{2}$ | 1 | 2 | cc | ≈0 | 0 | 3837.91 | 3621.40 |
| $\Xi_{cc}^{--}$ | $D^- + D_s^-$ | $\frac{1}{2}$ | $-\frac{1}{2}$ | −1 | −2 | $\overline{cc}$ | ≈0 | 0 | 3837.91 | – |

Note: All values of the baryon number $B_a$ are 0 and all $B$ value are 0.

At this point in our argument, we notice that the binding energy between quarks becomes smaller as the mass of each bound quark becomes heavier. Thus, we set the binding energy for cc to be nearly 0. A meson pair of $\Sigma_c$ baryons is determined using the following argument. $\Sigma_c^+$ is originally considered as a pair of $D^+$ and $\eta^0$ because $\Sigma^+$ is composed by $\pi^+$ and $\eta^0$. However, the existence of the double charged charm sigma baryon $\Sigma_c^{++}$ indicates that $\Sigma_c^{++}$ is composed of $D^+$ and $\pi^+$. Because $\Sigma_c^+$ should have a mass that is equal to the sum of the masses of $D^+$ and $\eta^0$ (1869.61 + 547.86 = 2417.47 MeV), the composing pions must be excited.

The excited energy of a pion is determined by the difference between the sum of the masses of $D^+$ and $\eta^0$ and the sum of the masses of $D^+$ and $\pi^0$ (2417.47 − 2286.46 = 131.01 MeV). To extend this consideration to the bottom sigma baryons case, we use the same excited energy (131.01 MeV) even though there are no double-charged bottom sigma baryons. Interestingly, there is no entry for $\Xi_{cc}^+$ ($\Xi_{cc}^-$) values in Table 6. It is possible that the composition of a meson with isospin $\frac{1}{2}$ is $D^0 + D_s^+$ ($D^0 + D_s^-$), but the third component of isospin $I_3$ becomes $-\frac{1}{2}$ ($\frac{1}{2}$) to hold to the Gell-Mann-Nishijima relation equation. This cannot be allowed if the consistency of isospin argument is to be maintained. Thus, $\Xi_{cc}^+$ ($\Xi_{cc}^-$) is forbidden in our consideration.

Table 7 shows the properties of heavy baryons with spin $\frac{1}{2}$ composed by b quarks.

The determination of binding energy is based on the same considerations used in the charm baryon case.

The reason that the strangeness of $\Omega_b^-$ ($\Omega_b^+$) is 0 is that the strangeness of $\overline{B_s^0}$ ($B_s^0$) is +1 (−1) and that of $\kappa^-$ ($\kappa^+$) is −1 (+1) so that the total of strangeness becomes 0.

Table 8 shows the properties of heavy baryons with spin $\frac{3}{2}$ composed by c quarks.

Table 9 shows the properties of heavy baryons with spin $\frac{3}{2}$ composed by b quarks.

## 3. Baryon Decay Mode

We show here several examples of baryon decay modes. The basic consideration

**Table 7.** Properties of heavy baryons (b quark; spin 1/2).

| Baryon | Pair of mesons | $I$ | $I_3$ | $S$ | $B$ | Binding quarks | Binding energy (MeV) | Excited Energy (MeV) | Mass (estimated) (MeV) | Mass (measured) (MeV) |
|---|---|---|---|---|---|---|---|---|---|---|
| $\Lambda_b^0$ | $B^+ + \pi^-$ or $B^- + \pi^+$ | 0 | 0 | 0 | 0 | $\bar{b}u, bu$ | 200.57 | 0 | 5619.40 (setting) | 5619.4 |
| $\Sigma_b^+$ | $B^+ + \pi^0$ | $\frac{1}{2}$ | $\frac{1}{2}$ | 0 | 1 | $\bar{b}u, \bar{b}d$ | 200.57 | 131.01 | 5745.82 | 5811.3 |
| $\Sigma_b^-$ | $B^- + \pi^0$ | $\frac{1}{2}$ | $-\frac{1}{2}$ | 0 | −1 | bu, bd | 200.57 | 131.01 | 5745.82 | 5815.5 |
| $\Sigma_b^0$ | $B^+ + \pi^-$ or $B^- + \pi^+$ | 0 | 0 | 0 | 0 | $\bar{b}u, bu$ | 200.57 | 131.01 | 5750.41 | – |
| $\Xi_b^+$ | $B^+ + \kappa_s^0$ or $B^+ + \kappa_L^0$ | $\frac{1}{2}$ | $\frac{1}{2}$ | 0 | 1 | $\bar{b}\bar{s}$ | 18.98 | 0 | 5795.85 | – |
| $\Xi_b^-$ | $B^- + \kappa_s^0$ or $B^- + \kappa_L^0$ | $\frac{1}{2}$ | $-\frac{1}{2}$ | 0 | −1 | bs | 18.98 | 0 | 5795.85 | 5791.1 |
| $\Xi_b^0$ | $B^+ + \kappa^-$ or $B^- + \kappa^+$ | 0 | 0 | 0 | 0 | $\bar{b}s, b\bar{s}$ | 18.98 | 0 | 5791.92 | 5787.8 |
| $\Xi_b'^+$ | $B^+ + \kappa_s^0$ or $B^+ + \kappa_L^0$ | $\frac{1}{2}$ | $\frac{1}{2}$ | 0 | 1 | $\bar{b}d$ | 200.57 | 0 | 5957.44 | – |
| $\Xi_b'^-$ | $B^- + \kappa_s^0$ or $B^- + \kappa_L^0$ | $\frac{1}{2}$ | $-\frac{1}{2}$ | 0 | −1 | bd | 200.57 | 0 | 5957.44 | – |
| $\Xi_b'^0$ | $B^+ + \kappa^-$ or $B^- + \kappa^+$ | 0 | 0 | 0 | 0 | $\bar{b}u, bu$ | 200.57 | 0 | 5973.51 | – |
| $\Omega_b^+$ | $B_s^0 + \kappa^+$ | $\frac{1}{2}$ | $\frac{1}{2}$ | 0 | 1 | $\bar{b}u$ | 200.57 | 0 | 6061.02 | – |
| $\Omega_b^-$ | $\overline{B_s^0} + \kappa^-$ | $\frac{1}{2}$ | $-\frac{1}{2}$ | 0 | −1 | $b\bar{u}$ | 200.57 | 0 | 6061.02 | 6071 |

Note: All values of the baryon number $B_a$ are all 0 and all $C$ value are 0.

**Table 8.** Properties of heavy baryons (c quark; spin 3/2).

| Baryon | Pair of mesons | $I$ | $I_3$ | $S$ | $C$ | Binding quarks | Binding energy (MeV) | Excited energy (MeV) | Mass (estimated) (MeV) | Mass (measured) (MeV) |
|---|---|---|---|---|---|---|---|---|---|---|
| $\Sigma_c^{*++}$ | $D^{*+} + \pi^+$ | $\frac{3}{2}$ | $\frac{3}{2}$ | 0 | 1 | cu | 281.87 | 131.01 | 2562.71 | 2517.9 |
| $\Sigma_c^{*+}$ | $D^{*+} + \pi^0$ | $\frac{3}{2}$ | $\frac{1}{2}$ | 0 | 1 | cu, cd | 281.87 | 131.01 | 2558.12 | 2517.5 |
| $\Sigma_c^{*-}$ | $D^{*-} + \pi^0$ | $\frac{3}{2}$ | $-\frac{1}{2}$ | 0 | −1 | $\bar{c}u, \bar{c}d$ | 281.87 | 131.01 | 2558.12 | – |
| $\Sigma_c^{*--}$ | $D^{*-} + \pi^-$ | $\frac{3}{2}$ | $-\frac{3}{2}$ | 0 | −1 | $\bar{c}u$ | 281.87 | 131.01 | 2562.71 | – |
| $\Sigma_c^{*0}$ | $D^{*+} + \pi^+$ or $D^{*-} + \pi^+$ | 0 | 0 | 0 | 0 | cd or $\bar{c}\bar{d}$ | 281.87 | 131.01 | 2562.71 | 2518.8 |
| $\Xi_c^{*+}$ | $D^{*+} + \kappa_s^0$ or $D^{*+} + \kappa_L^0$ | $\frac{1}{2}$ | $\frac{1}{2}$ | 0 | 1 | cs | 100.28 | 0 | 2608.22 | 2645.9 |
| $\Xi_c^{*-}$ | $D^{*-} + \kappa_s^0$ or $D^{*-} + \kappa_L^0$ | $\frac{1}{2}$ | $-\frac{1}{2}$ | 0 | −1 | $\bar{c}s$ | 100.28 | 0 | 2608.22 | – |
| $\Xi_c^{*0}$ | $D^{*+} + \kappa^-$ or $D^{*-} + \kappa^+$ | 0 | 0 | 0 | 0 | cs or $\bar{c}\bar{s}$ | 100.28 | 0 | 2604.85 | 2645.9 |
| $\Xi_{cc}^{*+++}$ | $D^{*+} + D_s^+$ | $\frac{1}{2}$ | $\frac{1}{2}$ | 1 | 2 | cc | ≈ 0 | 0 | 4122.36 | – |
| $\Xi_{cc}^{*--}$ | $D^{*-} + D_s^-$ | $\frac{1}{2}$ | $-\frac{1}{2}$ | −1 | −2 | $\bar{c}\bar{c}$ | ≈ 0 | 0 | 4122.36 | – |
| $\Omega_c^{*0}$ | $D_s^{*+} + \kappa^-$ or $D_s^{*-} + \kappa^+$ | 0 | 0 | 0 | 0 | $c\bar{u}$ or $\bar{c}u$ | 281.87 | 0 | 2887.65 | 2765.9 |

Note: All values of the baryon number $B_a$ are 0 and all $B$ values are 0.

**Table 9.** Properties of heavy baryons (b quark; spin 3/2).

| Baryon | Pair of mesons | $I$ | $I_3$ | $S$ | $B$ | Binding quarks | Binding energy (MeV) | Excited energy (MeV) | Mass (estimated) (MeV) | Mass (measured) (MeV) |
|---|---|---|---|---|---|---|---|---|---|---|
| $\Sigma_b^{*+}$ | $B^{*+}+\pi^0$ | $\frac{1}{2}$ | $\frac{1}{2}$ | 0 | 1 | $\bar{b}\bar{u}, \bar{b}d$ | 200.57 | 131.01 | 5791.76 | 5832.1 |
| $\Sigma_b^{*-}$ | $B^{*-}+\pi^0$ | $\frac{1}{2}$ | $-\frac{1}{2}$ | 0 | −1 | bu, bd | 200.57 | 131.01 | 5791.76 | 5835.1 |
| $\Xi_b^{*+}$ | $B^{*+}+\kappa_s^0$ or $B^{*+}+\kappa_L^0$ | $\frac{1}{2}$ | $\frac{1}{2}$ | 0 | 1 | $\bar{b}\bar{s}$ | 18.98 | 0 | 5841.79 | – |
| $\Xi_b^{*-}$ | $B^{*-}+\kappa_s^0$ or $B^{*-}+\kappa_L^0$ | $\frac{1}{2}$ | $\frac{1}{2}$ | 0 | −1 | bs | 18.98 | 0 | 5841.79 | – |
| $\Xi_b^{*0}$ | $B^{*+}+\kappa^-$ or $B^{*-}+\kappa^+$ | 0 | 0 | 0 | 0 | $\bar{b}s$ or $b\bar{s}$ | 18.98 | 0 | 5837.86 | 5945.5 |
| $\Omega_b^{*+}$ | $B_s^{*0}+\kappa^+$ | $\frac{1}{2}$ | $\frac{1}{2}$ | 0 | 1 | $\bar{b}u$ | 200.57 | 0 | 6109.65 | – |
| $\Omega_b^{*-}$ | $\overline{B_s^{*0}}+\kappa^-$ | $\frac{1}{2}$ | $-\frac{1}{2}$ | 0 | −1 | $b\bar{u}$ | 200.57 | 0 | 6109.65 | – |

Note: All values of the Baryon number $B_a$ are 0 and all $C$ values are 0.

is exactly the same as in the quark model case. Thus, we use the following weak decay and strong decay examples.

Example of weak decay

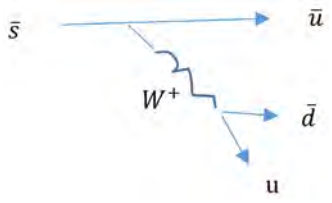


Example of strong decay

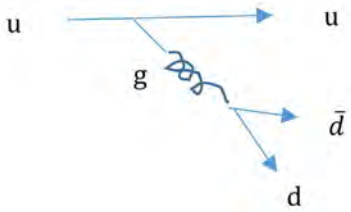


Following are examples of decay modes for $\Lambda^0, \Sigma^+, \Sigma^0, \Xi^-, \Omega^-, \Sigma_c^{++}, \Sigma_b^+, \Xi_{cc}^{++}$ cases.

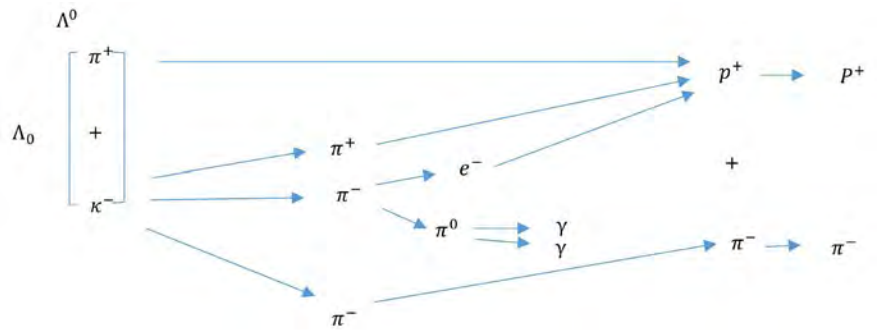

$$\Lambda^0 \to p^+ + \pi^-$$

Note that $\pi^-$ directly decays to $e^- + \gamma + \gamma$.

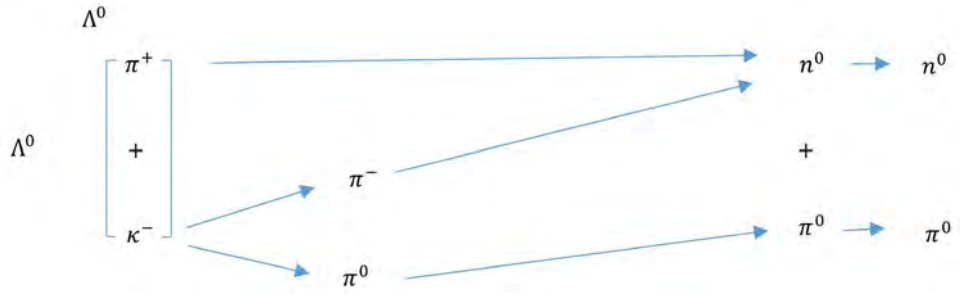


$$\Lambda^0 \to n^0 + \pi^0$$

In the case that $\Lambda^0$ is described as $\pi^+ + \kappa^-$, the decay mode is made obvious by noticing the fact that $\kappa^-$ decays to $\pi^+ + \pi^- + \pi^-$ or $\pi^- + \pi^0$.

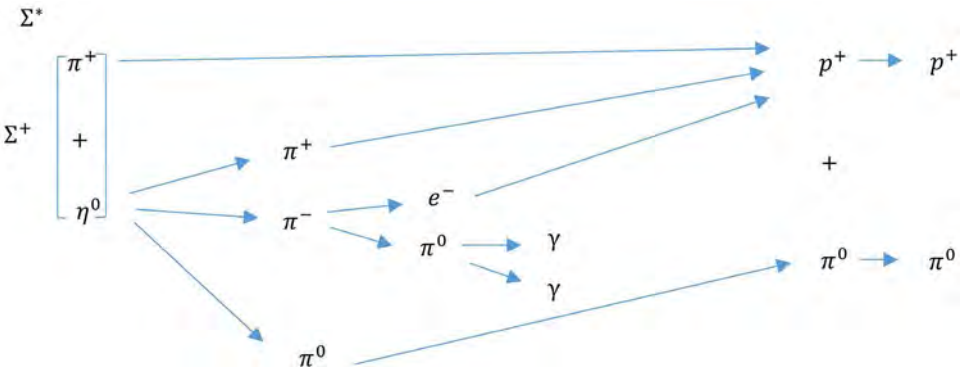


$$\Sigma^+ \to p^+ + \pi^0$$

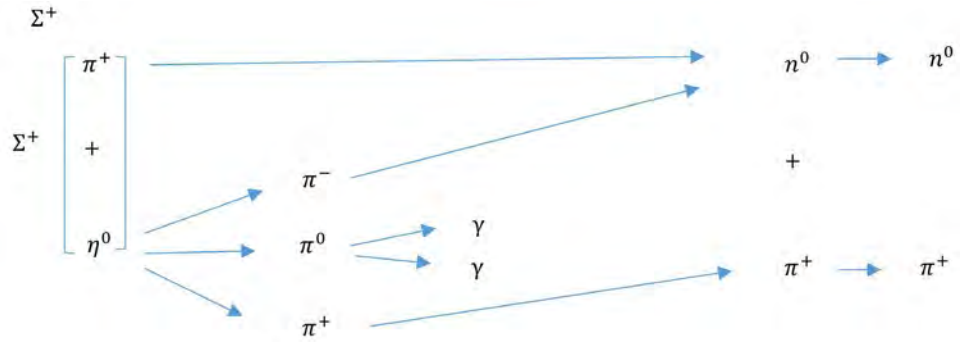


$$\Sigma^+ \to n^0 + \pi^+$$

The mass difference between the original baryon (in this case $\Sigma^+$) and the generated baryon (in this case $n^0$) is not large enough for two pions.

Thus, $\eta^0 \to \pi^+ + \pi^0 + \pi^- \to \pi^+ + \pi^- + \gamma + \gamma$ means that $\eta^0$ directly decays to $\pi^+ + \pi^- + \gamma + \gamma$.

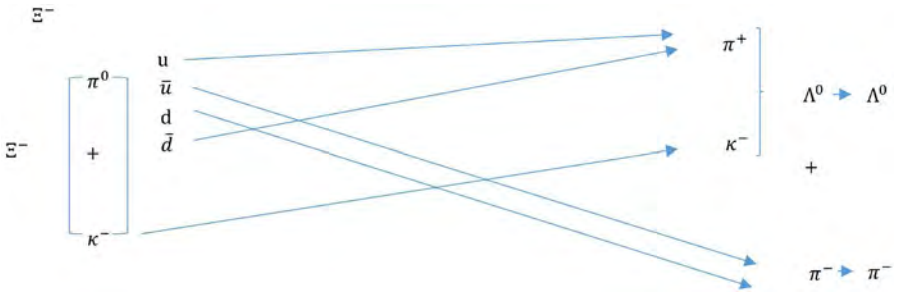


$$\Xi^- \to \Lambda^0 + \pi^-$$

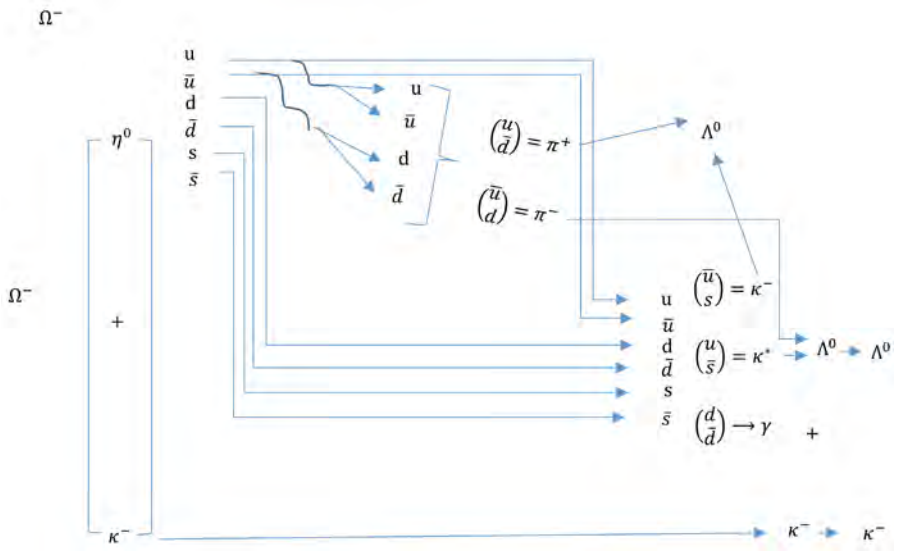


From the representation that $\Lambda^0 = \frac{1}{2}\left[\left(\pi^+ + \kappa^-\right) + \left(\pi^- + \kappa^+\right)\right]$ and the fact that the mass of $\Omega^-$ can afford to allow only one $\Lambda^0$, the graph above indicates

$$\Omega^- \to \Lambda^0 + \kappa^-$$

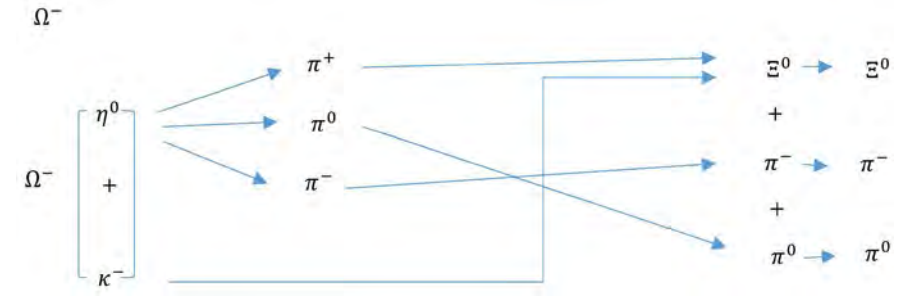


$$\Omega^- \to \Xi^0 + \pi^- + \pi^0$$

Note that the above graph uses $\Omega^- \to \Xi^0 + \pi^- + \pi^0$ instead of the more common form, $\Omega^- \to \Xi^0 + \pi^-$. We use this because the mass difference between $\Omega^-$ and $\Xi^0$ is large enough to generate two pions, unlike other baryon decay modes.

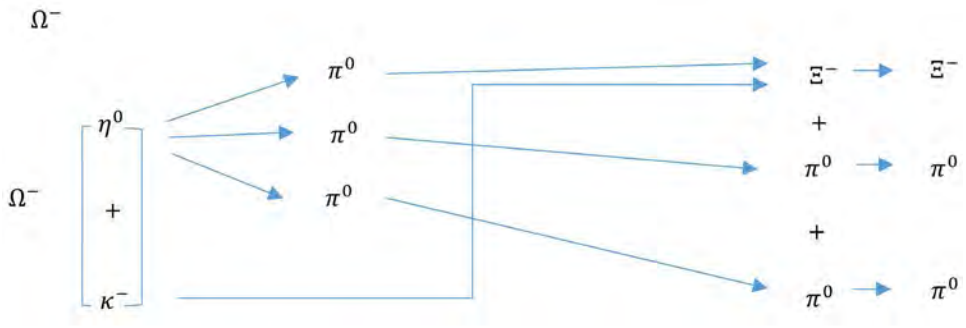


$$\Omega^- \to \Xi^- + \pi^0 + \pi^0$$

The reason this $\Omega^-$ decay mode has two $\pi^0$ instead of only one $\pi^0$ is the same as for the previous $\Omega^-$ decay mode.

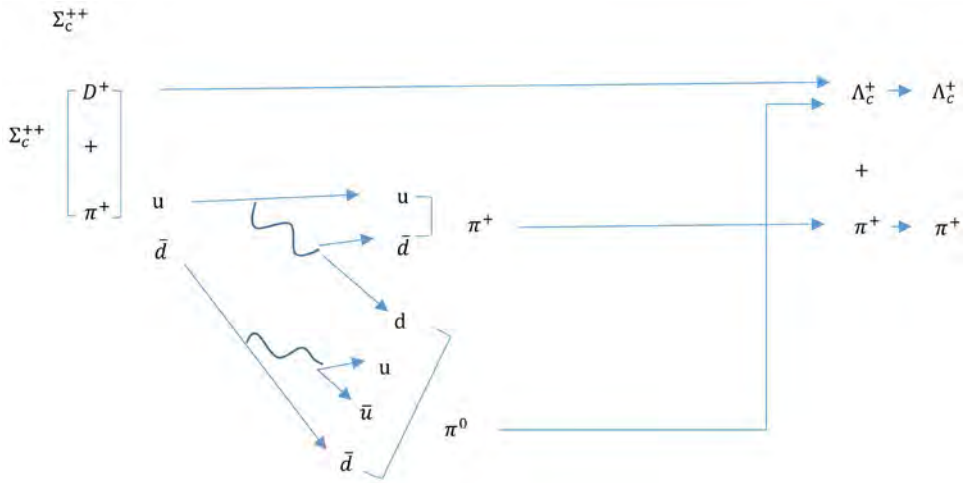


$$\Sigma_c^{++} \to \Lambda_c^+ + \pi^+$$

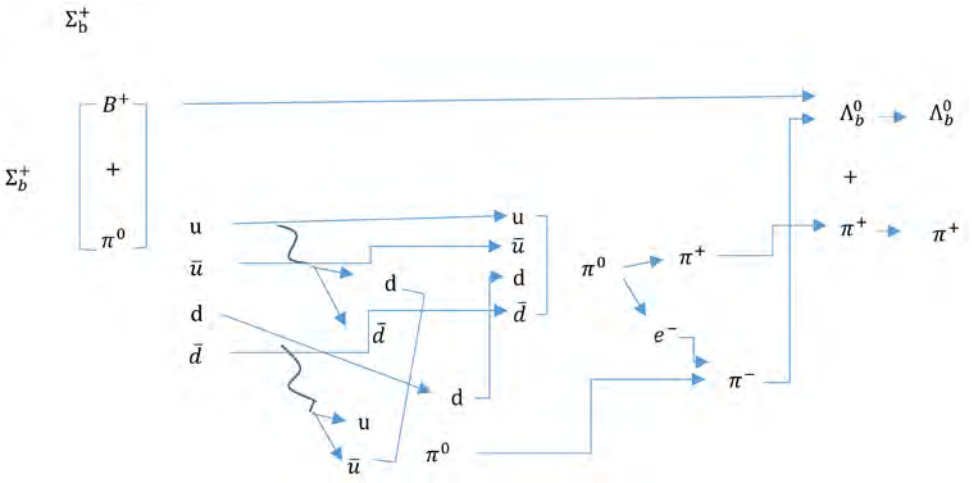


$$\Sigma_b^+ \to \Lambda_b^0 + \pi^+$$

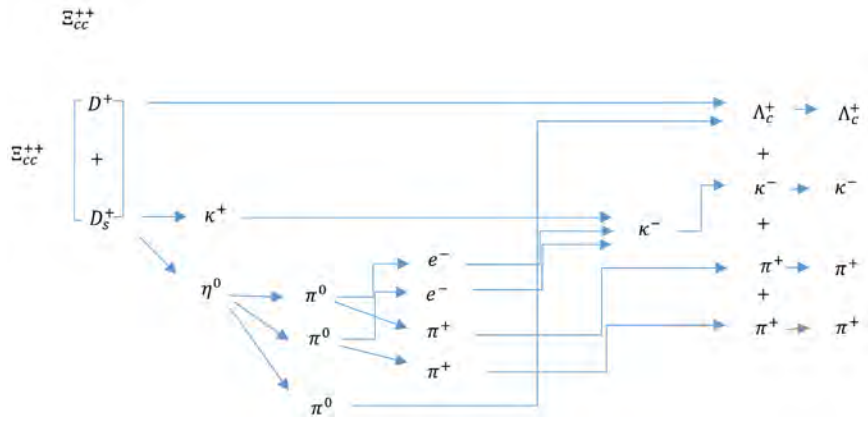


$$\Xi_{cc}^{++} \to \Lambda_c^+ + \kappa^- + \pi^+ + \pi^+$$

We do not know the decay mode of $D_s^+ \to \kappa^+ + \eta^0$, but if we assume it exists, then we could explain the above $\Xi_{cc}^{++}$ decay mode, which has been seen experimentally. These decay modes are given in Ref. [16].

## 4. Conclusions

In Section 2 and Section 3, we show the qualitative aspects of baryons described as a meson pair. From **Tables 4-9**, we can demonstrate that all baryons satisfy the generalized Gell-Mann-Nishijima relation Equation (5) with baryon number 0. This result supports our proposition [7] that all baryons have a baryon number of 0 instead of 1.

The difference between the estimated mass and the measured mass of any baryon is less than 100 MeV except for the $\Xi_{cc}^{++}$ case which is a difference about 200 MeV. Thus, the obtained results are reasonable even though the estimation method is simple. Also, baryon decay mode can be explained by a pair of mesons as shown in Section 3. These results indicate that the description of baryons as a meson pair shows the most important aspects of baryons.

## 5. Discussion

During the presentation of **Table 6**, we mention that the reason we omit $\Xi_{cc}^{+}$ and $\Xi_{cc}^{-}$ is for the consistency of the isospin argument. To be precise, the other $\frac{1}{2}$ isospin case shows that a positive charge particle has an $I_3$ of $\frac{1}{2}$ and the negative charge particle has an $I_3$ of $-\frac{1}{2}$, as is the case for $\Xi_c^+$ and $\Xi_c^-$ in the same table.

However, for $\Xi_{cc}^{+}$ and $\Xi_{cc}^{-}$, $I_3$ must be $-\frac{1}{2}$ and $\frac{1}{2}$, respectively, to satisfy the generalized Gell-Mann-Nishijima relation equation. Thus, we consider that $\Xi_{cc}^{+}$ and $\Xi_{cc}^{-}$ to be forbidden. To this point, the claimed discovery of $\Xi_{cc}^{+}$ has been controversial because of questionable experimental data [17]. If they are observed, our way of constructing isospin group may have to be reconsidered. In

this respect, whether or not $\Xi_{cc}^{+}$ and $\Xi_{cc}^{-}$ exist is an important point in our consideration.

The reason that the pair of mesons for $\Sigma_{c}^{0}$ (and other neutral particle) is a mixture of $D^{+}+\pi^{-}$ and $D^{-}+\pi^{+}$ (positive charge meson + negative charge meson) instead of a mixture of $D^{0}+\pi^{0}$ and $\overline{D^{0}}+\pi^{0}$ is that a neutron is composed of $\pi^{+}$ and $\pi^{-}$. We derived the charge distribution function of a neutron in a previous paper [7]. Because we consider that any neutral baryons should have a charge distribution, we adopt this mixture instead of that of a pair of neutral mesons.

## Conflicts of Interest

The author declares no conflicts of interest regarding the publication of this paper.

## References


[1] Greenberg, O.W. (1964) *Physical Review Letters*, **13**, 398. https://doi.org/10.1103/PhysRevLett.13.598

[2] Zweig, G. (1964) CERN Rep. No. 8182/TH, 401.

[3] Gell-Mann, M. (1961) OSTI GOV TID-12608, CTSL 20.

[4] Ne'eman, Y. (1961) *Nuclear Physics*, **26**, 222. https://doi.org/10.1016/0029-5582(61)90134-1

[5] Ashman, J., *et al.* (1988) *Physics Letters B*, **206**, 364.

[6] Thomas, A.W. (2008) arXiv: 0803. 2775v1 [hep-ph] JLAB-THY-08-780

[7] Kurai, T. (2020) *Journal of Modern Physics*, **11**, 741. https://doi.org/10.4236/jmp.2020.115048

[8] Okubo, S. (1962) *Progress of Theoretical Physics*, **27**, 949. https://doi.org/10.1143/PTP.27.949

[9] Suura, H. (1978) *Physical Review D*, **17**, 460. https://doi.org/10.1103/PhysRevD.17.469

[10] Suura, H. (1979) *Physical Review D*, **20**, 1429. https://doi.org/10.1103/PhysRevD.20.1412

[11] Kurai, T. (2014) *Progress of Theoretical and Experimental Physics*, **2014**, 053B01.

[12] Kurai, T. (2018) *Results in Physics*, **10**, 865-881. https://doi.org/10.1016/j.rinp.2018.07.034

[13] Noshijima, K. and Nakano, T. (1953) *Progress of Theoretical Physics*, **10**, 581. https://doi.org/10.1143/PTP.10.581

[14] Gellman, M. (1956) *Nuovo Ciment*, **4**, 848. https://doi.org/10.1007/BF02748000

[15] Olive, K.A., *et al.* (2014) *Chinese Physics C*, **38**, Article ID: 090001. https://doi.org/10.1088/1674-1137/38/9/090001

[16] Beringer, J., *et al.* (2012) *Physical Review D*, **86**, Article ID: 010001.

[17] CERN (2017) The LHCb Experiment Is Charmed to Announce Observation of a New Particle with Two Heavy Quarks.

Journal of Modern Physics, 2020, 11, 1842-1855
https://www.scirp.org/journal/jmp
ISSN Online: 2153-120X
ISSN Print: 2153-1196

# On Spontaneous Quantum-Events and the Emergence of Space-Time

**Andreas Schlatter**

Emeran AG, Küttigen, Switzerland
Email: schlatter.a@bluewin.ch

**How to cite this paper:** Schlatter, A. (2020) On Spontaneous Quantum-Events and the Emergence of Space-Time. *Journal of Modern Physics*, **11**, 1842-1855.
https://doi.org/10.4236/jmp.2020.1111115

**Received:** October 16, 2020
**Accepted:** November 13, 2020
**Published:** November 16, 2020





## Abstract

We show that the real existence of quantum-events, resulting from spontaneously broken unitary-evolution by quantum-transactions, can explain the dynamic metric of space-time, governed by Einstein's equation, if light-clocks are being used to measure the rhythm of events. In the derivation of Einstein's equation there naturally arises a term for a cosmological constant $\Lambda$.

## Keywords

Quantum-Events, Transactional Interpretation, Einstein Equation, Cosmological Constant

## 1. Introduction

There has been a long-standing quest for a theory of quantum-gravity and promising candidates like string-theory or loop-quantum gravity are widely discussed today. The straightforward way of treating the metric tensor as a spin-2 quantum field, however, has led to technical difficulties early. There are other routes towards harmonizing relativity with quantum theory, where gravity is not being treated as a fundamental but an emerging force. All these attempts are closely linked to the metaphysical question, what space, time and matter actually are, even if this question does normally not stand at the first place in developing mathematical models of nature [1]. In this paper we proceed the reverse way. Starting from a few foundational assumptions in quantum physics, we develop a theory of space-time in the flavor of emerging gravity.

One of the main differences between relativity and quantum theory is locality. While relativity is per design a local theory, quantum physics definitely shows non-local features, which are not easily reconciled [2][1]. A key notion of relativity theory is an "event" in space-time, which we define to be an (idealized) physical

[1]In fact, there are non-local phenomena in GR too, like the non-localizability of gravitational energy.

system of mass $m$ occurring at a point in space-time $(t,x)\in\mathbb{R}^4$. Einstein's equation encapsulates the local, metric relationship between events under the influence of gravity. By the collapse-postulate also quantum-fields can be localized in space-time and we call these localizations quantum-events. It is therefore a straightforward idea to link quantum-events to gravity. In order to do that, we must consequently take a quantum-event and the corresponding collapse for a real physical process. This is the foundational assumption, on which we are going to base our arguments. There has been extensive of work done in the field of collapse-theories and we chose ideas from the transactional theory of quantum mechanics [3] [4] [5] [6] as the technical basis of our work.

The paper is organized as follows: in paragraph 2 we briefly introduce the transactional interpretation and some of its key tenets, which are important for our work. We do this without entering into the details of the theory and the reader is referred to [6] for a comprehensive exposition. In the main paragraph 3 we derive local gravitational acceleration and the Einstein equation as a result of transactions between quantum-systems. Finally, we give a summary and draw some further conclusions in paragraph 4. In the appendices we prove some technical results.

## 2. Quantum Events and Light Clocks

### 2.1. Quantum Events

Quantum states of closed, isolated physical systems are represented as unit-elements of a complex Hilbert space $|\psi\rangle\in H_{\mathbb{C}}$, $\langle\psi|\psi\rangle=1$, and can under some realistic assumptions be uniquely assigned to the respective physical systems [7]. In the transactional interpretation [3] a quantum state $|\psi\rangle\in H_{\mathbb{C}}$ is launched as an "offer-wave" by an emitter and gets possible responses by "confirmation-waves" $\langle\psi_\iota|,\iota\in I$, which are the projections of the dual vector $\langle\psi|\in H_{\mathbb{C}}^*$ onto absorbers $\mathcal{A}_\iota$. The indices $\iota\in I$ denote a range of values, which the system can assume in a measurement of some physical operator[2]. The "selection" of a specific confirmation $\iota_0\in I$ leads to a "transaction", which is the actualization of emission and absorption as real events in space-time. The specific probability for a particular transaction $\iota_0\in I$ is $\left|\langle\psi_{\iota_0}|\psi\rangle\right|^2$ and the "selection" is purely random. The relativistic transactional interpretation [4] [5] additionally offers an explanation, why offer-waves (and confirmation-waves) are actually created. Quantum-fields are elements of abstract mathematical spaces and their components are indexed through space-time points. Relativistic interactions can be thought of as the mutual exchange of virtual bosons between fields, creating possibilities in a pre-space-time process. Transactions, in turn, are triggered by the exchange of real bosons and their four-momentum. The amplitude for emission or absorption of real bosons is the coupling amplitude between the matter-and gauge-fields and a specific transaction can happen spontaneously, if the conservation laws are satisfied. By the exchange of four-momentum the quan-

[2]They actually index the spectrum of a Hermitian operator.

tum states of the emitter and absorber collapse and the physical systems are found at the corresponding space-time points (regions). We will sometimes use the term "event-radiation" for the four-momentum transfer in transactions. Space-time thus becomes the connected set of emission-and absorption events corresponding to transactions, which define, by the four-momentum of the exchanged bosons, time-like (or null-like) space-time intervals, whose end points are these emission and absorption events. It is here, where the transactional view touches causal-set theory [8] [9], in which events spread in space-time by a stochastic Poisson-process. Boson-exchange, understood as a decay-process, is then a special case in this model[3]. Note that the actualization of a space-time interval amounts to spontaneously breaking the unitary evolution of the quantum states. At the same time the four-momentum, which is exchanged, determines a time direction, since positive energy is transmitted, and selects a space-direction. In this sense spatio-temporal symmetry is also spontaneously broken. We will in the sequel focus on the electromagnetic force and the related exchange of photons.

### 2.2. Light Clocks

It takes a (closed and isolated) quantum-system, represented by a vector in Hilbert space, $|\psi_0\rangle \in H_{\mathbb{C}}$, with average energy above ground state $\left(\bar{E}-E_0\right)$, minimally a time of

$$\overline{\Delta t}=\frac{h}{4\left(\bar{E}-E_0\right)}, \tag{1}$$

in order to unitarily evolve to an orthogonal state $|\psi_1\rangle$, $\langle\psi_0|\psi_1\rangle=0$, ($h \overset{\text{def}}{=}$ Planck's constant) [10]. We can use such a system as a clock[4] with period $\overline{\Delta t}$. Special interest will lie on the case, where the system is a photon of energy (above the ground-state) $\left(E-E_0\right)=h\nu$. The corresponding light-clock then has the period

$$\overline{\Delta t}=\frac{1}{4\nu}. \tag{2}$$

We will encounter the situation, where there is not a single photon but many of them over a range of frequencies in thermal equilibrium, and where the energy is given by a temperature $T$. For oscillators with $\bar{E}_\nu \approx k_B T$ ($h\nu \ll k_B T$, $k_B \overset{\text{def}}{=}$ Boltzmann constant) we get a corresponding clock with period

$$\overline{\Delta t}=\frac{h}{4k_B T}. \tag{3}$$

We call the special light-clock (3) a thermal clock.

## 3. Space-Time

There is an intricate interplay between space-time and quantum-fields, which we

[3]The transactional interpretation thinks of space-time slightly different than the causal-set-approach does. This has no impact on our mathematical result.

[4]We actually use it as the "core" of a clock, *i.e.* as an abstract periodic process without ability to "indicate" time.

will now start to explore.

### 3.1. Minkowski Space-Time

For any photon in vacuum the ratio between its energy $E$ and its 3-momentum $p = |\boldsymbol{p}|$ is a constant, namely the speed of light $c$

$$\frac{E}{p} = c. \tag{4}$$

Equation (4) is a quantum-identity and, if expressed in space-time, must hold in every inertial reference frame. If we write energy and momentum in space-time coordinates, we get $E = h\Delta\nu = \frac{h}{\Delta t}$ and, by the de Broglie-relation, $p = \frac{h}{\Delta x}$. Therefore (4) takes the form

$$\frac{E}{p} = \frac{\Delta x}{\Delta t} = c. \tag{5}$$

Since Equation (5) must hold in every inertial reference frame $\overline{x} = (t, x) \in \mathbb{R}^4$, it constrains the metric in $\mathbb{R}^4$ and the result is Minkowski space-time $\mathbb{M}^4$ with its metric tensor $\eta_{ab} = -\delta_{ab}, 1 \le a, b \le 3, \eta_{0a} = \delta_{0a}, 0 \le a \le 3$, and its linear isometries $O(1,3)$, the Lorentz transformations. As indicated in paragraph 2.1, we take the ontological standpoint that quantum-systems spontaneously break the unitary time-evolution through the exchange of real bosons and thus become manifest in space-time. This is what we call "quantum-events" or synonymously "actualizations". The kind of bosons depends upon the force in action. So we treat space and time as distinct attributes of matter, represented by a four-dimensional continuum, which adopts its metric structure by the "sprinkling" of matter through quantum-events. On the other hand the symmetries of $\mathbb{M}^4$ influence the structure of quantum states, which transform under suitable representations of the Lorentz group[5]. So the influence between space-time and quantum states is bidirectional.

The concept of a thermal clock (3) unfolds its power, if we consider multiple events of interacting quantum-systems. Multiple events manifest themselves in space-time by acceleration. In $\mathbb{M}^4$ physical systems of constant acceleration $\kappa$ in $x$-direction, say, can be expressed in Rindler-coordinates. This happens by choosing a co-moving coordinate system, defined in the wedge limited by $|x| = t$, and given by the transformations

$$x = \varrho\cosh(\kappa\vartheta),\ t = \varrho\sinh(\kappa\vartheta),\ \varrho \ge 0,\ -\infty < \vartheta < \infty. \tag{6}$$

The corresponding line-element is

$$\mathrm{d}s^2 = \left(\frac{\kappa\varrho}{c^2}\right)^2 c^2\mathrm{d}\vartheta^2 - \mathrm{d}\varrho^2 - \mathrm{d}y^2 - \mathrm{d}z^2. \tag{7}$$

Contrary to velocity, acceleration is not purely perspectival and cannot be transformed away by a Lorentz transformation. But there are local inertial reference-frames at $t = \vartheta = 0$, where systems are instantaneously at rest. By the

[5]The spin-number serves to classify these representations.

Tolman-Ehrenfest effect [11] we have in thermal equilibrium for systems being instantaneously at rest and located at arbitrary $\varrho_1, \varrho_2$

$$T_{\varrho_1} \frac{\kappa \varrho_1}{c} \mathrm{d}\vartheta = T_{\varrho_2} \frac{\kappa \varrho_2}{c} \mathrm{d}\vartheta. \tag{8}$$

For a system at the origin $\varrho_1 = \frac{c^2}{\kappa}$ and an arbitrary one at $\varrho_2$ we get with $T_\kappa = T_{\varrho_1}$

$$T_\kappa \frac{c^2}{\kappa} = T_{\varrho_2} \varrho_2 = const. \tag{9}$$

The constant on the right does no longer depend on $\kappa$. Assume that in this chart (coordinate system) there is a thermal bath of temperature $T_\kappa$, and we want to gauge proper time by a corresponding thermal clock. By (3), (6) and (9) we get for a system instantaneously at rest at the origin and with $\mathrm{d}\hat{s} = \frac{c}{\kappa}\mathrm{d}s$

$$\mathrm{d}\tau = \frac{\mathrm{d}\hat{s}}{\Delta t} = \frac{4}{h} k_B T_\kappa \frac{c^2}{\kappa} \mathrm{d}\vartheta. \tag{10}$$

We want to fix the constant in (9) and for this purpose synchronize[6] (10) with a quantum-clock, defined by a matter-wave with rest mass $m_0$, frequency $\omega = 2\pi\nu$ and corresponding acceleration $\kappa_\omega$. In its respective oscillatory rest-frame and for $m_0 \ll \frac{\hbar\omega}{c^2}$, the matter-clock measures time in analogy to (10) in units of

$$\mathrm{d}\tau_\omega = \frac{4}{h} E_\omega \frac{c^2}{\kappa_\omega} \mathrm{d}\vartheta. \tag{11}$$

By the de Broglie-relation there holds with $k = |\boldsymbol{k}|$ denoting the wave number

$$E_\omega^2 = \hbar^2\omega^2 = c^2\hbar^2k^2 + m_0^2c^4. \tag{12}$$

Further with $u_\omega = \frac{\omega}{k}$ and $v_\omega = c^2\frac{k}{\omega}$ denoting the phase-and group velocity, respectively, we have

$$\kappa_\omega = 2\pi u_\omega \omega. \tag{13}$$

By (12) and (13) Equation (11) turns into

$$\mathrm{d}\tau_\omega = \frac{4}{h}\hbar\omega \frac{c^2k}{2\pi\omega^2} \mathrm{d}\vartheta = \frac{c^2k}{\pi^2\omega} \mathrm{d}\vartheta = \frac{v_\omega}{\pi^2} \mathrm{d}\vartheta. \tag{14}$$

If we synchronize the two clocks, $\mathrm{d}\tau = \mathrm{d}\tau_\omega$, we therefore get

$$\frac{4}{h} k_B T_\kappa \frac{c^2}{\kappa} = \frac{v_\omega}{\pi^2}. \tag{15}$$

For the temperature $T_\kappa$ this implies

$$T_k = \frac{\hbar\kappa v_\omega}{2\pi k_B c^2}. \tag{16}$$

[6]By "synchronization" we just understand equality of periods.

Expression (16) is a generalized Davies-Unruh temperature. If we choose a massless wave ( $m_0 = 0$ ), then we are in the situation $u_\omega = v_\omega = c$ and (16) turns into the familiar Davies-Unruh temperature formula [12] [13]

$$T_\kappa = \frac{\hbar\kappa}{2\pi k_B c}. \tag{17}$$

We will use formula (17) in pargraph 3.2.3 in a concrete physical situation.

## 3.2. Lorentz Space-Time

We now want to generalize our approach by assuming that space-time is just locally flat[7]. In order to apply formula (17) we must have an appropriate acceleration. Of course, we want it to be gravitational acceleration. In the next pargraph we will show how transactions can give rise to local gravitational acceleration $g_R$.

### 3.2.1. Gravitational Acceleration

The following argument bases on an exposition in [14]. Let a quantum-event be given by two physical systems of mass $m$ and $M$, respectively, which come into being by a photon-transaction in locally flat space-time at relative rest and distance $R$ to each other. Let further an elementary bit of information be connected to the existence or non-existence of a physical system in space-time. Since a photon offer-wave is a priori emitted symmetrically in all space-directions, we find that the information about the spatial existence of (actualized) systems at time $\Delta t = \frac{1}{\nu} = \frac{R}{c}$ is located on the surface of the sphere with radius $R$ around $M$[8]. This is a kind of holographic principle. We may also assume that a bit of information is part of the surface-information, once it is at a distance of its Compton length $\lambda = \frac{\hbar}{mc}$ from the sphere, and that this information changes linearly with the distance $0 \le \Delta x \le \frac{\hbar}{mc}$ [14] [15][9]. This holds because structureless systems can reasonably be supposed to have the size of their Compton-length. So the quantum-event causes an entropy change of

$$\Delta S = 2\pi k_B \frac{mc}{\hbar}\Delta x. \tag{18}$$

For the total energy within the ball of radius $R$ we have by the holographic principle

$$E = Mc^2 = \frac{1}{2}k_B NT. \tag{19}$$

The number $T$ is the surface-temperature on the sphere of radius $R$ and $N$

[7]"Locally flat" means approximately flat in small regions around a point $x_0$. Technically this amounts to $g_{ab}(x_0) = \eta_{ab}$, $\Gamma^k_{ij}(x_0) = 0$, but generally $\Gamma^k_{ij,\nu}(x_0) \neq 0$, $0 \le i, j, k, \nu \le 3$.

[8]Since transactions can go either way, there is a priori a symmetry regarding the question, which of the two masses is actually in the center. This is why all masses mutually gravitate.

[9]This assumption implies $R > \lambda$.

denotes the number of bits on the surface, for which we have with the Planck-length $l_P = \sqrt{\frac{G\hbar}{c^3}}$ [10]

$$N = \frac{A_R}{l_P^2} = \frac{4\pi R^2 c^3}{G\hbar}. \tag{20}$$

By (19) and (20) we get for the surface-temperature $T$

$$T = \frac{MG\hbar}{2\pi R^2 k_B c}. \tag{21}$$

For the total energy-change on the surface we have the entropic-force equation

$$\Delta S \cdot T = F \cdot \Delta x. \tag{22}$$

By plugging (18) and (21) into (22), we arrive at

$$F = G \cdot \frac{Mm}{R^2} = m \cdot g_R. \tag{23}$$

Therefore we can think of local gravitational acceleration as the result of a kind of "osmotic pressure" towards the other emerging parts of space-time. Local gravity is a consequence of light-induced quantum-events and the second law.

### 3.2.2. Einstein Equation

Let a test-system at small distance $R$ be actualized by exchanging photons with $M$ and consequently feel the acceleration $g_R$. The energy-emission by the photons must appear in the local rest-frame of the accelerated system as a spontanous emission from a heat bath in the environment. The temperature is $T_{g_R}$ (17), since the period of the corresponding thermal clock must be synchronous with the one of the underlying light-clock (11). This synchronization amounts by (15) to the equation

$$\frac{4}{h} k_B T_{g_R} \frac{c}{g_R} = \frac{1}{\pi^2}. \tag{24}$$

with $E = Mc^2, l_P = \sqrt{\frac{G\hbar}{c^3}}$ and $A_R = 4\pi R^2$ we derive from (24)

$$k_B T_{g_R} A_R = 4 l_P^2 E. \tag{25}$$

By using (17), this leads to

$$g_R A_R = \frac{4\pi G}{c^2} E. \tag{26}$$

Note that Equation (26) is interesting per se, since it encapsulates the Gauss-Bonnet theorem for compact orientable surfaces in $\mathbb{R}^3$ of genus 2 (*i.e.* without handles) (see **Appendix B**). We are interested, however, in a dynamic development of (26). In the sequel we will continue to work in the local inertial coordinate-chart around the origin ($M$) and develop Einstein's equation for the $oo(tt)$-

[10]The Planck-length can be understood as a minimal Schwarzschild radius, as shown in **Appendix A**.

component of the metric-tensor. This will suffice to reveal the structure of the equation. With $V_R(t)$ denoting the volume of a small ball of test-systems at radius $R(t)$ around the origin, with $R(0)=R$, $\dot{R}(0)=0$ and $\ddot{R}(0)=g_R$, we can rewrite (26) as [16] [17]

$$\left.\frac{\mathrm{d}^2}{\mathrm{d}t^2}\right|_{t=0} V_R = \frac{4\pi G}{c^2}E. \tag{27}$$

If we introduce the energy-momentum tensor $T_{ab}, 0\le a,b\le 3$, with zero-component $T_{00}=\lim_{R\to 0}\frac{E_R}{V_R}$ [11], denoting the energy density at the origin, and use the local properties of the Ricci tensor $R_{ab}, 0\le a,b\le 3$, we have at the origin [16] [17] (see **Appendix C**)

$$\left.\frac{\ddot{V}_R}{V_R}\right|_{t=0} \xrightarrow{R\to 0} c^2 R_{00}. \tag{28}$$

Hence (26) turns in the limit $R\to 0$ into

$$R_{00}=\frac{4\pi G}{c^4}T_{00}. \tag{29}$$

### 3.2.3. Momentum-Flow

In a transaction there is a transfer of four-momentum through photons connected to a quantum-event. In paragraph 3.1 we called this momentum-transfer "event-radiation". In order to synchronize local light-clocks (24) we have so far only made use of the energy (zero)-component of event-radiation. Let $A_i, i=1,2,3$, be small surface elements with $\left\langle \boldsymbol{n}_{A_i} \middle| \boldsymbol{e}_j \right\rangle = 0, i\neq j$. From the 3-momentum there arises pressure in the spatial-directions, which defines the Laue-scalar at the origin

$$T=\sum_{i=1}^3 T_{ii}=\lim_{A_i\to 0}\sum_{i=1}^3 \frac{F_i}{A_i}=\lim_{A_i\to 0}\sum_{i=1}^3 \frac{1}{A_i}\frac{\mathrm{d}p_i}{\mathrm{d}t}. \tag{30}$$

This quantity also contributes to the energy density in (29). Let $N_R(t)$ be the number of actualizations within volume $V_R$ at time *t*. We have with $x_0=ct, \tilde{N}_R(x_0)=N_R\left(\frac{x_0}{c}\right)$ and the de Broglie-relation $p=\frac{h}{R}$

$$T=3\frac{\mathrm{d}N_R(t)}{\mathrm{d}tA_R}\cdot\frac{h}{R}=3\frac{c\cdot h}{3}\cdot\frac{\mathrm{d}\tilde{N}_R(x_0)}{\mathrm{d}x_0 V_R}=c\cdot h\cdot\frac{\mathrm{d}\lambda(x_0)}{\mathrm{d}x_0}. \tag{31}$$

The function $\lambda(x_0)=\frac{\tilde{N}_R(x_0)}{V_R}$ denotes the number of events per 3-volume at time $x_0$ and therefore $\frac{\mathrm{d}\lambda(x_0)}{\mathrm{d}x_0}$ is the change-rate of actualizations per 3-volume. We assumed in (31) that $\lambda(x_0)$ is constant over 3-space (*i.e.* in particular independent of *R*), which amounts to the homogeneity and isotropy of space with respect to actualizations. We have also tacitly assumed that $\lambda(x_0)$ is

[11] We assume *E* to be homogeneously distributed over $V_R$.

a differentiable function in $x_0$. This is an assumption, which cannot hold in the quantum-realm, since events represent discrete sets and are not deterministic, but obey a random-process. The only known Lorentz-invariant stochastic law for the spreading of events in $\mathbb{M}^4$, such that $N \sim V$, is a Poisson-process with constant average (photon) transaction-rate $\varrho_\gamma$ [18]. The homogeneity and isotropy of space-time are thus an immediate consequence of this law. Hence, in the above terminology we have for the averages (expectation values) and $\Delta x_0 > 0$ [12]

$$\bar{\lambda}\left(x_0 + \Delta x_0\right) = \bar{\lambda}\left(x_0\right) + \varrho_\gamma \cdot \Delta x_0 . \tag{32}$$

So by (32) we can define in analogy to (31)

$$\bar{T}_\gamma = 3\frac{c \cdot h}{3} \cdot \frac{\Delta\bar{\lambda}\left(x_0\right)}{\Delta x_0} = c \cdot h \cdot \varrho_\gamma . \tag{33}$$

If we set $T = \left(T_{00} - \bar{T}_\gamma\right)$ we can complete the right hand side of (29) to

$$\frac{4\pi G}{c^4} T_{00} \to \frac{8\pi G}{c^4}\left(T_{00} - \frac{1}{2} T \delta_{00}\right). \tag{34}$$

We may alternatively shift the added amount $\bar{T}_\gamma$ to the left of (29). We have by (33)

$$\frac{4\pi G}{c^4}\bar{T}_\gamma = \frac{4\pi G h}{c^3}\varrho_\gamma = 8\pi^2 l_P^2 \varrho_\gamma . \tag{35}$$

Therefore, with

$$\Lambda = 8\pi^2 l_P^2 \varrho_\gamma , \tag{36}$$

the synchronization-equation takes the form

$$R_{00} - \Lambda\delta_{00} = \frac{4\pi G}{c^4} T_{00} . \tag{37}$$

Note that $\Lambda$ has the dimension of $\frac{1}{(\text{length})^2}$. If matter-energy does not only stem from a static mass $M$, but from more complicated material systems, which also exercise pressure $T$, we finally get our main result by repeating the procedure in (34)

$$R_{00} - \Lambda\delta_{00} = \frac{8\pi G}{c^4}\left(T_{00} - \frac{1}{2} T \delta_{00}\right). \tag{38}$$

Under the assumption of known transformation rules, the full Einstein equations are equivalent to the fact that (38) holds in every local inertial coordinate system around every point in space-time [17].

## 4. Summary

To derive Equation (38) we have used three ideas. The first one is that quantum-events are real actualizations of quantum-systems in space-time and are accompanied by the transfer of four-momentum through bosons, so called

[12] We can expect that there is a lower bound $0 < ct_0 \le \Delta x_0$.

event-radiation. The number of events follows a Poisson-process, and the type of bosons depends on the respective force in action [3] [4] [5] [6]. The second idea is that quantum-systems can serve as (abstract) clocks and that the rhythm of actualizations induced by the electromagnetic force is best measured by the light-clocks, naturally given by the transferred photons. The third idea is that quantum-events induce an "osmotic" force, which locally leads to gravitational acceleration and that clock-periods from the perspective of unequally accelerated systems need to be synchronized, in order to define the same rhythm of time. If the acceleration is of gravitational origin, then the full synchronization-equation turns out to be (38).

The dynamic and expanding space-time of general relativity is hence a consequence of quantum-events and their corresponding event-radiation together with a fixed "yardstick", namely the locally constant speed of light $c$, implicit in the light-clocks used to measure time. There is in particular no direct connection of the constant $\Lambda$ to the energy of the quantum-vacuum. This is a fundamentally different picture to the one we get by trying to attribute fundamental reality to the metric field and quantize it. It furthermore explains quite naturally, why gravitational influence spreads with the speed of light.

Our result was derived under the assumption of a constant cosmological term $\Lambda$ (*i.e.* $\varrho_\gamma$). It is well possible that the value of $\Lambda$ is in fact varying with cosmic time and only appears to be constant over the time periods, which we can possibly oversee. This allows the connection to the Hubble "constant" $\Lambda \sim H^2$, which seems to hold, given the empirical data and the theoretical models at our disposal today [19].

## Conflicts of Interest

The author declares no conflicts of interest regarding the publication of this paper.

## References

[1] Grünbaum, A. (1973) Philosophical Problems of Space and Time: Boston Studies in the Philosophy and History of Science. 2nd Edition, Alfred A. Knopf, Boston. https://doi.org/10.1007/978-94-010-2622-2

[2] Maudlin, T. (2011) Quantum Non-Locality and Relativity. 3rd Edition, Wiley-Blackwell, Malden. https://doi.org/10.1002/9781444396973

[3] Cramer, J.G. (1986) *Review of Modern Physics*, **58**, 647-687. https://doi.org/10.1103/RevModPhys.58.647

[4] Kastner, R.E. (2012) *Foundations of Physics*, **42**, 1094-1113. https://doi.org/10.1007/s10701-012-9658-4

[5] Kastner, R.E. and Cramer, J.G. (2018) *International Journal of Quantum Foundations*, **4**, 210-212.

[6] Kastner, R.E. (2013) The Transactional Interpretation of Quantum Mechanics. Cambridge University Press, Cambridge.

[7] Pusey, M.F., Barret, J. and Rudolph, T. (2012) *Nature Physics*, **8**, 475-478.

https://doi.org/10.1038/nphys2309

[8] Sorkin, R.D. (2006) *Einstein Online*, **2**, 1007.

[9] Knuth, K. and Bahreyni, N.A. (2014) *Journal of Mathematical Physics*, **55**, Article ID: 112501. https://doi.org/10.1063/1.4899081

[10] Margolus, N. and Levitin, L.B. (1998) *Physica D*, **120**, 188-195. https://doi.org/10.1016/S0167-2789(98)00054-2

[11] Rovelli, C. and Smerlak, M. (2011) *Classical and Quantum Gravity*, **20**, Article ID: 075007. https://doi.org/10.1088/0264-9381/28/7/075007

[12] Unruh, W.G. (1076) *Physical Review D*, **14**, 870. https://doi.org/10.1103/PhysRevD.14.870

[13] Davies, P.C.W. (1975) *Journal of Physics A*: *Mathematical and General*, **8**, 609-616. https://doi.org/10.1088/0305-4470/8/4/022

[14] Verlinde, E. (2011) *JHEP*, **4**, 29. https://doi.org/10.1007/JHEP04(2011)029

[15] Bekenstein, J.D. (1973) *Physical Review D*, **7**, 2333. https://doi.org/10.1103/PhysRevD.7.2333

[16] Fischer, K. (2009) Einsteins-Gleichung der Gravitation ausgedrückt in Tensoren: Relativitätstheorie in einfachen Worten. Springer Spektrum, Berlin, 160.

[17] Baez, J. and Bunn, E. (2007) *American Journal of Physics*, **73**, 644-652. https://doi.org/10.1119/1.1852541

[18] Bombelli, L., Henson, J. and Sorkin, R.D. (2006) *Modern Physics Letters A*, **24**, 2579-2587. https://doi.org/10.1142/S0217732309031958

[19] Sorkin, R.D. (2007) *AIP Conference Proceedings*, **957**, 142-152. https://doi.org/10.1063/1.2823750

[20] Rovelli, C. and Vidotto, F. (2015) Foundations: Covariant Loop Quantum Gravity. Cambridge University Press, Cambridge, 3-27.

## Appendix A

We follow the exposition in [20]. It is well known that an amount of energy $E \sim M$ has an associated Schwarzschild radius $r_S = r_S(M) = \frac{2GM}{c^2}$, which screens it off from the rest of space-time, if it is concentrated within a sphere of radius $r \le r_S$. The question is, whether there is some lower bound $r_S^{\min}$ on the radii, below which no mass can concentrate. Indeed such a minimum exists due to quantum considerations. Assume that there is a system of energy $E$ with corresponding mass $M = \frac{E}{c^2}$. By the uncertainty relation we know that, if the object is localized within a range $\sim L$, then its momentum satisfies $p \ge \frac{\hbar}{L}$. We further assume that clssically $r_S \sim \frac{GM}{c^2}$, because the horizon-radius varies for spinning black holes, and we are looking for a minimum[13]. Further, since we want to localize very precisely, we will be in the relativistic limit and $E \sim pc$. If we take $L$ arbitrarily small, then $M$ will grow so much that $r_S$ becomes larger than $L$ and we lose localization. So we can lower $L$ only until we have $r_S = L$. Hence there is the following sequence for a minimal radius $L_{\min}$

$$L_{\min} = \frac{GM}{c^2} = \frac{GE}{c^4} = \frac{Gp}{c^3} = \frac{G\hbar}{c^3 L_{\min}}. \tag{A1}$$

Therefore we get the Planck-length $L_{\min} = l_P$

$$l_P = \sqrt{\frac{\hbar G}{c^3}}. \tag{A2}$$

No object in space-time can be concentrated blow the Planck-length and $l_P$ becomes an absolute "edge" of space-time. Therefore the Planck-length can consistently be thought of as a kind of minimum Schwarzschild radius

$$r_S^{\min} = l_P. \tag{A3}$$

## Appendix B

Let $K_S = \frac{1}{R^2}$ denote the Gaussian curvature of the 2-sphere $S \subset \mathbb{R}^3$ of radius $R$. With a suitable constant $\alpha$ we can rewrite Equation (26) in integral form

$$\alpha \int_S K_S \mathrm{d}A = \frac{4\pi G}{c^2} E. \tag{B1}$$

Let $\mathcal{S}$ denote a diffeomorphic surface without any additonal energy enclosed. We then have

$$\alpha \int_{\mathcal{S}} K_{\mathcal{S}} \mathrm{d}A = \frac{4\pi G}{c^2} E. \tag{B2}$$

Since $\alpha = MG$ we finally get with the Euler characterisitc $\chi(\mathcal{S}) = 2$

[13]The radius lies between $r_S = \frac{2GM}{c^2}$ for non-rotating black holes and $r_S = \frac{GM}{c^2}$ for maximally spinning ones.

$$\int_S K_S \mathrm{d}A = 4\pi = 2\pi\chi(S). \tag{B3}$$

## Appendix C

For the sake of completeness, we want to indicate how to derive the key relation (28). For this we follow the exposition in [17]. Let two nearby particles at relative rest to each other start to fall freely. If the initial velocity of particle one was $v$, then the one of the second particle follows from parallel transport along the connecting vector $\varepsilon u$. If we compare the two velocities after some small time $\varepsilon$, then the first one moved along $\varepsilon v$ and we have to again parallel transport it to $v_1$ in order to compare it to the corresponding $v_2$. Over the passage of time the avarage relative accelertion of the two particles $a_\varepsilon$ is $a_\varepsilon = \frac{v_2 - v_1}{\varepsilon}$. By the definition of the curvature tensor $R$ there holds

$$\lim_{\varepsilon\to 0} \frac{v_2 - v_1}{\varepsilon^2} = R(u,v)v. \tag{C1}$$

Hence, by the symmetries of the tensor $R$,

$$\lim_{\varepsilon\to 0} \frac{a_\varepsilon}{\varepsilon} = -R(v,u)v, \tag{C2}$$

or in coordinate-components

$$\lim_{\varepsilon\to 0} \frac{a_\varepsilon^j}{\varepsilon} = -R^j_{klm} v^k u^l v^m. \tag{C3}$$

A small ball $V_R$ of test particles, starting at relative rest and moving geodesically, changes in second order to an ellipsoid whose axes initially don't rotate. We can therefore chose local inertial coordinates in which (to second order) the center of the ball doesn't move and the principal axes of the ellipsoid stay aligned with the coordinate axes. If the ball's initial radius is $\varepsilon$, then $r^j(t) = \varepsilon + \frac{1}{2}a^j t^2 + O(t^3)$. Hence

$$\lim_{t\to 0} \frac{\ddot{r}^j}{r^j} = \frac{a_\varepsilon^j}{\varepsilon}. \tag{C4}$$

with $u$ denoting the unit-vector in $j$-direction and $v$ the one in time-direction we have by C3 withtout summation over $j$

$$\lim_{\varepsilon\to 0}\lim_{t\to 0} \frac{\ddot{r}^j(t)}{r^j(t)} = -R^j_{tjt}. \tag{C5}$$

Since the volume of our ball is proportinate to the radii,

$\lim_{t\to 0}\left(\frac{\ddot{V}}{V}\Big|_t\right) = \lim_{t\to 0}\sum_j \frac{\ddot{r}^j(t)}{r^j(t)}$, so with summation over all four $j$ (since $R^t_{ttt} = 0$)

$$\lim_{V\to 0} \frac{\ddot{V}}{V}\Big|_{t=0} = -R^j_{tjt} = -R_{00}. \tag{C6}$$

We get the reverse sign in (28) because in (26) we are actually working with $-g_R$, and the factor $c^2$ in front of the Ricci-curvature stems from the line-element $\mathrm{d}\tau = c\mathrm{d}t$.

Journal of Modern Physics, 2020, 11, 1856-1873
https://www.scirp.org/journal/jmp
ISSN Online: 2153-120X
ISSN Print: 2153-1196

# Motion in Clifford Space

**Magd E. Kahil**[1,2]

[1]Faculty of Engineering, Modern Sciences and Arts University, Giza, Egypt
[2]Egyptian Relativity Group, Cairo, Egypt
Email: e.mailmkahil@msa.eun.eg, magdelias.kahil@gmail.com

**How to cite this paper:** Kahil, M.E. (2020) Motion in Clifford Space. *Journal of Modern Physics*, **11**, 1856-1873.

https://doi.org/10.4236/jmp.2020.1111116

**Received:** October 22, 2020
**Accepted:** November 17, 2020
**Published:** November 20, 2020



## Abstract

Clifford algebra as an approach of geometrization of physics plays a vital role in unification of micro-physics and macro-physics, which leads to examine the problem of motion for different objects. Equations of charged and spinning of extended objects are derived. Their corresponding deviation equations as an extension of geodesics and geodesic deviation of vectors in Riemannian geometry have been developed in case of Clifford space.

## Keywords

Cifford Space, Poly-Vectors-Geodesics, Geodesic Deviation, Spinning Objects, Extended Objects

## 1. Clifford Space: Aims and Prospects

Motion of objects is regarded as a mirror to identify the behavior of field equations on manifolds. This may give rise to examine the trajectories of different particles to ensure the existence of any theory and its viability. From this perspective, we ought to study the problem of spinning objects in depth, as it is very close to the reality, rather than examining its simplicity by means of determining the equation of motion of test particles, *i.e.* the geodesic equation. The spinning object has been studied by many authors long time ago, Mathisson [1] started the idea; Papapetrou amended its content [2] and then it was developed to include charged objects by Dixon [3], which led many of their followers to obtain the corresponding equations of motion of moving objects in different types of geometries [4–9]. Not only these path equations but also their deviation equations play a fundamental role in regulating the stability of objects [10]. This is mandatory in case of examining the perturbation problem of an object orbiting a gravitational field. Yet, such a description may be in need to be revisited thoroughly for sake of unification of physics. Since the problem of unification of all fields of nature is a far fetched goal, it is wise enough to search for different methods and concepts that enable us to achieve this goal one day.

Accordingly, examining the problem of unification may be found by studying the motion of particles subject to these fields. This may give rise to search for different types of geometries or philosophies to achieve this task. One of proposals is to reconsider a specific geometry based strings, 1 loop, 2-loops, 3-loops, etc. In general it can be described as p-branes rather than points. This shows vectors as candidates of poly-vectors to represent objects in nature as extended ones rather than point-like. Consequently, it has been found that Clifford Algebra is a good candidate to describe these quantities, leading to the concept of Clifford space (C-space) [11]. From this perspective, and relying to examine the problem of motion for those extended objects, Pezzaglia (1997) performed an introductory step toward this task by studying the equations of motion [11,12]. Throughout his work, he focussed on the nature of the bases of C-space that are non-orthogonal, which widens the scope to reveal some obscure relations that are already untested. Such an approach has been given an additional role for quantities like the tetrad formalism as a tool for defining skew symmetric quantities like torsion of space-time, and spin connection in non-Riemaniann geometries. This tendency would be able to revise the absolute parallelism approach [13–15], as well as the Poincare gauge theories of gravity [16, 17]. Moreover, it gives a clear vision to detect the effect of spin of space-time as appeared in skew part of $g_{\mu\nu}$ [12]. Accordingly, the principle geometrization of physics has been applied in an extensive way rather than before in the conventional point-like manifold theories [18] .

Consequently, the concept of a manifold composing points to identify space-time is amended to include, lines, ares, volumes, ... etc. According to this descriptive vision particles may be defined as extended objects, rather than point-like ones [19]. This is performed by means of applying the Clifford algebra, which is regarded as pan-dimensional continuum or Clifford space (C-space). Due to this type of classification it is worth mentioning that, Castro and Pavsic (2005) revisited Clifford space to perform its extended relativity [18]. This theory has two fundamental parameters: the speed of light $c$ and a length scale which can be set to the Planck length. The poly vector coordinates $x^{\mu}, x^{\mu\nu}, x^{\mu\nu\rho}$... are now connected with basis poly-vector, bi-vector, tri-vector, ... r-vector, the generators $\gamma_{\mu_1} \wedge .... \wedge ... \wedge \gamma_{\mu_r}$ of the Clifford algebra, including the Clifford algebra unit element [20].

From this perspective, it can be found that strings and p-branes are expressed in the following way:

For a closed string (1-loop) which is embedded in a target flat background of D-dimensions whose projection is appeared within coordinate-planes in terms of variables $x_{\mu\nu}$. Similarly, a closed membrane (a 2-loop) may be described by anti-symmetric variables $x_{\mu\nu\rho}$ representing the corresponding 3-volume enclosed by the the 2-loop [21].

The aim of the present work is to extend the Castro-Pavsic approach of poly-vectors in C-space to derive modified equations of motion for extended objects and spinning ones. The significance of the derivation of these equations is in examining the existence of the notion of mass, charge and spin of an extended object associated with poly-vectors and compare them with the conventional ones as described within the context of vectors.

The paper is organized as follows: Section (2) displays briefly the geometry of C-space and its implications in physics. Section (3) per-

forms the trajectories of poly-vectors in C-space. Section (4) discusses the relationship between geodesics and geodesic deviations of poly-vectors and their link with charged and spinning poly-vectors. Section (5) displays a modified Lagrangian which enables us to determine both charged and spinning poly-vector equations as well as their deviation equations. Section (6) discusses the impact of determining these equations in revisiting the old notations of problem of motion using the conventional methods of a point-like manifold of describing space-time.

## 2. C-Space: A Brief Introduction

Following the geometrization scheme of physics, a new elegant formalism has been performed, which may explore new hidden physics to show an insightful vision for revisiting the old notations of physics. Such a trend is a crystal clear using Clifford Algebra which leads to express many physical quantities in a compact form [22]. Due to the richness of Clifford algebra, scalars, vectors, bi-vectors and r-vectors are expressed in one form called Clifford aggregate or poly-vector. The coordinates of poly-vectors contain, vectors, areas, volumes ... etc expressed as follows The poly-vector $X^M$ is defined as follows [23]

$$X^M \equiv X^{\mu_1\mu_2\mu_3\cdots}. \tag{2.1}$$

Accordingly, it can be shown that poly-vector coordinates of C-space are parameterized not only by 1-vector coordinates $x^\mu$ but also by the 2-vector coordinates $x^{\mu\nu}$, 3-vector coordinates $x^{\mu\nu\rho}$ ... etc called holographic coordinates, such that

$$\begin{aligned} X^M =& s\mathbf{1} + x^\mu\gamma_\mu \\ =& x^{\mu\nu}\gamma_\mu\wedge\gamma_\nu + x^{\mu\nu\rho}\gamma_\mu\wedge\gamma_\nu\wedge\gamma_\rho \\ &+ x^{\mu\nu\rho\sigma}\gamma_\mu\wedge\gamma_\nu\wedge\gamma_\rho\wedge\gamma_\sigma, \end{aligned} \tag{2.2}$$

where the component $s$ is the Clifford scalar components of a poly-vector valued coordinates.

Thus, in C-space proper time interval may be described as in Minkowski space [18]

$$(dS)^2 = (ds)^2 + dx_\mu dx^\mu + dx_{\mu\nu}dx^{\mu\nu} + \ldots\ldots \tag{2.3}$$

### 2.1. C-Space: Underlying Geometry

A point in C-Space is defined as a set of holographic coordinates $(s, x^\mu, x^{\mu\nu}, \ldots)$ forming the coordinates of a poly-vector. Each one is expressed within bases $\{\gamma_A\} = \{1, \gamma_{a_1}, \gamma_{a_1a_2}, \gamma_{a_1a_2a_3}\ldots.\}$ , $a_1 < a_2 < a_3 < a_4 < a_5 < \ldots$, $r = 1, 2, 3\ldots.$, where $\gamma_{a_1a_2a_3\ldots} = a_1\wedge a_2\wedge a_3\ldots.$ [23]. It is well known that the local basis $\gamma_\mu$, is related to the tetrad field $e^a_\mu$ such that

$$\gamma_\mu = e^a_\mu\gamma_a.$$

An element of a Clifford algebra is a superposition, called Clifford aggregate or poly-vector:

$$A = a + \frac{1}{1!}a^\mu\gamma_\mu + \frac{1}{2!}a^{\mu\nu}\gamma_\mu\wedge\gamma_\nu + \ldots\ldots\ldots\frac{1}{n!}a^{\mu_1\ldots.\mu_n}\gamma_{\mu_1}\wedge\ldots\ldots\gamma_{\mu_n}. \tag{2.4}$$

The differential of C-space is defined as follows [21]

$$dA = \frac{\partial A}{\partial X^B}dX^B, \tag{2.5}$$

i.e

$$dA = \frac{\partial A}{\partial s} + \frac{\partial A}{\partial x^{\mu}} dx^{\mu} + \frac{\partial A}{\partial x^{\mu\nu}} dx^{\mu\nu} + ..... \tag{2.6}$$

If one takes $A = \gamma_{\mu}$, then

$$d\gamma_{\mu} = \frac{\partial \gamma}{\partial s} + \frac{\partial \gamma_{\mu}}{\partial x^{\mu}} dx^{\mu} + \frac{\partial \gamma_{\mu}}{\partial x^{\mu\nu}} dx^{\mu\nu} + ....., \tag{2.7}$$

which becomes

$$d\gamma_{\mu} = \frac{\partial \gamma}{\partial s} + \Gamma^{\alpha}_{\mu\nu} dx^{\nu} + \Gamma^{\alpha}_{\mu[\nu,\rho]} dx^{\nu\rho} + ....., \tag{2.8}$$

and can be reduced to

$$d\gamma_{\mu} = \frac{\partial \gamma}{\partial s} + \Gamma^{\alpha}_{\mu\nu} dx^{\nu} + \frac{1}{2} R^{\alpha}_{\beta\nu\rho} dx^{\nu\rho} + ....., \tag{2.9}$$

where $R^{\alpha}_{\beta\nu\rho}$ is the curvature of space-time.

Also, it can be found that for an arbitrary poly-vector $A^{M}$

$$\frac{DA^{M}}{Dx^{\mu\nu}} = [D_{\mu}, D_{\nu}]A^{M}. \tag{2.10}$$

where $\frac{D}{Dx^{\mu\nu}}$ is the covariant derivative with respect to a plane $x^{\mu\nu}$, such that

$$\frac{Ds}{Dx^{\mu\nu}} = [D_{\mu}, D_{\nu}]s = K^{\rho}_{\mu\nu}\partial_{\rho}s, \tag{2.11}$$

such that $K^{\rho}_{\mu\nu}$ is the torsion tensor.

$$\frac{Da^{\alpha}}{Dx^{\mu\nu}} = [D_{\mu}, D_{\nu}]a^{\alpha} = R^{\alpha}_{\rho\mu\nu}a^{\rho} + K^{\rho}_{\mu\nu}D_{\rho}a^{\alpha}, \tag{2.12}$$

Yet, this type of torsion (2.12) can related to the notion of torsion as mentioned by Hammond as commutator the potential associated by a prescribed scalar field $\phi$ [25]

$$K^{\alpha}_{\mu\nu} = \frac{1}{2}(\delta^{\alpha}_{\mu}\phi_{,\nu} - \delta^{\alpha}_{\nu}\phi_{,\mu}). \tag{2.13}$$

Thus, we can figure out that the torsion as defined in C-space (Riemannian-type) by means of the parameter(s) $s$ may act like an independent scalar field defined in the usual context of the Riemann-Cartan geometry.

From examining Equation (2.11) and Equation (2.12), one can find the existence of torsion tensor even in the presence of symmetric affine connection apart from its conventional notation definition of being the antisymmetric part of an affine connection as in the context of non-Riemannian geometries [13–15]. Accordingly, owing to C-space one may realize the dispute between the reliability of torsion propagating or non-propagating this can be resolved by means of of we describe torsion as a result of covariant differentiation of areas of holographic coordinates and non-propagating as being defined as anti-symmetric parts of an affine connection of poly-vectors or vectors, if one utilizes in the internal or external coordinate and its corresponding non-symmetric affine connection.

Consequently, we can regard that the geometry described within the coordinates of poly-vector described not only Riemannian but also a non-Riemannian, *i.e.* the composition of a Riemannian affine

connection for the poly-vector is not necessarily Riemannian as well. This may shed some light to find out that a Riemannian Poly-vector affine connection and curvature (external coordinate capital Latin letters) may be described by non Riemannian quantities as describing its holographic coordinates (internal coordinate (Greek letters).

Accordingly, in C-space it is convenient to distinguish two frame fields [21]:

(i) Coordinate frame field, whose bases elements $\gamma_M, M = 1,2,3....2^n$ depend on the position of $X$ in C-space such that their expressions as the wedge products of vectors can not be preserved globally. Thus, one writes

$$\gamma_M \equiv \gamma_{\mu_1....\mu_r}. \tag{2.14}$$

The scalar product of two such basis elements gives the metric tensor of the C-space

$$^{\ddagger}\gamma_M.\gamma_N = G_{MN}, \tag{2.15}$$

(ii) Orthonormal frame field, whose bases elements $\gamma_{(A)}$, $(A) = 1,2,3,...2$ can at every point be expressed as a wedge product,

$$\gamma_{(A)} \equiv \gamma_{a_1....a_r} = \gamma_{a_1} \wedge \gamma_{a_2} \wedge \gamma_{a_3}..... \wedge \gamma_{a_r}, \tag{2.16}$$

The scalar product of the latter basis elements gives

$$^{\ddagger}\gamma_{(A)}.\gamma_{(B)} = \eta_{AB} \tag{2.17}$$

where $\eta$ is the metric tensor in flat space.

The derivative of a poly-vector is classified as follows [24]:

(i) Scalar field: Acting on a scalar field, it behaves as an ordinary partial derivative, *i.e.*

$$\partial_M \phi = \frac{\partial \phi}{\partial X^M}. \tag{2.18}$$

(ii) Coordinate bases: Acting on coordinate basis elements, it gives

$$\partial_M \gamma_N = \Gamma^Q_{MN} \gamma_Q \tag{2.19}$$

where $\Gamma^Q_{MN}$ is an affine connection. The commutator of the derivatives acting on $\gamma_J$ gives the Riemann tensor in $C$-space:

$$[\partial_M, \partial_N]\gamma_J = R^K_{\ .JMN}\gamma_K \tag{2.20}$$

(iii) Orthonormal bases (local frame field): These types of bases turn to be as follows

$$\partial_M \gamma_{(A)} = -\Omega^N_{A\ .\ M}\gamma_{(B)} \tag{2.21}$$

such that $\Omega^N_{A\ .\ M}$ acts as its appropriate spin connection.

Thus, the commutator of the derivatives acting on $\gamma_A$ gives

$$[\partial_M, \partial_N]\gamma_A = R^B_{\ .AMN}\gamma_B. \tag{2.22}$$

Thus, for an aggregate poly-vector $A$ one finds that:

$$\begin{aligned}\partial_M(A^N\gamma_N) =& \partial_M A^N \gamma_N + A^N \partial_M \gamma_N \\ =& (\partial_M A^N + \Gamma^N_{MK} A^K)\gamma_N \equiv (D_M A^N)\gamma_N,\end{aligned} \tag{2.23}$$

where $D_M A^N$ is the covariant derivative acting on the plyvector components $A^N$.

## 2.2. C-space and the Tetrad Field

The relationship between the two bases are related by the tetrad field $E^A$ associated with poly-vectors [24]

$$\gamma_M = E_M^{(A)}\gamma_{(A)}, \tag{2.24}$$

where $E_M^A$ is the C-space vielbein, such that

$$G_{MN} = E_M^{(A)}E_N^{(B)}\eta_{AB}. \tag{2.25}$$

Such a description does not preclude the non-Riemannian version of poly-vectors, which is a step to revisit the definition of the fundamental quantities that play an active role of describing such a type of geometry.

Accordingly, it is vital to note that the covariant derivative of C-space associated with Vielbein of poly-vector takes the following condition [20]

$$\partial_N E_M^C - \Gamma_{MN}^P E_P^C - E_M^A \Omega_{A\ .\ N}^C = 0, \tag{2.26}$$

Consequently, the covariant derivative acting on the tetrad field is invariant under general coordinate transformation by means of $\Gamma_{NQ}^M$ and local Lorentz invariance as expressed in terms of $\Omega_{A\ .\ N}^C$ representing the spin connection in C-space.

The curvature of C-space is defined, as usually, by the commutator of derivatives acting on basis poly-vectors [23]:

$$[D_M, D_N]\gamma_J = R_{MNJ}^K\gamma_K, \tag{2.27}$$

or

$$[D_M, D_N]\gamma_{(A)} = R_{MNJ}^{(B)}\gamma_{(B)}, \tag{2.28}$$

where $D_M$ is its associate covariant derive.

Meanwhile, introducing the reciprocal basis poly-vectors $\gamma^M$ and $\gamma^A$ satisfying

$$(\gamma^M)^\ddagger * \gamma_N = \delta_N^M, \tag{2.29}$$

$$(\gamma^{(A)})^\ddagger * \gamma_{(B)} = \delta_{(B)}^{(A)}. \tag{2.30}$$

The components of curvature in the corresponding bases are defined as follows

$$R_{MNJ}^K = \partial_M\Gamma_{NJ}^K - \partial_N\Gamma_{MJ}^K + \Gamma_{NJ}^L\Gamma_{ML}^K - \Gamma_{MJ}^L\Gamma_{NL}^K \tag{2.31}$$

or

$$\begin{aligned} R_{MN(A)}^K =& \partial_M\Omega_{(A)\ N}^{K} - \partial_N\Omega_{(A)\ M}^{K} \\ &+ \Omega_{(A)\ N}^{(C)}\Omega_{(C)\ M}^{K} - \Omega_{(A)\ M}^{(C)}\Omega_{(C)\ N}^{K}. \end{aligned} \tag{2.32}$$

The latter expression is a generalization to $C$-space of the analogous expression in Riemannian geometry for manifolds of point-like objects [26].

Moreover, there is a counterpart version of non-vanishing curvature and torsion as defined in non-Riemannian geometry, in C-space leading to define torsion of poly-vectors to become

$$\Lambda_{MN}^J = \bar{\Gamma}_{MN}^J - \bar{\Gamma}_{NM}^J. \tag{2.33}$$

Also, the contortion of poly-vectors $\Omega_{BCM}$ is given by

$$\Omega_{BCM} = \frac{1}{2} E_M^{(A)} (\Delta_{[(A)(B)](C)} - \Delta_{[(B)(C)](A)} + \Delta_{[(C)(A)](B)}) \quad (2.34)$$

where $\Delta_{[(A)(B)](C)}$ is defined as the Ricci coefficient of rotation [23]

$$\Delta_{[(A)(B)](C)} = E_{(A)}^M E_{(B)}^N (\partial_M E_{N(C)} - \partial_M E_{N(C)}).$$

Moreover, another covariant derivative associated with non-symmetric affine connection $\bar{\Gamma}_{NK}^M$ is defined as follows

$$X_{|N}^M = \partial_N X^M + \bar{\Gamma}_{NS}^M X^S, \quad (2.35)$$

such that

$$\bar{\Gamma}_{NS}^M X^S = \Gamma_{NS}^M X^S + \Delta_{NS}^M \quad (2.36)$$

$$X_{|NS}^M - X_{|SN}^M = \bar{R}_{QNS}^M X^Q + \Lambda_{NS}^Q X_{|Q}^M. \quad (2.37)$$

such that

$$R_{MNJ}^K = \partial_M \bar{\Gamma}_{NJ}^K - \partial_N \bar{\Gamma}_{MJ}^K + \bar{\Gamma}_{NJ}^L \bar{\Gamma}_{ML}^K - \bar{\Gamma}_{MJ}^L \bar{\Gamma}_{NL}^K. \quad (2.38)$$

Due to richness of these quantities this type work will be going to examine the behavior of extended objects subjects having sensitivity to these quantities in our future work ; while in our present work we focus on deriving the equations of motion and their deviation paths for different extended objects spinning and charged for poly-vectors defined within the context of Riemannian-like C-Space as explained in the following sections .

## 2.3. C-Space: An Arena of Unifying Physics

It is worth mentioning that, physical objects considered as matter in space-time, can be in the form of membranes (brane) of various dimensions (p-branes) [18]

From this perspective, the notation of Clifford aggregate as described in (2.1) , it may be important to revisit the conventional notations of mass and charge in the presence of C-space to be

$$M = m\mathbf{1} + p^\mu \gamma_\mu + S^{\mu\nu} \gamma_{\mu\nu}, \quad (2.39)$$

and

$$\epsilon = e\mathbf{1} + A^\mu \gamma_\mu + F^{\mu\nu} \gamma_{\mu\nu}, \quad (2.40)$$

where $M$ and $\epsilon$ are mass and charge of extended objects respectively.

Nevertheless, it is vital to be noted that in Clifford Space, there is a striking virtue, unlike the conventional string theory which expressed within 26 dimensions in which gauge fields are described as compact dimensions; while in C-space there is only 16 non-compact dimensions. Consequently, Pavsic (2005) generalized the conventional 4-dimensional space-time into 16 dimensional à la Klauza-Klein theory [23].

(i) There is no need for extra-dimensions of its corresponding space-time.

(ii) There is no need to have compact extra-dimensions. The extra-dimensions of C-space, namely $x^\mu, x^{\mu\nu}, x^{\mu\nu\rho}$, and $x^{\mu\nu\rho\sigma}$ describe the extended objects, therefore they are regarded as physical dimensions.

(iii) The number of components $G_{\mu\tilde{M}}$ , $\mu = 0, 1, 2, 3$ and $\tilde{M} \neq \mu$ is 12, which is the same as the number of gauge fields in the standard models.

Thus, the line element of poly-vectors in C-space become

$$|dX|^2 = dS^2 = G_{MN} dX^M dX^N, \tag{2.41}$$

i.e.

$$dS^2 = ds^2 + L^{-2} dx_\mu dx^\mu + L^{-4} dx_{\mu\nu} x^{\mu\nu} + L^{-6} dx_{\mu\nu\rho} x^{\mu\nu\rho} + ....,$$

where $G_{MN} = E_M^\dagger E_N$ is C-space metric, $L$ is the Planck length [12]. Consequently, Equation (2.43) can be expressed as

$$\begin{aligned} dS^2 =& c^2 dt^2 (1 + \frac{L^{-2}}{c^2} \frac{dx_\mu}{dt} \frac{dx^\mu}{dt} \\ &+ \frac{L^{-4}}{c^2} \frac{dx_{\mu\nu}}{dt} \frac{dx^{\mu\nu}}{dt} + \frac{L^{-6}}{c^2} \frac{dx_{\mu\nu\rho}}{dt} \frac{dx^{\mu\nu\rho}}{dt} + ....) \end{aligned} \tag{2.42}$$

with taking into account that the parameter $s$ is described only in the ordinary space-time *i.e.* $(ds)^2 = g_{\mu\nu} dx^\mu dx^\nu$ [22].

Meanwhile, in C-space, Castro and Pavsic (2005), showed that, there are some principles must be revisited especially the speed of light which is no longer the upper limit to be reached, but another combination of constants made of Planck's length in the following way [18]:

(i) Maximum 1-vector speed $\frac{dx^\mu}{ds} = 3 \times 10^8 m s^{-1}$ ,

(ii) Maximum 2-vector speed $\frac{dx^{\mu\nu}}{ds} = 1.6 \times 10^{-35} m^2 s^{-1}$ ,

(iii) Maximum 3-vector speed $\frac{dx^{\mu\nu\rho}}{ds} = 7.7 \times 10^{-62} m^3 s^{-1}$ ,

(iv) Maximum 4-vector speed $\frac{dx^{\mu\nu\rho}}{ds} = 7.7 \times 10^{-96} m^4 s^{-1}$ ... etc.

Also, it is worth mentioning that by means of C-space a particle as observed from 4-dimensional space, that can be speed of particles may be more than the conventional speed of light due to involvement of holographic coordinates $x^{\mu\nu}$, $x^{\mu\nu\rho}$ ... etc ; but does not exceeds the modified speed of light due to C-space. This can lead us to consider there will be specific upper limit to objects due to p-brans as $p = 0, 1, 2, 3, ...$

The Line element of poly-vectors in C-space is defined as follows [23]:

$$dS^2 = G_{MN} dX^M \times dX^N, \tag{2.43}$$

provided that the matrix $G_{MN}$ is defined as

$$G_{MN} = \begin{bmatrix} g_{\mu\nu} & G_{\mu\bar{N}} \\ G_{\bar{M}\nu} & G_{\bar{M}\bar{N}} \end{bmatrix}. \tag{2.44}$$

These degrees of freedom are in principle not hidden by which we describe the extended objects, therefore we do not need to compact dimensions of its internal space.

The metric of C-space $G_{MN}$ is subdivided into $G_{\mu\nu} = g_{\mu\nu}$ which relates to gravity, while gauge fields $G_{\mu\bar{M}}$, where $\mu \neq \bar{M}$ assumes 12 possible values, excluding the four values of $\nu = 0, 1, 2, 3$, and other 12 gauge fields ,to be defined as follows: 1 photon, 3 weak gauge bosons and 8 gluons described $A_\mu$, $A_\mu^a, a = 1, 2, 3$ and by $A_\mu^c c = 1, 1, 3, ...8.$ respectively.

It can be found that the number of mixed components in $G_{\mu\bar{M}} = (G_{\mu\mathbf{1}}, G_{\mu[\alpha\beta]}, G_{\mu[\alpha\beta\gamma]}, G_{\mu[\alpha\beta\gamma\delta]})$ of Clifford metric coincides with the

number of gauge fields in the standard model. For a fixed $\mu$, there are 12 mixed components of $G_{\mu\bar{M}}$ and 12 gauge fields $A^a_\mu, W^c_\mu, A^c_\mu$. This coincidence is fascinating and it may indicate that the known interactions are incorporated in curved Clifford space. The number of mixed metric $G_{\mu\bar{M}}$ is 12 the same numbers as the number of gauge fields in the standard model.

In addition, there are also interaction due to components $G_{\bar{M}\bar{N}}$ but do not have the properties of Yang-Mills fields. Thus, Pavsic (2006) has considered it as a metric of an internal space [24], which may be a glimpse to express bi-metric theory of gravity within the context of C-space . Such a study will be examined in our future work.

# 3. Trajectories of Poly-Vectors in C-Space

## 3.1. Equations of Motion in C-Space

Pavsic [24] considered the classical action for a point particle in C-space:

$$I[X^\mu, G_{MN}] = \int d\tau \sqrt{[G_{MN}\dot{X}^M\dot{X}^N)]} + \frac{\kappa}{16\pi}\int d[x]R. \tag{3.45}$$

The above classical action is a combined action for path equations and gravitational field equations respectively. One obtains its path equation by taking the variation with respect to $X^C$ to der ve corresponding geodesic equation *i.e.*

$$\frac{1}{\sqrt{\dot{X}^2}}\frac{d}{d\tau}\frac{\dot{X}^M}{\sqrt{\dot{X}^2}} + \Gamma^M_{NK}\frac{\dot{X}^M\dot{X}^N}{\dot{X}^2} = 0. \tag{3.46}$$

Also, from the same function (3.47) by taking the variation with respect to $G_{MN}$ one obtains its corresponding field equation

$$R^{MN} - \frac{1}{2}G^{MN}R = 8\pi\kappa\int \delta_{(C)}(x-X)\dot{X}^M\dot{X}^N, \tag{3.47}$$

where $\delta_{(C)}$ is the delta function in C-space. The latter equation can be expressed as

$$R^{MN} - \frac{1}{2}G^{MN}R = 8\pi T_{MN}, \tag{3.48}$$

where $T_{MN}$ is the energy-momentum tensor as defined in C-space.

## 3.2. C-Space and Problem of Motion: Pezzaglia's Approach

As an introductory step to the C-space formalism obtained by Castro-Pavsic [18], it is worth to mention that Pezzaglia had presented a speculative vision about the need to utilize Clifford space, the problem of unification can be passed by stages of composing scalar, vectors and bi-vectors in one form with taking into consideration that the corresponding bases vectors are described in non-orthonormal curved space in the following way [11].

$$\gamma_\mu.\gamma_\nu \equiv \frac{1}{2}\{\gamma_\mu\gamma_\nu\} = \frac{1}{2}\{\gamma_\mu\gamma_\nu + \gamma_\nu\gamma_\mu\} = g_{\mu\nu}, \tag{3.49}$$

where $g_{\mu\nu}$ is the metric tensor which may be a function of position. The outer product of two different bases vectors yields a new object

called a bi-vector, which is the basis of a plane spanned by two basis vectors

$$\gamma_{\mu\nu} = -\gamma_{\nu\mu} =\equiv \gamma_\mu \wedge \gamma_\nu \equiv \frac{1}{2}[\gamma_\mu\gamma_\nu] = \frac{1}{2}(\gamma_\mu\gamma_\nu - \gamma_\nu\gamma_\mu) = s_{\mu\nu}, \quad (3.50)$$

where $s_{\mu\nu}$ acts as the skew symmetric part of the metric $g_{\mu\nu}$ *i.e.*

$$g_{[\mu\nu]} = s_{\mu\nu}.$$

This illustration can be clarified by describing the momentum poly-vector and spin bi-vector angular momentum

$$M \equiv \frac{1}{\lambda} p^\mu \gamma_\mu + \frac{1}{\lambda^2} S^{\mu\nu}\gamma_{\mu\nu}, \quad (3.51)$$

such that $\lambda$ is a universal length constant

$$p^\mu = m\frac{dx^\mu}{ds},$$

and

$$S^{\mu\nu} = m\frac{da^{\mu\nu}}{ds},$$

where $S^{\mu\nu}$, in which is defined to be a bi-vector coordinate. In flat space one finds its corresponding equation of motion

$$\dot{M}^\mu = \frac{dM^\mu}{ds} = 0, \quad (3.52)$$

i.e.

$$\dot{p}^\mu = \frac{dp^\mu}{ds} = 0, \quad (3.53)$$

and

$$\dot{S}^{\mu\nu} = \frac{dS^{\mu\nu}}{ds} = 0. \quad (3.54)$$

It is worth mentioning that the modified momentum which include both linear and spin angular momentum may give rise to describe the momentum of the extended object not consider it as a test particle but a dipole one has an impact on its spinning case. Thus, studying momentum with taking its spinning motion may give rise to regard the spinning of the particle increases its mass as shown in Equation (3.51) and Equation (3.54) [12]. Now, the arising question is the situation of these equations in the presence of gravitational field, which may be expressed as follows

$$\frac{d^2x^\mu}{ds^2} + \Gamma^\mu_{\nu\rho}\frac{dx^\nu}{ds}\frac{dx^\rho}{ds} + \Gamma^\mu_{\nu[\rho,\delta]}\frac{dx^\nu}{ds}\frac{da^{\rho\delta}}{ds} = 0 \quad (3.55)$$

to become in the following way

$$\frac{d^2x^\mu}{ds^2} + \Gamma^\mu_{\nu\rho}\frac{dx^\nu}{ds}\frac{dx^\rho}{ds} + \frac{1}{2m}R^\mu_{\nu\rho\delta}\frac{dx^\nu}{ds}S^{\rho\delta} = 0 \quad (3.56)$$

and

$$\frac{dS^{\mu\nu}}{ds} + \Gamma^\mu_{\sigma\rho}S^{\sigma\nu}\frac{dx^\rho}{ds} + \Gamma^\nu_{\sigma\rho}S^{\mu\sigma}\frac{dx^\rho}{ds} = 0, \quad (3.57)$$

$$\frac{D^2x^\mu}{Ds^2} = \frac{1}{2m}R^\mu_{\nu\rho\sigma}S^{\rho\sigma}\frac{dx^\nu}{ds}, \quad (3.58)$$

and

$$\frac{DS^{\mu\nu}}{Ds} = \frac{da^{\alpha\beta}}{ds}(\Gamma^\mu_{\alpha[\beta,\sigma]}S^{\sigma\nu} + \Gamma^\nu_{\alpha[\beta,\sigma]}S^{\mu\sigma}) = 0, \quad (3.59)$$

*i.e.*

$$\frac{DS^{\mu\nu}}{Ds} = \frac{1}{2m} S^{\alpha\beta}(R^{\mu}_{\alpha\beta\sigma} S^{\sigma\nu} + R^{\nu}_{\alpha\beta\sigma} S^{\mu\sigma}), \tag{3.60}$$

such that $\frac{D}{Ds}$ is the conventional covariant derivative as defined in Riemannian Space. It can be figured out that the Equation (3.60) acts exactly as the Papapetrou equation for short; while extra terms in terms of curvature and spin tensor are added in Equation (3.61).

Following this stream of thinking in case of electro-magnetic field in the presence of flat space, one my find out that

$$\frac{d^2x^{\mu}}{ds^2} = \frac{e}{m} F^{\mu}_{\nu} \frac{dx^{\nu}}{ds}, \tag{3.61}$$

and

$$\dot{S}^{\mu\nu} = \frac{dS^{\mu\nu}}{ds} = \frac{e}{m} F^{[\mu}_{\rho} S^{\nu]\rho}, \tag{3.62}$$

where $F_{\mu\nu}$ is the elecro mangnetic tensor, which turns to be in case of gravitational field as

$$\frac{D^2x^{\mu}}{Ds^2} = \frac{1}{2m} R^{\mu}_{\nu\rho\delta} S^{\rho\delta} \frac{dx^{\nu}}{ds} + \frac{e}{m} F^{\mu\nu} \frac{dx^{\nu}}{ds}, \tag{3.63}$$

and

$$\frac{DS^{\mu\nu}}{Ds} = \frac{e}{m} F^{[\mu}_{\rho} S^{\nu]\rho} + \frac{1}{2} \frac{da^{\alpha\beta}}{ds} (R^{\mu}_{\alpha\beta\sigma} S^{\sigma\nu} + R^{\nu}_{\alpha\beta\sigma} S^{\mu\sigma}), \tag{3.64}$$

such that

$$\frac{DS^{\mu\nu}}{Ds} = \frac{e}{m} F^{[\mu}_{\rho} S^{\nu]\rho} + \frac{1}{2m} S^{\alpha\beta}(R^{\mu}_{\alpha\beta\sigma} S^{\sigma\nu} + R^{\nu}_{\alpha\beta\sigma} S^{\mu\sigma}). \tag{3.65}$$

Thus, it can be shown that Equation (3.66) acts as the Dixon equation, extra terms in terms of curvature and spin tensor are added in Equation (3.67). From studying these equations, we can see the involvement of bi-vector to be affected by additional factors of curvature of the space-time and spin tensor. This may give rise to make sure that in case of tri-vectors and other multi-vectors these effects will be added. Such an argument may impose the necessity to find a general formula capable to embody all these effects. It was found that using poly-vector coordinates may represent all these forms in a compact way. So it is essential to display the underlying geometry of poly-vectors prior to examining the corresponding equations of motion and the deviation ones.

## 3.3. The Bazanski Approach for Poly-Vectors

Equations of geodesic and geodesic deviation equations in Riemannian geometry are required to examine many problems of motion for different test particles in gravitational fields. This led many authors to derive them by various methods, one of the most applicable ones is the Bazanski approach [27] in which from one single Lagrangian one can obtain simultaneously equation of geodesic and geodesic deviations which has been applied in different theories of gravity [4–9],and [28–30]. Thus, by analogy this technique in case of Poly-vectors to become [31],

$$L = G_{MN} U^{M} \frac{D\Psi^{N}}{DS}, \tag{3.66}$$

where, $G_{MN}$ is the metric tensor, $U^{M} = \frac{dX^{M}}{dS}$, is a unit tangent poly-vector of the path whose parameter is $S$, and $\Psi^{\nu}$ is the deviation

poly-vector associated to the path $(S)$, $\frac{D}{DS}$ is the covariant derivative with respect to parameter $S$.

Applying the Euler Lagrange equation , by taking the variation with respect to the deviation poly-vector $\Psi^C$,

$$\frac{d}{dS}\frac{\partial L}{\partial \dot{\Psi}^C} - \frac{\partial L}{\partial \Psi^C} = 0, \tag{3.67}$$

to obtain the geodesic equation

$$\frac{DU^C}{DS} = 0, \tag{3.68}$$

and taking the variation with respect the the unit poly-vector $U^C$,

$$\frac{d}{dS}\frac{\partial L}{\partial U^C} - \frac{\partial L}{\partial x^C} = 0, \tag{3.69}$$

to obtain the geodesic deviation equation,

$$\frac{D^2\Psi^E}{DS^2} = R^E_{ABC}U^A U^B \Psi^C, \tag{3.70}$$

where $R^A_{BCD}$ is Riemann-Christoffel tensor described by poly-vectors.

### 3.4. Geodesic and Geodesic Deviation of C-Space: An Alternative Approach

Equations geodesic deviation of poly-vector are derived in a way of modifying the conventional Bazanski method, using the commutation relations and a condition between deviation poly-vector and poly-vector as well. This method has been worked successfully to derive deviation equation for extended objects with wobbling as shown in [6–9].

Applying the usual commutation relation [32] on Equation (3.70) we obtain:

$$\frac{D}{D\Omega}\frac{DA^D}{DS} - \frac{D}{DS}\frac{DA^D}{D\Omega} = \bar{R}^D_{BCE}A^B U^C \Psi^E, \tag{3.71}$$

provided that

$$\frac{DU^A}{DS} = \frac{D\Psi^A}{D\Omega}. \tag{3.72}$$

Thus, we obtain its corresponding geodesic deviation equations

$$\frac{D^2\Psi^C}{DS^2} = R^C_{BDE}U^B U^D \Psi^E. \tag{3.73}$$

## 4. Transformation of Geodesic Poly-Vectors to Charged and Spinning Poly-Vectors

### 4.1. From Geodesic Poly-Vector to Charged Object Poly-Vector

In this approach we are going to utilize the famous application for transforming geodesics to spinning object differently [32] to become reliable for charged object. In this case, one can assume that charged object travels on a deviated trajectory belongs to family of deviation parameters such that

$$W^C = U^C + \frac{\epsilon}{M}\frac{D\Psi^C}{DS}, \tag{4.74}$$

where $W^C = \frac{dX^C}{d\bar{\Xi}}$.

Thus, differentiating both sides by $\frac{D}{D\bar{S}}$ and taking that $\frac{dS}{d\bar{\Xi}} = 1$, one obtains,

$$\frac{DW^C}{D\bar{\Xi}} = \frac{D}{DS}[U^C + \frac{\epsilon}{M}\frac{D\Psi^C}{DS}]\frac{dS}{d\bar{\Xi}}. \tag{4.75}$$

Now, if we consider electro-magnetic tensor as follows

$$F^{AB}U^B = (R^A_{BDE}U^D\Psi^E)U^B, \tag{4.76}$$

then Equation (4.75) becomes

$$\frac{DW^C}{D\sigma} = \frac{\epsilon}{M}F^C_{.B}U^B\frac{dS}{d\bar{\Xi}} \tag{4.77}$$

which becomes the equivalent Lorentz force (Charged object) in Curved Clifford Space

$$\frac{DW^C}{D\Xi} = \frac{\epsilon}{M}F^{AB}W^B \tag{4.78}$$

### 4.2. From Geodesic Poly-Vector to Spinning Poly-Vectors

If we consider spinning poly-vectors are regarded as geodesics transferred from one path defined by a parameter $S$ into another one $\bar{S}$, such a translation may cause the object behave as a spinning particle rather moving as a test particle. We suggest the following poly-vector $V^C$ defined in the following way

$$V^C = U^C + \beta\frac{D\Psi^C}{DS}. \tag{4.79}$$

By taking the covariant derivative on both sides we obtain, with taking into account $\frac{dS}{d\bar{S}} = 1$,

$$\frac{DV^C}{D\bar{S}} = \frac{D}{DS}[U^C + \beta\frac{D\Psi^C}{DS}]\frac{dS}{d\bar{S}}. \tag{4.80}$$

Assuming that $\beta = \frac{\tilde{S}}{M}$ , and $\tilde{S}$ is the magnitude of the spin tensor as defined by

$$S^{AB} = \tilde{S}[U^A\Psi^B - U^B\Psi^A]. \tag{4.81}$$

Accordingly, substituting Equations (3.70), (3.72) and (4.83) into (4.82), provided that $\frac{dS}{d\bar{S}} = 1$ , we get after some manipulations:

$$\frac{DU^C}{DS} = \frac{1}{2m}R^C_{BDE}U^BS^{DE}, \tag{4.82}$$

which is the corresponding Papapetrou equation, for short, in C-space.

## 5. The Bazanki Approach for Extended Objects of C-Space

### 5.1. Equations of Charged and Charged Deviation Equations in C-Space

The Bazanski approach to obtain an equation of a charged object may be found as follows:

$$L = G_{AB}W^A\frac{D\Phi^B}{D\Xi} + \frac{\epsilon}{M}F_{AB}W^A\Phi^B. \tag{5.83}$$

Taking the variation with respect to $\Phi^C$ and $W^C$ we obtain after some manipulations one finds

$$\frac{DW^C}{DS} = F^{CB}W^B, \tag{5.84}$$

and

$$\frac{D^2\Phi^C}{D\bar{S}^2} = R^C_{BDE}W^E W^D \Phi^E + \frac{\epsilon}{M}(F^{CB}W^B)_{;D}\Phi^D. \tag{5.85}$$

## 5.2. Spinning and Spinning Deviation Equations of C-Space

We suggest the equivalent Bazanski Lagrangian for deriving the equations for spinning and spinning poly-vectors to be

$$L = G_{AB}P^A\frac{D\Psi^B}{D\bar{S}} + S_{AB}\frac{D\Psi^{AB}}{D\bar{S}} + F_A\Psi^A + M_{AB}\Psi^{AB}, \tag{5.86}$$

such that

$$P^A = mU^A + U_\beta\frac{DS^{AB}}{DS},$$

where $P^\mu$ is the momentum poly-vector $F^\mu = \frac{1}{2}R^\mu_{\nu\rho\delta}S^{\rho\delta}U^\nu$, $R^\alpha_{\beta\rho\sigma}$ is the Riemann curvature, $\frac{D}{DS}$ is the covariant derivative with respect to a parameter $\bar{S}$,$S^{\alpha\beta}$ is the spin poly-tensor, and $M^{\mu\nu} = P^\mu U^\nu - P^\nu U^\mu$ such that $U^\alpha = \frac{dx^\alpha}{ds}$ is the unit tangent poly-vector to the geodesic one. In a similar way as performed in (5.83), by taking the variation with respect to $\Psi^\mu$ and$\Psi^{\mu\nu}$ simultaneously in (5.86) one obtains

$$\frac{DP^M}{D\bar{S}} = F^M, \tag{5.87}$$

and

$$\frac{DS^{MN}}{D\bar{S}} = M^{MN}. \tag{5.88}$$

Using the following identity

$$A^D_{;NH} - A^D_{;HN} = R^D_{BNH}A^B, \tag{5.89}$$

on both Equation (5.87) and Equation (5.88), such that $A^D$ is an arbitrary poly-vector. Also, multiplying both sides with arbitrary poly-vectors, $U^H$ and $\Psi^B$ as well as using the following condition [33]

$$U^A_{;H}\Psi^H = \Psi^A_{;H}U^H, \tag{5.90}$$

and $\Psi^A$ is its deviation poly-vector associated to the unit poly-vector tangent $U^A$. And in a similar we can find out that:

$$S^{AB}_{;H}\Psi^H = \Psi^{AB}_{;H}U^H. \tag{5.91}$$

Consequently, one obtains the corresponding deviation equations which are inspired from the workings of Mohseni [34]

$$\frac{D^2\Psi^A}{DS^2} = \bar{R}^A_{BHC}P^B U^H \Phi^C + F^A_{;H}\Psi^H, \tag{5.92}$$

and

$$\frac{D^2\Psi^{AB}}{D\bar{S}^2} = S^{[BD}R^{A]}_{DHC}U^H\Psi^C + M^{AB}_{;H}\Psi^H. \tag{5.93}$$

### 5.3. The Generalized Dixon Equation in C-Space

In this part, we suggest the following Lagrangian which enables us to obtain the spinning charged poly-vector in Clifford space.

$$L = G_{AB}P^A\frac{D\Psi^B}{DS} + S_{AB}\frac{D\Psi^{AB}}{DS} + \tilde{F}_{AB}\Psi^A U^B + \tilde{M}_{AB}\Psi^{AB}, \quad (5.94)$$

such that

$$\tilde{F}_{AB} = \frac{1}{m}(eF_{AB} + \frac{1}{2}R_{ABCD}S^{CD})$$

and

$$\tilde{M}_{AB} = (P_A U^B - P_B U^U + F_{AC}S^C_{\cdot\,B} - F_{AC}S^{\cdot\,C}_{A\,\cdot}).$$

Taking the variation with respect to $\Psi^{\mu}$ and $\Psi^{\mu\nu}$ simultaneously in (5.94) we obtain

$$\frac{DP^M}{DS} = \frac{\epsilon}{M}F^M_B U^B + \frac{1}{2M}R^M_{NEQ}S^{EQ}U^N, \quad (5.95)$$

$$\frac{DS^{MN}}{DS} = P^M U^N - P^N U^M + F^{MC}S_{\dot{C}}{}^N - F^{CN}S^M_{\cdot\,C}. \quad (5.96)$$

Thus, applying the same laws of commutation as illustrated in (5.92) and (5.93) we obtain their corresponding deviation equations

$$\begin{aligned}\frac{D^2\Psi^A}{DS^2} =& R^A_{BHC}P^B U^H \Phi^C \\ &+ (\frac{\epsilon}{M}F^M_B U^B + \frac{1}{2m}R^M_{NEQ}S^{EQ}U^N)_{;H}\Psi^H, \end{aligned} \quad (5.97)$$

and

$$\begin{aligned}\frac{D^2\Psi^{AB}}{DS^2} =& S^{[BD}R^{A]}_{DHC}U^H\Psi^C + (P^M U^N - P^N U^M \\ &+ F^{MC}S_{\dot{C}}{}^N - F^{CN}S^M_{\cdot\,C})_{;H}\Psi^H. \end{aligned} \quad (5.98)$$

## 6. Concluding Remarks

In our approach, we have obtained the relevant equations of spinning and spinning of charged poly-vectors, as well as their deviation equations in C-space *i.e.* (4.84), (5.97) and (5.98). This type of work is regarded an extension to a previous work, obtaining equations of spinning and spinning objects in Riemannian and non-Riemannian geometries, using the Bazanski approach [4–9].

Throughout, this study, it has been found the necessity to regard extended objects, the most reliable ones to express the actual nature of objects, rather than relying to a point-like system. Due to this transition, the associate building block of space-time has to be revisited in the context of C-space. This approach has served to redefine different notations and quantities like mass and charge of any object as shown in (2.41) and (2.42). Not only the definitions of mass and charge for any object are needed to be revised, but also the notation of the torsion of space-time as defined in the internal coordinates (2.13) is obtained due to imposing the rules of differentiation of Clifford space as shown in equations (2.10), (2.11) and (2.12); while their corresponding external coordinates (poly-vector) are purely Riemannaian. This is due to taking the covariant derivative affected oriented areas $x^{\mu\nu}$ of holographic coordinates as shown in (2.10), and (2.11) from (2.12). Consequently,

the meaning of torsion is becoming as similar as being obtained in terms of commutation relation of differential operator on a potential scalar field as expressed by Hammond [25] on dealing with internal coordinates. While, the conventional definition of torsion (2.35) in the context of non-symmetric affine connection is also preserved, if one applies the associate geometry describing the external coordinates as a non-Riemaniann geometry [13–17].

Moreover, we have extended our study to derive the equivalent charged spinning equations and their deviation ones for poly-vectors in C-space, to be considered its corresponding generalized Dixon equation (5.97) and (5.98) in which their corresponding deviations (5.99) and (5.100) are obtained. This approach may help to examine the stability of extended objects in C-space.

To sum up, the problem of motion in C-space becomes a paradigm shift towards identifying the behavior of objects in a deterministic way which can be detected in terms of both internal coordinates and their external ones. Such a tendency may inspire many scientists to find out such a unified theory describing both micro-physics and macro-physics in one form.

## Conflicts of Interest

The author declares no conflicts of interest regarding the publication of this paper.

## References

[1] Mathisson, M. (1937) *Acta Physica Polonica*, **6**, 163-209. (In German)

[2] Papapetrou, A. (1951) *Proceedings of the Royal Society of London. Series A*, **209**, 248. https://doi.org/10.1098/rspa.1951.0200

[3] Dixon, W.G. (1970) *Proceedings of the Royal Society of London. Series A*, **314**, 499. https://doi.org/10.1098/rspa.1970.0020

[4] Kahil, M.E. (2006) *Journal of Mathematical Physics*, **47**, Article ID: 052501. https://doi.org/10.1063/1.2196749

[5] Pavšič, M. and Kahil, M.E. (2012) *Open Physics*, **10**, 414.

[6] Kahil, M.E. (2018) *Gravitation and Cosmology*, **24**, 83.

[7] Kahil, M.E. (2018) *ADAP*, **3**, 136.

[8] Kahil, M.E. (2020) *Gravitation and Cosmology*, **26**, 241-248. https://doi.org/10.1134/S0202289320030093

[9] Kahil, M.E. (2020) *Indian Journal of Physics*. https://doi.org/10.1007/s12648-020-01793-5

[10] Kahil, M.E. (2015) *Odessa Astronomical Publications*, **28**, 126. https://doi.org/10.18524/1810-4215.2015.28.70600

[11] Pezzaglia, W. (1997) Physical Applications of a Generalized Clifford Calculus (Papapetrou Equations and Metamorphic Curvature). arXiv:gr-qc/9710027

[12] Pezzaglia, W. (1999) Dimensionally Democratic Calculus and Principles of Polydimensional Physics. arXiv:gr-qc/99120251.

[13] Mikhail, F.I. and Wanas, M.I. (1977) *Proceedings of the Royal Society of London. Series A*, **356**, 471.

[14] Wanas, M.I. (2000) *Studii Si Cercetari Stiintifice. Seria Matematica*, No. 10, 297-309.

[15] Hayashi, K. and Shirifuji, T. (1979) *Physical Review D*, **19**, 3524. https://doi.org/10.1103/PhysRevD.19.3524

[16] Hehl, F.W., von der Heyde, P., Kerlik, G.D. and Nester, J.M. (1976) *Reviews of Modern Physics*, **48**, Article ID: 393416.

[17] Hehl, F.W. (1980) Four Lectures on Poincare Gauge Field Theory. In: Bergmann, P.G. and De Sabbata, V., Eds., *Cosmology and Gravitation. NATO Advanced Study Institutes Series (Series B. Physics)*, Vol. 58, Springer, Boston, MA, 5-61. https://doi.org/10.1007/978-1-4613-3123-0_2

[18] Castro, C. and Pavšič, M. (2005) *Progress in Physics*, **1**, 32.

[19] Castro, C. (2012) *Advances in Applied Clifford Algebras*, **23**, 39-62. https://doi.org/10.1007/s00006-012-0370-4

[20] Castro, C. (2006) *Annals of Physics*, **321**, 813-839. https://doi.org/10.1016/j.aop.2005.11.008

[21] Castro, C. and Pavšič, M. (2002) *Physics Letters B*, **539**, 133-142. https://doi.org/10.1016/S0370-2693(02)02068-3

[22] Castro, C. (2017) *Advances in Applied Clifford Algebras*, **27**, 2393-2405. https://doi.org/10.1007/s00006-017-0763-5

[23] Pavšič, M. (2005) *Physics Letters B*, **614**, 85-95. https://doi.org/10.1016/j.physletb.2005.03.052

[24] Pavšič, M. (2007) *Journal of Physics: Conference Series*, **66**, Article ID: 012022. https://doi.org/10.1088/1742-6596/66/1/012022

[25] Hammond, R. (2002) *Reports on Progress in Physics*, **65**, 599. https://doi.org/10.1088/0034-4885/65/5/201

[26] Collins, P.D., Martin, A.D. and Squires, E.J. (1989) Particle Physics and Cosmology. John Wily and Sons Inc., Hoboken.

[27] Bazanski, S.L. (1989) *Journal of Mathematical Physics*, **30**, 1018. https://doi.org/10.1063/1.528370

[28] Wanas, M.I., Melek, M. and Kahil, M.E. (1995) *Astrophysics and Space Science*, **228**, 273-276. https://doi.org/10.1007/BF00984980

[29] Wanas, M.I., Melek, M. and Kahil, M.E. (2000) *Gravitation and Cosmology*, **6**, 319.

[30] Kahil, M.E. (2017) *Gravitation and Cosmology*, **23**, 70-79. https://doi.org/10.1134/S0202289317010066

[31] Kahil, M.E. (2007) *AIP Conference Proceedings*, **957**, 329-332.

[32] Bini, D. and Geralico, A. (2011) *Physical Review D*, **84**, Article ID: 104012. https://doi.org/10.1103/PhysRevD.84.104012

[33] Heydrai-Fard, M., Mohseni, M. and Sepanigi, H.R. (2005) *Physics Letters B*, **626**, 230-234. https://doi.org/10.1016/j.physletb.2005.08.098

[34] Mohseni, M. (2010) *General Relativity and Gravitation*, **42**, 2477-2490. https://doi.org/10.1007/s10714-010-0995-3

Journal of Modern Physics, 2020, 11, 1874-1890
https://www.scirp.org/journal/jmp
ISSN Online: 2153-120X
ISSN Print: 2153-1196

# Research Progress of Magnesium Stabilized Aluminum Titanate and New Application of It in Pigment

**Junhua Chen[1], Li Yin[1], Guo Feng[2], Feng Jiang[1], Qianqian Zhao[1], Shanfang Lan[1], Mengting Liu[1], Feifei Zhong[1], Zuzhi Huang[3], Jianmin Liu[2], Qing Hu[1], Weihui Jiang[1,2]**

[1]Department of Material Science and Engineering, Jingdezhen Ceramic Institute, Jingdezhen, China
[2]National Engineering Research Center for Domestic & Building Ceramics, Jingdezhen Ceramic Institute, Jingdezhen, China
[3]School of Chemical Engineering and Technology, China University of Mining and Technology, Xuzhou, China
Email: fengguo@jci.edu.cn

**How to cite this paper:** Chen, J.H., Yin, L., Feng, G., Jiang, F., Zhao, Q.Q., Lan, S.F., Liu, M.T., Zhong, F.F., Huang, Z.Z., Liu, J.M., Hu, Q. and Jiang, W.H. (2020) Research Progress of Magnesium Stabilized Aluminum Titanate and New Application of It in Pigment. *Journal of Modern Physics*, **11**, 1874-1890.
https://doi.org/10.4236/jmp.2020.1111117

**Received:** October 26, 2020
**Accepted:** November 21, 2020
**Published:** November 24, 2020



## Abstract

Aluminum titanate has been widely used in low expansion applications and its thermal stability has been a hot topic. The stability of aluminium titanate research for improving product quality, and expanding its application field is of great significance. Aluminum titanate as glass melt erosion resistance and high temperature resistant, can be applied to high temperature pigment base. The medium temperature stability of aluminum titanate can be improved by ion doping, and magnesium stability of aluminum titanate has been widely studied. Therefore aluminium titanate is expected to become an ideal high temperature ceramic base material. In this paper, the preparation technology of magnesium-stabilized aluminum titanate powder was reviewed, and the preparation of magnesium-stabilized aluminum titanate powder by non-hydrolyzed sol-gel was mainly introduced.

## Keywords

Aluminum Titanate, Magnesium Stabilization, Preparation Methods, Progress, Heterogeneous Condensation, Non-Hydrolyzed Sol-Gel Method

## 1. Introduction

Aluminum titanate ($Al_2TiO_5$, abbreviated as $AT$) is characterized by high melting point (1860˚C ± 10˚C) and low expansion ($\alpha < 1.5 \times 10^{-6}$/˚C). It is a ceramic material with the best high-temperature resistance among low expansion materials (quartz glass, spodumene, cordierite and aluminum titanate). It has the characteristics of low thermal conductivity (1.5 W/m·K), good thermal shock re-

sistance, strong corrosion resistance and non-infiltration of metal and glass melt [1] [2]. Its melting point is higher than other low expansion materials, and it has a unique application in high-temperature area, so it is more and more noticed by material workers. The stable aluminum titanate can be obtained by ion doping, and the ion doping of solid solution color itself can effectively inhibit the decomposition of aluminum titanate. Therefore, aluminum titanate is expected to be an ideal new high temperature ceramic color base material. However, the crystal structure of aluminum titanate is shown in **Figure 1**. It can be seen that the coordination octahedrons [$AlO_6$] and [$TiO_6$] formed by $Al^{3+}$, $Ti^{4+}$ and $O^{2-}$ form the structural units of aluminum titanate crystal. These octahedrons are randomly distributed and cross connected with each other in the way of common arris or common top to form the spatial network structure of aluminum titanate. However, this spatial network structure also makes the bonding in aluminum titanate layer unstable, while the interlayer bonding is relatively stable [3]. In the aluminum titanate crystal structure, the radius of $Al^{3+}$ (0.05 nm) is quite different from that of $Ti^{4+}$ (0.068 nm), while the radius of $O^{2-}$ is 0.14 nm, so the ratio of $r_{Al^{3+}}/r_{O^{2-}}$ is only 0.357 < 0.414, and the ratio of $r_{Ti^{4+}}/r_{O^{2-}}$ is 0.486 > 0.414. According to Paulin's rule, the distortion of [$AlO_6$] is larger than that of [$TiO_6$]. At high temperature, the binding force of aluminum ion is weak, and it is easier to break away from the binding force of oxygen ion, so that the crystal structure of aluminum titanate is destroyed, leading to its decomposition [4] [5] [6]. Aluminum titanate is easy to decompose in the temperature range of 750˚C - 1280˚C. The thermal expansion rate of $\alpha$-$Al_2O_3$ and $TiO_2$ is higher than that of aluminum titanate, which results in the stress concentration in the material and the increase of the thermal expansion rate so that the thermal performance of the final sintered body becomes weak and the strength decreases, which limits its wide application [7].

In order to inhibit the thermal decomposition of aluminum titanate, stabiliser additive is the most effective method [8]. Studies have shown that although

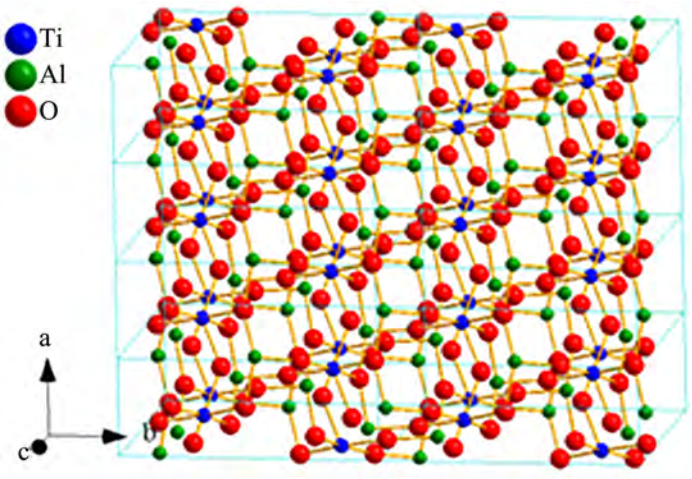


**Figure 1.** Crystal structure of aluminum titanate.

$Fe_2O_3$ can effectively inhibit the thermal decomposition of aluminum titanate, it will reduce its strength [9]. Aluminum titanate ($Al_2TiO_5$) belongs to the orbicular system and has the same structure as magnesium titanate ($MgTi_2O_5$), which can form $Al_{2(1-x)}Mg_xTi_{1+x}O_5$ solid solution. MgO is the most commonly used additive in the preparation of aluminum titanate [10]. An appropriate amount of MgO can not only partially or completely control the thermal decomposition of aluminum titanate, but also improve the mechanical properties of aluminum titanate, which has little impact on other excellent thermal properties. Therefore, stable aluminum titanate has become one of the hot spots in the research of aluminum titanate materials. At present, the main methods for preparing magnesium stabilized aluminum titanate include solid-phase method [11] [12] [13] [14] [15], co-precipitation method [16], hydrolyzed sol-gel method [17] [18] and nonhydrolytic sol-gel method [19] [20]. In this paper, the preparation methods of magnesium stabilized aluminum titanate are reviewed.

## 2. Materials and Methods

### 2.1. Solid-Phase Method

At present, the main method to prepare aluminum titanate ceramic powder is a solid-phase method. Aluminum titanate ($Al_2TiO_5$) should be prepared by the solid-phase method, which mainly uses the mixture of alumina and titanium dioxide powder and makes it solid by high-temperature calcination. The advantages of this method are simple equipment, convenient operation, mature process, low cost of raw materials and suitable for mass production. However, its shortcomings are also obvious, such as high synthesis temperature, low purity, coarse particle, uniformity and particle size are difficult to be effectively controlled, resulting in poor performance and instability of the material. Moreover, aluminum titanate ceramic powders prepared by a solid-phase method often need to be crushed, ball grinding and other post-treatment to improve the morphology and properties of the particles, and the post-treatment process is complex.

The current study of aluminum titanate ceramic pigment has just started, the Italian ceramic institute professor Michele [11], such as using high temperature solid phase method at 1400˚C was prepared by M (M = Cr (green)), Mn (brown), Co (pink) mixed with $Al_2TiO_5$ solid solution type ceramic pigment, the study found that Cr doped $Al_2TiO_5$ (green) and Mn doping $Al_2TiO_5$ (brown) pigment used in the glaze is still present a good shading effect, and Cr doped also effectively restrain the decomposition temperature of aluminium titanate. However, there are problems such as low doping concentration of color ions and Co ions dissolving out in the glaze, so the coloring effect is not ideal. The reason for this result is that the high temperature solid phase method is adopted in this study, which is limited by the uniformity of raw material mixing and solid reaction products, so it is often difficult to obtain high doping concentration and uniformity of color materials.

Fang Qing [12] synthesized $Al_{2(1-x)}Mg_xTi_{1+x}O_5$(AMT) ($x$ = 0, 0.01, 0.05, 0.1, 0.3) solid solution powder using $\alpha$-$Al_2O_3$, $TiO_2$ and MgO as raw materials and $MgO{\cdot}2TiO_2$ as stabilizer by solid-phase method. The raw materials of $\alpha$-$Al_2O_3$, $TiO_2$, MgO and the mixture were put into the plastic tank; the mixture was mixed for 12 hours, dried, and pressed into shape under the pressure of 10MPa. The sample material was synthesised in solid phase in a silicon-molybdenum furnace and held at 1450˚C for 2 h. The powder sample was obtained after grinding after natural cooling in the furnace. The $d$ values of (200), (060) and (006) of the diffraction pattern $AT$ of sample No.1 - No.5 powder and standard sample $\alpha$-$Al_2O_3$ uniformly mixed were taken, and the accurate values were obtained after checking with the standard sample and given in Table 1. Since aluminum titanate belongs to the rhombic crystal system and all the crystal planes taken are special ones, the three lattice constants $a$, $b$ and $c$ of the synthesized $Al_{2(1-x)}Mg_xTi_{1+x}O_5$ solid solution can be simply calculated by the following three formulas.

$$a = hd(h00)$$

$$b = kd(0k0)$$

$$c = ld(00l)$$

In the formula, $h$, $k$ and $l$ are the corresponding values in the crystal surface index. Any crystal surface can be expressed as ($h$, $k$ and $l$), where 2, 6 and 6 are respectively.

It is found that with the increase of $x$ value in $Al_{2(1-x)}Mg_xTi_{1+x}O_5$ solid solution, the lattice constant of solid solution increases, and the lattice constants $a$, $b$ and $c$ almost linearly increase, especially the linearity of c value is more significant. It is because the radius of $Mg^{2+}$ (65 pm) is larger than that of $Al^{3+}$ (51 pm) and closer to the radius of $Ti^{4+}$ (68 pm). When $AT$ and M2T form $Al_{2(1-x)}Mg_xTi_{1+x}O_5$ solid solution, $Mg^{2+}$ enters into the lattice of $AT$ to replace part of $Al^{3+}$ so that the lattice constant of AMT increases. With the increase of $MgO{\cdot}2TiO_2$ addition, the more $Mg^{2+}$ enters, the more $Al^{3+}$ is replaced, resulting in the linear increase of the lattice constant of AMT. The gradual increase of lattice constant further confirmed that $AT$ and M2T formed $Al_{2(1-x)}Mg_xTi_{1+x}O_5$ solid solution, and aluminum titanate completely decomposed into $\alpha$-$Al_2O_3$ and $TiO_2$ (rutile) without the addition of $MgO{\cdot}2TiO_2$. When $MgO{\cdot}2TiO_2$ with a mole fraction of 1% ($x$ = 0.01) was added, the diffraction peak of solid solution AMT was relatively strong. When $MgO{\cdot}2TiO_2$ with a mole fraction of 5% or 10% is added, it is basically the diffraction peak of the solid solution, indicating that $MgO{\cdot}2TiO_2$ can effectively

Table 1. $d$ values of AMT.

| Sample | No.1 | No.2 | No.3 | No.4 | No.5 |
|---|---|---|---|---|---|
| $d$(200) | 1.79405 | 1.79500 | 1.80003 | 1.80146 | 1.81329 |
| $d$(060) | 1.57385 | 1.57398 | 1.57000 | 1.58189 | 1.59086 |
| $d$(006) | 1.60560 | 1.60612 | 1.60817 | 1.61076 | 1.62419 |

inhibit the decomposition of aluminum titanate, resulting in good thermal stability of $Al_{2(1-x)}Mg_xTi_{1+x}O_5$ solid solution.

Aluminum titanate is composed of [$AlO_6$] and [$TiO_6$] octahedron. Because the radius of $Al^{3+}$ is smaller than that of $Ti^{4+}$, [$AlO_6$] is a distorted octahedron. From the perspective of a chemical bond, when aluminum titanate is heated, the vibration of all atoms intensifies, but $Al^{3+}$ is in a deformed octahedron, and the vibration intensifies with the rise of temperature. When the temperature rises to a certain value, the aluminum oxygen bond will break, making aluminum titanate decompose. So the more distorted [$AlO_6$] is, the more easily aluminum titanate will decompose. The radius of $Mg^{2+}$ is larger than $Al^{3+}$, which is closer to $Ti^{4+}$. The replacement of $Al^{3+}$ to form $Al_{2(1-x)}Mg_xTi_{1+x}O_5$ solid solution alleviates the distortion degree of [$AlO_6$]. Therefore, the thermal stability of $Al_{2(1-x)}Mg_xTi_{1+x}O_5$ is higher than that of pure aluminum titanate, which is not easy to decompose. With the increase of $x$ value, the more $Mg^{2+}$ replaces $Al^{3+}$, the weaker the overall distortion degree in the crystal is, so the thermal stability of $Al_{2(1-x)}Mg_xTi_{1+x}O_5$ is higher.

Zhang L.M, *et al.* [13] used $\alpha$-$Al_2O_3$, $TiO_2$ and MgO to form $Al_{2(1-x)}Mg_xTi_{1+x}O_5$ by solid reaction method at 1450˚C for 2 h. The lattice constants $a$, $b$ and $c$ of the solid solution $Al_{2(1-x)}Mg_xTi_{1+x}O_5$ all increase linearly with the increase of $x$ value. The thermal stability of $Al_{2(1-x)}Mg_xTi_{1+x}O_5$ was higher than that of pure aluminum titanate. The thermal stability of $Al_{2(1-x)}Mg_xTi_{1+x}O_5$ increases with the increase of $x$ value. When $x$ = 0.05, the decomposition rate of $Al_{2(1-x)}Mg_xTi_{1+x}O_5$ was only 9% at 1100˚C for 10h, while the pure aluminum titanate was almost completely decomposed. With the increase of the content of M2T, the relative density of the sintered body increases, indicating that the presence of M2T is conducive to the sintering of aluminum titanate. The solid-phase method has the advantages of low cost, simple preparation process and no special equipment. However, it is difficult to produce high purity, ultra-fine and uniform aluminum titanate powder.

Buscaglia V. *et al.* [8] studied the effect of adding 2 wt% MgO on reaction sintering of $Al_2TiO_5$. Solid reaction between $A1_2O_3$ and $TiO_2$ powders with different particle sizes was studied to generate $A1_2TiO_5$. Aluminum titanate powder was prepared by solid-phase method from raw materials of alumina and rutile. The equal molar aluminum oxide and rutile powder were mixed, and the aluminum oxide ball and polyethylene bottle were used for wet grinding for 100 h in water. After drying and sieving, the obtained powder was isostatic pressed on a 150 MPa cylinder with diameter = 10 mm and length = 100 mm. The material containing magnesium oxide was pretreated in the same manner with 2 wt% magnesium oxide (Aldrich, 99%). For simplicity, when prepared with $A1_2O_3$ and $TiO_2$, the sample will be displayed as K, while the corresponding sample prepared with magnesium oxide will be displayed as KM. The results showed that the overall reaction kinetics and microstructure of the alloy varied with the increase of temperature, and the formation of pure $Al_2TiO_5$ was firstly nucleation and rapid growth, and then the slow transformation of unreacted oxide under

the control of solid diffusion. The addition of MgO makes nucleation of the new phase easy. $MgAl_2O_4$ is first generated, and then the titanate solid solution particles rich in Mg are grown. Therefore, the final microstructure is mainly controlled by the density and size of spinel nucleus, followed by the growth process of titanate grain, leading to a strong decrease in titanate grain size and a significant increase in final density.

Synthesis [14] $Al_{0.8}Mg_{0.6}Ti_{1.6}O_5$ low-expansion ceramics with the same structure as aluminum titanate $Al_2TiO_5$ were prepared by solid reaction with $\alpha$-$Al_2O_3$, MgO and $TiO_2$ rutile. The three materials were mixed according to certain stoichiometry. The mixture was ground wet in water for 24 hours, and aluminum oxide ball was added in a polyethene bottle. Three different powders were obtained by different heat treatments: 1) the prepared mixture (M6); 2) Burn at 1100˚C for 2 h (M611) and 3) for 2 h (M613) at 1300˚C. M6 series corresponds to completely unreacted powder, M611 to partially reacted powder, and M613 to fully converted powder. M611 and M613 powder were burned at high temperature, then wet ground in water for 24 hours, dried and screened, and green bodies (cylinders with a diameter of +1 cm and length of +10 cm) were prepared under 150 MPa cold isostatic pressure. $Al_2TiO_5$-$MgTi_2O_5$ solid solution was formed from M6 loose powder within 0.5 - 7 h under the conditions of 1000˚C, 1100˚C, 1200˚C and 1300˚C. The sample was placed in the furnace and reached the reaction temperature within 2 - 3 min. After the reaction, the sample was taken out of the furnace for air quenching. The results showed that $Al_{0.8}Mg_{0.6}Ti_{1.6}O_5$ composite material did not decompose after being annealed for 250 hours in the temperature range of 900˚C - 1175˚C. Sintered ceramics at 1350˚C had a 97% relative density, a grain size of 5 m and an average coefficient of thermal expansion of $2 \times 10^{-6}$ $K^{-1}$ at 80˚C - 1000˚C. The measured coefficient of thermal expansion was comparable to that of other oxide ceramics (e.g. standard aluminum titanate ($\approx 1 \times 10^{-6}$ $K^{-1}$), porous cordierite ($\approx 1 \times 10^{-6}$ $K^{-1}$) and lithium aluminosilicate ($\approx 2 \times 10^{-6}$ $K^{-1}$). The materials obtained by direct reaction sintering with the same composition had higher thermal expansion coefficient ($\approx 4 \times 10^{-6}$ $K^{-1}$) and showed the presence of secondary phase ($TiO_2$, $Al_2O_3$ and $MgAl_2O_4$).

## 2.2. Microwave Sintering

This is a new solid-phase preparation technology in recent years. Compared with the traditional solid-phase method, microwave sintering method innovatively uses gamma $\gamma$-$Al_2O_3$, which greatly improves the activity of alumina. Shahab [15] $Al_{2(1-x)}Mg_xTi_{1+x}O_5$ ceramics prepared from $\gamma$-$Al_2O_3$, $TiO_2$ and MgO (0, 2, 5, 7 wt%). The $\gamma$-$Al_2O_3$, $TiO_2$ and MgO nanometer powder were mixed proportionally to form the stoichiometric solid solution $Al_{2(1-x)}Mg_xTi_{1+x}O_5$. Using alumina ball and methanol as grinding medium, the powder was ground in the plastic bottle for 2 hours to evenly mix the powder. The obtained slurry was first dried on a magnetic heater agitator and then dried in an oven at 120˚C for 24 hours. Then sieve the dry powder to 45 mesh. A 2 wt% polyvinyl alcohol solution was granulated in a container for 24 hours before passing through a 45

mesh sieve. The rectangular sample is $20 \times 6 \times 5$ mm$^3$ in a pressure of 50 MPa. At 180 MPa, the pressed sample is compacted again by cold isostatic pressure to eliminate any defects related to molding. The experimental parameters are shown in Table 2. A microwave oven (2.45 ghz, 900 W) was used for sintering in the temperature range of 1250˚C - 1400˚C. SiC crucible was used as the container, and the temperature rose to the maximum in a short time (the average heating rate was 52˚C/min). Phase transitions are performed during sintering at different temperatures (1250˚C, 1350˚C, and 1400˚C). The study found that when $x = 0.5$, the maximum strength of the sample was about 60 MPa. After annealing for 100 hours, the sample containing MgO still showed high thermal stability at 1100˚C and formed fine crystal structure at a low temperature of 1280˚C. In addition, the addition of MgO reduced the formation temperature of ilmenite and had a strong effect on its microstructure. Because of the advantages of using microwave radiation, ilmenite is formed at 1250˚C without heat preservation. However, the formation temperature of aluminum titanate using conventional heating has exceeded 1300˚C. Microwave heating reduces the formation temperature of ilmenite, but the diffusion time is insufficient due to rapid heating.

All the above preparation processes adopt the solid phase method. MgO is used as a magnesium source to stabilise the aluminum titanate material, to explore the properties of magnesium to stabilise the aluminum titanate. The solid-phase method has a high reaction temperature and poor uniformity of the prepared powder. Its cost is relatively low the preparation process is simple, does not need special equipment, but it is difficult to produce high purity, ultra-fine uniform powder.

### 2.3. Coprecipitation Method

The coprecipitation method overcomes the problems existing in the mixture, solid reaction and comminution of raw materials, the purity and the uniformity of composition, and the synthesis of powder raw materials with excellent properties. Coprecipitation method is to add precipitant to the mixed metal salt solution, that is, to get the evenly mixed precipitate of various components, and then conduct thermal decomposition. Compared with the solid reaction method, this method can produce a powder with good chemical uniformity and easy sintering. In common coprecipitation, all the cations in the excess precipitator solution precipitate simultaneously into a mixture. Under special circumstances,

Table 2. Samples composition with different amount of MgO.

| Sample | $AT$(wt%) | MgO (wt%) | Chemical formula |
|---|---|---|---|
| $AT$ | 100 | 0 | $Al_2TiO_5$ |
| $2AT$ | 98 | 2 | $Al_{1.8}Mg_{0.1}Ti_{1.1}O_5$ |
| $5AT$ | 95 | 5 | $Al_{1.4}Mg_{0.3}Ti_{1.3}O_5$ |
| $7AT$ | 93 | 7 | $AlMg_{0.5}Ti_{1.5}O_5$ |

there are precursor compounds with oxygen cation ratio meeting the requirements.

Yang [16] *et al.* prepared $Al_{2(1-x)}Mg_xTi_{1+x}O_5$ ($x$ = 0.05 - 0.3) composite powder by chemical coprecipitation with $TiCl_4$, $MgCl_2$ and $AlCl_3$ aqueous solutions as raw materials, ammonia water and ammonium bicarbonate as precipitators. $Al_2TiO_5$ and $MgTi_2O_5$ crystals belong to the rhombic system, with crystal plane spacing $d_{hkl}$ and lattice constants $a$, $b$ and $c$. In accordance with formula $d_{hkl} = 1/(h^2/a^2 + k^2/b^2 + l^2/c^2)$, the composite powder was prepared by co-precipitation method. By comparing the 3-strong peak of pure $Al_2TiO_5$, the crystal lattice constant of the sample, and the difference value between the crystal lattice constant and pure $Al_2TiO_5$ could be calculated [21]. The constant lattice $c$ of $Al_2TiO_5$ is closely related to stability. As the $c$ value increases, the stability of $Al_2TiO_5$ improves, and the more the $c$ value increases, the more stable $Al_2TiO_5$ becomes [22]. The results show that the chemical co-precipitation method is more effective in improving the thermal stability of aluminum titanate than the solid phase method. However, the powders prepared by this method have serious agglomeration and need later treatment. $MgTi_2O_5$ containing 5%, 10% of the composite powders, with furnace cooling does not appear in the process of generation of alpha $A1_2O_3$ $Al_2TiO_5$ decomposition, $TiO_2$, shows that using chemical coprecipitation synthesis of powder in $MgTi_2O_5$ mole fraction of 5% can effectively inhibit $Al_2TiO_5$ thermal decomposition, and using the method of solid-phase synthesis of composite powders in $MgTi_2O_5$ mole fraction of 10% $Al_2TiO_5$ there is still a small decomposition, which fully embodies the superiority of chemical coprecipitation.

## 2.4. Sol-Gel Method

Sol-Gel synthesis is a recently developed method which can replace the high-temperature solid-phase synthesis reaction to prepare ceramics, glass and many other solid materials. It starts from the solution of organometallic compounds or inorganic compounds, in the solution through the hydrolysis of compounds, polymerisation, from the solution into dissolved metal oxide particles of a sol, a further reaction occurs gelation. Then the gel can be heated into ceramics, glass, etc. At present, this method is one of the most important methods to prepare nano-thin films. The sol-gel method has won great interest from researchers of thin-film materials at home and abroad for its outstanding advantages.

Plinio Innocenzi [17] precursors of oxidative components were triply butanol ($Al(O\text{-}s\text{-}Bu)_3$), tetrply butanol ($Ti(OBu)_4$) and hexahydrate magnesium dichloride ($MgCl_2{\cdot}6H_2O$), using 2,4-pentanedione(acac) (Aldrich), nitric acid ($HNO_3$) (Prolabo) (1N) and anhydrous ethanol (Carlo Erba). In order to prepare thin films composed of $Al_2TiO_5$ (undoped aluminum titanate), $Al(O\text{-}s\text{-}Bu)_3$ was carefully added to reflux EtOH (80˚C) and $Ti(OBu)_4$ was slowly added under magnetic agitation. The sol was cooled to room temperature, then $HNO_3$(1N) was added, and the obtained sol was stirred for 1h and freshly used for impregnating coating. The preparation process of aluminum magnesium titanate was im-

proved as follows. After adding $Al(O\text{-}s\text{-}Bu)_3$ and $Ti(OBu)_4$ into EtOH, acac and $MgCl_2 \cdot 6H_2O$ were introduced into EtOH. Finally, $HNO_3$ was added to catalyse the sol. It was found that $Mg_xAl_{2(1-x)}Ti_{(1+x)}O_5$ thin films prepared by sol-gel method could produce stable aluminum titanate phase at a temperature much lower than that of solid-phase reaction. The thermal stability of the film is up to 90 hours at 1150˚C. During the long annealing time, the formation of microcracks on the surface of the film improved the heat resistance of the coating. At higher firing temperatures, Mg ions diffused to the surface of the film.

## 2.5. Gel Injection Molding

The equations are an exception to the prescribed specifications of this template. You will need to determine whether or not your equation should be typed using either the Times New Roman or the Symbol font (please no other font). Equations should be edited by Mathtype, not in text or graphic versions. Dai Binyu [18] prepared $Al_{2(1-x)}Mg_xTi_{1+x}O_5$ solid solution ceramics by gel injection molding with $\alpha$-$Al_2O_3$, rutile $TiO_2$ and MgO as initial powders. First, the organic monomer (methyl acrylamide) and cross-linking agent (methylene acrylamide) were dissolved in deionized water. Then, dispersant D-305 and defoaming agent C-582 were added to evenly stir to form premix. The pH value of premix was controlled to be 12 - 13. Then mix the powder evenly according to the molar fraction ratio in **Table 3** and add it into the premix to make the slurry with a solid phase volume fraction of 52%. After ball grinding for 2.5 h, vacuum degelling is carried out. After 15 min of treatment, appropriate amount of catalyst (tetramethylethylenediamine) and initiator (ammonium persulfate) was added to the slurry, fully stirred, and then vacuumized for 1 - 2 min. Then the slurry was injected into the metal mold, dried and demodulated at 50˚C, and discharged into 1560˚C after preservation for 2 h and burned.

The coefficient of thermal expansion was determined by differential method. WDW-200D microcomputer-controlled universal testing machine was used for the determination of flexural strength. The sample size was 7 mm × 8 mm × 60 mm. XRD test method was used to analyze the phase composition of sintered sample powder at 1560˚C and its thermal decomposition performance after being kept at 1100˚C for 50 h. The diffraction peak area of the aluminum titanate (101) crystal plane and rutile (110) crystal plane was measured on the X-ray diffraction pattern to obtain $I_{AT}$ and $I_T$, and then the thermal decomposition rate of the sample was calculated according to the following formula:

**Table 3.** Composition design of sample.

| number | $\alpha$-$Al_2O_3$ | MgO | $TiO_2$ |
|---|---|---|---|
| 1 | 100 | 0 | 1 |
| 2 | 95 | 5 | 1.05 |
| 3 | 90 | 10 | 1.10 |
| 4 | 85 | 15 | 1.15 |

$$\alpha_{AT} = \frac{I_T^{110}}{I_{AT}^{101} + I_T^{110}}$$

It is found that the introduction of MgO increases the thermal stability of $Al_2TiO_5$, reduces the number of microcracks, and increases the density. When the amount of MgO is not large, the strength of $Al_2TiO_5$ increases with the increase of *x* value. The coefficient of thermal expansion decreases slightly at first and then increases gradually.

## 2.6. Nonhydrolytic Sol-Gel Method (NHSG)

The nonhydrolytic sol-gel (NHSG) process simplifies the sol-gel process, in particular, homogenises the sol in the sol-gel process at the atomic level, thus greatly reducing the synthesis temperature of multi-component oxides [19] [20] [23] [24] [25] [26] [27]. NHSG method can synthesise aluminum titanate ($Al_2TiO_5$) at 750˚C, which is significantly lower than the solid-phase method and traditional sol-gel method [26]. Festive aluminum titanate ($Al_2TiO_5$) was prepared by the nonhydrolytic sol-gel method. However, to our knowledge, there is no formal report on the magnesium-stabilized modified aluminum titanate nonhydrolytic sol-gel (NHSG) process in the strict sense, except for the relevant patents of our research group.

Jiang Weihui *et al.* [19] prepared magnesium-stabilized aluminum titanate powder by nonhydrolytic sol-gel method using titanium tetrachloride and anhydrous aluminum chloride as precursors, anhydrous ethanol as oxygen supply, magnesium powder, magnesium fluoride, magnesium ethoxide and magnesium acetate as stabilizers. The effect of magnesium stabilizer on the synthesis of aluminum titanate at low temperature was studied. Anhydrous aluminum chloride ($AlCl_3$, AR, Shanghai) and titanium tetrachloride ($TiCl_4$, AR, Shanghai) were mixed in conical flask with anhydrous ethanol (EtOH, AR, Shanghai) as oxygen supply agent. The reaction mixture was refluxed continuously for 8 h at 110˚C, and aluminum titanate wet gel was obtained by nonhydrolytic sol-gel method. The wet gel was dissolved with $CHCl_3$ solution of magnesium fluoride, magnesium powder, magnesium acetate or magnesium ethanol, refluxed at 110˚C for 15 h, dried and ground at 110˚C, and calcined at 750˚C for 1.5 h to obtain powder samples. The powder was pressed into rods of 5 mm × 5 mm × 40 mm at a pressure of 12 MPa. Heat preservation for 20 h at 1100˚C was conducted for thermal decomposition test. The results showed that the introduction of magnesium powder or magnesium fluoride could not stabilize aluminum titanate, and the failure of low temperature synthesis of aluminum titanate at 750˚C was caused by the promotion of nonhydrolytic homogeneous condensation. In the precursor mixture, anhydrous magnesium acetate and ethoxy magnesium react with aluminol and titananol to form heterogeneous condensation bonds and promote the doping of magnesium ions into aluminum titanate lattice at 750˚C, thus improving its thermal stability. In order to study the thermal decomposition and stabilization mechanism of magnesium stabilizer to aluminum titanate, the lattice constants of samples $W^{\#}$, $M_3^{\#}$ and $M^{\#}$ are listed in **Table 4**. For comparison,

**Table 4.** Lattice parameters of samples.

| Sample | Lattice parameter [nm] | | |
|---|---|---|---|
| | *a* | *b* | *c* |
| $W^{\#}$ | 0.93589 | 0.95406 | 0.36025 |
| $M_3^{\#}$ | 0.94082 | 0.96033 | 0.35959 |
| $M_4^{\#}$ | 0.94387 | 0.96135 | 0.35927 |
| $M_3^{\#}$ (1100˚C, 20 h) | 0.94487 | 0.96613 | 0.35982 |
| $M_4^{\#}$ (1100˚C, 20 h) | 0.94919 | 0.97241 | 0.36013 |

Table 4 also gives sample lattice constants $M_3^{\#}$ and $M_4^{\#}$ holding 20 h after 1100˚C. As can be seen from Table 4, $M_3$ and $M_4^{\#}$ of the values of *a* and *b* are obviously about the same as *c* than $W^{\#}$. It is fully proved that magnesium introduced in the form of anhydrous magnesium acetate ($M_3^{\#}$) and ethoxylmagnesium ($M_4^{\#}$) has been doped into the lattice of aluminum titanate and stabilized it, which is the intrinsic reason for significantly improving the thermal decomposition ability of samples $M_3^{\#}$ and $M_4^{\#}$. After the thermal decomposition experiment held at 1100˚C for 20 h, the lattice constants of samples $M_3^{\#}$ and $M_4^{\#}$ further increased, indicating that magnesium ions continued to enter the lattice of aluminum titanate during the thermal decomposition process, thus improving the thermal stability of aluminum titanate. The process flow diagram 2 to be adopted in this experiment is shown in Figure 2. Heterogeneous bonding between magnesium acetate and titanium tetrachlide forms -Ti-O-Mg- and -Al-O-Mg-, which promotes the doping of magnesium ions into the lattice of aluminum titanate at 750˚C, changing the lattice constant of aluminum titanate, thus improving the thermal stability of aluminum titanate.

Feng Guo *et al.* [20] prepared magnesium stabilized aluminum titanate powder by nonhydrolytic sol-gel method with anhydrous aluminum chloride and titanium tetrachloride as the precursor, anhydrous ethanol as the oxygen supplier, and anhydrous magnesium acetate as the stabilizer. In the glove box, no water needed for measuring low carbon alcohol in 100 ml conical flask of dry, then put in ice water, according to the $TiCl_4$:$AlCl_3$:Ethanol = 1:2:5 (mole ratio), with a pipette measuring $TiCl_4$, and insert a pipette conical flask quickly alcohol level in the following, slow $TiCl_4$ mixed with alcohol, formation of $TiCl_4$-alcohol solution, then adding anhydrous aluminum chloride, stir to mix well. 1) For unadulterated $W^{\#}$ samples, reflux was directly performed at 110˚C for 24 h and then dried at 110˚C to form a dry gel; 2) For the $A^{\#}$ sample introduced by anhydrous magnesium acetate before the polycondensation reaction of aluminum and titanium precursor, add $TiCl_4$ 10 mol% anhydrous magnesium acetate, stir evenly, reflux at 110˚C for 24 h, and then dry at 110˚C to form a dry gel; 3) For the sample $B^{\#}$ introduced after the condensation reaction of anhydrous magnesium acetate in the precursor of aluminum and titanium, the sample was reflux for 12 h at 110˚C to form a wet gel. Then $TiCl_4$ 10 mol% of anhydrous magnesium acetate was added and reflux was repeated for 12 h at 110˚C to form a dry gel. For

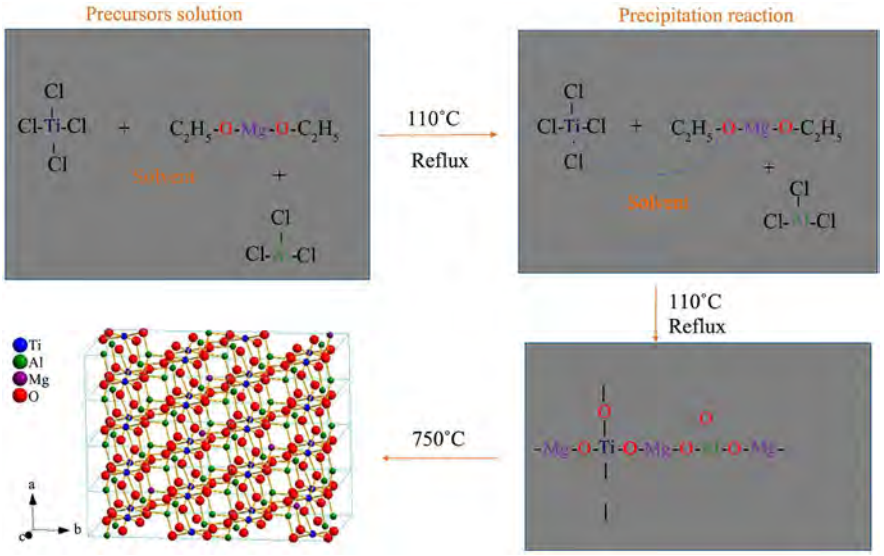


**Figure 2.** Schematic diagram of the process flow to be adopted in this experiment.

powder samples: the dry gel was directly obtained by calcination and grinding at 750˚C. For the test strips for thermal expansion coefficient test, the obtained dry gel was calcined at 300˚C for 0.5 h, then 3 wt% PVA was added for granulation, and then pressed into 40 mm × 5 mm × 5 mm test strips. Finally, magnesium stabilized aluminum titanate samples were obtained at 750˚C for 1.5 h. The anti-thermal decomposition effect was tested by holding the samples at 1100˚C for 20 hours. The results show that the introduction of anhydrous magnesium acetate before the polycondensation of aluminum and titanium precursor is not only detrimental to the stability of aluminum titanate at low temperature, but also greatly affects the synthesis of aluminum titanate at low temperature. When introduced after the polycondensation reaction of aluminum and titanium precursor, anhydrous magnesium acetate can further deester polycondensation reaction with the polycondensation product of aluminum and titanium precursor to form heterogeneous bonding, which ensures that magnesium can enter the aluminum titanate lattice at 750˚C to form a solid solution, thus improving its thermal stability.

**Figure 3** shows the XRD pattern of the powder prepared by 750˚C for 1.5 h after the addition of A# sample before the polycondensation of aluminum and titanium, the addition of B# sample after the polycondensation and the addition of W# sample without stabilizer. It can be seen from **Figure 3** that, compared with sample W#, sample A# not only has a significantly lower diffraction peak intensity than sample W#, indicating that the addition of anhydrous magnesium acetate before the condensation polymerization of aluminum and titanium inhibits the low-temperature synthesis of aluminum titanate. Moreover, A# sample showed a very strong corundum phase diffraction peak and a certain amount of rutile phase, and the synthesis effect of A# sample was much worse than that of A# sample. The relative strength of the aluminum titanate diffraction peak of B# sample was also slightly reduced compared with that of W# sample, and there

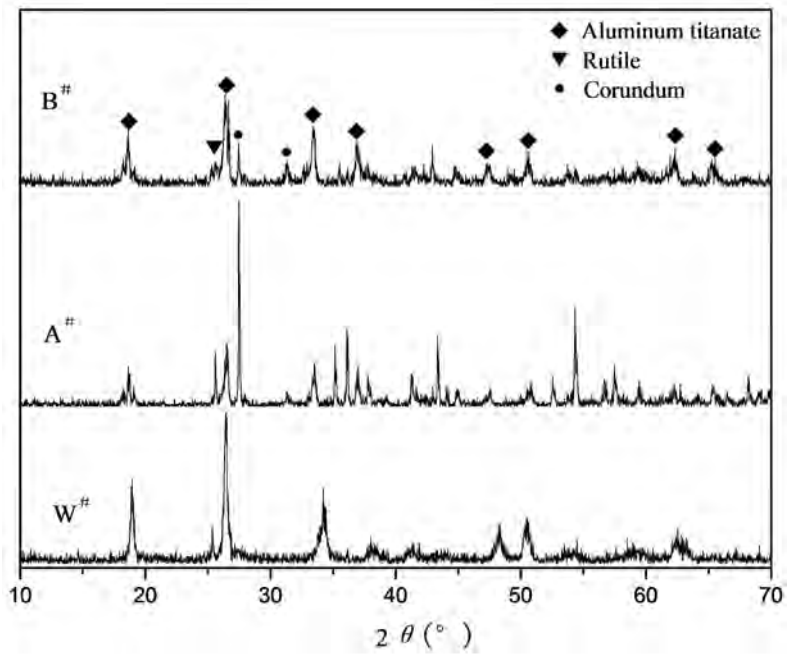


**Figure 3.** XRD patterns of samples W#, A# and B# treated at 750˚C for 1.5 h.

were a few corundum and rutile diffraction peaks, indicating that the low temperature synthesis effect of B# sample was also slightly worse. However, compared with A# sample, the synthesis effect of B# sample is obviously better than A# sample.

The thermal expansion coefficients of the three samples are listed in **Table 5**. It can be seen from **Table 5** that the thermal expansion coefficients of samples W# and B# are very similar, both approximately equal to $1.0 \times 10^{-6}$/˚C, indicating that the introduction of 10 mol% anhydrous magnesium acetate after the condensation polymerization of aluminum and titanium precursor does not affect the thermal expansion performance of aluminum titanate. The thermal expansion coefficient of A# sample introduced before the condensation polymerization of aluminum and titanium precursor was $3.67 \times 10^{-6}$/˚C, which was significantly higher than $0.99 \times 10^{-6}$/˚C of W# sample. The reason is that the content of rutile phase with high expansion coefficient in A# sample is relatively large (see **Figure 3**), which leads to the increase of thermal expansion coefficient of A# sample, while the content of rutile crystal phase in W# and B# samples is relatively low, and the content of aluminum titanate is not different, so the expansion coefficient of these two samples is very close.

**Figure 4** shows the XRD patterns of W#, A# and B# samples after being kept at 1100˚C for 20 h. The test results of their coefficient of expansion are listed in **Table 6**. **Figure 4** shows that the sample of W# has been completely decomposed into the crystal phase with high expansion coefficient of corundum ($8.6 \times 10^{-6}$/˚C) and rutile ($8.0 \times 10^{-6}$/˚C) after being kept at 1100˚C for 20 h, and its expansion coefficient has correspondingly increased from the initial $0.99 \times 10^{-6}$/˚C (see **Table 5**) to $8.78 \times 10^{-6}$/˚C (see **Table 6**). After being kept at 1100˚C

**Table 5.** Thermal expansion coefficients of samples treated at 750˚C for 1.5 h.

| specimen | coefficient of thermal expansion (×10$^{-6}$/˚C, 20˚C - 1000˚C) |
|---|---|
| A# | 3.67 |
| B# | 1.13 |
| W# | 0.99 |

**Table 6.** Thermal expansion coefficients of samples treated at 1100˚C for 20 h.

| Specimen | Coefficient of thermal expansion (×10$^{-6}$/˚C, 20˚C - 1000˚C) |
|---|---|
| A# | 7.12 |
| B# | 0.56 |
| W# | 8.78 |

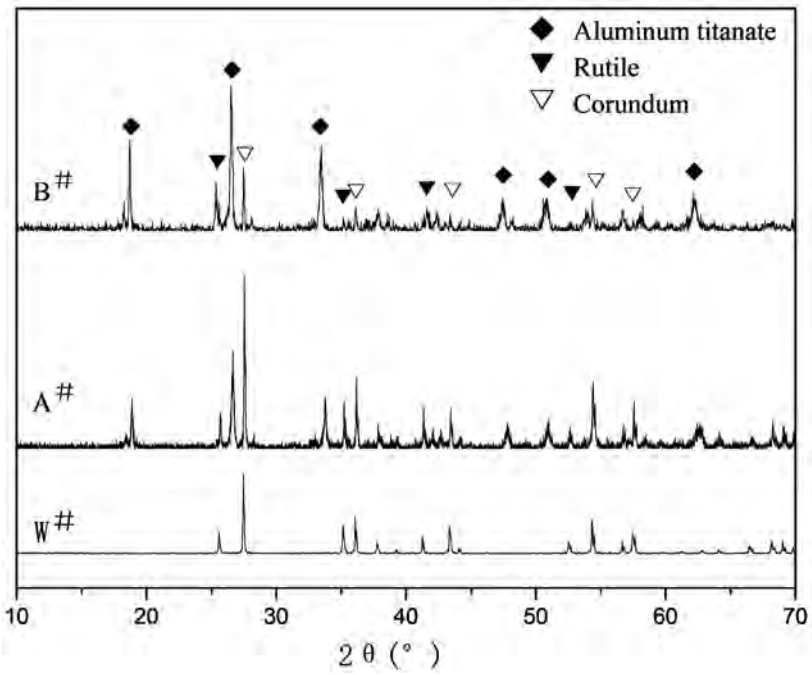


**Figure 4.** XRD patterns of samples W#, A# and B# treated at 1100˚C for 20 h.

for 20 h, A# was basically decomposed into rutile and corununde, and its expansion coefficient was also increased to 7.12 × 10$^{-6}$/˚C, indicating that the introduction of anhydrous magnesium acetate before the condensation polymerization of aluminum and titanium precursor could not effectively inhibit the thermal decomposition of aluminum titanate. However, from the increase of the thermal expansion coefficient of the sample, it can be determined that the aluminum titanate in the sample has not been completely decomposed, which is consistent with the XRD pattern corresponding to Figure 4, and there are still a small number of aluminum titanate diffraction peaks. In sharp contrast, the sample B# introduced after the condensation polymerization of aluminum and titanium precursor by anhydrous magnesium acetate was not decomposed by

aluminum titanate after 20 h heat treatment at 1100˚C. On the contrary, compared with the XRD pattern of the sample B# in Figure 4, the synthesis effect of aluminum titanate was significantly improved, which indicated that the newly synthesized aluminum titanate phase continuously appeared in the process of the sample B# rising from 750˚C to 1100˚C. Due to the increase of aluminum titanate crystalline phase and the disappearance of rutile phase, the expansion coefficient of B# sample was reduced from $1.59 \times 10^{-6}$/˚C to $0.56 \times 10^{-6}$/˚C (see Table 6).

Thus, it can be seen that although the synthesis effect of aluminum titanate at 750˚C is better than that of the sample of B#, it is completely decomposed at 1100˚C and its low expansion characteristics are completely lost. Therefore, the application of W# samples only outside the decomposition temperature of aluminum titanate makes sense. It is worth noting that after 1100˚C, the sample of B# not only shows excellent anti-decomposition ability, but also greatly improves the synthesis effect of aluminum titanate, highlighting the important value of the sample of B# that can be applied at the decomposition temperature of aluminum titanate, which is the purpose of improving the thermal decomposition ability of aluminum titanate.

When introduced before the polycondensation reaction of aluminum and titanium precursor, anhydrous magnesium acetate can promote the homogeneous polycondensation reaction in sol and form a large number of Al-O-Al and Ti-O-Ti bonds in gel. The low temperature synthesis of aluminum titanate at 750˚C is seriously affected. When introducing anhydrous magnesium acetate after the polycondensation reaction of aluminum and titanium precursor, it can further deester the polycondensation reaction product of aluminum and titanium precursor to form heterogeneous bonds of Mg-O-Al and Mg-O-Ti. Therefore, magnesium can enter the aluminum titanate lattice at 750˚C to form a solid solution, thus improving its thermal stability. Of the hydrolysis of sol-gel method in preparation of aluminum titanate material literature reported less, for this, based on the team in the hydrolysis of sol-gel research of hydrolysis of heterogeneous condensation reaction conditions. The type of aluminum titanate stabilizer, the influence law and mechanism of doping effect were studied. First adopted the hydrolytic sol-gel to 750˚C stabilization of modified aluminum titanate (reduced above 500˚C) than the traditional methods, both at home and abroad the first reveals the traditional anhydrous (low electronegativity) metal halide stabilizer cannot achieve aluminum titanate modified the root cause of the low temperature stabilization. Excessive ionic bond percentage (50%) of polar compounds to the hydrolysis of heterogeneous condensation reaction. Moreover, the magnesium stabilized aluminum titanate prepared by nonhydrolytic sol-gel method has achieved negative expansion property, and the preparation process has obvious advantages.

Our research group has developed a new high temperature stable aluminum titanate base ceramic color and its preparation method. The precursor was obtained by dissolving the aluminum source, titanium source and oxygen donor in solvent. Then the colorant raw material which plays a stabilizing role or the co-

lorant raw material and the stabilizer raw material are added together; Gel was formed by non-hydrolyzed sol-gel condensation reaction. The gel was dried, ground and calcined to obtain stabilized aluminum titanate base ceramic color. The new high-temperature stable aluminum titanate ceramic color developed by the invention has the characteristics of low synthesis temperature, low cost, small color difference and excellent coloring effect, etc., and is an ideal high-temperature color resistant material. The invention relates to a non-hydrolyzed sol-gel method for the preparation of a new stable aluminum titanate base ceramic pigment, which has the advantages of simple process, short period and easy control.

## 3. Conclusion

The preparation methods of magnesium-stabilized aluminum titanate powder have different characteristics. Magnesium stabilization improves the thermal stability of aluminum titanate. However, the temperature of non-hydrolyzed sol-gel method is relatively low, and aluminum titanate can be well synthesized at low temperature at 750˚C. Compared with the solid phase method, high-temperature reaction is required, and the powder in liquid phase method is easy to agglomerate, etc. The preparation technology of non-hydrolyzed sol-gel method has obvious advantages for the negative inflation of magnesium stable aluminum titanate materials. The synthesis of aluminum titanate powder by nonhydrolytic sol-gel method has great prospect. The medium temperature of aluminum titanate (800˚C - 1250˚C) is easy to decompose, but the poor stability of the medium temperature can be effectively inhibited by magnesium stabilization. Aluminum titanate itself has good corrosion resistance of glass melt and high temperature stability. Aluminum titanate stabilized with magnesium has good stability at medium temperature. Meanwhile, NHSG method has unique advantages. Because the non-hydrolytic heterogeneous polycondensation reaction is easy to form heterogeneous bonding and achieve uniform mixing of atomic levels, aluminum titanate stabilized with magnesium is expected to become an ideal new high-temperature ceramic color base material.

## Acknowledgements

This work was supported by the National Natural Science Foundation of China [grant numbers 52072162, 51662016, 51962014]; Jiangxi Provincial Natural Science Foundation [grant numbers 20202ACBL214006, 20202ACBL214008, 20192BBEL50022, 2020ZDI03004, 20202BABL214013]. Open fund project of the Key Laboratory of Inorganic Coating Materials, Chinese Academy of Science (ICM-202001).

## Conflicts of Interest

There are no conflicts to declare.

## References

[1] Thomas, H.A.J. and Stevens, R. (1989) *British Ceramic Transactions*, **88**, 144-151.

[2] Innocenzi, P., Martucci, A. and Armelao, L. (2000) *Chemistry of Materials*, **12**, 517-524. https://doi.org/10.1021/cm991134i

[3] Fang, Q., Zhang, L., Shen, Q., *et al.* (2003) *Chinese Journal of Ceramics*, **1**, 49-53.

[4] Zhang, C. (2012) Preparation and Properties of Aluminum Titanate Ceramics. Ph.D., Ocean University of China, Qingdao.

[5] Kato, E., Daimon, K. and Takahashi, J. (1980) *Journal of American Ceramics Society*, **63**, 355-356. https://doi.org/10.1111/j.1151-2916.1980.tb10745.x

[6] Thomas, H.A.J. and Stevens, R. (1989) *British Ceramic Transactions and Journal*, **88**, 44-90.

[7] Korim, T. (2009) *Ceramics International*, **35**, 1671-1675. https://doi.org/10.1016/j.ceramint.2008.07.017

[8] Buscaglia, V., Nanni, P., Battilana, G., *et al.* (1994) *Journal of the European Ceramic Society*, **13**, 411-417. https://doi.org/10.1016/0955-2219(94)90018-3

[9] Jiang, W.H., Xiao, X.C., Zhou, J.E., *et al.* (2000) *Journal of Inorganic Materials*, **15**, 437-440.

[10] Jiang, W.H., Xiao, X.C., Zhou, J.E., *et al.* (2000) *Journal of Inorganic Materials*, **15**, 163-168.

[11] Dondi, M., Lyubenova, T.S., Carda, J.B., *et al.* (2010) *Journal of the American Ceramic Society*, **92**, 1972-1980. https://doi.org/10.1111/j.1551-2916.2009.03172.x

[12] Fang, Q., Zhang, L.M. and Shen, Q. (1998) *Journal of Wuhan University of Technology*, **24**, 44-48.

[13] Zhang, L.M. and Fang, Q. (2002) *Journal of the Chinese Ceramic Society*, **30**, 451-455.

[14] Buscaglia, V., *et al.* (1997) *Journal of Materials Science*, **32**, 6525-6531.

[15] Shadab, L. and Touradj, E. (2014) *Ceramics International*, **40**, 12669-12674. https://doi.org/10.1016/j.ceramint.2014.04.114

[16] Yang, R., Shen, S.Y., Shen, Q., *et al.* (2005) *China Silicate Bulletin*, No. 3, 89-92.

[17] Plinio, I., Alessandro, M. and Lidia, A. (2004) *Journal of the European Ceramic Society*, **25**, 3587-3591.

[18] Dai, B.Y. and Liu, Z.B. (2015) *Special Casting and Nonferrous Alloys*, **35**, 453-456.

[19] Jiang, W.H., Hu, Z., Liu, J.M., *et al.* (2019) *Ceramics International*, **45**, 18704-18709. https://doi.org/10.1016/j.ceramint.2019.06.096

[20] Feng, G., Jang, W.H.J.M., Liu, Q., *et al.* (2017) *Acta Ceramica Sinica*, **38**, 471-475.

[21] Zhou, J.R., Zhang, Y.Z., Ma, G.H., *et al.* (1998) *China Ceramics*, **34**, 1-4.

[22] Xue, M.J. and Sun, C.X. (2001) *Journal of East China University of Science and Technology*, **27**, 76-79.

[23] Vioux, A. (1997) *Chemistry of Materials*, **9**, 2292-2299. https://doi.org/10.1021/cm970322a

[24] Vioux, A. and Leclercq, D. (1996) *Chemical Reviews*, **1**, 65-73. https://doi.org/10.1002/(SICI)1234-985X(199603)3:1<65::AID-HCR57>3.0.CO;2-7

[25] Hay, J.H. and Raval, H.M. (1998) *Journal of Sol-Gel Science and Technology*, **30**, 109-112. https://doi.org/10.1023/A:1008615708489

[26] Acosta, S., Arnal, P. and Vioux, A. (1994) *Materials Research Society Symposium Proceedings*, **346**, 43-54. https://doi.org/10.1557/PROC-346-43

[27] Jiang, W.H., Feng, G. and Liu, J.M. (2010) *Acta Silicate Sinica*, **38**, 783-787.

Journal of Modern Physics, 2020, 11, 1891-1910
https://www.scirp.org/journal/jmp
ISSN Online: 2153-120X
ISSN Print: 2153-1196

# Calculations Energy of the $(nl^2)\ ^1L^\pi$ Doubly Excited States of Two-Electron Systems via the Screening Constant by Unit Nuclear Charge Formalism

**Momar Talla Gning[1*], Ibrahima Sakho[1], Malick Sow[2]**

[1]Department of Experimental Sciences, UFR Sciences and Technologies University of Thies, Thies, Senegal
[2]Atoms Laser Laboratory, Department of Physics, Faculty of Sciences and Technologies, University Cheikh Anta Diop, Dakar, Senegal
Email: *gningpc85@hotmail.fr

**How to cite this paper:** Gning, M.T., Sakho, I. and Sow, M. (2020) Calculations Energy of the $(nl^2)\ ^1L^\pi$ Doubly Excited States of Two-Electron Systems via the Screening Constant by Unit Nuclear Charge Formalism. *Journal of Modern Physics*, **11**, 1891-1910.
https://doi.org/10.4236/jmp.2020.1111118

**Received:** July 11, 2020
**Accepted:** November 22, 2020
**Published:** November 25, 2020



## Abstract

In this work, the total energies of doubly excited states $(ns^2)\ ^1S^e$, $(np^2)\ ^1D^e$, $(nd^2)\ ^1G^e$, $(nf^2)\ ^1I^e$, $(ng^2)\ ^1K^e$, and $(nh^2)\ ^1M^e$ of the helium isoelectronic sequence with $Z \leq 10$ are calculated in the framework of the variational method of the Screening Constant by Unit Nuclear Charge (SCUNC). These calculations are performed using a new wavefunction correlated to Hylleraas-type. The possibility of using the SCUNC method in the investigation of high-lying Doubly Excited States(DES) in two-electron systems is demonstrated in the present work in the case of the $(nl^2)\ ^1L^\pi$ doubly excited states, where accurate total energies are tabulated up to $n = 20$. All the results obtained in this paper are in agreement with the values of the available literature and may be useful for future experimental and theoretical studies on the doubly excited $(nl^2)\ ^1L^\pi$ states of two-electron systems.

## Keywords

Doubly Excited States, Helium-Like Systems, Screening Constant by Unit Nuclear Charge (SCUNC), Wave Functions Correlated, Total Energy

## 1. Introduction

Studies of doubly-excited states of helium-like systems remain an active field of research since the early experiments of Madden and Codling [1] [2] concerning the observation of resonant structures in the absorption spectrum of helium using synchrotron radiation. The strong correlation between electrons in the

doubly excited state of two-electron atomic systems has attracted considerable attention from theorists and experimenters as evidenced by the efforts concentrated in the field over the last twenty years. Theoretical investigations in two-electron Doubly Excited States (DES) are of great interest in connection with the understanding of collisional and radiative processes which take place in hot astrophysical and laboratory plasma [3] [4] [5]. In these investigations, great attention has been paid to the study of symmetric ($nl^2$) DES where the electron-electron correlation effects may be predominant as revealed by the works of Fano [6]. Several experimental and theoretical studies on doubly excited ($nl^2$) states have been carried out using different methods. Experimentally, many of these doubly excited states have been observed in electronic impact experiments by Oda *et al.* [7] and Hicks and Comer [8]. In their studies, these authors have worked on the energy spectra of ejected electrons from autoionization states in helium excited by electron impact. Other doubly excited states were observed by ion impact by Rudd [9] and by Bordenave-Montesquieu *et al.* [10]. These doubly excited states were also studied by examining the spectra of ejected electrons by Gelabart *et al.* [11] and by Rodbro *et al.* [12]. From a theoretical point of view, several calculation methods have been used, the complex rotation method [13] [14] [15], the variational method of Hylleraas [16], the double sums over the total hydrogen spectrum formalism [17], the density functional theory [18], the formalism of the Feshbach projection operators [19] [20], the discretization technique [21], the truncated diagonalization method [22], the time-dependent variation perturbation theory [23], and the semi-empirical procedure of the screening constant by unit nuclear charge (SCUNC) method [24] [25] [26], to name a few. In all these *ab-initio* methods, energies of ($nl^2$) doubly-excited states of He isoelectronic sequence can't be expressed in an analytical formula. In addition, most of these preceding methods require large basis-set calculations involving a fair amount of mathematics complexity. But, it's widely believed that there are distinct advantages to viewing problems of physics within the framework of simple analytical models. Contrary to all these methods, the variational procedure of the SCUNC method makes it possible to calculate the energies of the ($nl^2$) doubly excited states without a complex mathematical program or calculation code but from a simple analytical expression. In addition, in the recent past the variational procedure of the SCUNC method has been successfully applied to calculations of the energies of doubly excited states $nlnl'$ ($n$ = 2 - 4) in helium-like ions by Sakho [27] using a special Hylleraas-type wave function. These reasons sufficiently justify our choice to apply the variational procedure of the SCUNC method in this study. The goal of the present work is to report accurate total energies and excitation energies of the doubly excited states ($nl^2$) using the variational procedure of the SCUNC formalism but also to show that it is possible to calculate total energies and precise excitation energies of high-lying up to $n$ = 20 of the doubly excited states ($nl^2$) without any calculation code or complex mathematical program, without a powerful computer but using a sim-

ple analytical expression. Section 2 gives the correlated wave functions and brief overview of the calculation method. Section 3 gives the presentation and the discussion of our results in the case of doubly excited states $(ns^2)\ ^1S^e$, $(np^2)\ ^1D^e$, $(nd^2)\ ^1G^e$, $(nf^2)\ ^1I^e$, $(ng^2)\ ^1K^e$, and $(nh^2)\ ^1M^e$ of the He-like ions up to $Z = 10$ are made. All our results are compared to available theoretical and experimental data.

## 2. Theory and Calculations

### 2.1. Hamiltonian and Hylleraas-Type Wave Functions

The time independent Schrödinger equation for the Helium atom, or the positive ions of its isoelectronic sequence, or of the negative Hydrogen ion, is

$$\hat{H}\Psi = E\Psi \tag{1}$$

where $\hat{H}$ represents the Hamiltonian operator of the considered system, $\Psi$ the trial wave function and $E$ the associated energy.

The Hamiltonian $H$ of the helium isoelectronic series in given by (in atomic units)

$$H = -\frac{1}{2}\Delta_1 - \frac{1}{2}\Delta_2 - \frac{Z}{r_1} - \frac{Z}{r_2} + \frac{1}{r_{12}} \tag{2}$$

In this equation, $r_1$ and $r_2$ denote the position of the two electrons from the nucleus, $Z$ is the nuclear charge, $\Delta_1$ is the Laplacian with reference to the coordinates of the vector radius $r_1$ which detect the position of the electron 1. $\Delta_2$ Laplacian defines the coordinates of the vector radius $r_2$ which detect the position of the electron 2 and $r_{12}$ inter-electronic distance.

Solving Equation (1) is very difficult because of the term $r_{12} = u = |r_1 - r_2|$ representing electron-electron repulsion. It is therefore necessary to implement a rough calculation method using a correlated wavefunction.

The groundbreaking work in this area was conducted by Hylleraas [28] [29] [30]. The simplest Hylleraas wave function is written as follow:

$$\Psi(r_1, r_2, r_{12}) = (1 + br_{12})\exp\left[-\alpha(r_1 + r_2)\right] \tag{3}$$

Since Hyllerass' original work, tremendous efforts have been made to improve upon that work, using larger and larger expansions, adding more complicated terms. In this present work, we have modified this Hylleraas wavefunction in order to adapt it to the study of symmetrical $(nf^2)\ ^1L^\pi$ doubly excited states in two-electron atomic systems. These wave functions are defined as follow:

$$\Psi(r_1, r_2, r_{12}) = \sum_{\upsilon=0}^{\upsilon=n-\ell-1}\left(n^2 r_0^2\right)^\upsilon \times (1 + C_0 Z r_{12})\exp\left[-\alpha(r_1 + r_2)\right] \tag{4}$$

In this expression, $n$ is the principal quantum number; $\ell$ is orbital quantum number, $r_0$ is Bohr radius, $C_0$ and $\alpha$ are the variational parameters to be determined by minimizing the energy, $Z$ is the nuclear charge number, $r_{12}$ represents the term electron-electron repulsion $r_1$ and $r_2$ are the coordinates of electrons with respect to the nucleus.

From the theoretical viewpoint, the Hylleraas variational method is based on the Hylleraas and Undheim theorem [31] according to which, a good approximation of the energy eigenvalue $E(\alpha, C_0)$ is obtained when the minima of the function ( $\mathrm{d}^2 E(\alpha, C_0) / \mathrm{d}\alpha \mathrm{d}C_0$ ) converge with increasing values of the dimension $D$ of the basis states and when the function exhibit a plateau.

Using this theorem, the values of the varitional parameters $\alpha$ and $C_0$ can be determined by the following conditions:

$$\frac{\partial E(\alpha, C_0)}{\partial C_0} = 0 \tag{5}$$

and

$$\frac{\partial E(\alpha, C_0)}{\partial \alpha} = 0 \tag{6}$$

In the framework of the Ritz' variation principle, the energy $E(\alpha, C_0) = \langle H \rangle (\alpha, C_0)$ is calculated from the relation:

$$E(\alpha, C_0) = \langle H \rangle (\alpha) = \frac{\langle \Psi(\alpha, C_0) | H | \Psi(\alpha, C_0) \rangle}{\langle \Psi(\alpha, C_0) | \Psi(\alpha, C_0) \rangle} \tag{7}$$

In this equation, the correlated wave functions are given by (4) and the Hamiltonian H of the helium isoelectronic series in given by (2) (in atomic units).

Furthermore, the closure relation represents the fact that $|\boldsymbol{r}_1, \boldsymbol{r}_2\rangle$ are continuous bases in the space of the two-electron space, written as follow:

$$\iint \mathrm{d}r_1^3 \mathrm{d}r_2^3 \, |\boldsymbol{r}_1, \boldsymbol{r}_2\rangle \langle \boldsymbol{r}_1, \boldsymbol{r}_2| = 1 \tag{8}$$

Using this relation, according to (7), we obtain:

$$\begin{aligned} & E(\alpha, C_0) \iint \mathrm{d}r_1^3 \mathrm{d}r_2^3 \langle \Psi(\alpha, C_0) || \boldsymbol{r}_1, \boldsymbol{r}_2\rangle \times \langle \boldsymbol{r}_1, \boldsymbol{r}_2 || \Psi(\alpha, C_0)\rangle \\ & = \iint \mathrm{d}r_1^3 \mathrm{d}r_2^3 \langle \Psi(\alpha, C_0) || \boldsymbol{r}_1, \boldsymbol{r}_2\rangle \hat{H} \langle \boldsymbol{r}_1, \boldsymbol{r}_2 || \Psi(\alpha, C_0)\rangle \end{aligned} \tag{9}$$

By developing this expression (9), we find:

$$E(\alpha, C_0) \iint \mathrm{d}r_1^3 \mathrm{d}r_2^3 \Psi(\alpha, C_0) \times \Psi^*(\alpha, C_0) = \iint \mathrm{d}r_1^3 \mathrm{d}r_2^3 \Psi(\alpha, C_0) \hat{H} \Psi^*(\alpha, C_0) \tag{10}$$

This means:

$$N^* E(\alpha, C_0) = \iint \mathrm{d}r_1^3 \mathrm{d}r_2^3 \Psi(\alpha, C_0) \hat{H} \Psi^*(\alpha, C_0) \tag{11}$$

with the normalization constant

$$N = \iint \mathrm{d}r_1^3 \mathrm{d}r_2^3 \left| \Psi(\alpha, C_0) \right|^2 \tag{12}$$

To make it easier to integrate Equation (11), we operate the variable changes in elliptic coordinates by:

$$s = r_1 + r_2; \quad t = r_1 - r_2; \quad u = r_{12} \tag{13}$$

On the basis of these variable changes, the elementary volume element

$$\mathrm{d}\tau = \mathrm{d}^3 r_1 \mathrm{d}^3 r_2 = 2\pi^2 \left(s^2 - t^2\right) u \mathrm{d}s \mathrm{d}u \mathrm{d}t \tag{14}$$

Using these elliptical coordinates, Equation (11) is written as follows

$$NE(\alpha,C_0)=\int_0^{\infty}\mathrm{d}s\int_0^{s}\mathrm{d}u\int_0^{u}\mathrm{d}t\left\{u\left(s^2-t^2\right)\times\left[\left(\frac{\partial\Psi}{\partial s}\right)^2+\left(\frac{\partial\Psi}{\partial t}\right)^2+\left(\frac{\partial\Psi}{\partial u}\right)^2\right]\right.$$
$$\left.+2\left(\frac{\partial\Psi}{\partial u}\right)\times\left[s\left(u^2-t^2\right)\times\frac{\partial\Psi}{\partial s}+t\left(s^2-u^2\right)\times\frac{\partial\Psi}{\partial t}-\Psi^2\times\left(4Zsu-s^2+t^2\right)\right]\right\} \tag{15}$$

with respect to the correlated wave functions given by expression (4), it is expressed as follow

$$\Psi(s,t,u,\alpha,C_0)=\sum_{\upsilon=0}^{\upsilon=n-\ell-1}\left(n^2r_0^2\right)^{\upsilon}\times\left(1+C_0Zu\right)\exp(-\alpha s) \tag{16}$$

Furthermore, according to (12), the normalization constant is written in elliptic coordinates as:

$$N=\int_0^{\infty}\mathrm{d}s\int_0^{s}\mathrm{d}u\int_0^{u}\mathrm{d}t u\left(s^2-t^2\right)\times\Psi^2 \tag{17}$$

## 2.2. General Formalism of the SCUNC Method

The Screening Constant by Unit Nuclear Charge (SCUNC) formalism is used in this work to calculate the total energies of the symmetrical $(n\ell)\ {}^1L^{\pi}$ doubly excited states of the helium-isoelectronic up to $Z=10$.

In the framework of the Screening Constant by Unit Nuclear Charge (SCUNC) formalism, total energies of the $(N\ell n\ell')\ {}^{2S+1}L^{\pi}$ doubly excited states are expressed in Rydberg (Ry) as below [24] [25]

$$E\left(N\ell n\ell',{}^{2s+1}L^{\pi}\right)=-Z^2\left(\frac{1}{N^2}+\frac{1}{n^2}\left[1-\beta\left(N\ell n\ell',{}^{2s+1}L^{\pi},Z\right)\right]^2\right)\mathrm{Ry} \tag{18}$$

In this equation, the principal quantum numbers $N$ and $n$, are respectively the inner and the outer electron of the helium-isoelectronic series. In this equation, the $\beta$-parameters are screening constant by unit nuclear charge expanded in inverse powers of $Z$ and given by

$$\beta\left(N\ell n\ell',{}^{2s+1}L^{\pi},Z\right)=\sum_{k=1}^{q}f_k\left(\frac{1}{Z}\right)^k \tag{19}$$

where $f_k=f_k\left(N\ell n\ell',{}^{2s+1}L^{\pi}\right)$ are screening constants to be evaluated based on variational predicable using a wavefunction.

For the states $(n\ell)\ {}^1L^{\pi}$, $N=n$ and $l=l'$. Hence, the total energy is written as follow:

$$E\left(n\ell^2,{}^1L^{\pi}\right)=-\frac{Z^2}{n^2}\left\{1+\left[1-\beta\left(n\ell^2,{}^1L^{\pi},Z\right)\right]^2\right\}\mathrm{Ry} \tag{20}$$

Furthermore, in the framework of the screening constant by unit nuclear charge formalism, the $\beta$-screening constant is expressed in terms of the variational $\alpha$-parameter as follow

$$\beta\left(n\ell^2,{}^1L^{\pi},Z,\alpha\right)=\frac{\alpha}{Z^2}\left(1+\frac{2L}{2n+4L-3}\right) \tag{21}$$

In this expression, $n$ denotes the principal quantum number, $L$ characterizes the considered quantum state (S, P, D, F etc.) and $\alpha$ is the variational parameter.

Then, using Equation (21), the total energies of the symmetrical $(n\ell^2)\ ^1L^\pi$ doubly excited states in the helium isoelectronic series is expressed in Rydberg (Ry) as below:

$$E\left(n\ell^2, {}^1L^\pi, Z\right) = -\frac{Z^2}{n^2}\left\{1+\left[1-\frac{\alpha}{Z^2}\left(1+\frac{2L}{2n+4L-3}\right)\right]^2\right\}\text{Ry} \tag{22}$$

In this equation, only the parameter $\alpha$ is unknown. Considering the $(2s^2)\ ^1S^e$ state of Helium-like ions ($Z$ = 2 - 10), we calculated the values of the variational parameters $\alpha$ and $C_0$, the results of which are presented in Table 1.

The Equation (22) is used to calculate the total energies of the $(n\ell^2)\ ^1L^\pi$ doubly excited states of helium-like ions without a complex calculation program.

## 3. Results and Discussions

The results obtained in the present study for $(ns^2)\ ^1S^e$, $(np^2)\ ^1D^e$, $(nd^2)\ ^1G^e$, $(nf^2)\ ^1I^e$, $(ng^2)\ ^1K^e$, and $(nh^2)\ ^1M^e$ with $n \le 20$ in the helium-like ions up to $Z$ = 10 are listed in Tables 1-16 and compared to various other calculations. Table 1 presents our results on the calculation of the variational parameters $\alpha$ and $C_0$. These variational parameters are calculated by determining the expression of $E = f(\alpha, C_0)$ from the expression (15) and the wavefunction (16), then according to conditions (5) and (6) we obtained a system of equations whose resolution to give the values of the variational parameters $\alpha$ and $C_0$ with $2 \le Z \le 10$. All calculations in this work were performed with the calculation program MAXIMA. In Tables 2-7 we have listed our present results $E$ on the calculation of the total energies of the $(n\ell^2)\ ^1L^\pi$ doubly excited states of the helium isoelectronic sequence with $2 \le Z \le 10$ and $2 \le n \le 20$ obtained using Equation (22). Table 2 shows our present results of the $(ns^2)\ ^1S^e$ ($n$ = 2 - 20) doubly excited states of helium - like systems ($Z$ = 2 - 10). Table 3 shows our present results of the $(np^2)\ ^1D^e$ ($n$ = 2 - 20) doubly excited states of helium-like systems ($Z$ = 2 - 10). Table 4 shows our present results of the $(nd^2)\ ^1G^e$ ($n$ = 3 - 20) doubly excited states of helium-like systems ($Z$ = 2 - 10). Table 5 shows our present results of the $(nf^2)\ ^1I^e$ ($n$ = 4 - 20) doubly excited states of helium-like systems ($Z$ = 2 - 10). Table 6 shows our present results of the $(ng^2)\ ^1K^e$ ($n$ = 5 - 20) doubly excited states of helium-like systems ($Z$ = 2 - 10). Table 7 shows our present results of the $(nh^2)\ ^1M^e$ ($n$ = 6 - 20) doubly excited states of helium-like systems ($Z$ = 2 - 10).

Table 8 shows a comparison of the present calculations for the $(ns^2)\ ^1S^e$ states with the results of the semi-empirical procedure of the screening constant by

Table 1. Values of variational parameters $\alpha$ and $C_0$ of helium-like ions ($Z$ = 2 - 10).

| $Z$ | 2 | 3 | 4 | 5 | 6 | 7 | 8 | 9 | 10 |
|---|---|---|---|---|---|---|---|---|---|
| $\alpha$ | 0.96105 | 1.40362 | 1.93837 | 2.47394 | 3.00997 | 3.54627 | 4.08276 | 4.61938 | 5.15608 |
| $C_0$ | 0.24982 | 0.26539 | 0.28139 | 0.29115 | 0.29771 | 0.30244 | 0.30600 | 0.30878 | 0.31102 |

**Table 2.** Total energy ($-E$) for ($ns^2$) $^1S^e$ ($n$ = 2 - 20) doubly excited states of helium-like systems ($Z$ = 2 - 10). The energies $E$ are in eV.

| $Z$ | 2 | 3 | 4 | 5 | 6 | 7 | 8 | 9 | 10 |
|---|---|---|---|---|---|---|---|---|---|
| $ns^2$ | $-E$ | $-E$ | $-E$ | $-E$ | $-E$ | $-E$ | $-E$ | $-E$ | $-E$ |
| $2s^2$ | 21.45940 | 52.42276 | 96.46002 | 154.07753 | 225.28724 | 310.09472 | 408.50290 | 520.51348 | 646.12749 |
| $3s^2$ | 9.53751 | 23.29900 | 42.87112 | 68.47890 | 100.12766 | 137.81987 | 181.55684 | 231.33932 | 287.16777 |
| $4s^2$ | 5.36485 | 13.10569 | 24.11501 | 38.51938 | 56.32181 | 77.52368 | 102.12572 | 130.12837 | 161.53187 |
| $5s^2$ | 3.43350 | 8.38764 | 15.43360 | 24.65241 | 36.04596 | 49.61515 | 65.36046 | 83.28216 | 103.38040 |
| $6s^2$ | 2.38438 | 5.82475 | 10.71778 | 17.11973 | 25.03192 | 34.45497 | 45.38921 | 57.83483 | 71.79194 |
| $7s^2$ | 1.75179 | 4.27941 | 7.87429 | 12.57776 | 18.39080 | 25.31385 | 33.34718 | 42.49090 | 52.74510 |
| $8s^2$ | 1.34121 | 3.27642 | 6.02875 | 9.62985 | 14.08045 | 19.38092 | 25.53143 | 32.53209 | 40.38297 |
| $9s^2$ | 1.05972 | 2.58878 | 4.76346 | 7.60877 | 11.12530 | 15.31332 | 20.17298 | 25.70437 | 31.90753 |
| $10s^2$ | 0.85838 | 2.09691 | 3.85840 | 6.16310 | 9.01149 | 12.40379 | 16.34012 | 20.82054 | 25.84510 |
| $11s^2$ | 0.70940 | 1.73298 | 3.18876 | 5.09347 | 7.44751 | 10.25107 | 13.50423 | 17.20706 | 21.35959 |
| $12s^2$ | 0.59609 | 1.45619 | 2.67945 | 4.27993 | 6.25798 | 8.61374 | 11.34730 | 14.45871 | 17.94799 |
| $13s^2$ | 0.50791 | 1.24078 | 2.28308 | 3.64681 | 5.33224 | 7.33952 | 9.66871 | 12.31985 | 15.29296 |
| $14s^2$ | 0.43795 | 1.06985 | 1.96857 | 3.14444 | 4.59770 | 6.32846 | 8.33679 | 10.62272 | 13.18628 |
| $15s^2$ | 0.38150 | 0.93196 | 1.71484 | 2.73916 | 4.00511 | 5.51279 | 7.26227 | 9.25357 | 11.48671 |
| $16s^2$ | 0.33530 | 0.81911 | 1.50719 | 2.40746 | 3.52011 | 4.84523 | 6.38286 | 8.13302 | 10.09574 |
| $17s^2$ | 0.29702 | 0.72557 | 1.33509 | 2.13256 | 3.11816 | 4.29197 | 5.65402 | 7.20434 | 8.94294 |
| $18s^2$ | 0.26493 | 0.64719 | 1.19086 | 1.90219 | 2.78132 | 3.82833 | 5.04325 | 6.42609 | 7.97688 |
| $19s^2$ | 0.23778 | 0.58086 | 1.06881 | 1.70723 | 2.49626 | 3.43595 | 4.52635 | 5.76746 | 7.15931 |
| $20s^2$ | 0.21459 | 0.52423 | 0.96460 | 1.54078 | 2.25287 | 3.10095 | 4.08503 | 5.20513 | 6.46127 |

**Table 3.** Total energy ($-E$) for the ($np^2$) $^1D^e$ ($n$ = 2 - 20) doubly excited states of helium-like systems ($Z$ = 2 - 10). The energies $E$ are in eV.

| $Z$ | 2 | 3 | 4 | 5 | 6 | 7 | 8 | 9 | 10 |
|---|---|---|---|---|---|---|---|---|---|
| $np^2$ | $-E$ | $-E$ | $-E$ | $-E$ | $-E$ | $-E$ | $-E$ | $-E$ | $-E$ |
| $2p^2$ | 19.40691 | 48.98779 | 91.46705 | 147.50214 | 217.11646 | 300.32082 | 397.12093 | 507.52007 | 631.52025 |
| $3p^2$ | 8.78089 | 22.04020 | 41.04506 | 66.07698 | 97.14529 | 134.25433 | 177.40638 | 226.60274 | 281.84424 |
| $4p^2$ | 5.00135 | 12.50334 | 23.24244 | 37.37258 | 54.89863 | 75.82286 | 100.14645 | 127.87008 | 158.99418 |
| $5p^2$ | 3.23051 | 8.05224 | 14.94822 | 24.01485 | 35.25507 | 48.67024 | 64.26108 | 82.02799 | 101.97124 |
| $6p^2$ | 2.25935 | 5.61862 | 10.41971 | 16.72838 | 24.54660 | 33.87526 | 44.71484 | 57.06561 | 70.92775 |
| $7p^2$ | 1.66926 | 4.14359 | 7.67801 | 12.32015 | 18.07141 | 24.93241 | 32.90349 | 41.98486 | 52.17663 |
| $8p^2$ | 1.28386 | 3.18216 | 5.89260 | 9.45120 | 13.85900 | 19.11648 | 25.22388 | 32.18135 | 39.98897 |
| $9p^2$ | 1.01824 | 2.52067 | 4.66512 | 7.47977 | 10.96542 | 15.12242 | 19.95098 | 25.45121 | 31.62316 |
| $10p^2$ | 0.82739 | 2.04609 | 3.78505 | 6.06690 | 8.89227 | 12.26146 | 16.17460 | 20.63180 | 25.63311 |
| $11p^2$ | 0.68564 | 1.69405 | 3.13258 | 5.01981 | 7.35623 | 10.14210 | 13.37752 | 17.06258 | 21.19731 |
| $12p^2$ | 0.57748 | 1.42570 | 2.63546 | 4.22227 | 6.18654 | 8.52846 | 11.24814 | 14.34564 | 17.82100 |
| $13p^2$ | 0.49305 | 1.21645 | 2.24800 | 3.60082 | 5.27527 | 7.27152 | 9.58964 | 12.22970 | 15.19171 |

**Continued**

| | | | | | | | | | |
|---|---|---|---|---|---|---|---|---|---|
| $14p^2$ | 0.42590 | 1.05014 | 1.94014 | 3.10718 | 4.55154 | 6.27337 | 8.27274 | 10.54969 | 13.10425 |
| $15p^2$ | 0.37159 | 0.91576 | 1.69148 | 2.70854 | 3.96718 | 5.46753 | 7.20965 | 9.19357 | 11.41933 |
| $16p^2$ | 0.32706 | 0.80563 | 1.48776 | 2.38200 | 3.48857 | 4.80759 | 6.33910 | 8.08313 | 10.03971 |
| $17p^2$ | 0.29008 | 0.71424 | 1.31875 | 2.11115 | 3.09165 | 4.26033 | 5.61723 | 7.16240 | 8.89585 |
| $18p^2$ | 0.25904 | 0.63757 | 1.17700 | 1.88402 | 2.75882 | 3.80148 | 5.01203 | 6.39051 | 7.93692 |
| $19p^2$ | 0.23273 | 0.57263 | 1.05694 | 1.69168 | 2.47700 | 3.41297 | 4.49963 | 5.73700 | 7.12510 |
| $20p^2$ | 0.21024 | 0.51712 | 0.95436 | 1.52736 | 2.23626 | 3.08112 | 4.06199 | 5.17886 | 6.43177 |

**Table 4.** Total energy ($-E$) for the ($nd^2$) $^1G^e$ ($n$ = 3 - 20) doubly excited states of helium-like systems ($Z$ = 2 - 10). The energies $E$ are in eV.

| $Z$ | 2 | 3 | 4 | 5 | 6 | 7 | 8 | 9 | 10 |
|---|---|---|---|---|---|---|---|---|---|
| $nd^2$ | $-E$ | $-E$ | $-E$ | $-E$ | $-E$ | $-E$ | $-E$ | $-E$ | $-E$ |
| $3d^2$ | 8.66987 | 21.84944 | 40.76532 | 65.70667 | 96.68358 | 133.70073 | 176.76056 | 225.86449 | 281.01340 |
| $4d^2$ | 4.92028 | 12.36512 | 23.04025 | 37.10534 | 54.56575 | 75.42399 | 99.68137 | 127.33865 | 158.39628 |
| $5d^2$ | 3.17227 | 7.95352 | 14.80410 | 23.82457 | 35.01823 | 48.38660 | 63.93048 | 81.65034 | 101.54646 |
| $6d^2$ | 2.21670 | 5.54666 | 10.31481 | 16.59001 | 24.37447 | 33.66919 | 44.47473 | 56.79139 | 70.61936 |
| $7d^2$ | 1.63727 | 4.08980 | 7.59970 | 12.21693 | 17.94306 | 24.77881 | 32.72457 | 41.78056 | 51.94691 |
| $8d^2$ | 1.25931 | 3.14100 | 5.83274 | 9.37235 | 13.76099 | 18.99922 | 25.08731 | 32.02543 | 39.81368 |
| $9d^2$ | 0.99901 | 2.48852 | 4.61839 | 7.41825 | 10.88897 | 15.03099 | 19.84451 | 25.32967 | 31.48654 |
| $10d^2$ | 0.81206 | 2.02051 | 3.74790 | 6.01801 | 8.83154 | 12.18883 | 16.09005 | 20.53529 | 25.52462 |
| $11d^2$ | 0.67323 | 1.67337 | 3.10257 | 4.98032 | 7.30720 | 10.08347 | 13.30928 | 16.98469 | 21.10977 |
| $12d^2$ | 0.56728 | 1.40875 | 2.61088 | 4.18993 | 6.14639 | 8.48047 | 11.19228 | 14.28189 | 17.74935 |
| $13d^2$ | 0.48458 | 1.20239 | 2.22761 | 3.57401 | 5.24199 | 7.23174 | 9.54334 | 12.17686 | 15.13234 |
| $14d^2$ | 0.41878 | 1.03834 | 1.92304 | 3.08470 | 4.52364 | 6.24003 | 8.23394 | 10.50542 | 13.05450 |
| $15d^2$ | 0.36555 | 0.90576 | 1.67701 | 2.68951 | 3.94357 | 5.43931 | 7.17681 | 9.15611 | 11.37723 |
| $16d^2$ | 0.32189 | 0.79709 | 1.47539 | 2.36575 | 3.46841 | 4.78350 | 6.31106 | 8.05115 | 10.00378 |
| $17d^2$ | 0.28563 | 0.70689 | 1.30810 | 2.09717 | 3.07430 | 4.23960 | 5.59311 | 7.13489 | 8.86493 |
| $18d^2$ | 0.25518 | 0.63119 | 1.16777 | 1.87190 | 2.74378 | 3.78351 | 4.99112 | 6.36666 | 7.91012 |
| $19d^2$ | 0.22936 | 0.56706 | 1.04888 | 1.68110 | 2.46388 | 3.39729 | 4.48139 | 5.71620 | 7.10173 |
| $20d^2$ | 0.20728 | 0.51223 | 0.94729 | 1.51807 | 2.22474 | 3.06737 | 4.04598 | 5.16061 | 6.41126 |

**Table 5.** Total energy ($-E$) for the ($nf^2$) $^1I^e$ ($n$ = 4 - 20) doubly excited states of helium-like systems ($Z$ = 2 - 10). The energies $E$ are in eV.

| $Z$ | 2 | 3 | 4 | 5 | 6 | 7 | 8 | 9 | 10 |
|---|---|---|---|---|---|---|---|---|---|
| $nf^2$ | $-E$ | $-E$ | $-E$ | $-E$ | $-E$ | $-E$ | $-E$ | $-E$ | $-E$ |
| $4f^2$ | 4.88462 | 12.30381 | 22.95032 | 36.98626 | 54.41728 | 75.24595 | 99.47366 | 127.10120 | 158.12904 |
| $5f^2$ | 3.14469 | 7.90632 | 14.73497 | 23.73314 | 34.90428 | 48.25001 | 63.77119 | 81.46828 | 101.34160 |
| $6f^2$ | 2.19522 | 5.51005 | 10.26127 | 16.51924 | 24.28632 | 33.56358 | 44.35159 | 56.65069 | 70.46106 |
| $7f^2$ | 1.62030 | 4.06098 | 7.55759 | 12.16131 | 17.87382 | 24.69587 | 32.62789 | 41.67010 | 51.82266 |
| $8f^2$ | 1.24569 | 3.11795 | 5.79909 | 9.32793 | 13.70571 | 18.93303 | 25.01016 | 31.93731 | 39.71456 |

**Continued**

| | | | | | | | | | |
|---|---|---|---|---|---|---|---|---|---|
| $9f^2$ | 0.98792 | 2.46980 | 4.59110 | 7.38224 | 10.84417 | 14.97736 | 19.78201 | 25.25829 | 31.40626 |
| $10f^2$ | 0.80291 | 2.00511 | 3.72546 | 5.98842 | 8.79474 | 12.14478 | 16.03872 | 20.47668 | 25.45872 |
| $11f^2$ | 0.66560 | 1.66055 | 3.08390 | 4.95571 | 7.27660 | 10.04685 | 13.26662 | 16.93598 | 21.05500 |
| $12f^2$ | 0.56085 | 1.39796 | 2.59518 | 4.16925 | 6.12067 | 8.44969 | 11.15644 | 14.24097 | 17.70334 |
| $13f^2$ | 0.47911 | 1.19322 | 2.21428 | 3.55645 | 5.22017 | 7.20563 | 9.51294 | 12.14215 | 15.09331 |
| $14f^2$ | 0.41408 | 1.03048 | 1.91163 | 3.06967 | 4.50496 | 6.21768 | 8.20792 | 10.47572 | 13.02111 |
| $15f^2$ | 0.36150 | 0.89898 | 1.66715 | 2.67654 | 3.92746 | 5.42004 | 7.15437 | 9.13050 | 11.34844 |
| $16f^2$ | 0.31836 | 0.79119 | 1.46683 | 2.35448 | 3.45441 | 4.76676 | 6.29158 | 8.02891 | 9.97877 |
| $17f^2$ | 0.28253 | 0.70173 | 1.30062 | 2.08731 | 3.06206 | 4.22496 | 5.57608 | 7.11544 | 8.84307 |
| $18f^2$ | 0.25245 | 0.62665 | 1.16118 | 1.86323 | 2.73302 | 3.77064 | 4.97615 | 6.34956 | 7.89091 |
| $19f^2$ | 0.22694 | 0.56304 | 1.04306 | 1.67344 | 2.45436 | 3.38592 | 4.46815 | 5.70109 | 7.08475 |
| $20f^2$ | 0.20513 | 0.50866 | 0.94211 | 1.51127 | 2.21629 | 3.05726 | 4.03422 | 5.14719 | 6.39618 |

**Table 6.** Total energy ($-E$) for the ($ng^2$) $^1K^e$ ($n$ = 5 - 20) doubly excited states of helium-like systems ($Z$ = 2 - 10). The energies $E$ are in eV.

| $Z$ | 2 | 3 | 4 | 5 | 6 | 7 | 8 | 9 | 10 |
|---|---|---|---|---|---|---|---|---|---|
| $ng^2$ | $-E$ | $-E$ | $-E$ | $-E$ | $-E$ | $-E$ | $-E$ | $-E$ | $-E$ |
| $5g^2$ | 3.12860 | 7.87865 | 14.69439 | 23.67940 | 34.83728 | 48.16967 | 63.67745 | 81.36112 | 101.22099 |
| $6g^2$ | 2.18229 | 5.48788 | 10.22878 | 16.47627 | 24.23275 | 33.49937 | 44.27669 | 56.56508 | 70.36472 |
| $7g^2$ | 1.60979 | 4.04301 | 7.53129 | 12.12654 | 17.83049 | 24.64395 | 32.56734 | 41.60091 | 51.74480 |
| $8g^2$ | 1.23704 | 3.10320 | 5.77753 | 9.29943 | 13.67022 | 18.89050 | 24.96058 | 31.88065 | 39.65082 |
| $9g^2$ | 0.98071 | 2.45755 | 4.57320 | 7.35860 | 10.81474 | 14.94209 | 19.74091 | 25.21133 | 31.35343 |
| $10g^2$ | 0.79685 | 1.99482 | 3.71044 | 5.96858 | 8.77005 | 12.11521 | 16.00426 | 20.43731 | 25.41443 |
| $11g^2$ | 0.66044 | 1.65182 | 3.07117 | 4.93891 | 7.25569 | 10.02181 | 13.23743 | 16.90264 | 21.01750 |
| $12g^2$ | 0.55643 | 1.39049 | 2.58428 | 4.15487 | 6.10279 | 8.42829 | 11.13149 | 14.21248 | 17.67130 |
| $13g^2$ | 0.47529 | 1.18677 | 2.20488 | 3.54406 | 5.20475 | 7.18718 | 9.49144 | 12.11760 | 15.06570 |
| $14g^2$ | 0.41075 | 1.02488 | 1.90347 | 3.05891 | 4.49158 | 6.20167 | 8.18926 | 10.45441 | 12.99715 |
| $15g^2$ | 0.35858 | 0.89408 | 1.66002 | 2.66713 | 3.91576 | 5.40604 | 7.13807 | 9.11188 | 11.32750 |
| $16g^2$ | 0.31579 | 0.78687 | 1.46055 | 2.34621 | 3.44413 | 4.75445 | 6.27724 | 8.01254 | 9.96037 |
| $17g^2$ | 0.28026 | 0.69791 | 1.29506 | 2.08000 | 3.05297 | 4.21408 | 5.56341 | 7.10097 | 8.82681 |
| $18g^2$ | 0.25042 | 0.62326 | 1.15624 | 1.85673 | 2.72494 | 3.76097 | 4.96489 | 6.33671 | 7.87646 |
| $19g^2$ | 0.22513 | 0.56001 | 1.03865 | 1.66763 | 2.44715 | 3.37729 | 4.45810 | 5.68962 | 7.07185 |
| $20g^2$ | 0.20350 | 0.50594 | 0.93816 | 1.50606 | 2.20982 | 3.04952 | 4.02521 | 5.13690 | 6.38462 |

**Table 7.** Total energy ($-E$) for the ($nh^2$) $^1M^e$ ($n$ = 6 - 20) doubly excited states of helium-like systems ($Z$ = 2 - 10). The energies $E$ are in eV.

| $Z$ | 2 | 3 | 4 | 5 | 6 | 7 | 8 | 9 | 10 |
|---|---|---|---|---|---|---|---|---|---|
| $ng^2$ | $-E$ | $-E$ | $-E$ | $-E$ | $-E$ | $-E$ | $-E$ | $-E$ | $-E$ |
| $6h^2$ | 2.17365 | 5.47302 | 10.20698 | 16.44740 | 24.19675 | 33.45620 | 44.22633 | 56.50750 | 70.29992 |
| $7h^2$ | 1.60263 | 4.03075 | 7.51331 | 12.10275 | 17.80083 | 24.60839 | 32.52586 | 41.55350 | 51.69145 |

**Continued**

| | | | | | | | | | |
|---|---|---|---|---|---|---|---|---|---|
| $8h^2$ | 1.23105 | 3.09296 | 5.76253 | 9.27960 | 13.64551 | 18.86088 | 24.92603 | 31.84117 | 39.60639 |
| $9h^2$ | 0.97565 | 2.44891 | 4.56056 | 7.34189 | 10.79392 | 14.91715 | 19.71182 | 25.17808 | 31.31603 |
| $10h^2$ | 0.79253 | 1.98746 | 3.69968 | 5.95436 | 8.75234 | 12.09399 | 15.97952 | 20.40904 | 25.38263 |
| $11h^2$ | 0.65672 | 1.64550 | 3.06193 | 4.92670 | 7.24049 | 10.00360 | 13.21620 | 16.87839 | 20.99022 |
| $12h^2$ | 0.55320 | 1.38501 | 2.57628 | 4.14431 | 6.08964 | 8.41253 | 11.11313 | 14.19150 | 17.64770 |
| $13h^2$ | 0.47247 | 1.18199 | 2.19790 | 3.53485 | 5.19329 | 7.17345 | 9.47544 | 12.09932 | 15.04514 |
| $14h^2$ | 0.40827 | 1.02068 | 1.89734 | 3.05082 | 4.48152 | 6.18962 | 8.17522 | 10.43837 | 12.97912 |
| $15h^2$ | 0.35638 | 0.89037 | 1.65461 | 2.66000 | 3.90688 | 5.39542 | 7.12568 | 9.09773 | 11.31160 |
| $16h^2$ | 0.31384 | 0.78358 | 1.45575 | 2.33987 | 3.43625 | 4.74502 | 6.26625 | 7.99999 | 9.94626 |
| $17h^2$ | 0.27851 | 0.69497 | 1.29078 | 2.07435 | 3.04594 | 4.20567 | 5.55361 | 7.08979 | 8.81423 |
| $18h^2$ | 0.24886 | 0.62062 | 1.15241 | 1.85167 | 2.71865 | 3.75344 | 4.95611 | 6.32669 | 7.86519 |
| $19h^2$ | 0.22372 | 0.55763 | 1.03520 | 1.66308 | 2.44149 | 3.37052 | 4.45021 | 5.68061 | 7.06172 |
| $20h^2$ | 0.20222 | 0.50380 | 0.93504 | 1.50195 | 2.20471 | 3.04341 | 4.01809 | 5.12877 | 6.37547 |

**Table 8.** Comparison of the present calculations on total energies of the doubly ($ns^2$) $^1S^e$ ($n$ = 2 - 7) excited states of helium-like systems ($Z$ = 2 - 10) with available literature values. All results are expressed in eV.

| States $ns^2\ ^1S^e$ | $Z$ | 2 | 3 | 4 | 5 | 6 | 7 | 8 | 9 | 10 |
|---|---|---|---|---|---|---|---|---|---|---|
| $2s^2\ ^1S^e$ | $-E^p$ | 21.45940 | 52.42276 | 96.46002 | 154.07753 | 225.28724 | 310.09472 | 408.50290 | 520.51348 | 646.12749 |
| | $-E^a$ | 21.19004 | 51.75672 | 95.92923 | 153.70728 | 225.09117 | 310.08075 | 408.67588 | 520.87683 | 646.68334 |
| | $-E^b$ | 21.16692 | 51.86067 | 96.15032 | 154.04035 | 225.53336 | 310.63042 | 409.33154 | 521.63766 | 647.54894 |
| | $-E^c$ | 21.19388 | 51.75719 | 95.92188 | 153.72003 | 225.09205 | 310.08931 | 408.67561 | 520.87758 | 646.68514 |
| | $-E^d$ | 21.16678 | 51.86054 | 96.15046 | 154.03995 | 225.53363 | 310.62879 | 409.33289 | 521.62923 | 647.54853 |
| | $-E^e$ | 21.16460 | 51.86312 | 96.14556 | 154.03886 | 225.53540 | 310.62852 | 409.33358 | 521.63576 | 647.54377 |
| | $-E^k$ | 21.19000 | 52.00000 | 96.43000 | 154.45000 | 226.09000 | 311.32000 | 410.17000 | 522.62000 | 648.67000 |
| $3s^2\ ^1S^e$ | $-E^p$ | 9.53751 | 23.29900 | 42.87112 | 68.47890 | 100.12766 | 137.81987 | 181.55684 | 231.33932 | 287.16777 |
| | $-E^a$ | 9.64562 | 23.38097 | 43.16324 | 68.99254 | 100.86877 | 138.79205 | 182.76224 | 232.77934 | 288.84349 |
| | $-E^c$ | 9.64065 | 23.48066 | 43.29425 | 69.06061 | 100.76559 | 138.39575 | 181.93676 | 231.37273 | 286.68564 |
| | $-E^f$ | 9.62031 | 23.40586 | 43.23344 | 69.10874 | 101.02769 | 138.99573 | 183.00878 | 233.07091 | 289.17806 |
| | $-E^g$ | 9.41772 | 23.00300 | 42.63519 | 68.31431 | 100.04059 | 137.81366 | 181.63365 | 231.50082 | 287.41489 |
| | $-E^d$ | 9.62017 | 23.40586 | 43.23316 | 69.10847 | 101.02837 | 138.99627 | 183.00918 | 233.06996 | 289.17887 |
| | $-E^e$ | 9.62466 | 23.40178 | 43.22527 | 69.10738 | 101.02224 | 138.98212 | 182.99653 | 233.05866 | 289.17125 |
| | $-E^h$ | 9.58385 | 22.83852 | 42.25657 | 67.85978 | | | | | |
| | $-E^k$ | 9.42000 | 23.11000 | 42.86000 | 68.65000 | 100.48000 | 138.37000 | 182.30000 | 232.27000 | 288.30000 |
| $4s^2\ ^1S^e$ | $-E^p$ | 5.36485 | 13.10569 | 24.11501 | 38.51938 | 56.32181 | 77.52368 | 102.12572 | 130.12837 | 161.53187 |
| | $-E^a$ | 5.49139 | 13.25971 | 24.42944 | 39.00059 | 56.97332 | 78.34732 | 103.12276 | 131.29961 | 162.87803 |
| | $-E^j$ | 5.46963 | 13.25848 | 24.45079 | 39.03978 | 57.02243 | 78.41957 | 103.20357 | 131.40206 | 162.99422 |
| | $-E^g$ | 5.29751 | 12.93915 | 23.98235 | 38.42684 | 56.27276 | 77.52023 | 102.16899 | 130.21932 | 161.67093 |

**Continued**

| | | | | | | | | | | |
|---|---|---|---|---|---|---|---|---|---|---|
| | $-E^{j}$ | 5.35000 | 13.18000 | 24.49000 | 38.08000 | 57.95000 | 78.43000 | 103.18000 | 130.42000 | 163.20000 |
| | $-E^{k}$ | 5.30000 | 13.00000 | 24.11000 | 38.61000 | 56.52000 | 77.83000 | 102.54000 | 130.65000 | 162.17000 |
| | $-E^{p}$ | 3.43350 | 8.38764 | 15.43360 | 24.65241 | 36.04596 | 49.61515 | 65.36046 | 83.28216 | 103.38040 |
| $5s^2\ ^1S^e$ | $-E^{a}$ | 3.53993 | 8.52792 | 15.69281 | 25.03462 | 36.55320 | 50.24884 | 66.12138 | 84.17083 | 104.39706 |
| | $-E^{g}$ | 3.39040 | 8.28111 | 15.34872 | 24.59325 | 36.01455 | 49.61291 | 65.38816 | 83.34034 | 103.46942 |
| | $-E^{j}$ | 3.22000 | 8.15000 | 15.33000 | 24.28000 | 36.45000 | 49.69000 | 65.29000 | 83.20000 | 103.67000 |
| | $-E^{k}$ | 3.39000 | 8.32000 | 15.43000 | 24.71000 | 36.17000 | 49.81000 | 65.63000 | 83.62000 | 103.79000 |
| | $-E^{p}$ | 2.38438 | 5.82475 | 10.71778 | 17.11973 | 25.03192 | 34.45497 | 45.38921 | 57.83483 | 71.79194 |
| $6s^2\ ^1S^e$ | $-E^{a}$ | 2.47025 | 5.94161 | 10.92483 | 17.41965 | 25.42606 | 34.94460 | 45.97447 | 58.51647 | 72.57007 |
| | $-E^{k}$ | 2.35000 | 5.78000 | 10.71000 | 17.16000 | 25.12000 | 34.59000 | 45.57000 | 58.07000 | 72.07000 |
| | $-E^{p}$ | 1.75179 | 4.27941 | 7.87429 | 12.57776 | 18.39080 | 25.31385 | 33.34718 | 42.49090 | 52.74510 |
| | $-E^{j}$ | 1.72000 | 4.27000 | 7.82000 | 12.63000 | 18.46000 | 25.39000 | 33.44000 | 42.58000 | 52.83000 |
| $7s^2\ ^1S^e$ | $-E^{k}$ | 1.73000 | 4.24000 | 7.87000 | 12.61000 | 18.46000 | 25.41000 | 33.48000 | 42.66000 | 52.95000 |
| | $-E^{a}$ | 1.821259 | 4.37559 | 8.04042 | 12.81602 | 18.70239 | 25.69953 | 33.80717 | 43.02557 | 53.35447 |

[p]Present work, values calculated from Equation (22), [a]sakho [32], [b]Ho [33], [c]Sow *et al.* [36], [d]Gning *et al.* [37], [e]Konte *et al.* [38], [f]Ho [34], [g]Sakho *et al.* [24], [h]Ray *et al.* [23], [i]Ho [35], [j]Diouf *et al.* [39], [k]Sakho [40].

unit nuclear charge method of Sakho *et al.* [24] [32], with the results of the complex rotation of Ho [33] [34] [35], with the results of Sow *et al.* [36] who used the variational method of the SCUNC formalism, with the complex rotation values of Gning *et al.* [37], with the Konté *et al.* [38] data, with the data from the time-dependent variation perturbation theory of Ray *et al.* [23], with the results of Diouf *et al.* [39] and finally with the data from the modified slater theory of Sakho [40]. The observation of our results shown in this table shows that our present calculations are generally in good agreement with the results of the cited authors up to $Z = 10$.

In **Table 9**, we compare our calculations for $(np^2)\ ^1D^e$ states with the results of the calculations of Badiane *et al.* [41], with the data of Sakho [24] [32] [40], with the results of the complex rotation calculations (CRC) of Ho and Bhatia [13], with the values of Ivanov and Safronova [17], with the results of the variational method calculations of Hylleraas de Biaye *et al.* [16] and finally with those obtained by Roy *et al.* [18] who applied the functional density theory (FDT). Here, the agreements between the calculations are considered good. **Table 10** compares our results for the $(nd^2)\ ^1G^e$ ($n$ = 3 - 10) states with those obtained by Badiane *et al.* [41], sakho [32] [40], Bachau *et al.* [19], Biaye *et al.* [16], Ivanov and Safronova [17], Diouf *et al.* [39], Ray *et al.* [23] and Roy *et al.* [18]. As regards the $(nd^2)\ ^1G^e$-levels, comparison shows also a good agreement up to $Z = 10$. **Table 11** shows the results of our present calculations of the total energies of the doubly excited $(nf^2)\ ^1I^e$ ($n$ = 4 - 10) states of helium-like systems up to $Z = 10$, which we compare with those obtained by Biaye *et al.* [16], Badiane *et al.* [41], Sakho *et al.* [32] [40], Ho [20], Diouf *et al.* [39], and Sow *et al.* [36]. A comparative

**Table 9.** Comparison of the present calculations on total energies of the doubly ($np^2$) $^1D^e$ ($n$ = 2 - 5) excited states of helium-like systems ($Z$ = 2 - 10) with available literature values. All results are expressed in eV.

| States $np^2\ ^1D^e$ | $Z$ | 2 | 3 | 4 | 5 | 6 | 7 | 8 | 9 | 10 |
|---|---|---|---|---|---|---|---|---|---|---|
| | $-E^p$ | 19.40691 | 48.98779 | 91.46705 | 147.50214 | 217.11646 | 300.32082 | 397.12093 | 507.52007 | 631.52025 |
| | $-E^a$ | 19.12145 | 48.19274 | 90.86974 | 147.15243 | 217.04218 | 300.53626 | 397.63604 | 508.34153 | 632.65271 |
| | $-E^b$ | 19.12008 | 48.19002 | 90.86565 | 147.14835 | 217.03537 | 300.52809 | 397.62652 | 508.33201 | 632.64183 |
| | $-E^c$ | 19.10104 | 48.18049 | 90.81667 | 147.03678 | 216.85169 | 300.26551 | 397.28229 | 507.90071 | 632.12481 |
| $2p^2\ ^1D^e$ | $-E^d$ | 19.41533 | 48.39138 | 90.97314 | 147.16059 | 216.95238 | 300.35123 | 397.35577 | 507.96601 | 632.18195 |
| | $-E^e$ | 19.18403 | 48.39138 | 91.14321 | 147.47352 | 217.39320 | 300.90769 | 398.02245 | 508.73746 | 633.05408 |
| | $-E^f$ | | 47.78049 | 90.54592 | 146.90888 | | | | | |
| | $-E^g$ | 19.12000 | 48.19000 | 90.87000 | 147.15000 | 217.03000 | 300.53000 | 397.63000 | 508.33000 | 632.64000 |
| | $-E^h$ | 19.12000 | 48.73000 | 91.95000 | 148.77000 | 219.20000 | 303.24000 | 400.88000 | 512.13000 | 636.9800 |
| | $-E^p$ | 8.78089 | 22.04020 | 41.04506 | 66.07698 | 97.14529 | 134.25433 | 177.40638 | 226.60274 | 281.84424 |
| | $-E^a$ | 8.98656 | 22.56777 | 42.23345 | 67.96182 | 99.74201 | 137.57401 | 181.45511 | 231.38394 | 287.36187 |
| | $-E^b$ | 9.19065 | 22.62219 | 42.10011 | 67.62440 | 99.19642 | 136.81482 | 180.48094 | 230.19344 | 285.95368 |
| | $-E^c$ | 9.33759 | 22.91608 | 42.54502 | 68.22033 | 99.94474 | 137.71687 | 181.53675 | 231.40299 | 287.31561 |
| $3p^2\ ^1D^e$ | $-E^d$ | 8.98929 | 22.11198 | 41.28241 | 66.49785 | 97.76238 | 135.07193 | 178.43056 | 227.83422 | 283.28559 |
| | $-E^e$ | 8.66955 | 21.80585 | 41.03206 | 66.37676 | 97.83993 | 135.44200 | 179.18160 | 229.06009 | 285.07883 |
| | $-E^f$ | | 21.82626 | 41.09465 | 66.40669 | | | | | |
| | $-E^g$ | 8.50000 | 21.42000 | 40.38000 | 65.40000 | 96.46000 | 133.57000 | 176.72000 | 225.92000 | 281.17000 |
| | $-E^h$ | 8.50000 | 21.66000 | 40.87000 | 66.12000 | 97.42000 | 134.77000 | 178.17000 | 227.61000 | 283.10000 |
| | $-E^p$ | 5.00135 | 12.50334 | 23.24244 | 37.37258 | 54.89863 | 75.82286 | 100.14645 | 127.87008 | 158.99418 |
| | $-E^a$ | 5.11302 | 12.82881 | 23.97187 | 38.52453 | 56.48269 | 77.84364 | 102.61009 | 130.77661 | 162.34727 |
| | $-E^b$ | 5.383774 | 13.08187 | 24.18141 | 38.68236 | 56.58609 | 77.88989 | 102.59512 | 130.70314 | 162.21121 |
| $4p^2\ ^1D^e$ | $-E^c$ | | 13.12678 | 24.26168 | 38.79937 | 56.73984 | 78.08038 | 102.82642 | 130.97117 | 162.51598 |
| | $-E^e$ | 4.893969 | 12.23560 | 22.93921 | 37.02246 | 54.49354 | 75.36060 | 99.629084 | 127.30035 | 158.37441 |
| | $-E^f$ | | 12.37982 | 23.26166 | 37.543563 | | | | | |
| | $-E^g$ | 4.78000 | 12.05000 | 22.72000 | 36.79000 | 54.26000 | 75.13000 | 99.41000 | 127.08000 | 158.16000 |
| | $-E^h$ | 4.78000 | 12.18000 | 22.99000 | 37.19000 | 54.80000 | 75.81000 | 100.22000 | 128.03000 | 159.24000 |
| | $-E^p$ | 3.23051 | 8.05224 | 14.94822 | 24.01485 | 35.25507 | 48.67024 | 64.26108 | 82.02799 | 101.97124 |
| | $-E^a$ | 3.28849 | 8.24777 | 15.40029 | 24.73652 | 36.25238 | 49.94652 | 65.81892 | 83.86824 | 104.09583 |
| $5p^2\ ^1D^e$ | $-E^b$ | 3.53068 | 8.51309 | 15.67240 | 25.00863 | 36.52178 | 50.21047 | 66.07743 | 84.12131 | 104.34209 |
| | $-E^f$ | | 7.95117 | 14.92953 | 24.08344 | | | | | |
| | $-E^g$ | | 7.71000 | 14.54000 | 23.54000 | 34.72000 | 48.08000 | 63.62000 | 81.33000 | 101.22000 |
| | $-E^h$ | 3.06000 | 7.80000 | 14.71000 | 23.80000 | 35.07000 | 48.52000 | 64.14000 | 81.94000 | 101.92000 |

[p]Present work, values calculated from Equation (22), [a]Badiane *et al.* [41], [b]Sakho *et al.* [32], [c]Ho and Bhatia [13], [d]Ivanov and Safronova [17], [e]Biaye *et al.* [16], [f]Roy *et al.* [18], [g]Sakho *et al.* [24], [h]Sakho [40].

**Table 10.** Comparison of the present calculations on total energies of the doubly $(nd^{\ell})\ ^1G^e$ ($n$ = 3 - 10) excited states of helium-like systems ($Z$ = 2 - 10) with available literature values. All results are expressed in eV.

| States $nd^{\ell}\ ^1G^e$ | $Z$ | 2 | 3 | 4 | 5 | 6 | 7 | 8 | 9 | 10 |
|---|---|---|---|---|---|---|---|---|---|---|
| | $-E^p$ | 8.66987 | 21.84944 | 40.76532 | 65.70667 | 96.68358 | 133.70073 | 176.76056 | 225.86449 | 281.01340 |
| | $-E^a$ | 8.31716 | 20.87794 | 39.56401 | 64.34271 | 95.23988 | 132.11133 | 175.08356 | 224.11306 | 279.19300 |
| | $-E^b$ | 8.30492 | 21.07114 | 39.88374 | 64.74271 | 95.64942 | 132.60385 | 175.60466 | 224.65184 | 279.74676 |
| | $-E^c$ | 8.38927 | 21.14053 | 39.89191 | 64.68148 | 95.48479 | 132.35623 | 175.26860 | 224.22190 | 279.18892 |
| $3d^{\ell}\ ^1G^e$ | $-E^d$ | 8.58383 | 21.54734 | 40.49464 | 65.45157 | 96.431745 | 133.44332 | 176.491754 | 225.57839 | 280.70732 |
| | $-E^e$ | 8.57703 | 21.24938 | 39.97082 | 64.73727 | 95.551456 | 132.41065 | 175.321664 | 224.27632 | 279.27872 |
| | $-E^f$ | 8.50000 | 21.73000 | 41.06000 | 65.52000 | 96.77000 | 134.03000 | 178.740000 | 227.96000 | 282.92000 |
| | $-E^g$ | 8.48996 | 21.15414 | 39.84021 | 64.56448 | | | | | |
| | $-E^i$ | 8.35000 | 21.43000 | 40.55000 | 65.72000 | 96.94000 | 134.21000 | 177.52000 | 226.87000 | 283.28000 |
| | $-E^p$ | 4.92028 | 12.36512 | 23.04025 | 37.10534 | 54.56575 | 75.42399 | 99.68137 | 127.33865 | 158.39628 |
| | $-E^a$ | 4.78104 | 12.03016 | 22.74328 | 36.89048 | 54.45816 | 75.43951 | 99.82773 | 127.62417 | 158.82476 |
| $4d^{\ell}\ ^1G^e$ | $-E^b$ | 4.85315 | 12.17709 | 22.90383 | 37.03063 | 54.55884 | 75.48985 | 99.82092 | 127.55342 | 158.68869 |
| | $-E^d$ | 4.89397 | 12.23560 | 22.93785 | 37.02110 | 54.49218 | 75.35787 | 99.62500 | 127.29354 | 158.77713 |
| | $-E^g$ | 5.31166 | 12.51724 | 23.33105 | 37.55445 | | | | | |
| | $-E^i$ | 4.70000 | 12.05000 | 22.81000 | 36.97000 | 54.53000 | 75.49000 | 99.85000 | 127.62000 | 158.78000 |
| | $-E^p$ | 3.17227 | 7.95352 | 14.80410 | 23.82457 | 35.01823 | 48.38660 | 63.93048 | 81.65034 | 101.54646 |
| | $-E^a$ | 3.09394 | 7.79198 | 14.71456 | 23.83718 | 35.14896 | 48.64581 | 64.32502 | 82.18386 | 102.22233 |
| $5d^{\ell}\ ^1G^e$ | $-E^b$ | 3.17965 | 7.92259 | 14.84245 | 23.93786 | 35.21155 | 48.66214 | 64.28964 | 82.09406 | 102.07538 |
| | $-E^h$ | 3.06672 | 7.81375 | 14.73769 | 23.83854 | | | | | |
| | $-E^f$ | 3.04000 | 7.59000 | 14.57000 | 23.600000 | 34.80000 | 48.31000 | 63.87000 | 81.59000 | 101.68000 |
| | $-E^i$ | 3.01000 | 7.71000 | 14.60000 | 23.66000 | 34.90000 | 48.31000 | 63.91000 | 81.67000 | 101.62000 |
| | $-E^p$ | 2.21670 | 5.54666 | 10.31481 | 16.59001 | 24.37447 | 33.66919 | 44.47473 | 56.79139 | 70.61936 |
| $6d^{\ell}\ ^1G^e$ | $-E^a$ | 2.16331 | 5.45044 | 10.28591 | 16.64929 | 24.53379 | 33.93533 | 44.85254 | 57.28271 | 71.22855 |
| | $-E^f$ | 2.04000 | 5.34000 | 10.12000 | | 24.28000 | 33.51000 | 44.31000 | 56.74000 | 70.50000 |
| | $-E^h$ | | 5.45997 | 10.28182 | 16.61392 | | | | | |
| | $-E^i$ | 2.09000 | 5.36000 | 10.14000 | 16.43000 | 24.23000 | 33.55000 | 44.38000 | 56.72000 | 70.57000 |
| | $-E^p$ | 1.63727 | 4.08980 | 7.59970 | 12.21693 | 17.94306 | 24.77881 | 32.72457 | 41.78056 | 51.94691 |
| $7d^{\ell}\ ^1G^e$ | $-E^a$ | 1.59595 | 4.02456 | 7.58926 | 12.27914 | 18.08469 | 25.00727 | 33.04279 | 42.18991 | 52.44861 |
| | $-E^f$ | 1.50000 | 3.93000 | 7.44000 | 12.04000 | 17.87000 | 24.57000 | 32.64000 | 41.68000 | 51.83000 |
| | $-E^h$ | | 3.87490 | 7.57293 | 12.23152 | | | | | |
| | $-E^i$ | 1.53000 | 3.94000 | 7.45000 | 12.07000 | 17.80000 | 24.65000 | 32.60000 | 41.67000 | 51.85000 |
| $8d^{21}G^e$ | $-E^p$ | 1.25931 | 3..14100 | 5.83274 | 9.37235 | 13.76099 | 18.99922 | 25.08731 | 32.02543 | 39.81368 |
| | $-E^a$ | 1.22587 | 3.09257 | 5.82867 | 9.42738 | 13.88052 | 19.18810 | 25.34740 | 32.35841 | 40.22114 |
| $9d^{\ell}\ ^1G^e$ | $-E^p$ | 0.99901 | 2.48852 | 4.61839 | 7.41825 | 10.88897 | 15.03099 | 19,84451 | 25.32967 | 31.48654 |
| | $-E^a$ | 0.97145 | 2.44902 | 4.61641 | 7.46408 | 10.98659 | 15.18531 | 20.05614 | 25.60046 | 31.81826 |
| $10d^{\ell}\ ^1G^e$ | $-E^p$ | 0.81206 | 2.02051 | 3.74790 | 6.01801 | 8.83154 | 12.18883 | 16.09005 | 20.53529 | 25.52462 |
| | $-E^a$ | 0.78777 | 1.98779 | 3.74565 | 6.05589 | 8.91173 | 12.31587 | 16.26424 | 20.75820 | 25.79638 |

[p]Present work, values calculated from Equation (22), [a]Badiane *et al.* [41], [b]Sakho *et al.* [32], [c]Bachau *et al.* [19], [d]Biaye *et al.* [16], [e]Ivanov and Safronova [17], [f]Diouf *et al.* [39], [g]Ray *et al.* [23], [h]Roy *et al.* [18], [i]Sakho [40].

**Table 11.** Comparison of the present calculations on total energies of the doubly ($nf^2$) $^1I^e$ ($n$ = 4 - 10) excited states of helium-like systems ($Z$ = 2 - 10) with available literature values. All results are expressed in eV.

| States $nf^2\ ^1I^e$ | $Z$ | 2 | 3 | 4 | 5 | 6 | 7 | 8 | 9 | 10 |
|---|---|---|---|---|---|---|---|---|---|---|
| | $-E^p$ | 4.88462 | 12.30381 | 22.95032 | 36.98626 | 54.41728 | 75.24595 | 99.47366 | 127.10120 | 158.12904 |
| | $-E^a$ | 4.88580 | 12.21518 | 22.89565 | 36.94625 | 54.37377 | 75.18776 | 99.38820 | 126.98190 | 157.96206 |
| | $-E^b$ | 4.34429 | 11.11585 | 21.49427 | 35.32989 | 52.59824 | 73.28841 | 97.39225 | 124.90568 | 155.82597 |
| $4f^2\ ^1I^e$ | $-E^c$ | 4.40552 | 11.35530 | 21.70788 | 35.46051 | 52.61456 | 73.17140 | 97.12829 | 124.48662 | 155.24772 |
| | $-E^d$ | 4.63682 | | | | | | | | |
| | $-E^e$ | 5.03000 | 12.12000 | 23.43000 | 37.54000 | 55.20000 | 76.38000 | 100.82000 | 128.65000 | 159.25000 |
| | $-E^f$ | 5.02139 | 12.43411 | 23.27892 | 37.66635 | 55.38959 | 76.43250 | 100.78073 | 128.41943 | 159.33212 |
| | $-E^g$ | 4.62000 | 11.92000 | 22.63000 | 36.74000 | 54.25000 | 75.16000 | 99.47000 | 127.18000 | 158.30000 |
| | $-E^p$ | 3.14469 | 7.90632 | 14.73497 | 23.73314 | 34.90428 | 48.25001 | 63.77119 | 81.46828 | 101.34160 |
| $5f^2\ ^1I^e$ | $-E^b$ | 2.80685 | 7.35524 | 14.16352 | 23.18954 | 34.41423 | 47.82944 | 63.42973 | 81.21236 | 101.17735 |
| | $-E^e$ | 2.93000 | 7.59000 | 14.41000 | 23.50000 | 34.69000 | 48.17000 | 63.55000 | 81.41000 | 100.29000 |
| | $-E^g$ | 2.95000 | 7.63000 | 14.48000 | 23.51000 | 34.72000 | 48.10000 | 63.66000 | 81.40000 | 101.31000 |
| | $-E^p$ | 2.19522 | 5.51005 | 10.26127 | 16.51924 | 24.28632 | 33.56358 | 44.35159 | 56.65069 | 70.46106 |
| $6f^2\ ^1I^e$ | $-E^b$ | 1.97691 | 5.18241 | 9.96072 | 16.27921 | 24.12697 | 33.49448 | 44.38040 | 56.78062 | 70.69789 |
| | $-E^e$ | 2.07000 | 5.28000 | 10.04000 | 16.22000 | 24.10000 | 33.41000 | 44.22000 | 56.54000 | 70.38000 |
| | $-E^g$ | 2.05000 | 5.30000 | 10.06000 | 26.33000 | 24.11000 | 33.40000 | 44.21000 | 56.53000 | 70.35000 |
| | $-E^p$ | 1.62030 | 4.06098 | 7.55759 | 12.16131 | 17.87382 | 24.69587 | 32.62789 | 41.67010 | 51.82266 |
| $7f^2\ ^1I^e$ | $-E^b$ | 1.46533 | 3.83817 | 7.36884 | 12.03287 | 17.81937 | 24.72289 | 32.74209 | 41.87423 | 52.11931 |
| | $-E^e$ | 1.50000 | 3.88000 | 7.36000 | 11.95000 | 17.75000 | 24.57000 | 32.48000 | 41.51000 | 51.63000 |
| | $-E^g$ | 1.51000 | 3.89000 | 7.39000 | 11.99000 | 17.71000 | 24.54000 | 32.48000 | 41.53000 | 51.69000 |
| $8f^2\ ^1I^e$ | $-E^p$ | 1.24569 | 3.11795 | 5.79909 | 9.32793 | 13.70571 | 18.93303 | 25.01016 | 31.93731 | 39.71456 |
| | $-E^b$ | 1.12791 | 2.95379 | 5.66677 | 9.20697 | 13.68732 | 18.98537 | 25.135152 | 32.13663 | 39.99120 |
| $9f^2\ ^1I^e$ | $-E^p$ | 0.98792 | 2.46980 | 4.59110 | 7.38224 | 10.84417 | 14.97736 | 19.78201 | 25.25829 | 31.40626 |
| | $-E^b$ | 0.89389 | 2.34289 | 4.49124 | 7.32666 | 10.84101 | 15.03156 | 19.89560 | 25.43447 | 31.64547 |
| $10f^2\ ^1I^e$ | $-E^p$ | 0.80291 | 2.00511 | 3.72546 | 5.98842 | 8.79474 | 12.14478 | 16.03872 | 20.47668 | 25.45872 |
| | $-E^b$ | 0.72654 | 1.90208 | 3.64632 | 5.94568 | 8.796078 | 12.19342 | 16.13771 | 20.62758 | 25.66169 |

[p]Present work, values calculated from Equation (22), [a]Biaye *et al.* [16], [b]Badiane *et al.* [41], [c]Sakho *et al.* [32], [d]Ho [20], [e]Diouf *et al.* [39], [f]Sow *et al.* [36]; [g]Sakho [40].

reading of the results mentioned in this table shows a good agreement between the present SCUNC results and the data found in the literature. For level $4f^2$, it should be noted that comparison with the results of Biaye *et al.* [16] indicates satisfactory agreement for $Z$ = 2 - 10.

In Table 12 and Table 13, we compare the results of our calculations of the total energies of the doubly excited states ($ng^2$) $^1K^e$ and ($nh^2$) $^1M^e$ with those of Sakho [40] and Diouf *et al.* [39]. The agreements between the calculations are seen to be generally good. It is worth mentioning that there are not many results

**Table 12.** Comparison of the present calculations on total energies of the doubly $(ng^2)\ ^1K^e$ ($n$ = 5 - 10) excited states of helium-like systems ($Z$ = 2 - 10) with available literature values. All results are expressed in eV.

| States $ng^2\ ^1K^e$ | $Z$ | 2 | 3 | 4 | 5 | 6 | 7 | 8 | 9 | 10 |
|---|---|---|---|---|---|---|---|---|---|---|
| | $-E^p$ | 3.12860 | 7.87865 | 14.69439 | 23.67940 | 34.83728 | 48.16967 | 63.67745 | 81.36112 | 101.22099 |
| $5g^2\ ^1K^e$ | $-E^a$ | 2.93000 | 7.59000 | 14.42000 | 23.44000 | 34.63000 | 47.99000 | 63.54000 | 81.26000 | 101.16000 |
| | $-E^b$ | 2.93000 | 7.59000 | 14.41000 | 23.41000 | 34.69000 | 47.90000 | 63.71000 | 81.24000 | 101.28000 |
| | $-E^p$ | 2.18229 | 5.48788 | 10.22878 | 16.47627 | 24.23275 | 33.49937 | 44.27669 | 56.56508 | 70.36472 |
| $6g^2\ ^1K^e$ | $-E^a$ | 2.03000 | 5.27000 | 10.02000 | 16.27000 | 24.05000 | 33.33000 | 44.12000 | 56.43000 | 70.25000 |
| | $-E^b$ | 2.04000 | 5.23000 | 10.04000 | 16.22000 | 24.10000 | 33.41000 | 44.22000 | 56.54000 | 70.38000 |
| | $-E^p$ | 1.60979 | 4.04301 | 7.53129 | 12.12654 | 17.83049 | 24.64395 | 32.56734 | 41.60091 | 51.74480 |
| $7g^2\ ^1K^e$ | $-E^a$ | 1.49000 | 3.87000 | 7.36000 | 11.96000 | 17.67000 | 24.49000 | 32.42000 | 41.46000 | 51.61000 |
| | $-E^b$ | 1.50000 | 3.88000 | 7.36000 | 11.95000 | 17.75000 | 24.43000 | 32.48000 | 41.51000 | 51.63000 |
| $8g^2\ ^1K^e$ | $-E^p$ | 1.23704 | 3.10320 | 5.77753 | 9.29943 | 13.67022 | 18.89050 | 24.96058 | 31.88065 | 39.65082 |
| $9g^2\ ^1K^e$ | $-E^p$ | 0.98071 | 2.45755 | 4.57320 | 7.35860 | 10.81474 | 14.94209 | 19.74091 | 25.21133 | 31.35343 |
| $10g^2\ ^1K^e$ | $-E^p$ | 0.79685 | 1.99482 | 3.71044 | 5.96858 | 8.77005 | 12.11521 | 16.00426 | 20.43731 | 25.41443 |

[p]Present work, values calculated from Equation (22), [a]sakho [40], [b]Diouf *et al.* [39].

**Table 13.** Comparison of the present calculations on total energies of the doubly $(nh^2)\ ^1M^e$ ($n$ = 6 - 10) excited states of helium-like systems ($Z$ = 2 - 10) with available literature values. All results are expressed in eV.

| States $nh^2\ ^1M^e$ | $Z$ | 2 | 3 | 4 | 5 | 6 | 7 | 8 | 9 | 10 |
|---|---|---|---|---|---|---|---|---|---|---|
| | $-E^p$ | 2.17365 | 5.47302 | 10.20698 | 16.44740 | 24.19675 | 33.45620 | 44.22633 | 56.50750 | 70.29992 |
| $6h^2\ ^1M^e$ | $-E^a$ | 2.02000 | 5.25000 | 9.99000 | 16.24000 | 24.01000 | 33.28000 | 44.07000 | 56.37000 | 70.18000 |
| | $-E^b$ | 2.04000 | 5.23000 | 9.97000 | 16.22000 | 24.10000 | 33.27000 | 44.06000 | 56.37000 | 70.18000 |
| | $-E^p$ | 1.60263 | 4.03075 | 7.51331 | 12.10275 | 17.80083 | 24.60839 | 32.52586 | 41.55350 | 51.69145 |
| $7h^2\ ^1M^e$ | $-E^a$ | 1.48000 | 3.86000 | 7.34000 | 11.93000 | 17.64000 | 24.45000 | 32.38000 | 41.42000 | 51.56000 |
| | $-E^b$ | 1.46000 | 3.82000 | 7.36000 | 11.95000 | 17.63000 | 24.43000 | 32.33000 | 41.51000 | 51.63000 |
| $8h^2\ ^1M^e$ | $-E^p$ | 1.23105 | 3.09296 | 5.76253 | 9.27960 | 13.64551 | 18.86088 | 24.92603 | 31.84117 | 39.60639 |
| $9h^2\ ^1M^e$ | $-E^p$ | 0.97565 | 2.44891 | 4.56056 | 7.34189 | 10.79392 | 14.91715 | 19.71182 | 25.17808 | 31.31603 |
| $10h^2\ ^1M^e$ | $-E^p$ | 0.79253 | 1.98746 | 3.69968 | 5.95436 | 8.75234 | 12.09399 | 15.97952 | 20.40904 | 25.38263 |

[p]Present work, values calculated from Equation (22), [a]Sakho [40], [b]Diouf *et al.* [39].

on the states and the only ones available to our knowledge are those of the authors Sakho [40] and Diouf *et al.* [39]. Moreover for $n > 7$ there are no results available so we think that the results cited up to $n = 20$ in this work may be interesting for future experimental and theoretical studies on these states.

In Tables 14-16 are quoted results for excitation energies of helium-like ions with $Z \leq 10$. Our excitation energies are calculated with respect to the accurate ground state energies of Frankowski and Pekeris [42]. Comparison indicates that our excitation energies for $(ns^2)\ ^1S^e$, $(np^2)\ ^1D^e$ and $(nd^2)\ ^1G^e$ levels agree well

**Table 14.** Comparison of the present calculations on the variationnal calculation of the excitation energies of the doubly excited states $(ns^2)\ ^1S^e$ ($n$ = 2 - 5) of the He-like systems with some theoretical results available in the literature consulted for $Z$ = 2 - 5. All the results are expressed in eV: 1 Ryd = 13.605698 eV.

| States $ns^2\ ^1S^e$ | $Z$ | 2 | 3 | 4 | 5 |
|---|---|---|---|---|---|
| $2s^2\ ^1S^e$ | $E^p$ | 57.5548 | 145.6737 | 275.1269 | 445.4159 |
| | $E^a$ | 57.8487 | 146.2476 | 275.4882 | 445.5893 |
| | $E^b$ | 58.6460 | 147.7633 | 277.6814 | 448.4165 |
| | $E^c$ | 57.8200 | 146.3400 | 275.6600 | 445.7800 |
| $3s^2\ ^1S^e$ | $E^p$ | 69.4768 | 174.7975 | 328.7157 | 531.0145 |
| | $E^b$ | 69.4299 | 175.2577 | 329.3314 | 531.6345 |
| | $E^c$ | 69.5900 | 175.1000 | 328.9600 | 531.1800 |
| | $E^d$ | 69.3972 | 174.7026 | 328.4035 | 530.5215 |
| $4s^2\ ^1S^e$ | $E^p$ | 73.6494 | 184.9908 | 347.4719 | 560.9740 |
| | $E^a$ | 73.5469 | 184.8470 | 347.1820 | 560.5819 |
| | $E^b$ | 73.4218 | 184.9939 | 347.5358 | 561.0989 |
| | $E^c$ | 73.7100 | 185.1600 | 347.6100 | 561.0600 |
| $5s^2\ ^1S^e$ | $E^p$ | 75.5808 | 189.7089 | 356.1533 | 574.8410 |
| | $E^b$ | 75.1905 | 189.4457 | 355.9523 | 574.7972 |
| | $E^c$ | 75.6200 | 189.8200 | 356.2400 | 574.9000 |

[p]Present work, [a]Ho [33], [b]Ray and Mukherjee [23], [c]Sakho *et al.* [24], [d]Ho [34].

**Table 15.** Comparison of the present calculations on the variationnal calculation of the excitation energies of the doubly excited states $(np^2)\ ^1D^e$ ($n$ = 2 - 5) of the He-like systems with some theoretical results available in the literature consulted for $Z$ = 2 - 5. All the results are expressed in eV: 1 Ryd = 13.605698 eV.

| States $np^2\ ^1D^e$ | $Z$ | 2 | 3 | 4 | 5 |
|---|---|---|---|---|---|
| $2p^2\ ^1D^e$ | $E^p$ | 59.6074 | 149.1087 | 280.1198 | 451.9913 |
| | $E^a$ | 59.8900 | 149.9100 | 280.7200 | 452.3400 |
| | $E^b$ | | 149.9157 | 280.7699 | 452.4575 |
| | $E^c$ | 60.3249 | 150.6749 | 281.6815 | 453.8316 |
| | $E^d$ | | 150.3239 | 281.0420 | 452.5854 |
| | $E^e$ | | 150.0599 | 280.9522 | 452.6670 |
| $3p^2\ ^1D^e$ | $E^p$ | 70.2334 | 176.0563 | 330.5418 | 533.4165 |
| | $E^a$ | 70.5100 | 176.6900 | 331.2100 | 534.0900 |
| | $E^b$ | | 176.4251 | 330.8008 | 533.5502 |
| | $E^c$ | 70.0693 | 175.9788 | 330.1368 | 533.3216 |
| | $E^d$ | | 176.2699 | 330.4933 | 533.0876 |
| | $E^f$ | | 176.4441 | 330.8253 | 533.5611 |

**Continued**

| | | | | | |
|---|---|---|---|---|---|
| $4p^2\ ^1D^e$ | $E^p$ | 74.0129 | 185.5932 | 348.3444 | 562.1209 |
| | $E^a$ | 74.2300 | 186.0500 | 348.8700 | 562.7000 |
| | $E^c$ | 73.5851 | 185.3858 | 347.9848 | 561.5942 |
| | $E^d$ | | 185.7178 | 348.3249 | 561.9479 |
| $5p^2\ ^1D^e$ | $E^p$ | 75.7838 | 190.0443 | 356.6386 | 575.4786 |
| | $E^a$ | 75.9500 | 190.3900 | 357.2000 | 575.9500 |
| | $E^c$ | | 189.6852 | 358.2598 | 575.0067 |
| | $E^d$ | | 190.1451 | 356.6570 | 575.4095 |

[p]Present work, [a]Sakho *et al.* [24]; [b]Ho and Bhatia [13]; [c]Ray and Mukherjee [23]; [d]Roy *et al.* [18]; [e]Macias *et al.* [21]; [f]Bachau *et al.* [19].

**Table 16.** Comparison of the present calculations on the variationnal calculation of the excitation energies of the doubly excited states $(nd^2)\ ^1G^e$ ($n$ = 2 - 5) of the He-like systems with some theoretical results available in the literature consulted for $Z$ = 2 - 5. All the results are expressed in eV.

| States $nd^2\ ^1G^e$ | $Z$ | 2 | 3 | 4 | 5 |
|---|---|---|---|---|---|
| $3d^2\ ^1G^e$ | $E^p$ | 70.3444 | 176.2471 | 330.8215 | 533.7867 |
| | $E^a$ | 70.6245 | 176.9557 | 331.6960 | 534.8128 |
| | $E^b$ | 71.0544 | 177.3529 | 332.0144 | 535.0495 |
| | $E^c$ | 70.5238 | 176.9421 | 331.7477 | 534.9298 |
| $4d^2\ ^1G^e$ | $E^p$ | 74.0939 | 185.7314 | 348.5466 | 562.3881 |
| | $E^b$ | 74.3089 | 186.0362 | 348.7685 | 562.5167 |
| | $E^c$ | 73.7021 | 185.5789 | 348.2569 | 561.9398 |
| $5d^2\ ^1G^e$ | $E^p$ | 75.8420 | 190.1429 | 356.7827 | 575.6688 |
| | $E^b$ | 75.9470 | 190.2838 | 356.8475 | 575.6543 |
| | $E^c$ | 75.6667 | 189.8185 | 358.3822 | 575.0611 |
| $6d^2\ ^1G^e$ | $E^p$ | 76.7975 | 192.5498 | 361.2720 | 582.9034 |
| | $E^b$ | 76.8667 | 192.6376 | 361.3047 | 582.8789 |
| $7d^2\ ^1G^e$ | $E^p$ | 77.3770 | 194.0067 | 363.9872 | 587.2765 |
| | $E^b$ | 77.4273 | 194.0717 | 364.0150 | 587.2600 |

[p]Present work; [a]Bachau *et al.* [19]; [b]Roy *et al.* [18]; [c]Ray and Mukherjee [23].

with results obtained by the authors cited in **Tables 14-16**. Overall, we find a good agreement between our results and those of these authors. For all the states studied, the results obtained are in good agreement with the theoretical results we have consulted. The small difference noted between our results and those of the authors mentioned above is explained by the used method and the choice of the correlated wavefunction. The actual results presented in these different tables sufficiently show the good agreements between the current calculations and the different *ab-initio* results for the doubly excited states $(ns^2)\ ^1S^e$, $(np^2)\ ^1D^e$, $(nd^2)$

$^1G^e$, $(nl^2)$ $^1I^e$, $(ng^2)$ $^1K^e$, and $(nh^2)$ $^1M^e$ of the He-like ions up to $Z = 10$. This very good agreement sufficiently justifies the validity of the variational procedure of the SCUNC method to give the precise values obtained directly from an analytical expression, unlike all the *ab-initio* methods cited in this document. Furthermore, the results quoted up to $n = 20$ in this work may be interesting for future experimental and theoretical studies in the doubly excited states $(nl^2)$ $^1L^\pi$. In summary, the manuscript reports on new calculations for key atomic-structure parameters of important fundamental few-body systems (helium and helium-like ions). While not allowing more precision tests of physics due to the neglect of relativistic, spin, and QED effects, such results can still be helpful in the future development of theories to describe more complex atoms, or may be further developed to study the time-dependent evolution of atoms in external (e.g. laser) fields.

## 4. Conclusion

In this paper, the total energies and excitation energies of the doubly excited $(ns^2)$ $^1S^e$, $(np^2)$ $^1D^e$, $(nd^2)$ $^1G^e$, $(nf^2)$ $^1I^e$, $(ng^2)$ $^1K^e$, and $(nh^2)$ $^1M^e$ states of helium-like ions up to $Z$ =10 are reported. These energies are calculated in the framework of the variationnal procedure of the Screening Constant by Unit Nuclear Charge (SCUNC) formalism. In this present work, a new wavefunction correlated to Hylleraas-type adapted to the correct description of electron-electron correlation phenomena in the $(nl^2)$ doubly excited states of helium-like systems has been constructed. Our results for total energies and the excitation energies are in good agreement with the values cited in the experimental and theoretical literature. Furthermore, for $n > 10$, no theoretical and experimental values from the literature are available for direct comparison. The good precision obtained in this work underlines that the results quoted up to $n = 20$ in this work may be interesting for future experimental and theoretical studies in the doubly excited states $(nl^2)$ $^1L^\pi$. The results presented in this paper show that it is therefore possible to perform an analytical calculation of the total energies of the $(nl^2)$ doubly excited states for helium-like ions, without having to resort to excessively complicated calculations or a computer program.

## Conflicts of Interest

The authors declare no conflicts of interest regarding the publication of this paper.

## References

[1] Madden, R.P. and Codling, K. (1963) *Physical Review Letters*, **10**, 516. https://doi.org/10.1103/PhysRevLett.10.516

[2] Codling, K., Madden, R.P. and Ederer, D.L. (1967) *Physical Review Journals Archive*, **155**, 26. https://doi.org/10.1103/PhysRev.155.26

[3] Kahn, M.S. (1999) *Physica Scripta T*, **80**, 23-27. https://doi.org/10.1238/Physica.Topical.080a00023

[4] Keller, S. and Dreizler, R.M. (1999) *Physica Scripta T*, **80**, 93-94. https://doi.org/10.1238/Physica.Topical.080a00093

[5] Faenov, A.Ya., Skobelev, I.Yu. and Rosmej, F.B. (1999) *Physica Scripta T*, **80**, 43-45. https://doi.org/10.1238/Physica.Topical.080a00043

[6] Fano, U. (1983) *Reports on Progress in Physics*, **46**, 97-165. https://doi.org/10.1088/0034-4885/46/2/001

[7] Oda, N., Nishimura, F. and Tashira, S. (1970) *Physical Review Letters*, **24**, 42-45. https://doi.org/10.1103/PhysRevLett.24.42

[8] Hicks, P.J. and Comer, J. (1975) *Journal of Physics B*: *Atomic and Molecular Physics*, **8**, 1866-1879. https://doi.org/10.1088/0022-3700/8/11/022

[9] Rudd, M.E. (1965) *Physical Review Letters*, **15**, 580-581. https://doi.org/10.1103/PhysRevLett.15.580

[10] Bordenave-Montesquieu, A., Gleizes, A., Rodiere, M. and Benoit-Cattin, P. (1973) *Journal of Physics B*: *Atomic and Molecular Physics*, **6**, 1997. https://doi.org/10.1088/0022-3700/6/10/016

[11] Gelebart, F., Tweed, R.J. and Peresse, J. (1976) *Journal of Physics B*: *Atomic and Molecular Physics*, **9**, 1739. https://doi.org/10.1088/0022-3700/9/10/018

[12] Rodbro, M., Bruch, R. and Bisgaard, P. (1979) *Journal of Physics B*: *Atomic and Molecular Physics*, **12**, 2413-2447. https://doi.org/10.1088/0022-3700/12/15/009

[13] Ho, Y.K. and Bhatia, A.K. (1991) *Physical Review A*, **44**, 2895-2855. https://doi.org/10.1103/PhysRevA.44.2895

[14] Lindroth, E. (1994) *Physical Review A*, **49**, 4473-4480. https://doi.org/10.1103/PhysRevA.49.4473

[15] Ho, Y.K. and Callaway, J. (1985) *Journal of Physics B*: *Atomic and Molecular Physics*, **18**, 3481. https://doi.org/10.1088/0022-3700/18/17/010

[16] Biaye, M., Konté, A., Faye, B.A.N. and Wagué, A. (2005) *Physica Scripta*, **71**, 39-42. https://doi.org/10.1088/0031-8949/71/1/006

[17] Ivanov, A.I. and Safronova, I.U. (1993) *Optika.Spectrosk*, **75**, 516.

[18] Roy, K.A., Singh, R. and Deb, M.B. (1997) *Journal of Physics B*: *Atomic*, *Molecular and Optical Physics*, **30**, 4763. https://doi.org/10.1088/0953-4075/30/21/014

[19] Bachau, H., Martin, F., Riera, A. and Yanez, M. (1991) *Atomic Data Nuclear Data Tables*, **48**, 167-212. https://doi.org/10.1016/0092-640X(91)90006-P

[20] Ho, Y.K. (1989) *Z Physics D Atoms*, *Molecules and Clusters*, **11**, 277-281. https://doi.org/10.1007/BF01438499

[21] Macias, A., Martin, F., Riera, A. and Yanez, M. (1987) *Physical Review A*, **36**, 4187-4202. https://doi.org/10.1103/PhysRevA.36.4187

[22] Conneely, M.J. and Lipsky, L. (1978) *Journal of Physics B*: *Atomic and Molecular Physics*, **24**, 4135. https://doi.org/10.1088/0022-3700/11/24/008

[23] Ray, D. and Mukherjee, P.K. (1991) *Journal of Physics B*: *Atomic*, *Molecular and Optical Physics*, **24**, 1241. https://doi.org/10.1088/0953-4075/24/6/013

[24] Sakho, I., Ndao, A.S., Biaye, M. and Wagué, A. (2008) *European Physical Journal D*, **47**, 37-44. https://doi.org/10.1140/epjd/e2008-00018-2

[25] Sakho, I., Ndao, A.S., Biaye, M. and Wagué, A. (2008) *Physica Scripta*, **77**, Article ID: 055303. https://doi.org/10.1088/0031-8949/77/05/055303

[26] Sakho, I. (2011) *European Physical Journal D*, **61**, 267-283. https://doi.org/10.1140/epjd/e2010-10294-8

[27] Sakho, I. (2011) *Journal of Atomic and Molecular Sciences*, **2**, 20-42. https://doi.org/10.4208/jams.062910.072810a

[28] Hylleraas, E.A. (1928) *Zeitschrift für Physik*, **48**, 469-494. https://doi.org/10.1007/BF01340013

[29] Hylleraas, E.A. (1929) *Zeitschrift für Physik*, **54**, 347-366. https://doi.org/10.1007/BF01375457

[30] Hylleraas, E.A. (1930) *Zeitschrift für Physik*, **65**, 209-225. https://doi.org/10.1007/BF01397032

[31] Hylleraas, E.A. and Undheim, B. (1930) *Zeitschrift für Physik*, **65**, 759-772. https://doi.org/10.1007/BF01397263

[32] Sakho, I., Ndao, A.S., Biaye, M. and Wagué, A. (2010) *Physica Scripta*, **82**, Article ID: 035301. https://doi.org/10.1088/0031-8949/82/03/035301

[33] Ho, Y.K. (1981) *Physical Review A*, **23**, 2137. https://doi.org/10.1103/PhysRevA.23.2137

[34] Ho, Y.K. (1979) *Journal of Physics B*: *Atomic and Molecular Physics*, **12**, 387. https://doi.org/10.1088/0022-3700/12/3/016

[35] Ho, Y.K. (1980) *Physics Letters A*, **79**, 44-46. https://doi.org/10.1016/0375-9601(80)90313-8

[36] Sow, B., Sow, M., Gning, Y., Traore, A., Ndao, A.S. and Wague, A. (2016) *Radiation Physics and Chemistry*, **123**, 25-30. https://doi.org/10.1016/j.radphyschem.2016.01.037

[37] Gning, *et al.* (2015) *Radiation Physics and Chemistry*, **106**, 1-6. https://doi.org/10.1016/j.radphyschem.2014.06.015

[38] Konté, A., Ndao, A.S., Biaye, M. and Wagué, A. (2006) *Physica Scripta*, **74**, 605. https://doi.org/10.1088/0031-8949/74/6/002

[39] Diouf, A., *et al.* (2017) *International Journal of Applied Mathematics and Theoretical Physics*, **3**, 78-85. https://doi.org/10.11648/j.ijamtp.20170304.11

[40] Sakho, I. (2010) *Journal of Atomic and Molecular Sciences*, **1**, 103-117. https://doi.org/10.4208/jams.022510.031010a

[41] Badiane, J., *et al.* (2018) *International Journal of Applied Mathematics and Theoretical Physics*, **4**, 27-41. https://doi.org/10.11648/j.ijamtp.20180402.11

[42] Frankowski, F. and Pekeris, L.C. (1966) *Physical Review*, **146**, 46-49. https://doi.org/10.1103/PhysRev.146.46

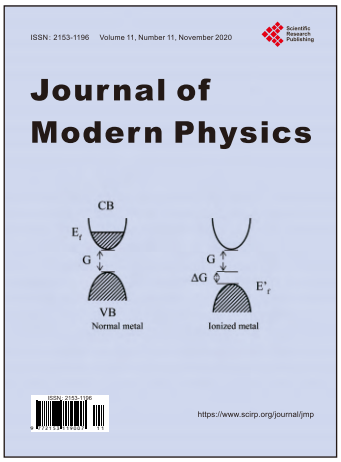


# Call for Papers

# Journal of Modern Physics

ISSN: 2153-1196 (Print) ISSN: 2153-120X (Online)
https://www.scirp.org/journal/jmp

***Journal of Modern Physics*** **(JMP)** is an international journal dedicated to the latest advancement of modern physics. The goal of this journal is to provide a platform for scientists and academicians all over the world to promote, share, and discuss various new issues and developments in different areas of modern physics.

## Editor-in-Chief

**Prof. Yang-Hui He** City University, UK

## Subject Coverage

Journal of Modern Physics publishes original papers including but not limited to the following fields:

Biophysics and Medical Physics
Complex Systems Physics
Computational Physics
Condensed Matter Physics
Cosmology and Early Universe
Earth and Planetary Sciences
General Relativity
High Energy Astrophysics
High Energy/Accelerator Physics
Instrumentation and Measurement
Interdisciplinary Physics
Materials Sciences and Technology
Mathematical Physics
Mechanical Response of Solids and Structures
New Materials: Micro and Nano-Mechanics and Homogeneization
Non-Equilibrium Thermodynamics and Statistical Mechanics
Nuclear Science and Engineering
Optics
Physics of Nanostructures
Plasma Physics
Quantum Mechanical Developments
Quantum Theory
Relativistic Astrophysics
String Theory
Superconducting Physics
Theoretical High Energy Physics
Thermology

We are also interested in: 1) Short Reports—2-5 page papers where an author can either present an idea with theoretical background but has not yet completed the research needed for a complete paper or preliminary data; 2) Book Reviews—Comments and critiques.

## Notes for Intending Authors

Submitted papers should not have been previously published nor be currently under consideration for publication elsewhere. Paper submission will be handled electronically through the website. All papers are refereed through a peer review process. For more details about the submissions, please access the website.

## Website and E-Mail

**https://www.scirp.org/journal/jmp** **E-mail: jmp@scirp.org**

## What is SCIRP?

Scientific Research Publishing (SCIRP) is one of the largest Open Access journal publishers. It is currently publishing more than 200 open access, online, peer-reviewed journals covering a wide range of academic disciplines. SCIRP serves the worldwide academic communities and contributes to the progress and application of science with its publication.

## What is Open Access?

All original research papers published by SCIRP are made freely and permanently accessible online immediately upon publication. To be able to provide open access journals, SCIRP defrays operation costs from authors and subscription charges only for its printed version. Open access publishing allows an immediate, worldwide, barrier-free, open access to the full text of research papers, which is in the best interests of the scientific community.

- High visibility for maximum global exposure with open access publishing model
- Rigorous peer review of research papers
- Prompt faster publication with less cost
- Guaranteed targeted, multidisciplinary audience


Scientific Research Publishing

**Website: https://www.scirp.org**

**Subscription: sub@scirp.org**

**Advertisement: service@scirp.org**